Dissertation

New liver cancer and colorectal cancer biomarkers: PI3K/AKT/mTOR pathway members and eukaryotic translation initiation factors

submitted by

Nicole Golob-Schwarzl, BSc MSc

for the Academic Degree of

Doctor of Medical Science

(Dr. scient. med.)

at the

Medical University of Graz

Institute of Pathology

under the Supervision of

Univ.-Prof. Dr. med. Univ. Dr. sc. Nat. Johannes Haybaeck

2017

Declaration

I hereby declare that this thesis is my own original work and that I have fully acknowledged by name all of those individuals and organizations that have contributed to the research for this thesis. Due acknowledgment has been made in the text to all other material used.
Throughout this dissertation and in all related publications I followed the guidelines of "Good Scientific Practice."

Graz, July, 2017

Parts of this thesis have been published in: Nicole Golob-Schwarzl[1, 2], Stefanie Krassnig[1], Anna M. Toeglhofer[1], Young Nyun Park[3], Margit Gogg-Kamerer[1], Klemens Vierlinger[4], Fabian Schröder[4], Hyungjn Rhee[5], Rudolf Schicho[6], Peter Fickert[7], Johannes Haybaeck[1, 2, 8]. "New liver cancer biomarkers: PI3K/AKT/mTOR pathway members and eukaryotic translation initiation factors", at European Journal of Cancer, 2017; 83:56-70.

[1]Department of Pathology, Medical University of Graz, Austria
[2]Center for Biomarker Research in Medicine, Graz, Austria
[3]Department of Pathology, Yonsei University, College of Medicine, Seoul, South Korea
[4]AIT Austrian Institute of Technology GmbH, Vienna, Austria
[5]Department of Pathology, Yonsei University, University College of Medicine, Seoul, South Korea
[6]Institute of Experimental and Clinical Pharmacology, Medical University of Graz, Austria
[7]Division of Gastroenterology and Hepatology, Medical University of Graz, Austria
[8]Department of Pathology, Otto-von-Guericke-University Magdeburg, Germany

I confirm that all co-authors have agreed to the use of their data in my thesis.

Acknowledgements

I want to thank

Univ.-Prof. Dr. med. univ. Dr. sc. nat. Johannes Haybäck for giving me the opportunity to work on this fascinating topic and for his supervision and guidance throughout the whole dissertation.

My colleagues Stefanie, Anna, Nadine, Christina, Florian, Sabine and Julia for their assistance, motivating conversations and memorable moments in the lab.

Margit Gogg-Kamerer for her assistance and excellent help with the immunohistochemistry.

Prof. Rudolf Schicho and Prof. Peter Fickert for their assistance and support as members of the thesis committee.

The members of the OncoTrack consortium for the opportunity to work on this European project in particular Dr. Christian Regenbrecht, Dr. Jens Hoffmann, Dr. David Henderson and Univ.-Prof. Dr. Hans Lehrach.

I received funding from “Cbmed – Center for Biomarker Research in Medicine” and the Medical University of Graz through the Doctoral School “Molecular Medicine and Inflammation”.

Cbmed – Center for Biomarker Research in Medicine for the allowance to work in the company and the whole Cbmed team for their support during my time there.

I want to thank my mother and my sister for their endless support throughout my whole life and especially during my PhD thesis. Without them I would have never finished this thesis. It’s impossible to express my thankfulness in words.

Last but not least I want to thank my beloved husband for his endless love, endurance and support. He always pushed me to give my best.

This work is dedicated to my beloved father, who is not able to witness my graduation anymore.

Content

Abbreviation

AD	Aqua dest
AJCC	American Joint Committee on Cancer
AKT	Protein Kinase B
ASH	Alcoholic steatohepatitis
ATCC	American Type Culture Collection
AUC	Area under the Curve
BRAF	v-Raf murine sarcoma viral oncogene homolog B
BSA	Bovine Serum Albumin
CC	Colon Carcinoma
CC-Met	Liver metastases of primary colon carcinomas
cDNA	copy Deoxyribo-nucleic acid
CD34	Heamatopoietic progenitor cell antigen 34
CK-7	Cytokratin-7
CRC	Colorectal cancer
CO_2	Carbon dioxide
Ct	Cycle threshold
DMEM	Dulbecco Modified Eagle Medium
DNA	Deoxyribo-nucleic acid
DTT	Dithiothreitol
4E-BP1	4E-binding protein 1
EGFR	Epidermal Growth Factor Receptor
eIF	eukaryotic initiation factors

ERK	Extracellular Signal-Regulated Kinase
FCS	Fetal Calf Serum
FFPE	Formalin-fixed paraffin-embedded tissue
Fwd	Forward
GAP	GTPase-activator protein
GAPDH	Glyceraldehyde 3-phosphate dehydrogenase
GEF	Guanine Nucleotide Exchange Factor
GTP	Guanosine triphosphate
HCC	Hepatocellular carcinoma
HCl	Hydrochloric acid
HBV	Hepatitis B virus
HCV	Hepatitis C virus
H/E	Hematoxilin and Eosin Stain
HG	High Grade
HRP	Horse radish peroxidase
IRES	Internal ribosomal entry site
KCl	Potassium chloride
KRAS	V-Ki-ras2 Kirsten rat sarcoma viral oncogene homolog
LG	Low Grade
M	Metastasis
MEK	Methyl ethyl ketone
MEM	Minimum Essential Medium Eagle
$MgCl_2$	Magnesium chloride
MMTV	Mouse mammary tumor virus

mRNA	Messenger RNA
MSS4	Mammalian phosphatidylinositol-4-phosphate
MSI	Microsatellite instability
MSI-H	Microsatellite instability
MSI-L	Microsatellite instability
MTT	3-(4,5-dimethylthiazol-2-yl)-2,5-diphenyltetrazolium bromide
mTOR	Mammalian Target of Rapamycin
N	Regional Lymph Nodes
NaCl	Sodium chloride
NASH	Nonalcoholic induced steatohepatitis
NF-ƙB	Nuclear factor 'kappa-light-chain-enhancer' of activated B-cells
NH_4Cl	Ammonium chloride
NNLT	Non-neoplastic liver tissues
NNM	Non-neoplastic mucosa
NNT	Non-neoplastic tissues
OD	Optical density
PABP	Poly-A-binding protein
PARP	Poly (ADP-ribose) polymerase
PAS	Periodic acid-Schiff reaction
PBS	Phosphate Buffered Saline
PCR	Polymerase chain reaction
PDX	Patient Derived in Xenograft
PIC	Preinitiation complex
PI3K	Phosphatidylinositol-4,5-bisphosphate 3-kinase

PIK3CA	Phosphatidylinositol-4,5-Bisphosphate 3-Kinase Catalytic Subunit
POI	Protein of Interest
PTEN	Phosphatase and tensin homolog
qRT-PCR	Quantitative Real-Time PCR
RAF	Rapidly accelerated fibrosarcoma
RAS	Rat sarcoma
RC	Rectum Carcinoma
RC-Met	Liver metastases of primary rectum carcinomas
Rev	Reverse
RISC	RNA-induced silencing complex
RT	Reverse transcribed
S6K	Ribosomal S6 kinase
SDS	Sodium dodecyl sulfate
siRNA	Small interfering RNA
T	Primary Tumor
TBST	Tris Buffered Saline Tween
T/C	Tumor volume of treatment in comparison to control
TCGA	The Cancer Genome Atlas
TMA	Tissue Micro Array
UICC	Union internationale contre le cancer
UV	Ultraviolet radiation
WHO	World Health Organization
WT	Wild type

Zusammenfassung

Theoretischer Hintergrund & Zielsetzung:

Das hepatozelluläre Karzinom (HCC) zählt zu den häufigsten Lebertumoren .Trotz der guten Ergebnisse, die im Krankheitsmanagement und in der Diagnose erzielt worden sind, beträgt die Überlebensrate von Patienten mit HCC weniger als 8 Monate. Chirurgische Resektion, Lebertransplantation und lokale Entfernung bilden die Behandlungsstrategien für HCC. In 70 % der Patienten rezidiviert dieser Tumor innerhalb von 5 Jahren nach der Resektion. Entzündung und chronische Verletzung fördern dabei die Tumorentwicklung. Das HCC ist eines der besten Beispiele hierfür. Mehr als 90% der HCC Fälle entwickeln sich aus einer hepatischen Verletzung oder Entzündung. Deshalb sind Biomarker, die HCC von Entzündungen und Zirrhose unterscheiden, erforderlich um die Prognose der Patienten zu verbessern.

Das kolorektale Karzinom (CRC) stellt mit mehr als 1,2 Millionen diagnostizierten Fällen pro Jahr weltweit die dritthäufigste Todesursache der Tumorerkrankungen dar. Die Proteinderegulierung spielt bei der Entwicklung des Tumors eine wesentliche Rolle. Der erste Schritt in diesem Entstehungsprozess wird durch die eukaryotischen Initiationsfaktoren (eIFs) geregelt und wird als limitierender Schritt in der Proteinsynthese angesehen. Die eIFs bilden die Hauptbestandteile in der Tumortherapie und stehen in funktioneller Verbindung mit dem PI3K/AKT/mTOR Signalweg.

Der erste Teil dieser Arbeit richtet den Fokus auf eIF5 und seiner potentiellen Rolle als prognostischer Biomarker für die chronische Leberentzündung Hepatitis B Virusinfektion (HBV) und Hepatitis C Virusinfektion (HCV), das HBV- und HCV-assoziierte hepatozelluläre Karzinom, das nicht viral induzierte HCC, ASH und Morbus Wilson.

Das zweite Hauptaugenmerk dieser Arbeit galt der Rolle von eIFs und den mTOR Mitgliedern im kolorekaten Karzinom. Neben patientenbasierenden Analysen wurden *in vitro* siRNA –knockdown Experimente gegen eIF1, eIF5 und eIF6 in zwei Kolorektalkarzinomzelllinien durchgeführt. Die untersuchten Parameter umfassten Zellproliferation, Zellviabilität, Invasion und Koloniebildung.

Methoden:

Die Expression von eIFs und mTOR Mitgliedern wurde in HBV, HCV, HBV- und HCV-assoziiertem HCC, nicht viral induziertem HCC, ASH und Morbus Wilson im Vergleich zu nicht-neoplastischem Gewebe auf Proteinebene mittels Immunhistochemie und Immunblots untersucht.

Die Expression von eIFs und mTOR Mitgliedern wurde in primären niedrig- und hochgradigen Kolonkarzinomen (CC) und Rektumkarzinomen (RC) im Vergleich zu nicht-neoplastischem Gewebe ohne krankheitszusammenhängender Pathologie auf Protein und mRNA Ebene analysiert. Um das therapeutische Potenzial zu bewerten, wurden siRNA–Knockdowns gegen eIF1, eIF5 und eIF6 in HCT116 und HT29 Zelllinien durchgeführt. Der eIF–Silencing Effekt wurde auf Protein- und mRNA-Ebene analysiert gefolgt von Untersuchungen zur Zellproliferation, Zellviabilität, Invasion und Koloniebildung. Alterationen in der Proteinsynthese wurde mittels Darstellung eines Polysomenprofils analysiert. Zusätzlich wurden immunhistochemische Analysen auf Tissue Mirco Arrrays mit 9 eIF-Untereinheiten an Lebermetastasen von primären CC und RC im Vergleich zu nicht-neoplastischem Lebergewebe durchgeführt. Darüber hinaus folgten *in vivo* Experimente mit CC und RC Tumoren in xenotransplantierten Nacktmäusen, welche mit unterschiedlichen Therapeutika behandelt wurden, um anschließend die eIF und mTOR Expression zu analysieren.

Ergebnisse:

Auf Proteinebene wurde eine erhöhte Expression von eIF5 in HBV, HCV, in HBV- und HCV-assoziiertem HCC, nicht viral induziertem HCC, ASH und Morbus Wilson nachgewiesen.

In niedrig- und hochgradigen CC- und RC-Patienten zeigte sich eine signifikante Überexpression auf Protein- und mRNA-Ebene für mTOR Mitglieder und den meisten eIF-Untereinheiten. Da sich eIF1, 5 und 6 als vielversprechendste Kandidaten in der Therapie von CRC darstellten, untersuchten wir diese drei eIF Untereinheiten ausführlicher in Silencing-Experimenten. Nach erfolgreichem Silencing von eIF1, eIF5 und eIF6 zeigte sich sowohl in der Proliferationsrate als auch in der Klonogenität von HCT116- und HT29-Zellen eine signifikante Reduktion. Zu späteren Zeitpunkten des Knockdowns wurde eine deutliche Erhöhung der Apoptose beobachtet. Das Silencing von eIF1, eIF5 und eIF6 führte zu einer Reduktion von Polysomen, was auf eine generelle Reduktion der Proteintranslation hinweist. Zusätzlich zu Chemosensitivitätsaustestungen wurden CRC-PDX Modelle auf Proteinebene

analysiert. Es konnten keine signifikanten Änderungen im eIF-Expressionsmuster in behandelten CRC-PDX Modell beobachtet werden.

Schlussfolgerung:

eIF5 wurde sowohl als prädiktiver und auch als prognostischer Biomarker in HBV, HCV, HBV- und HCV-assoziiertem HCC, nicht viral induzierten HCC, ASH und Morbus Wilson identifiziert.

eIF Untereinheiten zeigten eine signifikante Überexprimierung in Lebermetastasen des primären CRC, Diese Ergebnisse lassen die Schlussfolgerung zu, dass eIFs in der Translationsinitiation von Lebermetastasen des primären CRC und in der Tumorentstehung eine wichtige Rolle spielen. Um einen tieferen mechanistischen Einblick in die vielfältige Rolle von eIF1, eIF5 und eIF6 in der Tumorentstehung zu gewinnen, sind zukünftige Studien erforderlich. Allerdings kann man schlussfolgern, dass vor allem eIF1, eIF5 und eIF6 in niedrigen und hochgradigen CRCs sowohl als prognostische als auch als prädiktive Biomarker eingesetzt werden können.

Abstract

Theoretical background & aim:

The most common type of liver cancer is hepatocellular carcinoma (HCC). Despite progressive achievements in management and diagnosis, the mean survival of patients with HCC is less than 8 months. Treatment strategies for HCC are surgical resection, liver transplantation, and local ablation. Recurrence occurs in up to 70% of patients within 5 years after resection. Inflammation and chronic injury are known to benefit tumor development. HCC is one of the best examples, and more than 90% of HCCs arise from hepatic injury and inflammation. Therefore, biomarkers differentiating HCC from inflammation and cirrhosis are needed in order to improve the prognosis of the respective patients.

Colorectal cancer (CRC) is the third most common cause of cancer-related death worldwide. With more than 1.2 million cases registered per year, it constitutes the third most frequently diagnosed cancer entity worldwide.

Protein deregulation has received considerable attention as a major step in cancer development and progression. The step of initiation, regulated by eukaryotic initiation factors (eIFs), is regarded as rate-limiting step in protein synthesis. eIFs become major targets for cancer therapy and are functionally linked to PI3K/AKT/mTOR signaling. However, little is known about their contribution to CRC.

The first part of this thesis focuses on eIF5 to find out if this gene could serve as a prognostic biomarker in chronic hepatitis B (HBV) and C (HCV), HBV- and HCV-associated HCC, non-virus related HCC, ASH, and Wilson´s disease.

In the second part, the thesis focuses on eIF1, eIF5, and eIF6 in CRC. The aim of the *in vitro* studies was to establish a siRNA knockdown system in CRC cell lines to down-regulate the levels of eIF1, eIF5, and eIF6. Using CRC cell lines, we analyzed the response to eIF1, eIF5, and eIF6 knockdown in preparation in the search for changed translation, proliferation, and viability.

Methods:

eIF and mTOR expression was analysed in HBV and HCV, HBV- and HCV-associated HCC, non-virus related HCC, ASH, and Wilson´s disease. A comparison was made with non-neoplastic tissue without any disease-related pathology on the protein level using immunohistochemistry and immunoblot.

eIF and mTOR expression was analysed in primary low and high grade colon carcinoma (CC) and rectum carcinoma (RC) samples, and compared with non-neoplastic tissue without any disease-related pathology on the protein and mRNA level. To assess the therapeutic potential of targeting eIF1, eIF5, and eIF6, siRNA knockdown in HCT116 and HT29 cells was performed. We evaluated the eIF knockdown on protein and mRNA level, and investigated proliferation, apoptosis, invasion, colony-forming, and polysome-associated fractions. In addition, CC and RC liver metastasis and non- neoplastic liver tissue served as controls, and were studied by immunohistochemistry investigating 9 eIF subunits on tissue micro-arrays (TMAs). *In vivo,* CC and RC patients-derived xenograft models were treated with different drugs and the protein expression of eIFs and mTOR members was analyzed.

Results:

On the protein level, eIF5 turned out to be a prognostic biomarker in HBV, HCV, HBV- and HCV-associated HCC, non-virus related HCC, ASH, and Wilson´s disease.

Protein and mRNA levels of low and high grade CC and RC patients revealed a significant up-regulation for mTOR members and most eIF subunits. As the eIF subunits 1, 5, and 6 turned out to be the most promising candidates in targeting CRC, we investigated them in more detail in silencing experiments. After successful down-regulation of *eIF1*, *eIF5,* and *eIF6,* both the proliferation rate and the clonogenicity of HCT116 and HT29 cells were significantly reduced. Apoptosis significantly increased during longer treatment periods. Silencing of *eIF1*, *eIF5,* and *eIF6* resulted in a reduction of polysomes, indicating reduced overall translation. In addition to chemosensitivity testing, CRC PDX models were analyzed on the protein level. No significant changes in eIF expression pattern could be observed when comparing CRC and control tissues upon treatment.

Conclusion:

eIF5 turned out to serve as a predictive and prognostic biomarker in HBV, HCV, HBV- and HCV-associated HCC, non-virus related HCC, ASH, and Wilson´s disease.

Various eIF subunits were found to be significantly overexpressed in liver metastases of primary CRC. This might lead to the conclusion that eIFs are key drivers in the carcinogenesis of liver metastases of primary CRC. The question of whether eIFs could serve as predictive biomarkers, not only for cisplatin and related therapies, will be a subject of intense research in the following years. To gain a deeper mechanistic insight into the multifaceted role of eIF1, eIF5, and eIF6 in carcinogenesis, future studies are needed.

However, it can be concluded that eIF1, 5, and 6 might serve as prognostic tumor markers especially in low and high grade CRC.

1 Introduction

1.1 Hepatocellular carcinoma

1.1.1 Epidemiology, Relevance and Risk Factors

Liver cancer is the second leading cause of cancer mortality worldwide, with approximately 600,000 cancer related deaths [1, 2]. The most common type of liver cancer is hepatocellular carcinoma (HCC), which has increased in its incidence in the United States in recent years and is expected to double in the next 10 to 20 years [3, 4]. Despite progressive achievements in management and diagnosis, the mean survival of patients with HCC is less than 8 month and thus HCC is still one of the most fatal cancers [3, 2]. Relevant treatment strategies for HCC are surgical resection, liver transplantation, and local ablation. Recurrence occurs in up to 70% of patients within 5 years after resection [2, 5, 6].

Two pronounced types of recurrence are known in HCC. The early recurrence develops from primary cancer cells spreading to the surrounding liver and is usually observed within the first 2 years after surgery. In comparison, late recurrence, which is typically monitored more than 2 years after surgery, appears to be a result of chronic liver damage known as the field effect, and creates *de novo* tumors that are irrespective of resected primary tumors [5]. The two types of recurrence follow different clinical courses and presumably appear in distinct biological contexts [7]. For improving the disease treatment, it is therefore important to recapitulate and understand the biological characteristics of each type of recurrence and to generate distinct molecular prognostication systems that are capable of determining patients at high risk for either type. Above all the importance of managing recurrence, our knowledge about the genetic alterations appendant with either type, primarily late recurrence, is incomplete [2].

Inflammation and chronic injury are known to promote tumor development. HCC is one of the best examples, and more than 90% of HCCs arise from hepatic injury and inflammation [8, 9]. Chronically unresolved inflammation is often associated with continuing hepatic injury and simultaneously regeneration, which prime the liver for the development of HCC. This process resembles a continuing wound-healing response, regardless of the differences among various etiological factors such as alcohol, viruses, and fatty liver [10, 11]. However, the coexistence of cirrhosis and inflammation bedevils early diagnosis of HCC. Therefore, biomarkers differentiating HCC from inflammation and cirrhosis are needed in order to improve prognosis of the respective patients. Besides, biomarkers may influence the

evolution of novel chemopreventive strategies for benefit during HCC surveillance of patients with liver cirrhosis [12].

1.1.2 Histology of Hepatocellular Carcinoma

The typical histological features of HCC are well vascularized tumors with extensive trabeculae (> 3 cells), small changes in the cells, cytological atypia, characteristic acinar pattern, mitotic activity, vascular invasion, loss of Kupffer cells and deficiency of the reticulin network [13]. The most frequent histological growth patterns are the trabecular-resembling normal liver tissue, the compressed or solid pattern and pseudo glandular or acinar pattern with possible bile or fibrin content. Moreover, the bile production can be observed and within the tumor cells Mallory-Denk-bodies and pale bodies can be monitored [14]. The histomorphologic epiphany of HCC varies greatly from patient to patient, variable stages of intratumoral differentiation and growths pattern can be observed. By contrast, advanced HCC displays an expansive and infiltrative histologic growth pattern with entire neovascularization with unpaired arteries and potential vascular infiltration. No classical histological pattern like pseudo glandular, trabecular or sinusoidal, solid and undifferentiated and portal tracts is seen within the tumor [15].

Angioarchitecture performs a major role during tumor growth and is part of modern imaging modalities. Advanced HCC shows classical unpaired arteries positive for SMA and CD34 but these arteries are not associated with a portal tract and have no contact to bile ducts. Early stage HCC of the vaguely nodular type displays an increase in density of unpaired arteries in contrast to advanced HCC [16, 17]. Early stage HCC of the distinctly nodular type as well as advanced stage HCC indicates hyper vascularity because of earlier neovascularization with unpaired arteries.

1.1.2.1 *Fibrolamellar HCC*

This uncommon subtype was first described by Edmondson occurring in less than 1% of all tumors [18]. Fibrolamellar HCC is often seen in young patients without liver cirrhosis and shows no other predisposing factors. This type displays a better prognosis for the patient than classical HCC [19, 20]. The tumor cells histologically develop in sheets and trabeculae that are separated by collagen fibers which are often hyalinized and display a lamellar pattern [15]. This subtype often shows inclusions like ground glass pale bodies and cytoplasmic

globules which are Periodic acid-Schiff reaction (PAS)-positive and immunoreactivity to anti-fibrinogen [21].

1.1.2.2 *Sarcomatous HCC*

This subtype can develop by itself, but also in classical HCC. The tumor cells are spindle-shaped, and display eccentric anaplastic figures. Sarcomatous HCC often shows giant cells, but this is not exclusively for this subtype. In patients without advanced HCC, it is difficult to differ from fibrosarcoma and leiomyosarcoma [22, 23].

1.1.2.3 *Scirrhous HCC*

In this HCC subtype fibrotic changes can be observed, which can arise after antitumor treatments and unusual in untreated tumors. Histologically, scirrhous HCC shows fibrosis along the sinusoid-like blood spaces, with atrophy of the trabeculae. In immunohistochemistry, Hep-Par-1 and CK7 are often used to identify positive tumor cells [24].

1.1.2.4 *Clear-cell Variant HCC*

This subtype shows a clear cytoplasm which contains glycogen, a different amount of fat vesicles and displays a trabecular pattern [25], only in parts of the tumor. Clear-cell variant HCC is predominantly in male [26].

1.1.2.5 *Steatohepatitic HCC*

This subtype is characterized through steatotic arisen of > 5% of the tumor. It consists of Mallory-Denk-bodies, fibrosis, ballooning of the hepatocytes as in steatohepatitis and inflammation. The fibrosis arises in a trabecular and pericellular form and the inflammatory infiltrate compound of lymphocytes, plasma cells and neutrophils. Most of the patients suffer from non-alcoholic steatohepatitis but this subtype is also recognized in patients without steatohepatitic transformations in the non-neoplastic liver tissue [27].

1.1.2.6 *HCC with Lymphoid Stroma*

This subtype is very rare and is described only in a few case reports. It contains a massive inflammatory infiltrate with few tumor cells. Most of the cells are lymphocytes, giant cells, plasma cells, macrophages and neutrophils [28, 29].

1.1.3 TNM Classification of Hepatocellular Carcinoma

The most common staging system is the American Joint Committee on Cancer (AJCC) TNM system. This system is based on three key factors. These determine the depth of tumor invasion (T), the extent of nodal metastasis (N) and the spreading of the cancer (M). T describes the extent to which the primary tumor has grown into the wall of the intestine. N characterizes proliferation to nearby lymph nodes, and M indicates if the cancer has spread to other organs [30].

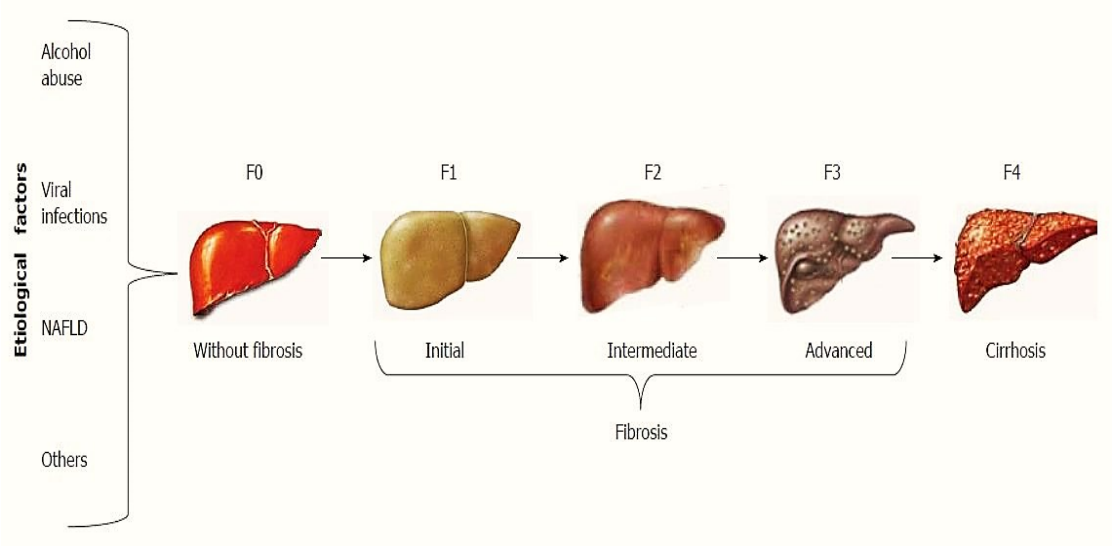

Figure 1: Scheme of hepatic fibrogenesis of HCC. Reproduced from [31] with permission of publisher (World J Gastroenterol.).

1.2 Colorectal Cancer

1.2.1 Epidemiology, Relevance and Risk Factors

Colorectal cancer (CRC) is the third most common cause of cancer-related death. With more than 1.2 million cases registered per year, it constitutes the third most frequently diagnosed cancer entity worldwide [32 - 35]. Over the past few decades, the mortality of CRC has been steadily on the decline, as revealed by early detection through screening methods [36]. The pathogenesis of CRC is complex and usually manifests in the three following patterns: sporadic, inherited or familial.

The sporadic development of the disease is seen in approximately 75% of CRC cases. The familial form of the disease occurs in 25% of cases. Some of the family members of these cases have been reported to be affected by CRC as well. This group has developed a higher risk of developing CRC compared to the general population. However, most of the CRC cases represent a sporadic type; this means there is neither a family history nor a genetic predisposition [37].

The most important risk factor is increasing age, and 90% of the patients diagnosed with CRC are older than 50 years. Younger patients (in their 40s) exhibit a much more aggressive form of this disease, whereas patients older than 70 mostly develop this disease at an early stage [38]. The incidence of developing CRC is equal in men and women. Compared to men, women seem to suffer more frequently from right-sided tumors. Moreover, the overall 5-year survival rate is significantly higher in women than in men [39]. A major risk factor for developing CRC lies in dietary factors, such as high intake of red meat (beef and pork), which has been associated with the development of advanced CRC compared to patients not consuming these meat products [40,41]. Epidemiologic studies show that smoking and alcohol abuse are further factors that increase the risk of developing CRC. Chronic inflammatory bowel diseases, such as Ulcerative Colitis and Crohn Disease, increase the CRC risk. A genetics-based explanation for this predisposition has not yet been identified [39].

Anatomically, CRC is divided into proximal colon cancer (right from the splenic flexure), distal colon cancer (left from the splenic flexure) and rectal cancer. The proximal colon cancer originates from the midgut, while the distal colon and rectum cancer arise from the hindgut. In CRC, several genetic abnormalities have been reported to affect other sites as well [42].

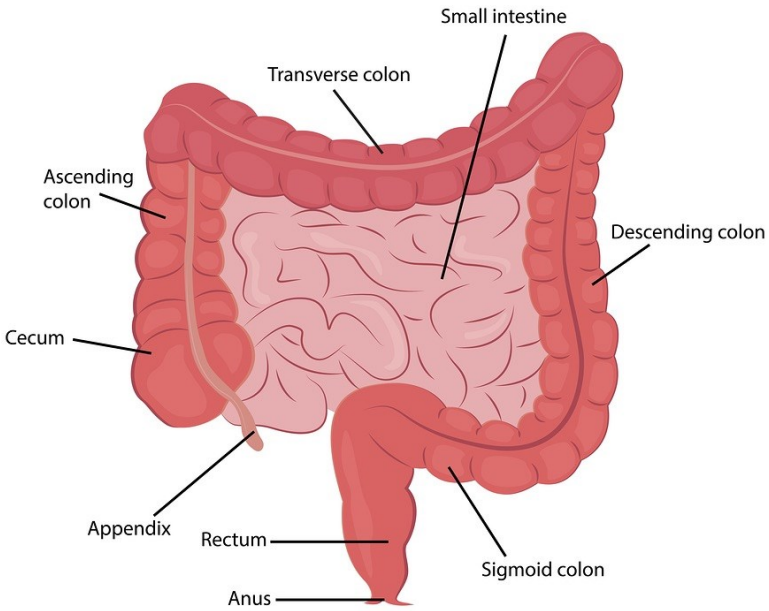

Figure 2: Anatomy of colon and rectum. Reproduced from [43] with permission of publisher.

1.2.2 Histology of Colorectal Cancer

Colon and rectum consist of a tunica mucosa, a tela submucosa, a tunica muscularis propria (externa) and a tunica serosa.

The mucosa displays a glandular epithelium, with lamina propria and the muscularis mucosae. Both parts show no plicae circulares and villi. Deep crypts of Lieberkühn are visible and depth increases in anal direction. The mono layered columnar epithelium contains a large number of goblet cells for mucus secretion. The lamina propria is small and extends to a distinctive muscularis mucosae. The musculature of the tunica muscularis displays an outer longitudinal and an inner circular form. The teniae coli is formed by three separate bands of longitudinal musculature [44, 45].

The histology of the rectum is similar to that of the colon, but there are still differences at the histological level. There are no epithelial cells in the rectum; they are replaced by goblet cells. The tenia structure in the rectum shows outer longitudinal and inner circular muscle fibers, and the crypts are longer than in the colon [46].

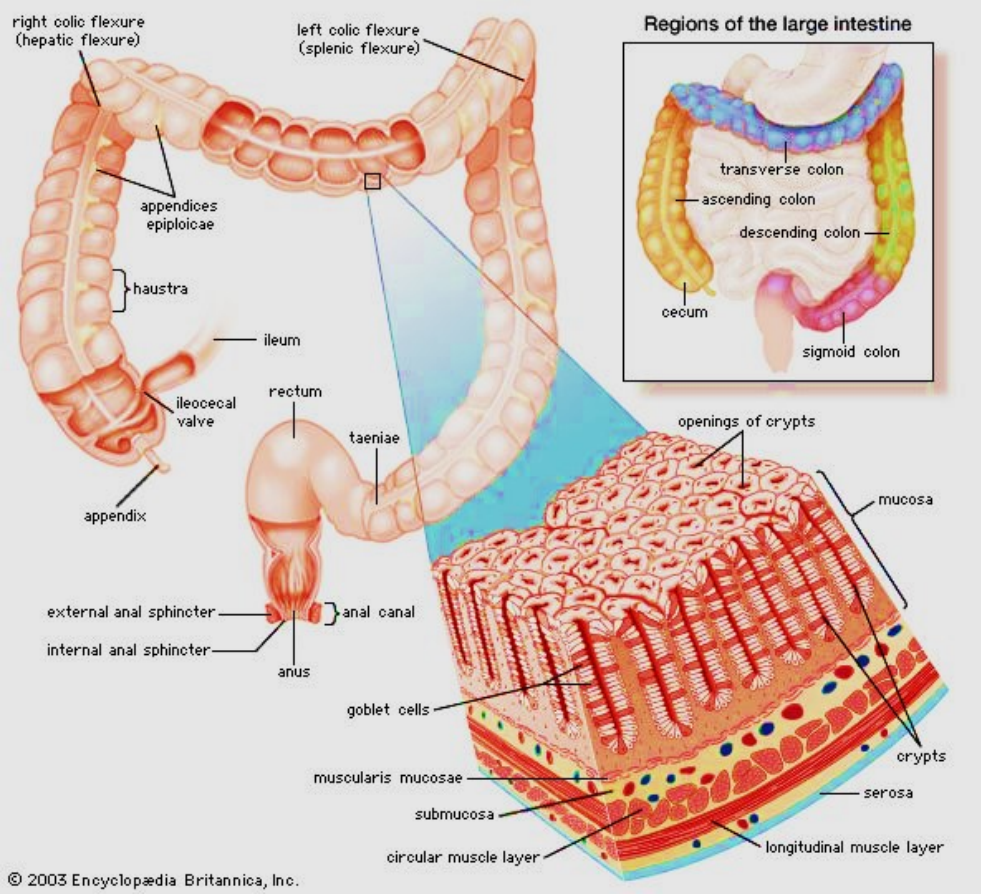

Figure 3: Histology of Colorectal. Reproduced from [47] with permission of publisher (wordpress).

Colorectal carcinomas can be subdivided into the following types: mucinous, signet ring cell, medullary, micropapillary, serrated, cribriform comedo-type, adenosquamous, carcinosarcoma, spindle cell and undifferentiated CRC [48].

1.2.2.1 *Mucinous Adenocarcinoma*

This carcinoma type, diagnosed in more than 50%, consists of an extracellular mucin. Mucinous adenocarcinoma shows glandular structures with pools of extracellular mucin that include malignant epithelium presenting as acinar structure. This tumor region also contains single tumor cells, such as signet ring cells. Low grade tumors very often show micro-satellite instability. By contrast, adenocarcinomas with stable microsatellites are more aggressive, and the tumors are in an advanced stage of the disease [48, 49].

1.2.2.2 Signet Ring Cell Carcinoma

Signet ring cell carcinoma is a very rare form, constituting only 1% of all colorectal carcinomas. In this carcinoma type, more than 50% of the tumor cells show distinguished intracytoplasmic mucin. The main feature is a prominent intracytoplasmic mucin vacuole that fills the cytoplasm and pushes the nucleus to the periphery. Signet ring cell carcinoma can arise in the extracellular mucin pool or shows infiltrative processes. Some signet ring cell carcinomas show micro-satellite instability, mainly in low grade tumors [50 - 52].

1.2.2.3 Medullary Carcinoma

This carcinoma type is very rare, affecting about 5 – 8 cases in 10,000 colorectal cancer patients [53]. Sheets of neoplastic cells with vesicular nuclei and abundant cytoplasm are typical of this type of carcinoma. Medullary carcinoma is associated with MSI-H and shows successful prognosis compared to other poorly differentiated and undifferentiated CRCs [54, 55].

1.2.2.4 Adenosquamous Carcinoma

Adenosquamous carcinoma, which displays characteristics of squamous carcinomas and adenocarcinomas, is represented either as mixed form or as separate part of the tumor. Primary adenosquamous carcinomas of the colon and rectum are extremely rare clinical entities. However, most of the data are obtained from case reports. The rarity of these tumors has made it a challenge to understand the biology of the disease. Also, the clinical pathological behavior and optimal management of these rare tumors are not defined yet [48].

1.2.2.5 Undifferentiated Carcinoma

This rare carcinoma type shows different histological characteristics. Undifferentiated carcinoma shows DNA replication errors (RERs) or DNA microsatellite instability [48]. Mutations of DNA mismatch repair genes produce destabilization of tracts of simple repetitive DNA in yeast and like this to sporadic colorectal cancer and hereditary non-polyposis colorectal cancer.

1.2.3 TNM Classification of Colorectal Cancer

Staging is described as the extent to which cancer has spread and is one of the decisive factors in the treatment of colorectal cancer.

The most commonly used staging system is the AJCC TNM system. This system is based on three key factors. Same as for liver cancer, the key factors determine the depth of tumor invasion (T), the extent of nodal metastasis (N) and the spreading of the cancer (M). T describes the extent to which the primary tumor has grown into the wall of the intestine. N characterizes proliferation to nearby lymph nodes, and M indicates if the cancer has spread to other organs [30]. Colorectal cancer can spread to all organs in the body, but the most common metastases of patients suffering from CRC are metastases to the liver and lung [54, 55].

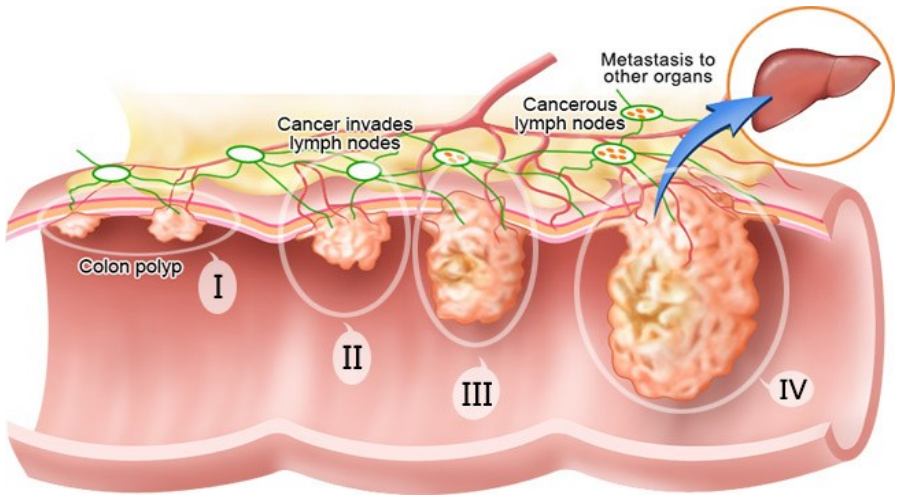

Figure 4: TNM classification of colorectal cancer stages. Reproduced from [58] with permission of publisher.

I. <u>Primary Tumor (T)</u>

TX	Primary tumor cannot be assessed
T0	No evidence of primary tumor
Tis	Carcinoma in situ: intraepithelial or invasion of lamina propria

T1 Tumor invades submucosa

T2 Tumor invades muscularis propria

T3 Tumor invades through muscularis propria into subserosa

T4 Tumor directly invades other tissues or organs

II. Regional Lymph Nodes (N)

NX Regional lymph nodes cannot be assessed

N0 No regional lymph node metastasis

N1 Metastasis in one to three regional lymph nodes

N2 Metastases in four or more regional lymph nodes

III. Distant Metastases (M)

MX Distant metastasis cannot be assessed

M0 No distant metastasis

M1 Distant metastasis [30]

1.2.4 Therapeutic Strategies

CRC can be treated in different ways, depending on the tumor. The standard treatment option for colon cancer (CC) stage 0-II is open resection of the primary tumor and nearby lymph nodes Stage III CC is presently treated with chemotherapy. For stage IV, the treatment strategies are surgery, chemotherapy and targeted therapy. About 20% of CRC patients have liver metastases at the time of diagnosis, and 60% of all patients develop liver metastases during the course of disease [42, 61, 62]. The standard treatment options for liver metastases are surgery, neoadjuvant and adjuvant chemotherapy, local ablation, and intra-arterial chemotherapy [63, 64].

For rectum cancer (RC), the treatments differ by reason of the local recurrence risk and poorer overall prognosis [65]. For stage I RC patients, the standard procedure is surgery with or without chemoradiation. However, for RC at stage II and III, surgery, pre- and postoperative chemoradiation therapy, and short-course preoperative radiation therapy are

the treatment options. For stage IV and recurrent RC, therapy includes surgery with or without chemotherapy or radiation therapy, first-line or second-line chemotherapy, targeted therapy, and palliative therapy.

Liver metastases treatment involves surgery, neoadjuvant or adjuvant chemotherapy, local ablation, and intra-arterial chemotherapy [66]. Different drugs have been reported to be effective against primary or metastatic CRC, but the effectiveness of current medications still needs to be improved. Despite their biologically similarity, CC and RC are treated differently with respect to surgery and radiotherapy [66].

1.2.5 Molecular Genetics of Colorectal Cancer and Relevance to Prognosis

CRC shows heterogeneous molecular profiles and displays distinguishable tumor phenotypes. Malignant transformations develop gradually and are mediated through activation of proto-oncogenes, as well as by inactivation of tumor suppressor genes and epigenetic mutations. Previous studies displayed the complexity of the genomic landscape of CRC [68].

1.2.5.1 Microsatellite Instability

Microsatellite instability (MSI), as part of CRC, has gradually gained interest. MSI stands for DNA segments with repeated sequences of nucleotides of set length [60]. Nucleotide insertion or deletions are summarized under the term MSI, which is a defect in DNA mismatch repair genes. MSI tumors are grouped into three categories: high (MSI-H), intermediate (MSI-L) and stable (MSS) tumors. MSI-H tumors indicate instability in 30% or more of the microsatellites, MSI-L tumors display instability in 10 – 30 %, and MSS tumors are instable in less than 10% [67 -71].

1.2.5.2 RAS-RAF-MEK-ERK-MAP Kinase Pathway Mutation

The RAS-RAF-MEK-ERK-MAP kinase pathway is involved in survival, cell-cycle arrest, cell proliferation and apoptosis [72, 73]. This pathway covers a major part in signal transduction, which is mediated through cellular response and growth signals. RAS is connected to the inner surface of the plasma membrane. RAF, MEK, and ERK are protein kinases of the cytosolic pathway and activate each other [74]. In CRC, KRAS or BRAF mutations, which arise in about 50% of the patients, are associated with poor prognosis. These mutations

mediate the activation of the MEK-ERK-MAP kinase pathway. The BRAF gene acts as downstream effector of KRAS signaling and is mediated by a protein kinase [75 – 78].

1.2.5.3 KRAS

The proto-oncogene KRAS converts guanosine triphosphate/ guanosine diphosphate and transmits thereby the signals of an activated cell surface receptor to the nucleus [69]. In metastatic CRC, EGFR-targeted monoclonal antibodies (cetuximab and panitumumab) significantly improve disease response, but only in tumors with wild type KRAS [79, 80]. In metastatic CRC, it is now state of the art to routinely test for the KRAS gene mutation. Patients with mutated KRAS status should not undergo EGFR therapy. Studies reported conformity between primary CRC and their respective lung and liver metastases. Another study displayed the connection between higher KRAS mutation and primary tumors with lung metastases [81]. Nevertheless, no predictive value has been reported for KRAS mutation and response to chemotherapy [82].

1.2.5.4 BRAF

BRAF mutation has been found to act as prognostic marker for decreased survival in CRC patients. Prognosis is poor especially in MSI-L and MSS tumors, and it is also resistant to EGFR monoclonal antibodies [83 – 85]. In multivariate studies, the mutation was connected to female patients with a high grade right side tumor and MSI-high tumors. Souglakos et al. reported that patients treated with cetuximab and affected by BRAF mutation displayed lower progression-free survival compared to wild type BRAF patients [85]. Treatment with irinotecan or oxaliplatin showed no effect in patients with KRAS/BRAF mutations [76, 86].

1.2.5.5 PI3K and PTEN

Deletion of PTEN and PI3KCA mutation indicates resistance to anti-EGFR therapy, such as cetuximab and panitumumab. In CRC, especially mutations in PIK3CA and loss of PTEN expression have been suggested as markers for anti-EGFR therapy resistance. The resistance to anti-EGFR therapy and the relation between the alterations in this pathway are unusual. However, this evidence suggests a predictive role of EGFR monoclonal antibody-based treatment therapy. The PIK3CA mutations and loss of PTEN are believed to be connected with KRAS and BRAF mutations. Up to 70% of patients with these mutations did not response to cetuximab or panitumumab [87, 88].

1.3 Eukaryotic Translation Initiation

Eukaryotic gene expression is mainly regulated at the transcriptional and translational levels.

To encode mRNA information for the translation into a protein, recruitment of the mRNA to the ribosome is necessary. The protein synthesis can be divided into four major steps: initiation, elongation, termination and ribosome recycling. Translation initiation is the most complex and rate-limiting step, and is highly regulated [89]. Initiation is most often incorporated in cancer development and progression. During initiation, the mRNA is recruited to the 40S ribosome at the AUG start codon and joined by the 60S ribosome to form the 80S ribosome. The 80S ribosome moves along the mRNA, translating each nucleotide in triplicates to an amino acid integrated into the growing polypeptide chain. In the step of translation termination, the newly formed protein is released [88, 89]. The last step in the translation initiation is ribosome recycling. The mRNA is released, the 80S ribosome is split into 40S and 60S subunits, and the translation loop can start once again. These protein factors, which are involved in the translation initiation, are called eukaryotic translation initiation factors (eIFs) [88, 89, 90].

During translation initiation, the mRNA recognizes the eIF4F cap-binding complex and binds to it. The eIF4F complex consists of eIF4E, eIF4A and eIF4G. The 40S ribosome recruits the mRNA with several factors, including eIF1, eIF1A, eIF2/met-$tRNA_i$, eIF3 and eIF5 to form the 43S preinitiation complex (PIC). The ribosome scans along the 5' UTR of the mRNA in the 5' to 3' direction until the initiation codon is recognized. eIF5B promotes the binding of the 60S and forms the 80S ribosome. The factors are released, and elongation can take place [90, 91]. Elongation is followed by termination and recycling [90 – 94].

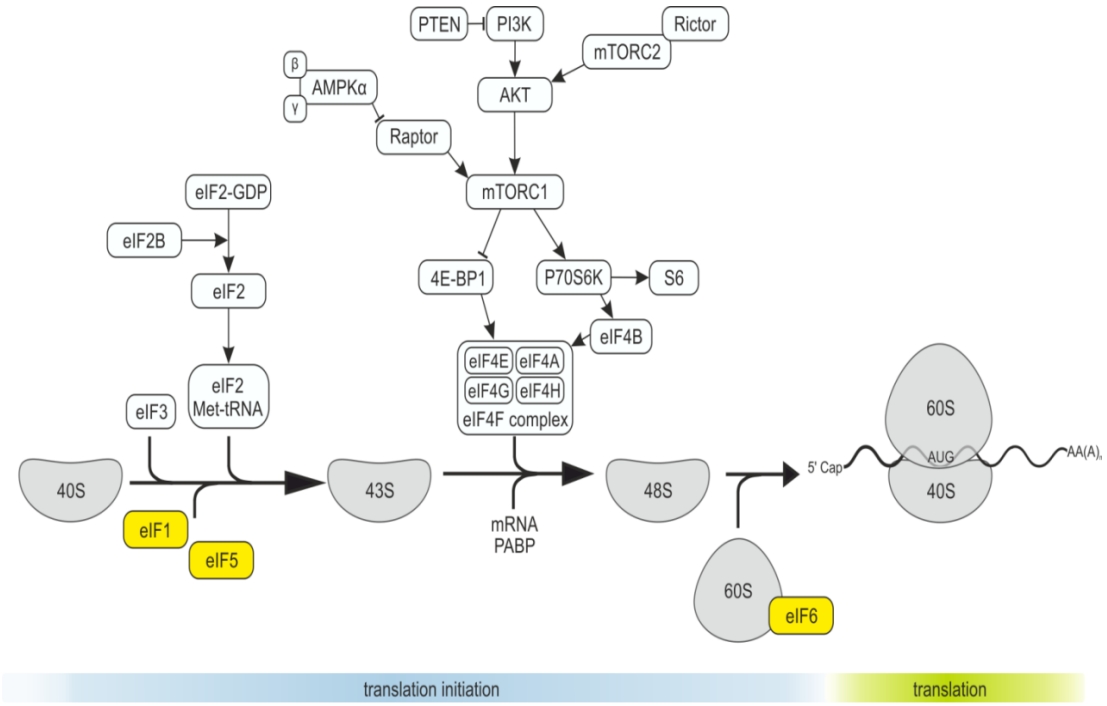

Figure 5: eIF1, eIF5 and eIF6 expression in CRC. Schematic model representing main molecular regulators of translation initiation. eIF1 acts as mediator of start codon recognition and is essential for the recruitment of the 40S ribosomal subunit by eIF3 during initiation of protein translation. eIF5 interacts with the 40S initiation complex to promote hydrolysis of bound GTP and joining of the 60S ribosomal subunit to the 80S ribosome. eIF6 has anti-association properties by blocking premature 60S joining to 40S.

1.3.1 Eukaryotic Translation Initiation Factors

The regulation of translation initiation is mostly controlled by 12 eukaryotic initiation factors (eIFs): eIF1, eIF1A, eIF2, eIF2B, eIF3, eIF4A, eIF4E, eIF4G, eIF4B, eIF4H, eIF5, eIF5B and eIF6, a non-core eIF [90].

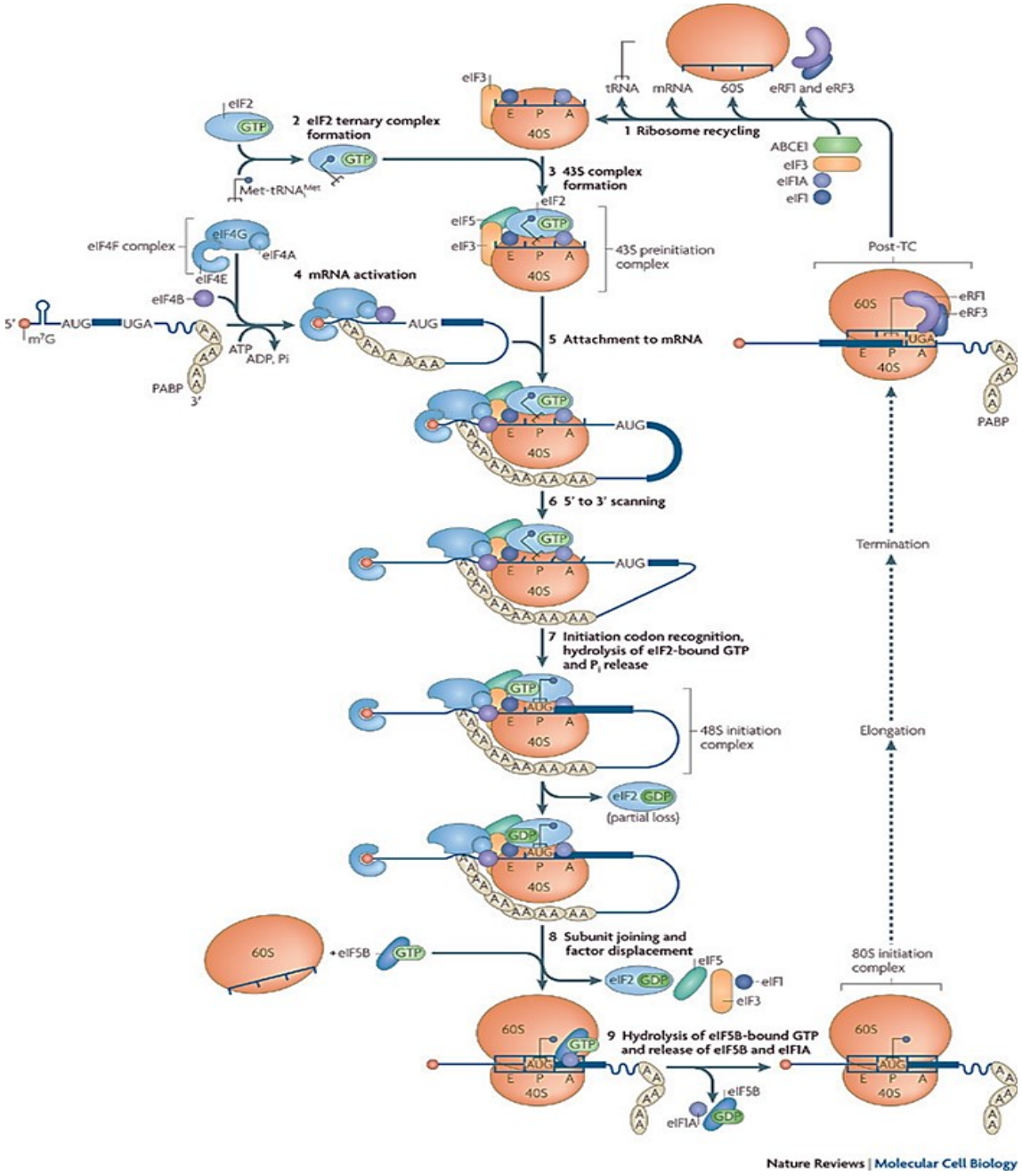

Figure 6: Graphic represent eukaryotic translation initiation and principles of its regulation; Reproduced from [95] with permission of publisher (*Nat. Rev. Cell Biol.*). (**1**) The eukaryotic translation initiation starts with the separation of 40S and 60S ribosomal subunits, and formation of an 80S ribosomal initiation complex. (**2**) Formation of a 43S preinitiation complex comprising a 40S subunit, eIF1, eIF1A, eIF3, eIF2–GTP–Met-tRNA$^{Met}_i$ and probably eIF5. (**3**) The next step is mRNA activation, (**4**) followed by attachment of the 43S complex to the activated mRNA region. (**5**) Scanning of the 5′ UTR by 43S complexes. (**6**) Recognition of the initiation codon and 48S initiation complex formation.

(**7**) The next step is joining of 60S subunits to 48S complexes and concomitant displacement of eIF2–GDP and other factors (eIF1, eIF3, eIF4B, eIF4F and eIF5). (**8**) GTP hydrolysis by eIF5B and release of eIF1A and GDP-bound eIF5B. (**9**) Termination follows elongation and leads to recycling [95].

1.3.1.1 Eukaryotic translation initiation factor 1 (eIF1) and 1A (eIF1A)

eIF1 is a highly conserved 113 amino acid long protein. eIF1A is a 144 amino acid long protein encoded on chromosome X [92]. These two proteins are essential for protein translation initiation and mRNA examination, where an initiation complex that binds the 5'-cap region is displaced to the first AUG initiation codon [93]. eIF1 is also fundamental to recognize the correct AUG region and binding. eIF1A initiates the formation of the pre-initiation complex with eIF2, eIF3, , eIF4B and eIF4F. Both factors have different functions, but eIF1 and eIF1A are required for 48S complex assembly and binding at the initiation codon. The eIF1 distribution is not uniform in human tissues, for example in brain, lung pancreas, liver, heart and skeletal muscle [92, 94].

CHO cells were processed, ranging from UV and UV simulation via ionization to heat shocks. In cells processed with UV and UV simulation, induction of eIF1 was monitored, leading to an UV effect that was simulated in different cancer cell lines. The interaction between eIF1 and eIF5 was first described in a yeast-two-hybrid system. eIF1 also binds to eIF3C. This step is important in the protein translation initiation for recruitment of the 40S ribosomal subunits through eIF3. Less information is available about eIF1 and eIF1A and translation initiation, but it seems that eIF1A plays a major role in the NF-ƙB signaling pathway [95, 96, 98, 99, 103].

1.3.1.2 Eukaryotic translation initiation factor 2 (eIF2)

eIF2 contains three subunits that generate the core of the eIF/GTP/Met-tRNA$_i$ ternary complex, which is a major part of the translation initiation. eIF2 arranges the active GTP-bound and the inactive GDP-bound form. This arrangement is regulated through the invertible phosphorylation of the α subunit via kinases that respond to different stress stimuli [97, 98]. The eIF2 complex, in particular eIF2α, seems to play an important role in cell proliferation, survival, malignant transformation, tumor progression, tumor initiation and the formation of metastases [92, 97, 104].

1.3.1.2.1 eIF2γ

The eIF2*γ* subunit is part of the eIF2 complex, and interacts with α and β subunits. It contains three domains, is characterized by a zinc-binding hinge, and is required for GTP binding. Biochemical and mutation analyses, as well as hybrid studies, revealed that eIF2*γ* binding to eIF2β subunit is necessary for GTP binding [99, 105, 106].

1.3.1.2.2 eIF2β

In *archaea* and eukaryotes, the C-terminal domain of eIF2β shows a C2-C2 zinc-binding motif [100]. The N-terminal part of eIF2β reveals a binding site for eIF2B that catalyzes GDP-GTP exchange on the eIF2-GDP binary complex and shows a binding site for the C-terminal domains of eIF5 that catalyzes GTP hydrolysis [101, 104, 107].

1.3.1.2.3 eIF2α

The structure of *eIF2*α displayed an N-terminal oligonucleotide/oligosaccharide binding part and a α-helix part [104, 106]. The major mechanism for the activity of eIF2 is regulated through Ser51 phosphorylation via eIF2α kinases. In eukaryotes, the translational control via phosphorylation of eIF*2*α is essential for an accurate process and modification of cellular stress during the life cycle.

Moreover, eIF*2*α displayed variable expression in different cancer types, including bronchioloaveolar carcinomas, as well as gastrointestinal and melanocytic neoplasms. eIF2 targeting seems to be a new approach in cancer therapy. The first publication of this kind dealt with Bortezomid for the treatment of multiple myeloma. Bortezomid activates ER stress and apoptosis. A decrease in eIF2α phosphorylation reduced the efficiency of the therapy. In this adjustment, eIF2α inhibited eIF2B activity and translation initiation [92, 108].

1.3.1.2.4 eIF2B

The eIF2B complex consists of five subunits from α to ε. The catalytic core of this complex is eIF2Bε. Its activity is significantly improved by binding to eIF2B*γ.*The eIF2Bε*γ* is the catalytic sub-complex, whose activity for GEF is similar to that of the full eIF2B complex. The regulatory sub-complex contains the subunits α, β and σ, and acts in high-affinity binding to phosphorylated eIF2α. The regulation of protein synthesis succumbs the high affinity by eIF2α phosphorylation [109].

1.3.1.3 Eukaryotic translation initiation factor 3 (eIF3)

The initiation factor 3 is the largest and most difficult complex with a size of 804 kDa. Thirteen subunits have been identified to build up the eIF3 complex, with a molecular weight ranging between 25 and 166 kDa, [92]. The eIF3 complex is highly conserved and is one part of the translation initiation, which are necessary for IRES-dependent translation initiation. The whole complex can be subdivided into three subclasses: eIF3a, b, l, g; eIF3f, h, m and eIF3K, l, e, d, c. The subunit eIF3J is not included in these three subclasses but interacts with eIF3B.

eIF3 is a key player in the steps of the initiation pathway, supporting Met-tRNAi and mRNA binding to the 40S ribosomal subunit. The exact effect for each eIF3 subunit in translation initiation remains to be refined [110, 111, 112].

1.3.1.3.1 eIF3A

eIF3A is the largest subunit and is increased in many cancer types, for example in cancer of the breast, cervix, esophagus, lung and stomach [113 - 115]. Studies have shown that a high level of eIF3 is often monitored at early stages of cancer progression in contrast to high grade malignancies. eIF3A exhibits RNA binding capacity and interacts with eIF4B and all eIF3 subunits. Mammalian eIF3A is a major target in cell cycle regulation. A study investigating HEK293 and NIH 3T3 cells described eIF3A as a negative controller of the ERK pathway.eIF3A seemed to be a major target in various signaling pathways and in carcinogenesis [92, 111].

1.3.1.3.2 eIF3B

eIF3B has a molecular weight of 116 kDa and is strongly expressed in the SW116 cell line and NIH 3T3 cell line. siRNA knockdown of eIF3B showed a reduction in proliferation and determined apoptosis. Human eIF3B binds at the C-terminus eIF3G and eIF3I and on the N-terminal to eIF3J [92].

1.3.1.3.3 eIF3C

The molecular weight of eIF3C is110 kDa, and the gene is located on chromosome 16 [92]. The N-terminal part binds to eIF1, which is rich in phosphorylation sites, implicating that those protein kinases regulate such interactions. eIF3C interacts with heat shock protein 90, as well as with the tumor suppressors schwannomin and merlin. Tumors with a high level of eIF3C indicate loss of schwannomin [116].

1.3.1.3.4 eIF3D

eIF3D is responsible for protein synthesis and is a marker for drug resistance in gastric cancer patients. eIF3D is over-expressed in these patients, possibly constituting a predictive marker in patients developing resistance against standard treatment, for example cisplatin and flurouracil [117]. In malignant mesothelioma, eIF3D was identified as a potential target after targeting 39 genes by siRNA [118].

1.3.1.3.5 eIF3E

eIF3E was first described as integration site of the mouse mammary tumor virus (MMTV), which shows homologues sites to herceptin 2 (Her-2) [119]. High levels of eIF3E are found in many human cancer types. Knockdown studies with eIF3E do not decrease protein synthesis, but they affect the translation of specific mRNAs. eIF3E is important for the interaction and recruitment of mRNA to the 40S PIC by binding of eIF4G and eIF3. eIF3E overexpression in NIH 3T3 cells led to a reduction in the binding of eIF3 and eIF4G, and to a repression of protein synthesis [120]. In full-length wild type (wt), eIF3E displayed no malignant transformation. Wt eIF3E expression was decreased in various human cancers, such as cancers of the colon, lung and breast. Wt eIF3e may act as a potential tumor suppressor [92].

1.3.1.3.6 eIF3F

eIF3F is down-regulated in human cancers, such as melanoma and pancreatic cancer. Knockdown experiments with siRNA stimulated protein synthesis and increased cell proliferation and apoptosis in pancreatic cancer and melanoma cell lines [121, 122]. eIF3F interacts with mTOR and its downstream target S6K1, key regulators of protein synthesis. eIF3F binds to a stress-stimulated protein (MSS4) and decreases translation, which may control its function. In contrast, muscle cells showed lower levels of eIF3Ff, leading to a reduced translation rate whereas high levels stimulated protein synthesis [92].

1.3.1.3.7 eIF3G

Only little is known about the role of 44 kDa protein in translation initiation and its potential involvement in carcinogenesis. eIF3G interacts directly with Pelota, which regulates cell proliferation and stem cell self-renewal [92].

1.3.1.3.8 eIF3H

The encoding gene of eIF3H is located on chromosome 8. In colorectal cancer, a splice variant of eIF3H was detected. These findings indicate that eIF3H has a role as a susceptibility gene for colorectal carcinoma [92].

1.3.1.3.9 eIF3I

eIF3I was overexpressed in various human cancer types and NIH 3T3 cells. Knockdown experiments in HeLa and PCI-1 cell lines displayed the opposite effect, namely a reduction in cell size and proliferation rates. Moreover, in these experiments, inhibition of mTOR diminished the transformation activity of eIF3I, suggesting a significant role of eIF3I phosphorylation [123, 124]. Regrettably, the specific role of eIF3I in protein synthesis has not been identified in these experiments.

1.3.1.3.10 eIF3J

This protein has a molecular weight of 35 kDa and binds to the 40S ribosome in the absence of mRNA. The eIF3 complex interacts with eIF3J, but this binding is poor and unstable. Only little is known about eIF3J and carcinogenesis [92].

1.3.1.3.11 eIF3K

This eIF, first described in 2003, was found to interact with the eIF3 subunits C, G and J. eIF3K cooperates with cyclin D3 and is involved in other processes linked to translation initiation. An important role of eIF3K in translation initiation has not been specified yet [92].

1.3.1.3.12 eIF3M

The eIF3M subunit has not yet been studied extensively, but a transformation in cell proliferation, cell cycle progression and cell death was observed after eIF3M knockdown in human colon cancer cell lines. It seems that eIF3M is oncogenic, but its mode of action remains unknown [92, 125].

1.3.1.4 Eukaryotic translation initiation factor 4 (eIF4)

The eIF4 complex plays a major part in translation initiation. The process of ribosomal recruitment to mRNA is rate-limiting and is mediated by the eIF4 protein complex. eIF4B contains parts rich in arginine, tyrosine, aspartic acid and glycine. These parts homodimerize or bind to eIF3A [126, 127]. eIF4B is involved in the creation auxiliary bridges between mRNA and the 40S ribosomal subunit. The eIF4B subunit is part of the mTOR pathway and activates S6K, which is responsible for the phosphorylation of eIF4B [128].

The eIF4F complex consists of three subunits: eIF4E, eIF4A and eIF4G. eIF4A, with a molecular mass of 50 kDa, is part of the DEAD-box family and is involved in different processes, such as pre-mRNA splicing and ribosome biogenesis [129]. It can react as RNA-dependent ATPase and bidirectional RNA helicase. eIF4B controls the helicase activation of eIF4A. The phosphoprotein eIF4E, with a molecular mass of 24 kDa, is involved in protein translation initiation via cap-binding activity. Phosphorylation of eIF4E led to increased translation and proliferation [129 - 131]. eIF4E is modulated through the 4E-binding protein 1 (4E-BP1), which is responsible for cellular stimulation by insulin and growth factors. If binding of 4E-BP1 to eIF4E decreases, eIF4E is released and can further interact in the eIF4F complex [92, 130]. eIF4E was overexpressed in breast, colon, ovarian, head and neck cancer [92]. The polypeptide eIF4G has a molecular mass of 220 kDa. eIF4G has three isoforms, both of which share 46% homology. eIF4G shows binding sites for various eIF subunits and Poly-A-binding protein (PABP) [132].

Targeting the eIF4 subunits is a major field in cancer therapy. One option is to target the eIF4F complex to split the cap-binding activity of eIF4E. In acute myeloid leukemia, inhibition of eIF4E cap interaction showed promising effects in clinical trials [129, 130]. Knockdown experiments also displayed a significant reduction in invasiveness and migration in breast cancer cells. In breast cancer cells and breast xenograft mice tumors, the translation initiation was reduced after treatment with the 4EGI-1 inhibitor [132].

1.3.1.5 Eukaryotic translation initiation factor 5 (eIF5)

eIF5 is a fundamental core protein of translation initiation. It acts on the N-terminal as a GTPase activator. eIF2 binds during translation initiation to GTP and hires the Met-tRNA to the 40S ribosomal subunit. The N-terminal function as a GTPase-activator protein (GAP) and is also connected to an independent GDP dissociation inhibitor (GDI) [133]. The C-terminal generates the ribosomal preinitiation complex. It also contains a couple of interaction sites for other components of the translation initiation, such as eIF1, eIF2, eIF3A and eIF4G. The C-

terminus has α-helices which can bind to eIF2 [134]. eIF5 is the only protein capable of undergoing hypusination. In mice experiments, this modification was thoroughly studied. It showed inflammation followed by dysfunction of islet β cells. In diabetic patients, inhibition of eIF5 hypusination led to promising effects and was also recommended for a combination therapy for treatment of leukemia [135, 136].

1.3.1.5.1 eIF5A

eIF5A is a major part of the elongation step in the protein synthesis of eukaryotes. It is important for cell growth and has been described in some human cancer types. eIF5 shows two isoforms (eIF5A-1 and eIF5A-2) participating in cellular regulation, differentiation, proliferation transformation, apoptosis and tumorigenesis. eIF5A-1 is expressed in all cells and tissues. In contrast, eIF5A-2 may be expressed in a tissue-dependent manner. eIF5A-2 has been recommended as a prognostic marker in human cancer types [92].

1.3.1.6 Eukaryotic translation initiation factor 6 (eIF6)

The eIF6 protein consists of 245 amino acids. Up to 70% are localized in the cytoplasm, and 30% are expressed in the nucleus. eIF6 has a double function. On the one hand, it is required for the maturation of the large 60S ribosomal subunit and ribosomal anti-association activity. Furthermore, it is also involved in translation initiation. After binding to 60S ribosomal subunit in the nucleus, eIF6 is phosphorylated via growth factors and is released into the cytoplasm. The interaction of 60S and 40S subunits is blocked, and therefore no translation is initiated [137, 138]. According to some studies, eIF6 restricts cell growth and transformation, and the regulation of translation is rate-limiting. eIF6 is also part of the RNA-induced silencing complex (RISC), suggesting a major role in the biogenesis of 60S ribosome [139, 140]. The role of eIF6 in cancer is still unclear, but overexpression was reported in various cancer types, such as head and neck cancer, also in lung metastasis and CRC, but the strongest expression was noted in metastatic diseases. eIF6 was shown to be a modulator of tumorigenesis and tumor growth [92].

1.3.2 mTOR Signaling Pathway

The mammalian target of rapamycin (mTOR) is a serine/threonine kinase, constituting a major component of the phosphoinositide 3-kinase (PI3K)/v-AKT murine thymoma viral oncogene homolog (AKT)/mTOR signaling pathway. This signaling pathway is involved in the

regulation of various cellular processes, including transcription and ribosome biogenesis, as well as in protein and lipid synthesis. Moreover, it influences cell proliferation, cell growth, apoptosis and autophagy. Most human cancers display a dysfunction in the mTOR pathway [141, 142]. mTOR exists in two multiprotein complexes: mTOR complex 1 (mTORC1) and mTOR complex 2 (mTORC2). Both share a catalytic mTOR subunit, and the mammalian lethal with sec-13 protein 8 (mLST8), the DEP domain-containing mTOR-interacting protein (DEPTOR) and TTI1/TEL2 complex. But regulatory-associated protein of mTOR (RAPTOR) and proline-rich AKT are specific for mTORC1. However, the rapamycin-insensitive attender of mTOR (RICTOR), target of rapamycin complex 2 subunit MAPKAP1 (mSIN1), and protein observed with RICTOR1 and 2 (PROTOR1/2) are part of mTORC2 [143]. It is also known that each complex regulates different biological processes. The activity of mTORC1 is regulated through five signals: growth factors, energy level, oxygen, stress and amino acids.

mTORC1 regulates diverse cellular processes through multiple downstream targets. Activated mTOR1 supports the translation initiation by phosphorylating the translation regulator eIF4E- binding protein (4E-BP) and the ribosomal protein S6 kinase (S6K). There are three 4E-BP variants: 4E-BP1, 4E-BP2 and 4E-BP3, with each form being encoded by a different gene. Mammalian cells have two RpS6 kinase proteins [144]. Ongoing activation of mTORC1 can block growth factor signaling via negative feedback loops which inhibit PI3K signaling.

On the other hand, only little is known about mTORC2. It is activated through growth factors, but this mechanism is not well understood. mTORC2 regulates metabolism, motility, cell survival and cytoskeletal organization by phosphorylating kinases, such as AKT and PKCα. mTORC2 has been reported to be resistant to rapamycin treatment [144 - 147].

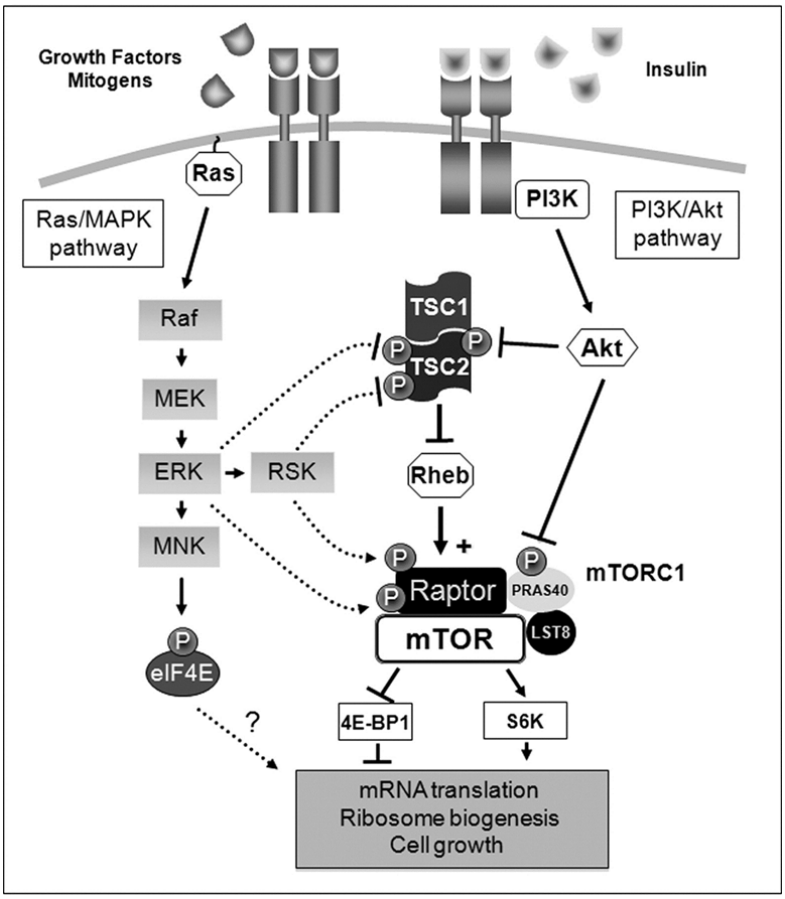

Figure 7: Graphic of the molecular mechanisms by the Ras/MAPK pathway to regulate mTORC1 signaling. Activation of the Ras/MAPK pathway stimulates mTORC1 activity through the coordinated action of the kinases ERK1/2 and RSK on the TSC protein complex upstream of mTORC1, and on Raptor, an important partner of mTOR within mTORC1. Reproduced from [145] with permission of publisher (J. Biol. Chem.).

2 Aim

Changes in translation initiation lead to degenerated gene expression and therefore to an increased risk of developing cancer. The translation initiation factors have been described to be overexpressed in different cancer entities, where they show an association with the progression of cancer. Therefore, the aim of this study was to characterize the expression of eIFs and important components of the mTOR pathway in chronic hepatitis B (HBV) and C (HCV), HBV- and HCV-associated HCC, non-virus related HCC, ASH and Morbus WilsonWilson´s disease.

In the first part, the PhD thesis focused on eIF5 to find out if it could serve as prognostic biomarkers in chronic hepatitis B and C, HBV- and HCV-associated HCC, non-virus related HCC, ASH and Morbus Wilson.

The literature classifies them as CRC, but it is recommended to subdivide these into two tumor entities: CC and RC. Therefore, the aim of this study was to characterize the expression of eIFs and important components of the mTOR pathway in CRC, to subdivide CRC into CC and RC, and to compare these findings with low and high grade tumors of CC and RC. For this purpose, we also included in this thesis the eIF expression in liver metastasis of primary CC and RC.

In the second part, the PhD thesis focused on eIF1, eIF5 and eIF6 to find out if these factors could serve as prognostic biomarkers in CRC.

The aim of the *in vitro* studies of this thesis was to establish a siRNA knockdown system in CRC cell lines to down-regulate the levels of eIF1, eIF5 and eIF6. Using two distinct cell lines, we analyzed the response to eIF1, eIF5 and eIF6 silencing, in the search for changed translation, proliferation and viability.

3 Material and Methods

3.1 Patient Samples

3.1.1 HCC Tissue

This retrospective study included 235 HCC patients operated at the Department of Surgery, Yonsei University College of Medicine, Seoul, Korea.

Clinical data were available from all patients. All tumor tissues and non-neoplastic liver tissues (NNLTs) were fixed in formalin and embedded in paraffin according to routine methods. The study was reviewed and approved by the institutional ethics committee of the Medical University of Graz in agreement to Austrian and European law (20-119 ex 08/09). Histological tumor type and grade were evaluated according to the cancer WHO classification and tumor stage according to UICC classification. The cohort included 196 (83.4%) male and 39 (16.6%) female patients. Age ranged between 30 and 81 years, with a median of 56 years. Disease etiology was as listed in Table 1: HBV in 194 patients (82.5 %), HCV in 12 patients (5.1 %), and alcoholic liver injury in 11 patients (4.7 %). Seventy-eight patients (40%) did not show cirrhosis, in comparison to 116 (60%) patients who did (Table 1). Fibrosis grade, Child-Pugh score and class were also analyzed. Child-Pugh score/class is an assessment tool for prognosis and liver function of cirrhotic patients. In our patient cohort, most patients revealed Child-Pugh class A with a score of 5, indicating favorable liver functional status. Ten patients revealed no fibrosis, eight of the cohort 1. A fibrosis grade of 2 was observed in 34 patients, whereas 49 patients displayed a grade of 3 and 124 patients showed a fibrosis grade of 4 [182].

Table 1: Summary of HCC patient data included in the HCC TMA [182].

Parameter	(%)
Sex	
Male	83.4
Female	16.6
Ethiology of liver disease	
HBV	82.5
HCV	5.1
ASH	4.7
Cirrhosis	60
No cirrosis	40
Survival	
Alive	87.3
Dead	12.7
Microvessel invasion	
No	48.2
Yes	51.8
Tumor number	
1	86.6
2	10.8
3	2.1
4	0.5
TNM	
1	44
2	53.6
3	2.4
Edmondson-Steiner grade	
1	8.3
2	74.4
3	17.3

3.1.2 CRC Tissue

Tumor material was obtained with informed consent from CRC patients at the Medical University of Graz and the St. John of God Hospital Graz under approval from the Ethics Committee of the Medical University of Graz, Austria, and the Ethics Committee of St. John of God Hospital, Graz (23-015 ex 10/11). FFPE (Formalin-fixed paraffin-embedded tissue) samples from primary CRC (31 patients), liver metastases from primary CRC (17 patients)

and non-neoplastic tissue from 48 patients were collected to generate two TMAs. All samples were recorded for statistical evaluation, considering tumor grade, stage, patient gender and patient age at the time of diagnosis. Specimens consisted of tumor resection material, fixed in formalin and treated according to routine pathological workup procedures, including diagnostic hematoxylin and eosin staining, upon which grading and staging were determined during routine diagnostics. Tumor type and grade were histologically diagnosed according to the current WHO classification. Tumor staging was based on UICC [181].

Table 2: Summary of liver metastases of primary CRC patient data, included in the liver metastasis TMA.

	n	%
Total	17	100
Male	14	82.4
Female	3	17.6
Colon	11	64.7
Rectum	6	35.3
Stage	IV	100

Table 3: Summary of CRC patient data included in the CRC TMA.

	n	%
Total	31	100
Male	18	58
Female	13	42
Colon	19	61.3
Rectum	12	38.7
Stage		
I	4	12.9
II	1	3.2
IIa	3	9.7
IIIB	7	22.6
IIIC	6	19.4
IV	5	16.1
IVa	4	12.9
IVb	1	3.2

3.1.3 Tissue Microarray CRC

The Tissue Microarray (TMA) technology is an important innovation in the field of pathology and is a unique opportunity to analyze specified regions of various tumors in a standardized way. Tumor staging was reviewed by an experienced, board-certified pathologist (J. H.) using hematoxylin- and eosin-stained sections. Relevant tumor areas were marked on the slide. TMAs are paraffin blocks generated by extracting cylindrical tissue cones from donor paraffin blocks and by embedding these into a single microarray block at defined array positions. The arrangement and the position of patient material in the grid have to be recorded adequately, in a way that guarantees a precise connection between samples and patient. Tissue sections were cut at 4 µm and mounted on adhesive-coated glass slides. A schematic diagram of how tissue microarrays are established is shown in Figure 7 [181, 182].

The liver metastases tissue microarray included liver metastases tissue from 11 colon and 6 rectum carcinoma patients with non-neoplastic liver tissue (Table 2). The colorectal carcinoma TMA was composed of 186 tissue spots, including carcinoma tissue and non-neoplastic colorectal tissue from 19 patients with colon carcinoma and 12 patients with rectum carcinoma (Table 3) [182].

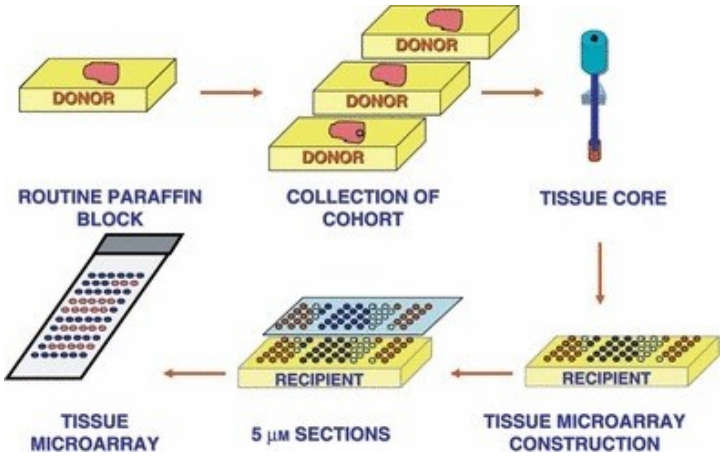

Figure 8: A schematic overview of the TMA generation procedure. Reproduced from [119] with permission of publisher (J. Virol.).

3.1.4 Tissue Microarray HCC

In this study, 12 different TMA blocks were analyzed in comparison to tissues of control patients.

3.2 Immunohistochemistry

For the immunohistochemical analysis of specific protein expression, slices (4 µm) were mounted on adhesive-coated glass slides and fixed at 65 °C for one hour. Antibodies used to determine the expression of various eIFs are given in Table 4. Staining was performed using a Ventana Immunostainer XT (Ventana Medical Systems, Tucson, USA) using an ultra-VIEW universal DAB Detection Kit (Ventana Medical Systems, Tucson, USA) and cell conditioning solution for 30 minutes using heat induced epitope retrieval (HIER). The primary antibodies were incubated for 30 minutes using different dilutions (Table 4). eIF expression was evaluated with respect to staining intensity (intensity score 0-3; 0 no staining, 1 weak, 2 moderate and 3 strong) and the percentage of positive cells (proportion score; 0-100%) [181, 182].

Table 4: Antibodies for immunohistochemistry used in this study [181].

Primary Antibody	Company	Dilution	Secondary Antibody
eIF1	Sigma Aldrich (HPA043003)	1:30	Rabbit
eIF2α (D7D3) XP	Cell Signaling (#5324)	1:100	Rabbit
eIF3A	Cell Signaling (#2538)	1:50	Rabbit
eIF3B (eIF3η D-9)	Santa Cruz (sc-137215)	1:100	Mouse
eIF3P110 (B-6)	Santa Cruz (sc-74507)	1:2000	Mouse
eIF3H (D9C1) XP	Cell Signaling (#3413)	1:750	Rabbit
eIF3M (V-21)	Santa Cruz (sc133541)	1:75	Rabbit
eIF4E	Cell Signaling (#9742)	1:100	Rabbit

eIF4G	Cell Signaling (#2498)	1:25	Rabbit
eIF5	Gene Tex	1:100	Rabbit
eIF6	Gene Tex (GTX63642)	1:250	Rabbit

3.3 *In situ* Detection Using Padlock Probes

Tissues were deparaffinized, permeabilized with pepsin, and subjected to in situ reactions. eIF1, eIF5 and eIF6 were detected *in situ* using a multiplexed reaction.

All oligonucleotides were designed using CLC Main Workbench software (CLC Bio Workbench Version 7.6, Qiagen; Venlo, Netherlands). mRNA sequences were retrieved from the National Center for Biotechnology Information (NCBI) with the GenBank accession numbers NM_005801(eIF1), NM_001969 (eIF5) and NM_002212 (eIF6). The padlock probes were designed and ordered 5´ phosphorylated (Integrated DNA Technologies; Coralville, IA, USA). The primers were purchased from IDT DNA detection oligos (Biomers; Ulm, Germany). Imaging was performed using a Zeiss Observer.Z1 inverted microscope (Carl Zeiss; Oberkochen, Germany) with a 20x objective and ZEN 2.3 software (Carl Zeiss, blue edition, Version 2.3.64.0). Z-Stacks were projected into one layer by a maximum intensity projection with ZEN 2012 black software (Carl Zeiss, Version 8.1). For a better visualization, the brightness and contrast of images were adjusted with ZEN 2012 black software (Carl Zeiss). CellProfiler software (Version 2.1.1) was used for the quantification of signals. The modification includes a background correction, removing fluorescent signals detectable in at least two fluorescent channels simultaneously as this indicates unspecificity. Statistical analyses were performed using the GraphPad Prism software, version 6.01 (GraphPad Prism, Inc., La Jolla, USA). An unpaired t-test was applied to compare cancer vs. non-neoplastic tissue in every group (colon and rectum). Results were considered statistically significant when $p < 0.05$ [181].

3.4 Biochemical Analyses

5.4.1 CRC Patient Samples

Table 5: Clinical and pathological characteristics of 40 patients with colorectal carcinoma [181].

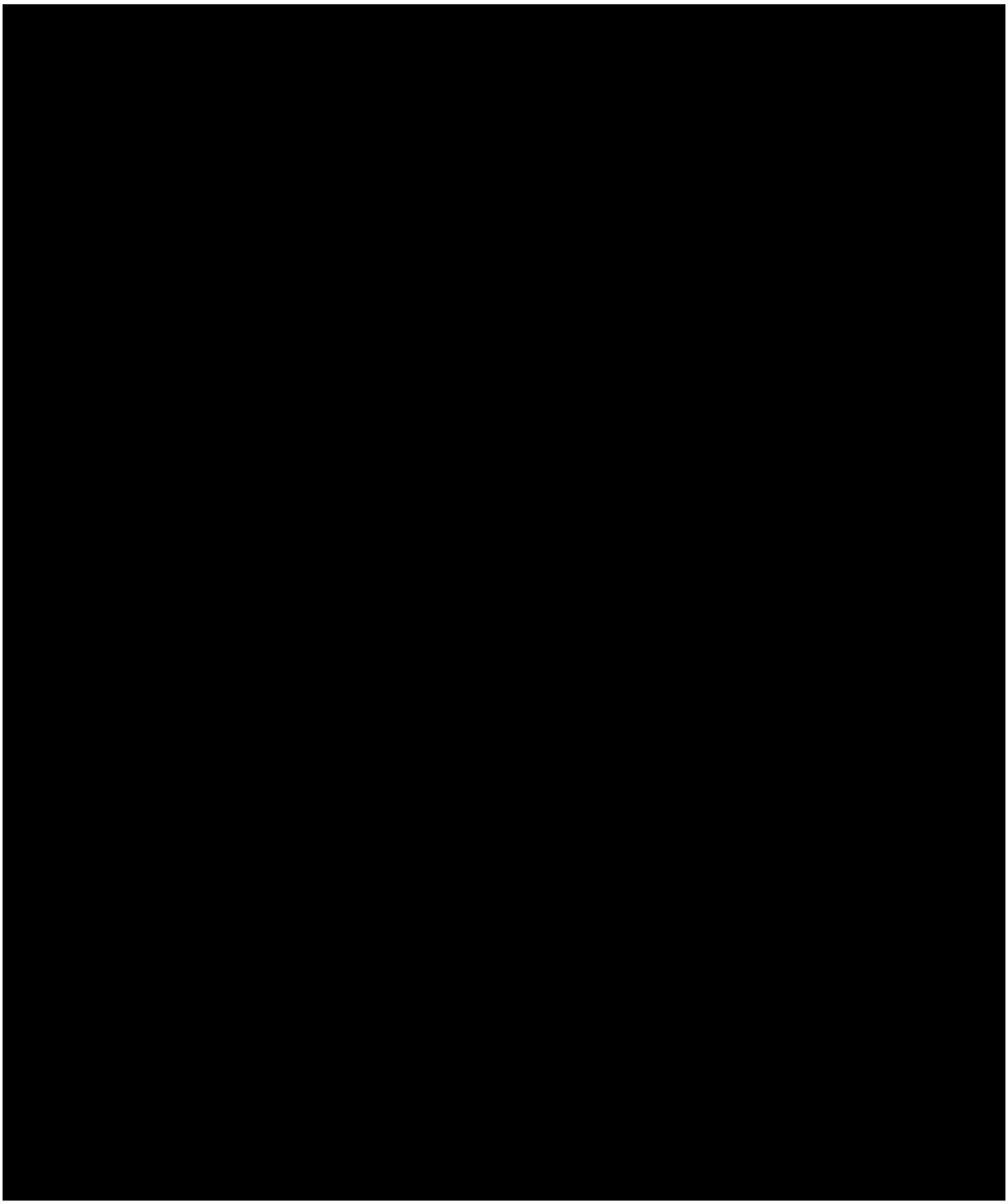

Tumor material was obtained with informed consent from 40 CRC patients for whom clinical and pathological data (Table 5) were available at the Medical University of Graz and the St. John of God Hospital Graz, under approval from the Ethics Committee of the Medical University of Graz and the Ethics Committee of St. John of God Hospital, Graz (23-015 ex 10/11) [181].

3.4.2 Liver Patient Samples

All tumor tissue samples were acquired during surgery, immediately frozen in liquid nitrogen and stored at -80°C. The study was reviewed and approved by the institutional ethics committee of the Medical University of Graz in agreement to Austrian and European law (20-119 ex 08/09).

Six patient-derived tumors from non-virus related HCC, eight patient-derived tumors from HCV-associated HCC, two patient-derived tumors from HCV, two patient-derived tumors from HBV-associated HCC, four patient-derived tumors from HBV, two patient-derived tumors from ASH and two Morbus Wilson patients were used for immunoblot analyses [182].

3.4.3 Kaplan-Meier Survival Curves for CRC

Kaplan-Meier curves were generated using the survival R package. The log rank test was applied to test for an association of survival with gene expression. A p-value <0.05 was considered statistically significant. To identify the association between gene expressions, stratified by median, and survival, we analyzed the TCGA public dataset, including 201 and 70 subjects suffering from colon adenocarcinoma and rectal carcinoma [181].

3.4.4 Kaplan-Meier Survival Curves for HCC

Kaplan-Meier curves were generated using the survival and survminer R package. The log rank test was applied to test for association of survival and gene expression. A p value <0.05 was considered statistically significant. To identify the association between gene expressions, stratified by median, and survival, the TCGA public dataset including 76 subjects with a low gene expression and 75 subjects with a high gene expression, respectively, was analyzed [182].

3.4.5 Immunoblot Analysis

All tumor tissue samples were acquired during surgery, immediately frozen in liquid nitrogen and stored at -80°C. For the isolation of protein from frozen tissue, samples were homogenized with a MagNA Lyser homogenizer (Roche Diagnostics, Risch-Rotkreuz, Switzerland) and lysed in NP-40 Lysis buffer (0.05 M Tris-HCl, 5 mM NaCl, 0.5% NP-40, 0.1 mM Pefabloc, 1 mM DTT, complete Mini, PhosSTOP). The lysate was transferred into a new tube and centrifuged at 10 000 rpm for 10 minutes at 4°C. The protein concentration was determined using Bradford protein assay (Biorad Protein Assay Dye Reagent, 500-0006; BioRad Laboratories GmbH, Munich, Germany) according to the manufacturer´s instructions. The sample concentration was determined by comparing samples with a BSA standard curve composed of the following concentrations: 0.5, 1, 2, 4, 6, 8, 10 µg/µl. Sample concentration was adapted to 3 µg/µl with SDS Sample Buffer. The samples were stored at -80°C until further usage. The protein samples were separated according to their molecular mass through SDS-PAGE and transferred onto a membrane for immunodetection. Depending on the molecular mass of the proteins of interest, 8% (4.6 ml ddH_2O; 2.5 ml 1.5 M Tris pH 8.8; 2.7 ml Acrylamide; 100 µl 10% SDS; 100 µl APS; 6 µl TEMED) or 12.5% (3.28 ml ddH_2O; 2.5 ml 1.5 M Tris pH 8.8; 4.06 ml Acrylamide; 100 µl 10% SDS; 100 µl APS; 7.5 µl TEMED) of polyacrylamide gels were casted using the four gel caster S235 (Hoefer Inc, Holliston, USA). Stacking gel composition was similar to all casted gels (3.1 ml ddH_2O; 1.25 ml 1.5 M Tris pH 6.8; 0.5 ml Acrylamide; 50 µl 10% SDS; 25 µl APS; 7.5 µl TEMED). The samples were prepared with SDS Sample Buffer (Bio-Rad) as mentioned above and heated for 5 minutes at 95°C. A total amount of 30 µg protein was loaded onto the gel. As molecular weight marker, the Novex Pre-Stained Protein Standard (Life Technologies, Carlsbad, USA) was used. Electrophoresis was performed for about 1.5 h at 120 V with the SE 250 Mini-Vertical Electrophoresis Chamber (Hoefer Inc) using a 1x SDS Running Buffer (25 mM Tris HCl (pH 8.4), 19.2 mM Glycine and 0.1% SDS in ddH_2O). After electrophoresis, the gel was blotted and immobilized onto a PVDF membrane (Immobilin-P transfer membrane, Merck Millipore, Darmstadt, Germany) using a Semi-Dry Blotting Unit (JH Bioinnovations, Bangalore, India) at 160 mA for 1.5 h. Prior to the electrotransfer, the membrane was activated by rinsing it for 20 seconds with Methanol, 2 minutes with ddH_2O and 5 minutes with Towbin Transfer Buffer (25 mM Tris, 190 mM Glycine, 20% Methanol in ddH_2O). The transfer was checked by Ponceau Red staining (Ponceau S solution, Sigma-Aldrich). For the immunodetection, the membrane was blocked in 5% non-fat dried milk powder (AppliedChemistry, Land) in TBS-Tween (0.1%) for 1 h to prevent non specific background binding of primary and secondary antibody to the

membrane. All primary antibodies were diluted in 5% bovine serum albumin (BSA) solution depending on the recommended concentration of the company. After three washing steps with 0.1% TBS- Tween for 5 minutes, the HRP (Horse radish peroxidase) - linked secondary antibody was diluted in 5% non-fat dried milk powder and incubated with the membrane for 1 hour at room temperature. Protein detection was done using the HRP compatible ECL Select Western Blot Detection Kit (GE Healthcare, Land), followed by exposure to the Image Quant LAS 500 (GE Healthcare). The camera of the Image Quant LAS 500 detected chemiluminescence emanating from the membrane and transformed it into a digital image. Exposure time depended on the intensity of the chemiluminescence signal [181, 182].

The signal was normalized using an anti-β-actin antibody (mAb dilution 1:2000, Sigma-Aldrich, Missouri, USA). A summary of all primary antibodies is given in Table 12 [181, 182].

Table 6: NP40 Lysis buffer.

Reagent	Final concentration
Tris HCl (pH 7.5)	50 mM
NaCl	150 mM
NP-40	1%

Table 7: Stacking gel.

Reagent	Volume
ddH_2O	3.1 ml
Tris 1.5 M pH 6.8	1.25 ml
Acrylamide	0.5 ml
10% SDS	50 µl
APS (Ammonium Persulfate)	25 µl
TEMED	7.5 µl

Table 8: Separation gel.

Reagent	8%	12.5%
ddH_2O	4.6 ml	3.3 ml
Tris 1.5 M pH 8.8	2.5 ml	2.5 ml
Acrylamide	2.7 ml	4.0 ml
10% SDS	100 µl	100 µl
APS	100 µl	100 µl
TEMED	6.0 µl	7.5 µl

Table 9: SDS Running buffer (10x).

Reagent	Final Concentration
TrisHCl (pH 8.4)	250 mM
Glycine	192 mM
SDS	1%

Table 10: Towbin Transfer buffer (1x).

Reagent	Final Concentration
Tris	25 mM
Glycine	190 mM
Methanol	20%

Table 11: TBS buffer (10x). Add 0.1% Tween-20 to 1x TBS buffer.

Reagent	Final Concentration
Tris	0.2 M
NaCl	1.4 M
adjust to pH 7.6 with HCl	

Table 12: Primary antibodies used for immunoblot analyses in this study [181, 182].

Primary Antibody	Company	Dilution	Secondary Antibody
Phospho-mTOR	Cell Signaling (#5536)	1:1000	Rabbit
mTOR	Cell Signaling (#2983)	1:1000	Rabbit
Phospho-PTEN	Cell Signaling (#9551)	1:1000	Rabbit
PTEN	Cell Signaling (#9559)	1:1000	Rabbit
Phospho-P70S6K	Cell Signaling (#9204)	1:1000	Rabbit
P70S6K	Cell Signaling (#9202)	1:1000	Rabbit
Phospho Akt	Cell Signaling (#4058)	1:1000	Rabbit
Akt	Cell Signaling (#9272)	1:1000	Rabbit
GAPDH	Cell Signaling (#2118)	1:3000	Rabbit
Phospho 4E-BP1	Cell Signaling (#9456)	1:1000	Rabbit
4E-BP1	Cell Signaling (#9452)	1:1000	Rabbit
Anti-Actin	Sigma (A2103)	1:1000	Rabbit
eIF1	Sigma (HPA043003)	1:500	Rabbit
Phospho-eIF2α	Cell Signaling (#3398)	1:1000	Rabid
eIF2α (D7D3) XP	Cell Signaling (#5324)	1:1000	Rabbit
eIF3A	Cell Signaling (#2538)	1:1000	Rabbit
eIF3β (A-8) = eIF3I	Santa Cruz (sc-374155)	1:1000	Mouse
eIF3C	Cell Signaling (#2068)	1:1000	Rabbit
eIF3H (D9C1) XP	Cell Signaling (#3413)	1:1000	Rabbit
eIF3J	Cell Signaling (#3261)	1:1000	Rabbit
eIF3K (2313C2a)	Santa Cruz (sc-81262)	1:1000	Mouse
eIF3M (V-21)	Santa Cruz (sc-133541)	1:500	Rabbit
eIF3B	Santa Cruz (sc-137215)	1:1000	Mouse
eIF3P110 (B-6)	Santa Cruz (sc-74507)	1:500	Mouse

eIF3θ (H-300)	Santa Cruz (sc-30149)	1:1000	Rabbit
eIF3D	Santa Cruz (sc-28856)	1:1000	Rabbit
Phospho eIF4b	Cell Signaling (#5399)	1.1000	Rabbit
eIF4B	Cell Signaling (#3592)	1.1000	Rabbit
eIF4E	Cell Signaling (#9742)	1:1000	Rabbit
eIF4G	Cell Signaling (#2498)	1:1000	Rabbit
eIF5	GeneTex (GTX114923)	1:500	Rabbit
eIF6	Gene Tex (GTX63642)	1:1000	Rabbit

3.4.6 Quantification of Immunoblots

Imaging of the blots was performed using the ECL Select Western Blot Detection Reagents (GE Healthcare). ImageJ (National Institute of Health) was used to compare the density of each band on the Immunoblot membrane. The aim of the analysis was to compare the density of samples on multiple membranes and to show differences between treatments in the experiments. Therefore, the non-neoplastic tissue was always used as standard sample, and GAPDH and β-actin were applied as internal loading controls.

$$\textbf{Relative density}_{\textbf{sample HKG}} = {\text{AUC}_{\text{sample HKG}}}\Big/{\text{AUC}_{\text{Control HKG}}}$$

$$\textbf{Relative density}_{\textbf{sample POI}} = {\text{AUC}_{\text{sample POI}}}\Big/{\text{AUC}_{\text{Control POI}}}$$

$$\textbf{Adjusted density}_{\textbf{sample POI}} = {\text{Relative density}_{\text{sample POI}}}\Big/{\text{Relative density}_{\text{sample HKG}}}$$

Figure 9: Relative quantification of immunoblot analysis. "Area under the Curve" is defined as AUC, "Protein of Interest" as POI.

Statistical analyses were performed using the GraphPad Prism software, version 6.01 (GraphPad Prism, Inc., La Jolla, USA).

3.4.7 RNA Isolation

Total RNA was isolated from fresh-frozen tissue of CRC, non-neoplastic tissue (NNT) and untreated/treated xenograft samples using a Trizol based protocol. 50-120 mg of tissue was homogenized with MagNA Lyser Green Beads (Roche) by addition of 1 ml Trizol reagent (Life Technologies) for 30 sec at 6500 rpm with the MagNA Lyser (Roche). The lysate was incubated for 10 minutes at room temperature. 200 µl of chloroform was added to the vial, incubated for 3 minutes at room temperature and centrifuged for 15 minutes at 10 000 rpm and 4°C. The upper RNA-containing phase was transferred into a fresh tube, mixed with 500 µl isopropanol and centrifuged for 20 minutes at 10 000 rpm and 4°C. After discarding the supernatant, the pellet was washed twice, with 1 ml of 80% ethanol and dried for 5 minutes at 37°C. Depending on the size of the pellet, it was dissolved in 100 – 200 µl RNase free water. After a 10-minute incubation step at 58°C, the RNA samples were stored at -80°C until further usage [181].

3.4.8 Reverse Transcription

RNA was reverse transcribed with the High-Capacity cDNA Reverse Transcription Kit (Applied Biosystems), essentially as described by the manufacturer. Briefly, 20 µg of RNA were added to 10 µl of 2x RT master mix ending up in a final volume of 20 µl, and PCR was performed using the PCR GeneAmp 9700 Thermocycler (Applied Biosystems). The PCR program was performed for 10 minutes at 25° C, followed by 37° C for 120 minutes, and the reaction was stopped at 85° C for 5 minutes (Table 7). cDNAs were either directly diluted 1:10 and added to PCR reactions or stored at -20° C for later usage [181].

Table 13: PCR program used for the reverse transcription.

	Temperature °C]	Time]min]
Step 1	25	10
Step 2	37	120
Step 3	85	5
Step 4	4	∞

Table 14: Components of the 2x Reverse Transcriptase Master Mix used for cDNA synthesis.

2x Reverse Transcriptase Master Mix	
Component	**Volume [µl]**
10x RT Buffer	2.0
25x dNTP Mix (100 mM)	0.8
10x RT Random Primers	2.0
MultiScribe™ Reverse Transcriptase	1.0
RNase Inhibitor	1.0
Nuclease-free H2O	3.2
Total Volume per Reaction	**10.0**

3.4.9 Quantitative Real-Time PCR

Quantitative Real-Time PCR (qRT-PCR) was performed using the Power SYBR Green PCR Master Mix Kit (Applied Biosystems). Oligonucleotides (Table 16) were self-designed with Primer-Blast and synthesized by Eurofins MWG operon (Germany). Efficiencies of all self-designed primers were calculated with known cDNA concentrations. The qRT-PCR was performed using the 7900HT Fast Real-Time PCR System (Applied Biosystems). The programs were set according to the manuals. mRNA expression data were analyzed by relative quantification using the $2^{\Delta\Delta CT}$ (cycle threshold) method and normalized to GAPDH and β-actin as internal housekeeping genes (HKG). The HKG is used to normalize possible variations during treatment, sample preparation, RNA isolation, reverse transcription and PCR set-up. The Ct-value of each carcinoma sample, which indicates the cycle number at which a fluorescence signal crosses the threshold, was compared with the Ct-value of the healthy control sample. Vertical scatter plots were created using GraphPad Prism (Version 6.01), showing the results of the fold change ratio and the mean [181].

Table 15: SYBR Green I Master Mix used for qRT-PCR.

Master Mix	
Component	**Volume [µl]**
Power SYBR Green PCR Master Mix (2x)	15
Forward Primer [10 pm]	1
Reverse Primer [10 pm]	1
Nuclease-free H2O	8
Total Volume per Reaction	**25**

Table 16: Oligonucleotides used for qRT-PCR in this study [181].

Gene	Primer	Sequence (5'-3')	Length	Tm [°C]
mTOR	Fwd	ATGCTTGGAACCGGACCTG	19	60
	Rev	TCTTGACTCATCTCTCGGAGTT	22	58
PTEN	Fwd	TGGATTCGACTTAGACTTGACCT	23	58
	Rev	GGTGGGTTATGGTCTTCAAAAGG	23	59
eIF2α	Fwd	TGGTGAATGTCAGATCCATTGC	22	60
	Rev	TAGAACGGATACGCCTTCTGG	21	61
eIF3A	Fwd	GCCGGAAAATGCCCTCAAAC	20	62
	Rev	TGGTTCGTGTATCTTTTGCCAT	22	60
eIF3B	Fwd	GGACCCGACCGACTTGAGA	19	63
	Rev	TTGACCCGGAATGTGTGCTG	20	63
eIF3J	Fwd	GTCAAGGATAACTGGGATGACG	22	60

	Rev	CGAGGTCTGACTCTTCCTGTAA	22	61
eIF4B	Fwd	CCTCCCAGTCCACTCGAGCTG	21	65
	Rev	GCTTGGGTGTCTCTCCCGAGG	21	65
eIF4G1	Fwd	CCCGAAAAGAACCACGCAAG	20	62
	Rev	TTCCCCTCGATCCTTATCAGC	21	61
eIF5	Fwd	AGCGTGTCAGACCAGTTCTAT	21	61
	Rev	CTGTCTTGATTCCATTGCCTTTG	23	60
eIF6	Fwd	CCGCGTGCGGAGCTTGTAT	19	61
	Rev	CGCCCTCGAACACACTGTAGAAGT	24	64
eIF4E	Fwd	GACCTGACCTCCCGCGGACAA	21	65
	Rev	TGCCCATCTGTTCTGTAGGGGATG	24	64
eIF3M	Fwd	TCAGAAGAGAACTCGGAAGGTG	22	60
	Rev	ACCACACTGTTCATCACACTTT	22	57
eIF3H	Fwd	TCGGGAGATTCAGCCGTGA	19	59
	Rev	CTCCGCATCATTTCCATCTGATA	23	59
eIF3C	Fwd	TTTGGGCCTCGTGCTTCGTGG	21	64
	Rev	TCGCTCAGCAAACAATGGCTGTTTG	24	63
eIF1	Fwd	GAAACGGCAGGAAGACCCTTA	21	60
	Rev	CGGATGCTCAATTACAGTACCAT	23	59

3.5 In vitro Experiments

3.5.1 Colorectal Cancer Cell Line (HCT116)

The HCT116 cell line was obtained from the American Type Culture Collection (ATCC). Cells were cultured at 37°C, 5% CO_2 and 95% humidity in McCoy 5A medium (Lonza, Belgium) containing 10% fetal bovine serum, 1% penicillin/ streptomycin (all Lonza).

3.5.2 Colorectal Cancer Cell Line (HT29)

The HT29 cell line was obtained from the American Type Culture Collection (ATCC). Cells were cultured at 37°C, 5% CO_2 and 95% humidity in DMEM medium (Lonza) containing 10% fetal bovine serum, 1% penicillin/ streptomycin and 1% MEM non-essential amino acids (all Lonza).

3.5.3 siRNA Transfection of Cell Lines

We targeted the gene of interest by using small interfering RNAs (siRNAs) from QIAGEN (Hilden, Germany). For each gene of interest, two target sequences were used. For eIF1; 5´-GACCAGACATATCCTAGCTAA-3´and 5´-AAGCAATACCGTCATGTTTCA-3, for eIF5; 5´-AGGCGCTTAATCGGCCTCCAA-3´ and 5´-CAGCCAGAAGTGCAACATGTA-3´; for eIF6; 5´-CTGCTTTGCCAAGCTCACCAA-3´and 5´-CTGGTGCATCCCAAGACTTCA-3´.

Transfection experiments were performed using Metafectene^{R}si^{+} transfection reagent (Biontex, Germany) according to the manufacturer´s instructions. For the transfection, 1x SI buffer, Metafectene SI+ and 20nM of each siRNA were mixed into a drop. After an incubation of 15 minutes at room temperature, 500 µl cells (80 000 cells/well) were seeded onto a 24-well plate. Cells with transfection mix were cultured at 37°C in a humidified atmosphere of 5% CO_2.

Cells were harvested at 24 hours, 48 hours and 72 hours on ice with the cell scraper using pre-chilled PBS, immediately centrifuged (150xg, 10 minutes, 4°C). The supernatant was removed, and the pellets were snap frozen in liquid nitrogen. The cell pellets were stored at -80°C until further usage [181].

3.5.4 Immunoblot Analyses of Cell Lysates

siRNA transfected cells were scraped off into ice cold phosphate buffered saline (PBS) and lysed. The protein concentration was determined using Bradford protein assay (Biorad Protein Assay Dye Reagent, 500-0006; BioRad Laboratories GmbH, Munich, Germany). Equal amounts of 30 µg protein were loaded onto SDS-PAGE gels (30% Acrylamid/Bisacrylamid solution; ROTH, Karlsruhe, Germany), subjected to electrophoresis in Mini-vertical electrophoresis units (Hoefer Inc, Richmond, USA) and blotted onto PVDF membranes (Immobilin-P Transfer Membrane; Millipore, Massachusetts, USA) using a Semi Dry Blotting Unit (SCIE-PLAS; Cambridge, England). The membranes were blocked in TBS-Tween (TBST) with 5% non-fat dried milk (AppliChem; Darmstadt, Germany) for 1h at room temperature. The primary antibodies (Table 12) were diluted in TBST, 5% BSA and applied overnight at 4°C. The membranes were washed with TBST, followed by incubation with a horseradish peroxidase-conjugated secondary antibody (anti-mouse 1:3000 and anti-rabbit 1:5000; GE Healthcare Life Sciences, Buckinghamshire, England). Proteins were visualized using a chemiluminescence ECL kit (GE Healthcare Life Sciences), followed by exposure on the Image Quant LAS 500 (GE Healthcare, Little Chalfont, UK). The signal was normalized using anti-β-actin antibody (mAb dilution 1:2000, Sigma-Aldrich, Missouri, USA) [181, 182].

3.5.5 qRT-PCT of Cell Lysates

siRNA transfected cells were washed three times with ice cold PBS, scraped off into ice cold PBS and lysed with Trizol Reagent. qRT-PCR was performed using the High-Capacity cDNA Reverse Transcription Kit (Applied Biosystems, FosterCity, USA) according to the manufacturer´s instructions and the GeneAmp 9700 Thermocycler (Applied Biosystems; Foster City, USA). Primers and dilutions used to determine the expression of eIF1, eIF5, eIF6, Caspase 3 and PARP are shown in Table 17. For the qRT-PCR, the Power SYBR Green PCR Master Mix Kit (Applied Biosystems, Foster City, USA) was used in a 7900HT Fast Real-Time PCR System (Applied Biosystems, Foster City, USA). β-actin was used as HKG, and the relative gene expression levels were calculated using the $2^{\Delta\Delta CT}$ analysis method [181].

Table 17: Oligonucleotides used for qRT-PCR [181].

Gene	Primer	Sequence (5'-3')	Length	Tm [°C]
Ki67	Fwd	AGACGCCTGGTTACTATCAAAG	19	60
	Rev	GGAAGCTGGATACGGATGTCA	22	58
PARP	Fwd	CGGTGACTTATCCTGTGGTCC	23	58
	Rev	ACATCCCGACAGAAAGGCAC	23	59
Caspase 3	Fwd	ATGGAAGCGAATCAATGGACTC	22	60
	Rev	CTGTACCAGACCCGAGATGTCA	21	61
eIF1	Fwd	GAAACGGCAGGAAGACCCTTA	21	60
	Rev	CGGATGCTCAATTACAGTACCAT	23	59
eIF5	Fwd	AGCGTGTCAGACCAGTTCTAT	21	61
	Rev	CTGTCTTGATTCCATTGCCTTTG	23	60
eIF6	Fwd	CCGCGTGCGGAGCTTGTAT	19	61
	Rev	CGCCCTCGAACACACTGTAGAAGT	24	64

3.5.6 Proliferation Assay

The number of viable cells was determined on the basis of mitochondrial conversion of 3-(4,5-dimethylthiazol-2-yl)-2,5-diphenyltetrazolium bromide (MTT, Sigma Aldrich, Missouri, USA) to formazine.

Transfected and control cells were seeded in 96-well plates (80 000 cells/well) and cultivated under low serum conditions (1% FCS) for 24 hours, 48 hours and 72 hours. Cells incubated with 16 µl of MTT solution (5.5 mg/ml) were added to a medium volume of 160 µl for 2 h at 37°C, 5% CO_2 and 95% humidity conditions. The supernatant was removed, and cells were lysed with sodium dodecyl sulphate. The MTT formazan crystals were dissolved with 95 µl

isopropanol/HCl (0.04 M) solution and shaken for 15 minutes at room temperature. Optical density was measured at 570 nm (Synergy^{TM}4, BioTek, Winooski, USA). The proliferation rate was also confirmed with Ki67 on mRNA level [181].

3.5.7 Apoptose Assay

Apoptotic cells were detected using YO-PRO®-1 (Thermo Fisher Scientific, Massachusetts, USA) reagent. The assay was performed in polystyrene black 96-well plates with optical bottom (Nunc, Bundesstatt, USA). siRNA-transfected and control cells were seeded onto 96-well plates (80 000 cells/well) and incubated at 37°C, 5% CO_2 and 95% humidity. After 24 hours, 48 hours and 72 hours, cells were incubated with YO-PRO®-1 for 15 minutes at 37°C, the supernatant was removed, and cells were washed with PBS. Finally, fluorescence was measured with the Synergy^{TM}4 (BioTek, Winooski, USA) at 485 nm (emission) to 535 nm (excitation). The apoptosis rate was also confirmed with *Caspase 3* and *PARP* on mRNA level [181].

3.5.8 Invasion Assay

For analysis of invasiveness of HCT116 cells, the CytoSelect TM 24-Well Cell Invasion Assay (Cell Biolabs, San Diego, USA) was performed according to the manufacturer's instructions. The underlying principle is migration through a basement membrane layer coated-transwell chamber to reach the serum-containing compartment. $1x10^5$ siRNA transfected and control cells were suspended in medium with 10% FCS, placed in the upper chamber and incubated for 48 hours at 37°C, 5% CO_2 and 95% humidity conditions. The cells which invaded the lower surface of the filter inserts were stained with crystal violet. The optical density was measured at 560 nm (Synergy^{TM}4, BioTek, USA) [181].

3.5.9 Colony Formation Assay

HCT116 cells transfected with siRNA against eIF1, eIF5 and eIF6, as well as scrambled control siRNA , were collected and seeded in six-well plates at a density of 500 cells/well, followed by incubation at 37°C, 5% CO_2 and 95% humidity . The medium was changed every three days. After two weeks of culture, cells were washed three times with PBS and fixed in

4% paraformaldehyde (Sigma-Aldrich, USA). Fixed cells were stained by adding freshly prepared diluted Giemsa solution (Sigma-Aldrich, Missouri, USA) for 20 minutes. Then the cells were rinsed with distilled water, and colonies were analysed using a microscope (Nikon TMS – Inverted Microscope, Japan) [181].

3.5.10 Polysome Profile Analyses

Sucrose density-gradient centrifugation was performed to analyze the cellular distribution of polysomes, 80S ribosomes and free 40S and 60S subunits. Cells were cultured in 100 mm dishes, transfected with siRNA and cultivated for 24h, 48h and 72h. Fifteen minutes prior to lysis, cells were incubated with 100 µg/ml cycloheximide (Sigma-Aldrich, Missouri, USA) to stall ribosomes on the mRNA strand. Lysis was performed on ice by washing cells in ice-cold PBS containing 100 µg/ml cycloheximide followed by suspension in lysis buffer (20 mM HEPES pH 7.4; 15 mM $MgCl_2$; 200 mM KCl; 1% Triton X-100; 2 mM DTT and 100 µg/ml cycloheximide), and nuclei were removed by centrifugation (14000g, 10 minutes, 4°C). The supernatant was snap frozen for analysis and stored at -80°C until further use. The supernatant was layered onto 15%-40% sucrose gradients (50 mM NH4Cl, 50 mM Tris-acetate pH 7.0, 12 mM $MgCl_2$, 100 µg/ml cycloheximide and freshly added 1 mM DTT). 2.2 ml of each solution, starting with the highest concentration, was layered on top of each other, with at least 4 h of freezing (-80°C) in between. Centrifugation tubes were from Beckman Coulter. Final gradients were put to 4°C o/n to equilibrate. Sample volumes equal to 2 OD values were loaded onto the gradients. The ultracentrifugation was performed in Beckman Coulter SW41 rotor (Beckman, Villepinte, France) for 150 min at 160000 g, 4°C in vacuum without breaking. Polysomal profiles were analysed via an ISCO density gradient analyser unit, which analyses and simultaneously blots ribosomal distribution measured by an UA-6 detector with 254 nm filter (Teledyne ISCO, Nebraska, USA) [181].

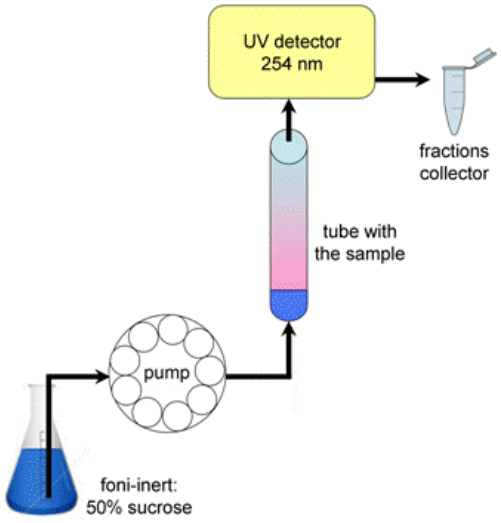

Figure 10: Fractionation of polysome gradient analysis. A peristaltic pump presses the gradient from the tube with a foni-inert through a spectrophotometer which monitors the absorbance, and the fractions where collected into tubes. Graph was adopted and taken from [149].

3.6 In vivo Experiments

3.6.1 Generation of Xenograft Models

Five primary rectum carcinoma samples and two liver metastases from patients suffering from rectum cancer, as well as four primary colon carcinoma samples and one liver metastasis from patients suffering from colon cancer, were sent to EPO Berlin-Buch GmbH (Berlin, Germany). The tissue samples were transplanted into 3 to 6 immunodeficient NOD/SCID mice. The tumor growth was monitored in a daily rhythm. At a size of about 1 cm^3, the tumors were removed and transferred to naive NMRI:nu/nu mice for chemosensitivity testing [122]. Xenotransplanted carcinomas and metastases were treated with different standard and novel chemotherapeutic drugs (Table 18). During chemosensitivity testing, the tumor volume was measured regularly and used to generate growth curves. After a time period of 30 - 40 days, the tumors were excised and analyzed by WImmunoblot and qRT-PCR. Chemosensitivity data were kindly provided by EPO Berlin-Buch GmbH. Tumor volume upon treatment, in comparison to the controls (T/C), was calculated in percent.

Table 18: Chemotherapeutic drugs used for chemosensitivity testing. Standard drugs for CRC treatment*; Novel drugs in preclinical testing*.

Drug	Subclass
Oxaliplatin*	Alkylating agent
Irinotecan*	Topoisomerase I inhibitor
5-FU*	Antimetabolite (Pyrimidinantagonist)
Cetuximab*	EGFR inhibitor
AZD8931	Reversible inhibitor of signaling by EGFR
AZD6244	Mitogen-activated protein kinase kinase (MEK or MAPK/ERK kinases) 1 and 2 inhibitor
Afatinib	Tyrosine Kinase inhibitor
Avastin*	Angiogenesis inhibitor
Regorafenib*	Multi-kinase inhibitor
Nintedanib	Angiokinase inhibitor for VEGFR1/2/3, FGFR1/2/3 and PDGFRα/β
mTOR FR	mTOR inhibitor
IGF 1/2 mAB *	IGF-1/IGF-2 co-neutralizing monoclonal antibody
AZ1*	Aziridinylbenzoquinone
Volitinib*	c-Met inhibitor

3.7 Statistical Analyses

3.7.1 Statistical Analyses for CRC

All statistical analyses and graphs were generated using Graph Pad Prism 6.01 software (La Jolla, CA, USA).

According to the results, non-parametric tests were used for not normally distributed data. For normally distributed groups, the data were analyzed with Student T-test or 1-way ANOVA. Mann-Whitney U test was used as non-parametric test for two groups.

Outliers for all analyses were identified by Grubb's test. Significance levels were set at $p < 0.05$.

3.7.2 Statistical Analyses for HBV, HCV, HCV-associated HCC, HBV-associated HCC and non-virus induced HCC

Patient survival curves have been depicted in association with different conditions. They illustrated the Kaplan-Meier estimator indicating the fraction of patient's alive (y-axis) after a given period of time in days (x-axis). As the sample size approaches the total population under consideration the survival curve will converge to the true survival function.

Furthermore, the p-value of the log-rank test was added to the plot. This non-parametric hypothesis test allows assessing the probability to observe the given survival curves under the null-hypothesis that the two or more groups have identical survival and hazard functions.

To evaluate the potential predictive power of eIF5 we conducted a number of proportional hazard models, also referred to as Cox regressions. This model assumes a multiplicative relation of the covariates to the hazard rate and non-informative censoring [182].

4 Results Hepatocellular Carcinoma

The following pages contain the manuscript “New liver cancer biomarkers: PI3K/AKT/mTOR pathway members and eukaryotic translation initiation factors” published in the European Journal of cancer [182]. This work is the central achievement of the PhD thesis.

4.1 Immunohistochemically Profile of Various eIF Subunits in HCC

eIF profiles were analyzed in HCC patients compared to non-neoplastic liver tissue (NNLT) using IHC.

The IHC data displayed stronger eIF2α, eIF3H and eIF5 expression in HCC samples compared to NNLT. The subunits eIF3C, eIF4E (p=0.408) and eIF6 did not display any differences in the tumor samples compared to NNLT (Figure 11 and Figure 12). The staining distribution of eIF subunits was found to be mainly cytoplasmic 182].

A significant difference was observed in patients with a high score of eIF5 (p=0.001), indicating that a score of 2 or 3 is associated with better overall survival. The same tendency was observed for eIF2α (p=0.115). For eIF3H (p=0.319), eIF3C (p=0.5), eIF4E (p=0.408) and eIF6 (p=0.544) no differences in overall survival were observed (Figure 11 and Figure 12) [182].

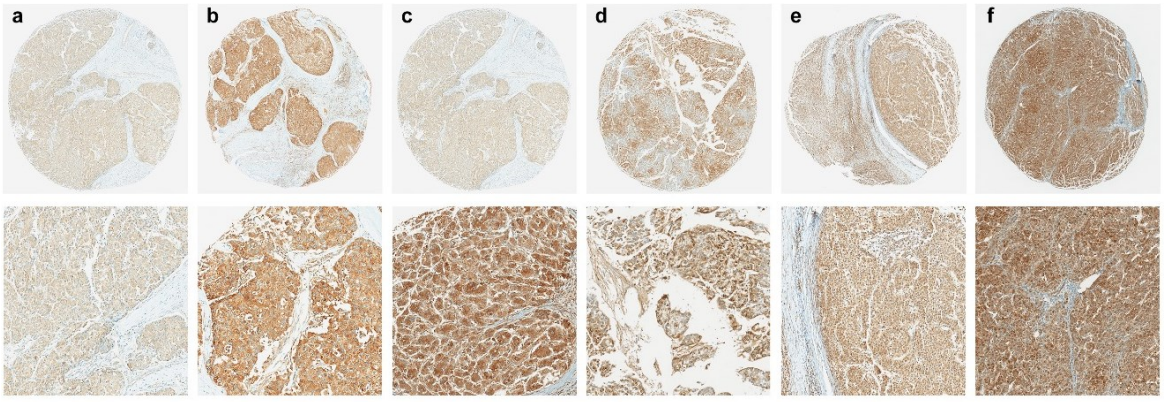

Figure 11: IHC of various eIF subunits in HCC patients. Expression of (a) eIF2α, (b) eIF3C, (c) eIF3H, (d) eIF4E, (e) eIF5, (f) eIF6 in HCC samples compared to NNT analyzed by IHC. The

interobserver variation between the two independent observers (J.H. and N.GS.) was calculated. Scale bars: 200 nm and 50nm [182].

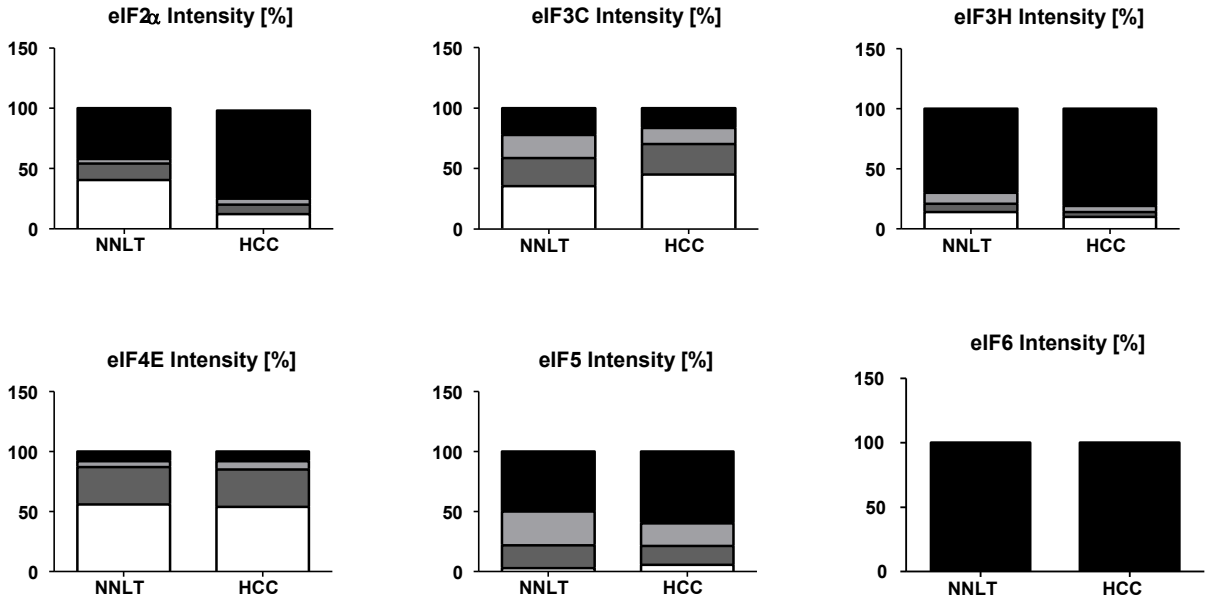

Figure 12: Densitometric analysis of immunohistochemical staining from various eIF subunits in HCC compared to non-neoplastic liver tissue (NNLT) [182].

4.2 Overall Survivals According to the Expression of Various eIF Subunits and Chronic hepatitis B and Chronic Hepatitis C

Patients with HBV (Figure 14a) and HCV infection (Figure 13d) and high eIF2α expression as well patients without HBV and HCV showed a better survival. For eIF3H, we observed the best survival in patients with a low eIF3H score and without HBV (Figure 13b). HCV infected patients with a high eIF3H (Figure 13e) score had a poor prognosis. For eIF3C we did not observe any differences in the survival with a high or low score and no significant differences neither with nor without HBV background (Figure 13c). The survival according to eIF3C in HCV showed no significant differences with or without HCV infection (Figure 13f). For eIF4E we did not observe any differences in the survival with a high or low score and also no significant differences with or without HBV infection background (Figure 14a). Patients with HCV displayed a shorter survival compared to patients without HCV infection, but eIF4E did not influence the survival in these patients (Figure 14d). A high score of eIF5 showed a

significantly influence on survival in HBV infected patients and in patients without HBV infection (Figure 14b). The eIF5 score did not have much influence in HCV positive patients. The survival in HCV infected patients is poor compared to patients without HCV induced hepatitis (Figure 14e).

Both, eIF6 expression and HBV positivity (Figure 14c) showed no significant differences in the patient overall survival. HCV infected patients displayed a poor survival with a high score of eIF6 (Figure 14f).

We noticed dramatic differences in the overall survival in the eIF expression and chronic hepatitis C but no changes in chronic hepatitis B [182].

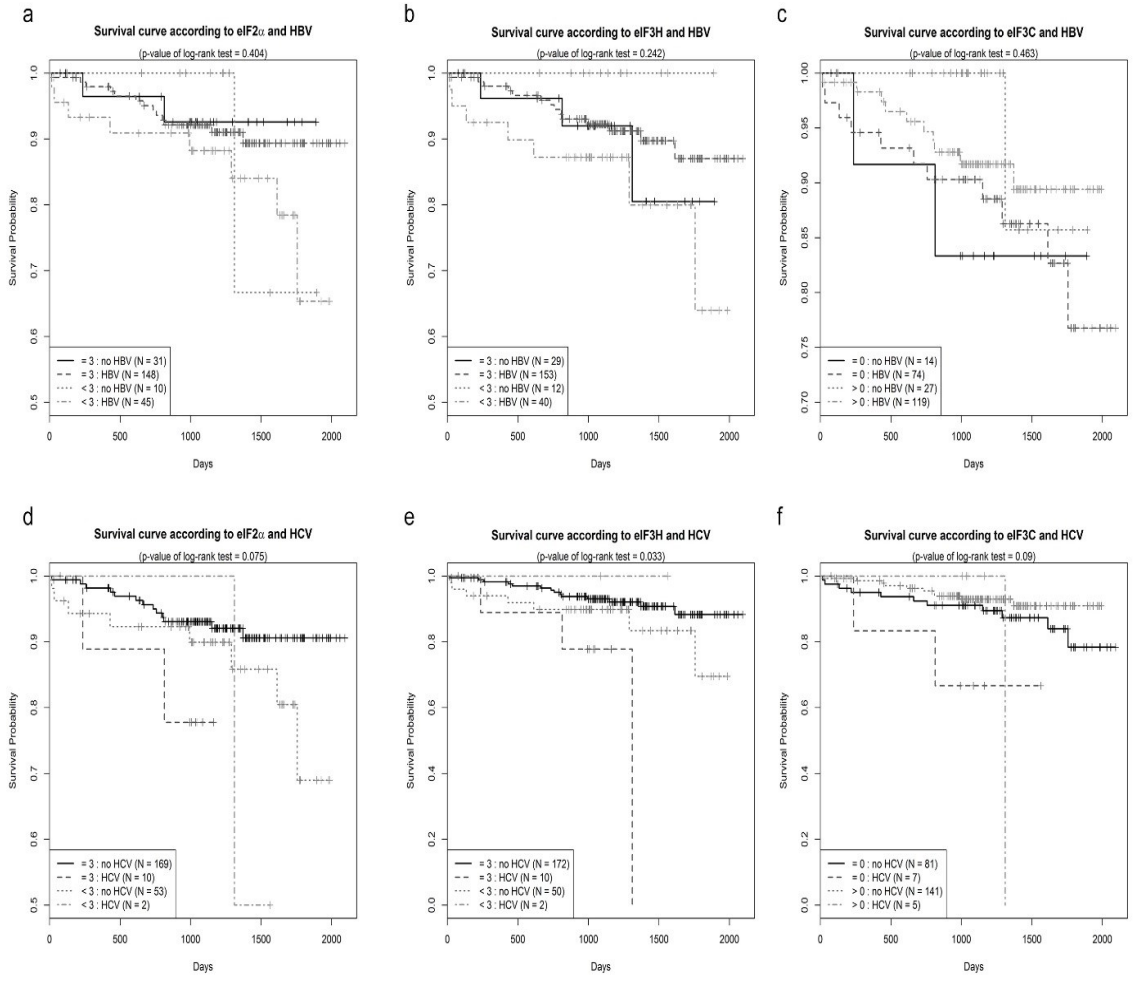

Figure 13: Kaplan Meier curves of various eIF subunits with respect to patients with chronic hepatitis B and C. (a) High score of eIF2α in HBV patients display a better survival. (b) We observed

the best survival in patients with a low eIF3H score and without HBV. (c) For eIF3C we did not observe any significant differences in the survival between patients with or without HBV. (d) A high score of eIF2α in HCV patients and as well in patients without HCV showed a better survival. (e) HCV patients with a high eIF3H score displayed a poor survival. (f) The survival according to eIF3C in HCV showed no significant differences in patients with or without HCV [182].

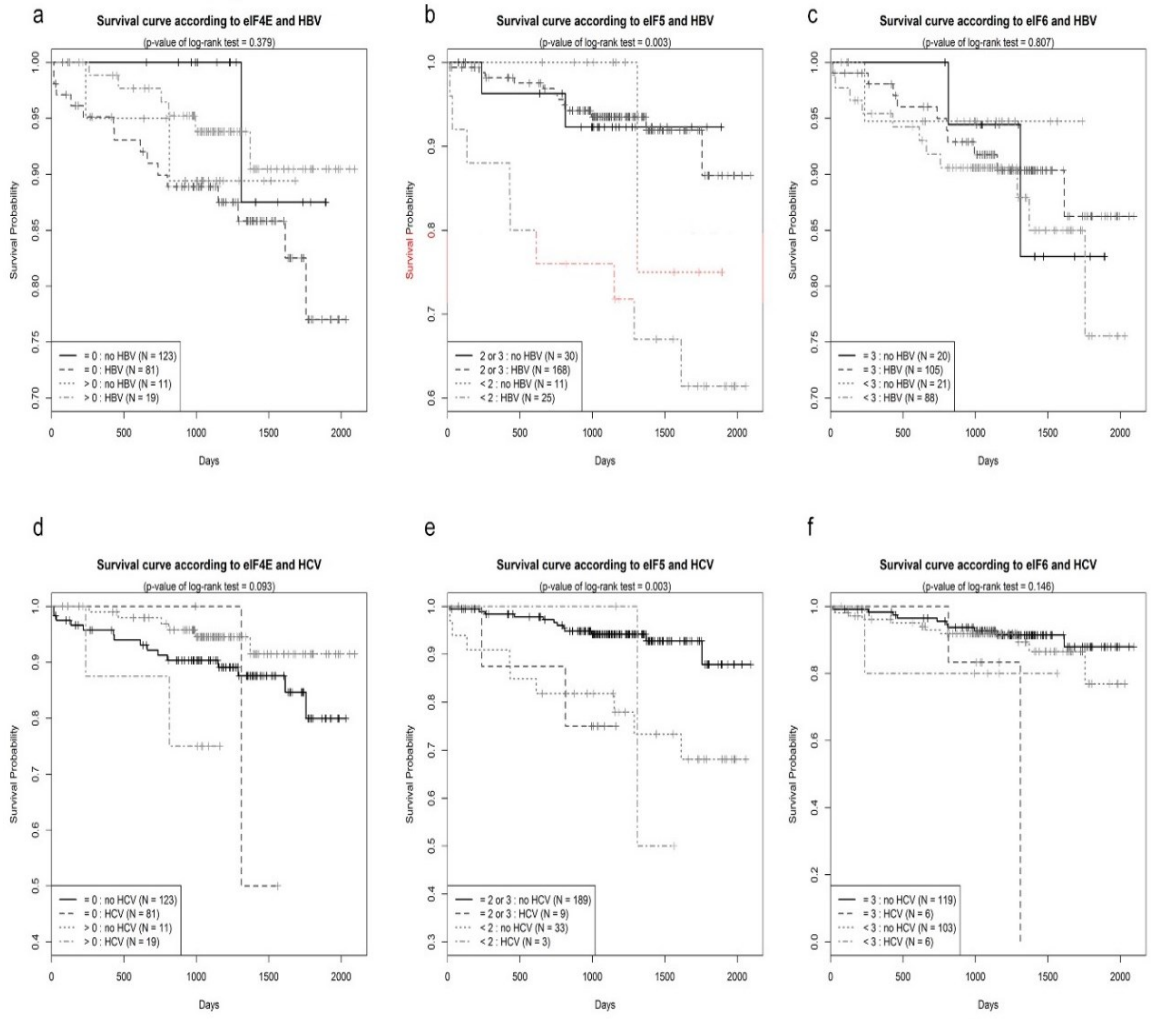

Figure 14: Kaplan Meier curves of various eIF subunits with respect to patients with chronic hepatitis B and C. (a) For eIF4E we did not observe any differences in patients overall survival with or without HBV. (b) High eIF5 scores revealed a significant influence on survival in patients with and without HBV. (c) The survival according to eIF6 expression and HBV showed no significant differences in the patients overall survival. (d) Patients with HCV displayed a poor survival compared to patients without HCV independent of eIF4E expression. (e) eIF5 scores did not influence the survival of HCV

patients. The survival in HCV patients was poor compared to patients without HCV. (f) HCV patients with a high score of eIF6 displayed a poor overall survival [182].

4.3 Expression Profile, Kaplan-Meier Curves and Prognostic Value

Survival of patients with two or more tumors, thus higher tumor load, was shorter, than of individuals with only one tumor nodule (Figure 15b). Survival was reduced in patients with microvessel invasion compared to patients without microvessel invasion (Figure 15d). Survival was shorter in patients with recurring tumors compared to patients without recurrences (p=0.019) (Figure 15e). Edmondson-Steiner grade from patients with HCC showed an expected correlation to overall survival (Figure 15f) [182].

The influence of HBV infection on overall survival did not display any clear difference between patients with and without chronic HBV (Figure 16 and 17). Patients with cirrhosis live shorter than patients without cirrhosis. HCV infection was associated with shorter overall survival (Figure 16 and 17) in HCC patients [182].

The investigated HCC cohort was representative as a lower T-stage correlated with a better prognosis (Figure 15a). The overall survival in patients with only one tumor, without cirrhosis, non-tumor recurrence and microvessel invasion correlated with a significantly better prognosis (Figure 15b). Patients with chronic HCV lived longer (Figure 16 and 17) compared to chronic HBV patients [182].

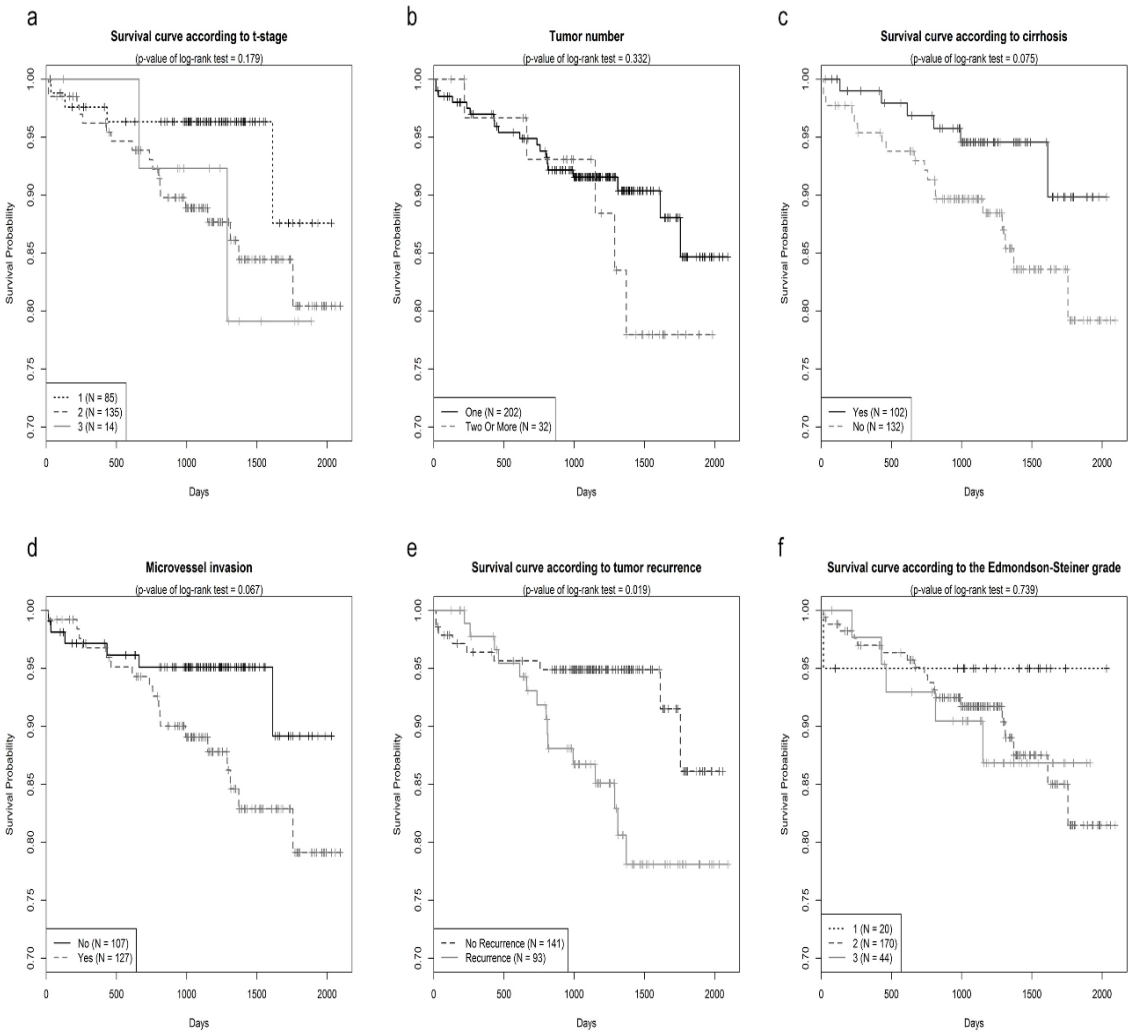

Figure 15: Kaplan Meier Curves of patients with HBV- and HCV-associated HCC and HCC without viral infection. (a) Survival curve according to t-stage. (b) Tumor number compared to survival shows a shorter survival with two or more tumors. (c) Overall survival of patients with and without cirrhosis. (d) Patients with microvessel invasion reveal a shorter survival compared to patients without microvessel invasion. (e) Patients with a tumor recurrence have a lower outcome with shorter survival compared to patients without recurrent tumor burden. (f) Survival according to Edmondson-Steiner grade of patients with HCC [182].

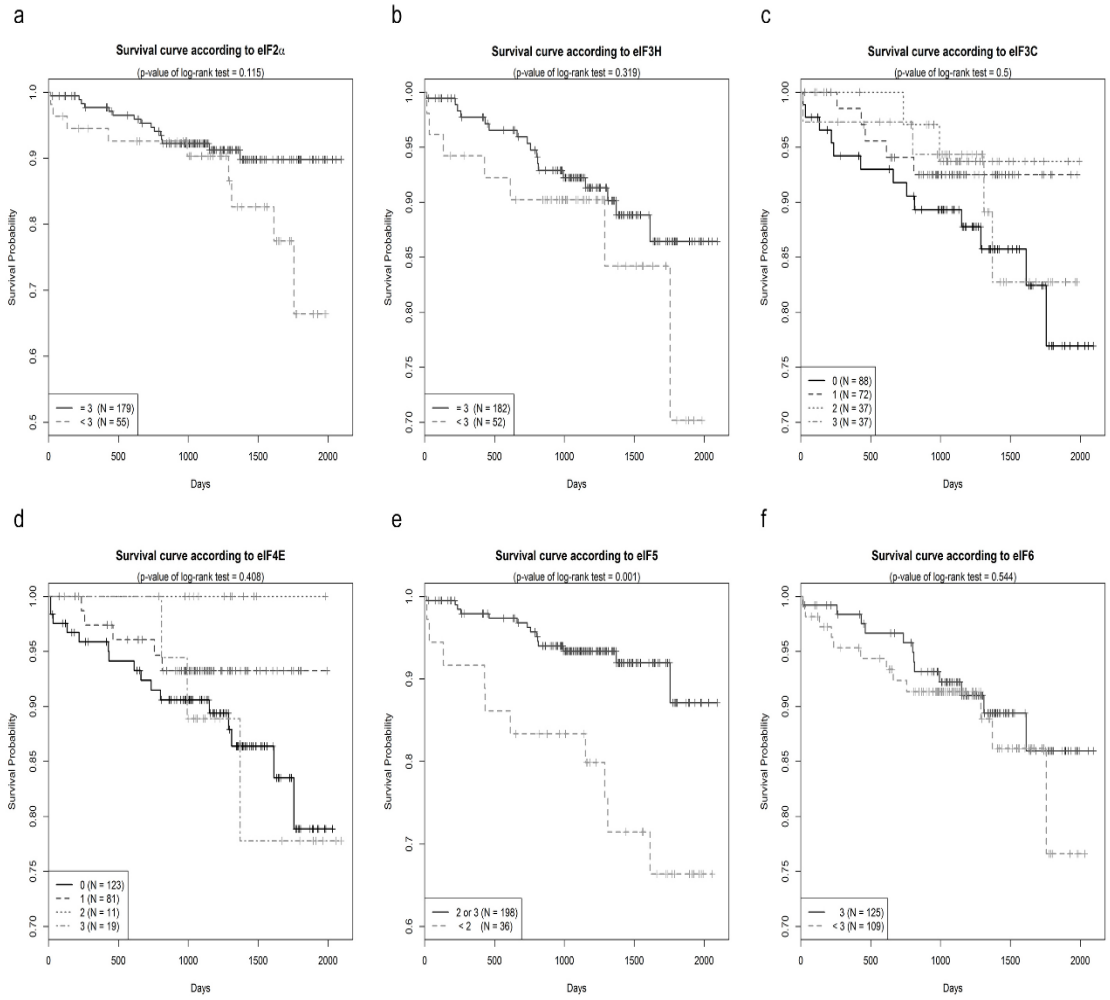

Figure 16: Kaplan Meier curves of various eIF subunits in patients with HBV- and HCV-associated HCC and HCC without viral infection. (a) Survival curve according to the eIF2α intensity. (b) Survival curve according to the eIF3H intensity. (c) Survival curve according to the eIF3C intensity. (d) Survival curve according to the eIF4E intensity. (e) Survival curve according to the eIF5 intensity. (f) Survival curve according to the eIF6 intensity [182].

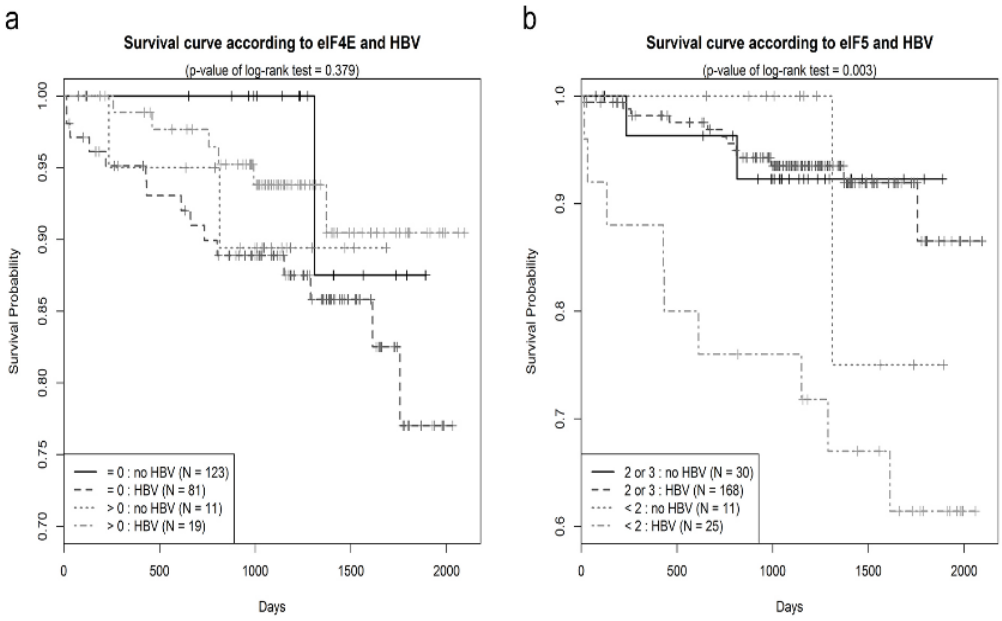

Figure 17: Kaplan Meier Curves of chronic hepatitis patients. (a) Overall survival of patients with and without HBV infection have a similar prognosis compared to non HBV infected patients. (b) Overall survival of patients with and without HBV infection have a poor prognosis compared to non HCV infected patients [182].

The TCGA database was investigated to identify eIF genes that are significantly altered in HCC. Kaplan-Meier curves were drawn to assess a potential association of eIF expression and overall survival in HCC, chronic hepatitis C and B and ASH patients. The median eIF mRNA expression in all HCC tissues was used as the cutoff point to divide all cases into low and high expressed HCC (n = 151) groups. The first group represent in medium grey lines low gene expression and the black lines high gene expression (Figure 18a – 29a). The second group displays the comparison between HCC with chronic hepatitis C and B. The light grey lines represent low gene expression for chronic hepatitis B, medium grey lines display high gene expression for chronic hepatitis B, the dark grey lines represent low gene expression for chronic hepatitis C and the black lines high gene expression for chronic hepatitis C (Fig. 18b – 29b). The third group displays the comparison between ASH and NASH induced HCC. The light grey lines represent low gene expression for NASH, medium grey lines display high gene expression for NASH, the dark grey lines represent low gene expression for ASH and the black lines high gene expression for ASH (Fig. 18c – 29c) [182].

As shown in Figure 22, there was a significant difference in the survival between patients of low and high gene expression in HCC group for eIF3D (p = 0.028). In Figure 25, there were significant differences in the survival between patients of low and high gene expression in NASH and ASH group (p = 0.045). Further analysis showed also significance for chronic HBV for eIF4G1 (p = 0.018) and eIF6 (p = 0.016) and also for NASH group for eIF4G1 (p 0 0.033) and ASH for eIF6 (0.029). In Figure 29, there was a significant difference in the survival between patients of low and high gene expression in HCC group for eIF6 (p = 0.015). However, there were no significant differences in overall survival between low and high grade groups for eIF2α (Figure 18), eIF3B (Figure 19), eIF3C (Figure 20), eIF3H (Figure 22), eIF3J (Figure 23), eIF4E (Figure 24), eIF4G2 (Figure 26), eIF4G3 (Figure 27) and eIF5 (Figure 28) [182].

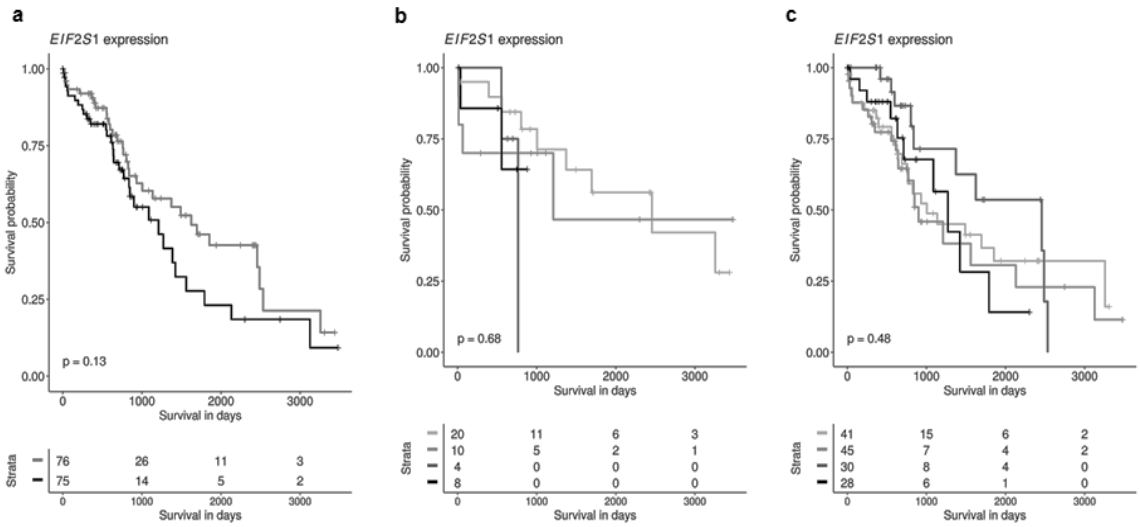

Figure 18: eIF2α is a clinically relevant candidate in HCC patients, patients with HBV- and HCV-associated HCC, non-alcoholic and alcoholic livers. Kaplan-Meier curves of eIF2α expression on overall survival for HCC, HBV- and HCV-associated HCC, and ASH. Cases are divided in low or high expressers according to whether expression is below or above median and survivals are compared using the log-rank test. (a) Represent the HCC dataset, medium grey lines display low gene expression and black line high gene expression for eIF2α. (b) Comparison between HCC with chronic hepatitis C and B. The light grey lines represent low gene expression for chronic hepatitis B, medium grey lines display high gene expression for chronic hepatitis B, the dark grey lines represent low gene expression for chronic hepatitis C and the black lines high gene expression for chronic hepatitis C. (c)

Comparison between ASH and NASH induced HCC. The light grey lines represent low gene expression for NASH, medium grey lines display high gene expression for NASH, the dark grey lines represent low gene expression for ASH and the black lines high gene expression for ASH [182].

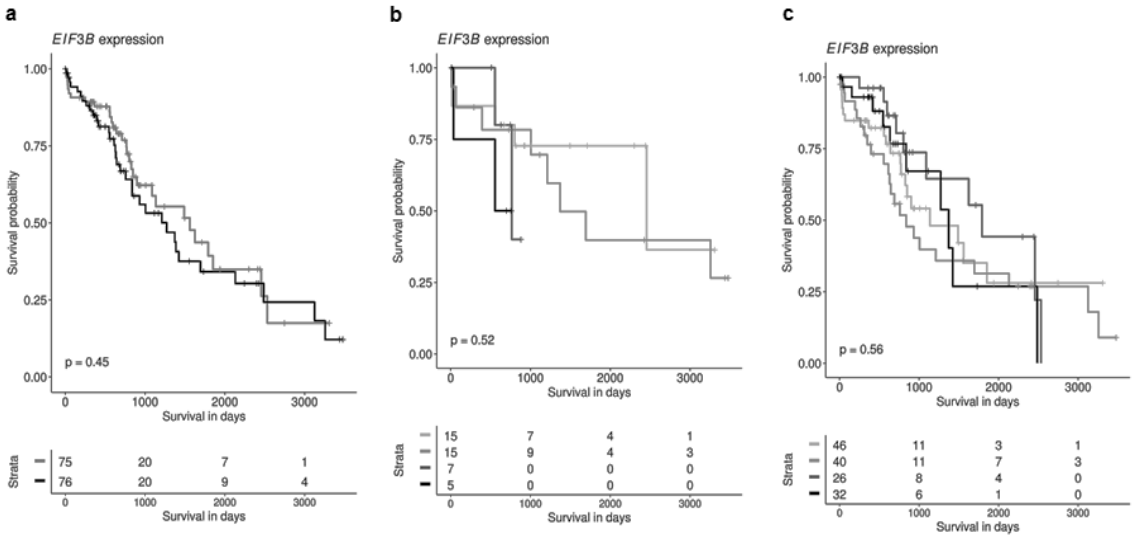

Figure 19: eIF3B is a clinically relevant candidate in HCC patients, patients with HBV- and HCV-associated HCC, non-alcoholic and alcoholic livers. Kaplan-Meier curves of eIF3B expression on overall survival for HCC, HBV- and HCV-associated HCC, and ASH. Cases are divided in low or high expressers according to whether expression is below or above median and survival are compared using the log-rank test. (a) Represent the HCC dataset, medium grey line displays low gene expression and black line high gene expression for eIF3B. (b) Comparison between HCC with chronic hepatitis C and B. The light grey lines represent low gene expression for chronic hepatitis B, medium grey lines display high gene expression for chronic hepatitis B, the dark grey lines represent low gene expression for chronic hepatitis C and the black lines high gene expression for chronic hepatitis C. (c) Comparison between ASH and NASH induced HCC. The light grey lines represent low gene expression for NASH, medium grey lines display high gene expression for NASH, the dark grey lines represent low gene expression for ASH and the black lines high gene expression for ASH [182].

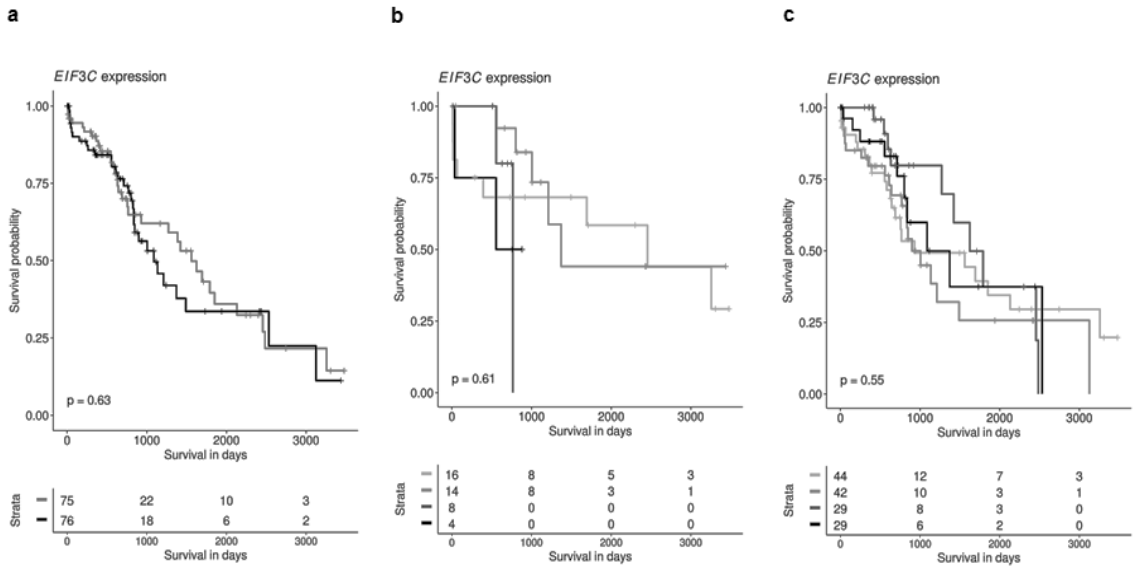

Figure 20: eIF3C is a clinically relevant candidate in HCC patients, patients with HBV- and HCV-associated HCC, non-alcoholic and alcoholic livers. Kaplan-Meier curves of eIF3C expression on overall survival for HCC, HBV- and HCV-associated HCC, and ASH. Cases are divided in low or high expressers according to whether expression is below or above median and survival are compared using the log-rank test. (a) Represent the HCC dataset, medium grey line displays low gene expression and black line high gene expression for eIF3C. (b) Comparison between HCC with chronic hepatitis C and B. The light grey lines represent low gene expression for chronic hepatitis B, medium grey lines display high gene expression for chronic hepatitis B, the dark grey lines represent low gene expression for chronic hepatitis C and the black lines high gene expression for chronic hepatitis C. (c) Comparison between ASH and NASH induced HCC. The light grey lines represent low gene expression for NASH, medium grey lines display high gene expression for NASH, the dark grey lines represent low gene expression for ASH and the black lines high gene expression for ASH [182].

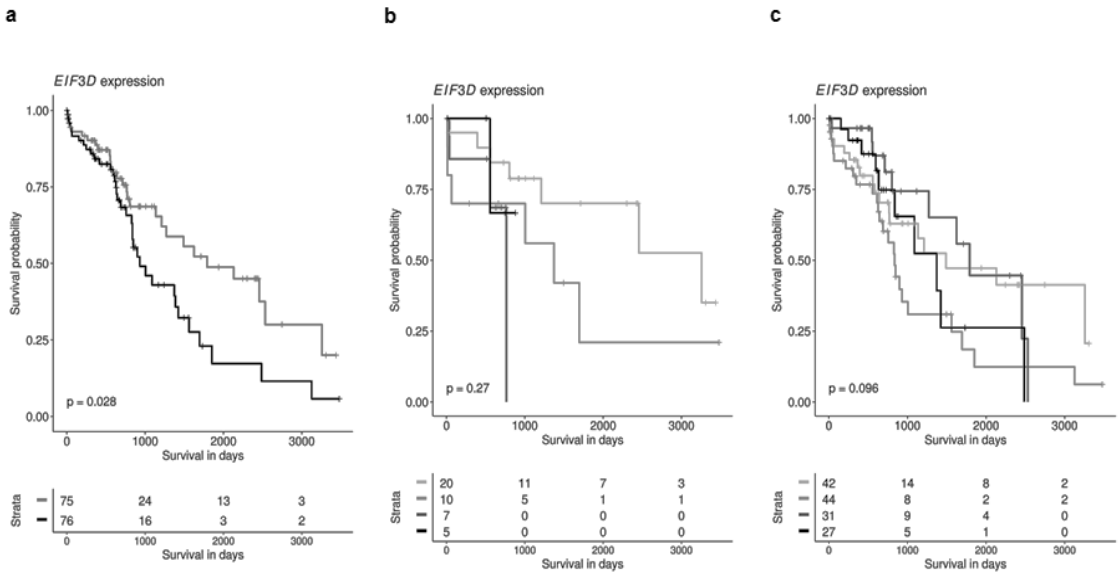

Figure 21: eIF3D is a clinically relevant candidate in HCC patients, patients with HBV- and HCV-associated HCC, non-alcoholic and alcoholic livers. Kaplan-Meier curves of eIF3D expression on overall survival for HCC, HBV- and HCV-associated HCC, and ASH. Cases are divided in low or high expressers according to whether expression is below or above median and survival are compared using the log-rank test. (a) Represent the HCC dataset, medium grey line displays low gene expression and black line high gene expression for eIF3D. (b) Comparison between HCC with chronic hepatitis C and B. The light grey lines represent low gene expression for chronic hepatitis B, medium grey lines display high gene expression for chronic hepatitis B, the dark grey lines represent low gene expression for chronic hepatitis C and the black lines high gene expression for chronic hepatitis C. (c) Comparison between ASH and NASH induced HCC. The light grey lines represent low gene expression for NASH, medium grey lines display high gene expression for NASH, the dark grey lines represent low gene expression for ASH and the black lines high gene expression for ASH [182].

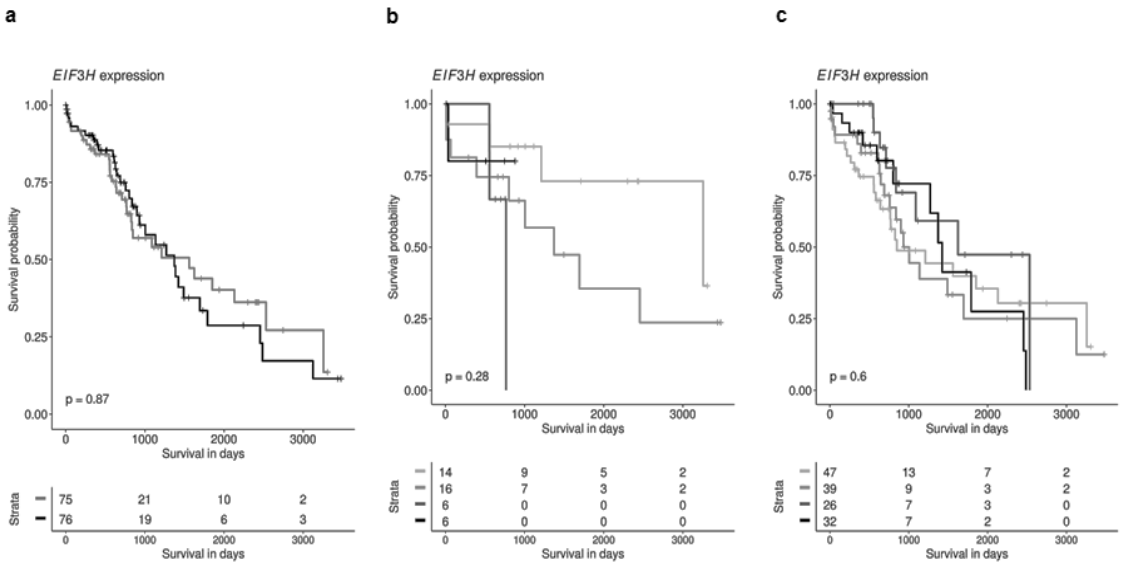

Figure 22: eIF3H is a clinically relevant candidate in HCC patients, patients with HBV- and HCV-associated HCC, non-alcoholic and alcoholic livers. Kaplan-Meier curves of eIF3H expression on overall survival for HCC, HBV- and HCV-associated HCC, and ASH. Cases are divided in low or high expressers according to whether expression is below or above median and survival are compared using the log-rank test. (a) Represent the HCC dataset, medium grey line displays low gene expression and black line high gene expression for eIF3H. (b) Comparison between HCC with chronic hepatitis C and B. The light grey lines represent low gene expression for chronic hepatitis B, medium grey lines display high gene expression for chronic hepatitis B, the dark grey lines represent low gene expression for chronic hepatitis C and the black lines high gene expression for chronic hepatitis C. (c) Comparison between ASH and NASH induced HCC. The light grey lines represent low gene expression for NASH, medium grey lines display high gene expression for NASH, the dark grey lines represent low gene expression for ASH and the black lines high gene expression for ASH [182].

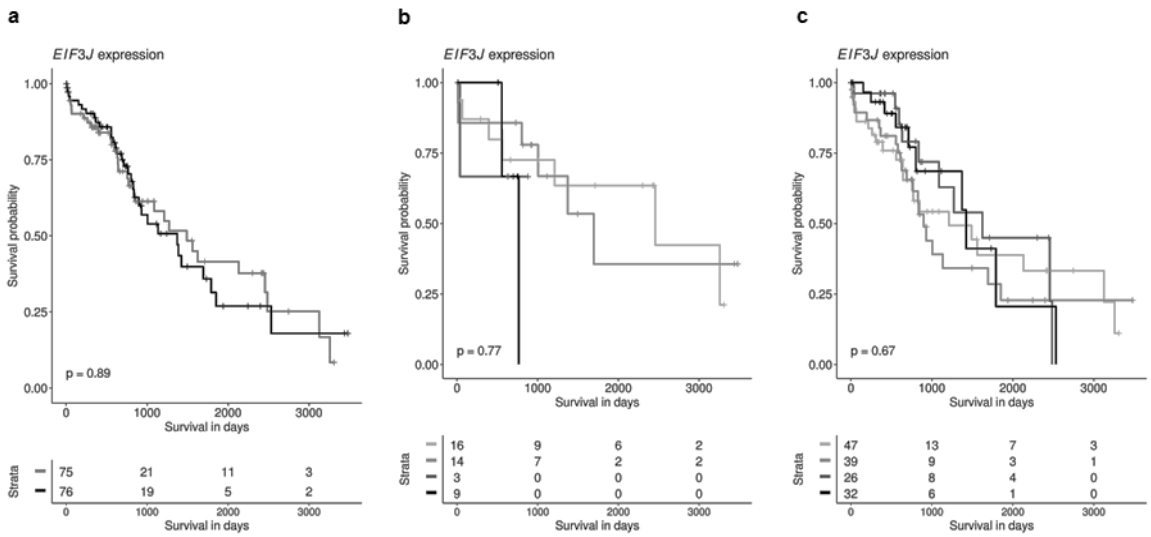

Figure 23: eIF3J is a clinically relevant candidate in HCC patients, patients with HBV- and HCV-associated HCC, non-alcoholic and alcoholic livers. Kaplan-Meier curves of eIF3J expression on overall survival for HCC, HBV- and HCV-associated HCC, and ASH. Cases are divided in low or high expressers according to whether expression is below or above median and survival are compared using the log-rank test. (a) Represent the HCC dataset, medium grey line displays low gene expression and black line high gene expression for eIF3J. (b) Comparison between HCC with chronic hepatitis C and B. The light grey lines represent low gene expression for chronic hepatitis B, medium grey lines display high gene expression for chronic hepatitis B, the dark grey lines represent low gene expression for chronic hepatitis C and the black lines high gene expression for chronic hepatitis C. (c) Comparison between ASH and NASH induced HCC. The light grey lines represent low gene expression for NASH, medium grey lines display high gene expression for NASH, the dark grey lines represent low gene expression for ASH and the black lines high gene expression for ASH [182].

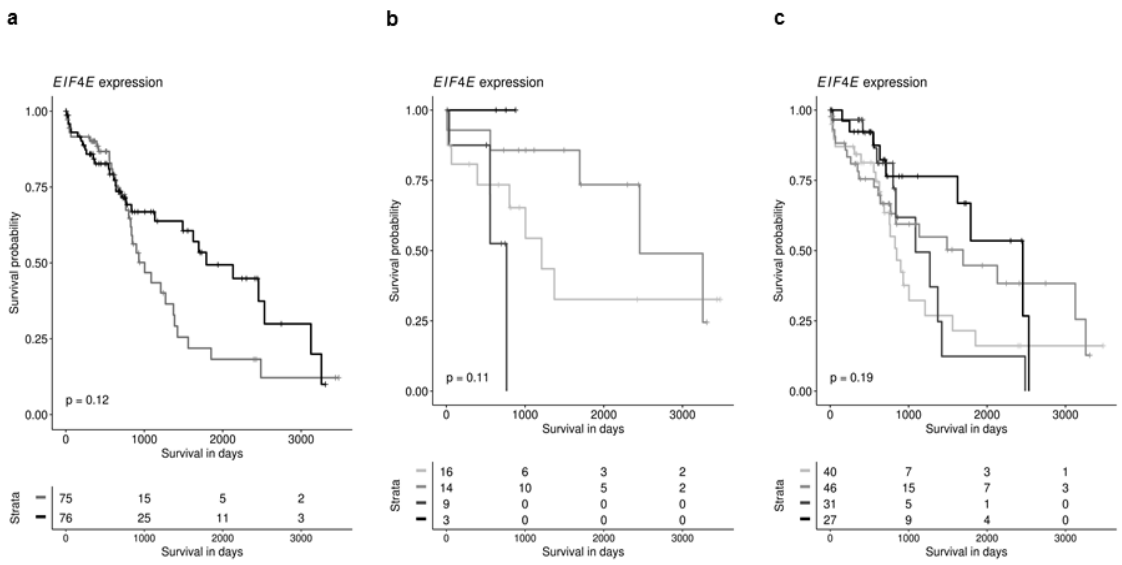

Figure 24: eIF4E is a clinically relevant candidate in HCC patients, patients with HBV- and HCV-associated HCC, non-alcoholic and alcoholic livers. Kaplan-Meier curves of eIF4E expression on overall survival for HCC, HBV- and HCV-associated HCC, and ASH. Cases are divided in low or high expressers according to whether expression is below or above median and survival are compared using the log-rank test. (a) Represent the HCC dataset, medium grey line displays low gene expression and black line high gene expression for eIF4E. (b) Comparison between HCC with chronic hepatitis C and B. The light grey lines represent low gene expression for chronic hepatitis B, medium grey lines display high gene expression for chronic hepatitis B, the dark grey lines represent low gene expression for chronic hepatitis C and the black lines high gene expression for chronic hepatitis C. (c) Comparison between ASH and NASH induced HCC. The light grey lines represent low gene expression for NASH, medium grey lines display high gene expression for NASH, the dark grey lines represent low gene expression for ASH and the black lines high gene expression for ASH [182].

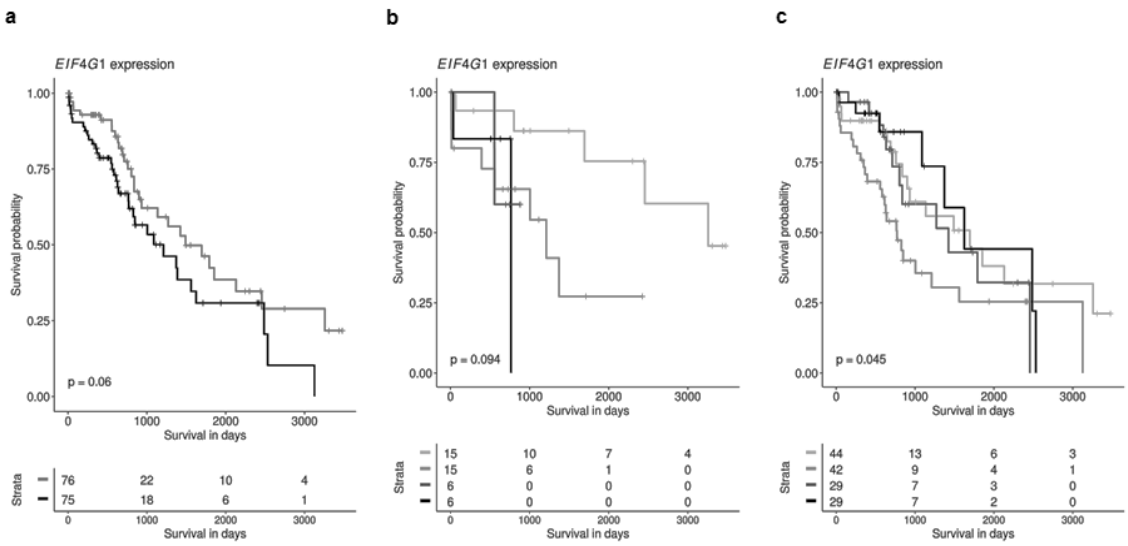

Figure 25: eIF4G1 is a clinically relevant candidate in HCC patients, patients with HBV- and HCV-associated HCC, non-alcoholic and alcoholic livers. Kaplan-Meier curves of eIF4G1 expression on overall survival for HCC, HBV- and HCV-associated HCC, and ASH. Cases are divided in low or high expressers according to whether expression is below or above median and survival are compared using the log-rank test. (a) Represent the HCC dataset, medium grey line displays low gene expression and black line high gene expression for eIF4G1. (b) Comparison between HCC with chronic hepatitis C and B. The light grey lines represent low gene expression for chronic hepatitis B, medium grey lines display high gene expression for chronic hepatitis B, the dark grey lines represent low gene expression for chronic hepatitis C and the black lines high gene expression for chronic hepatitis C. (c) Comparison between ASH and NASH induced HCC. The light grey lines represent low gene expression for NASH, medium grey lines display high gene expression for NASH, the dark grey lines represent low gene expression for ASH and the black lines high gene expression for ASH [182].

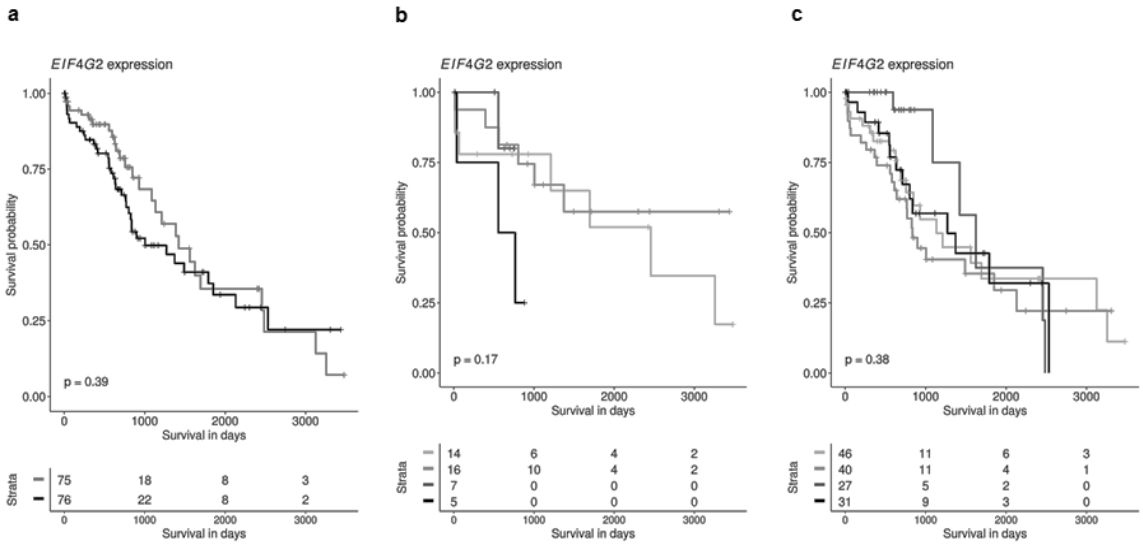

Figure 26: eIF4G2 is a clinically relevant candidate in HCC patients, patients with HBV- and HCV-associated HCC, non-alcoholic and alcoholic livers. Kaplan-Meier curves of eIF4G2 expression on overall survival for HCC, HBV- and HCV-associated HCC, and ASH. Cases are divided in low or high expressers according to whether expression is below or above median and survival are compared using the log-rank test. (a) Represent the HCC dataset, medium grey line displays low gene expression and black line high gene expression for eIF4G2. (b) Comparison between HCC with chronic hepatitis C and B. The light grey lines represent low gene expression for chronic hepatitis B, medium grey lines display high gene expression for chronic hepatitis B, the dark grey lines represent low gene expression for chronic hepatitis C and the black lines high gene expression for chronic hepatitis C. (c) Comparison between ASH and NASH induced HCC. The light grey lines represent low gene expression for NASH, medium grey lines display high gene expression for NASH, the dark grey lines represent low gene expression for ASH and the black lines high gene expression for ASH [182].

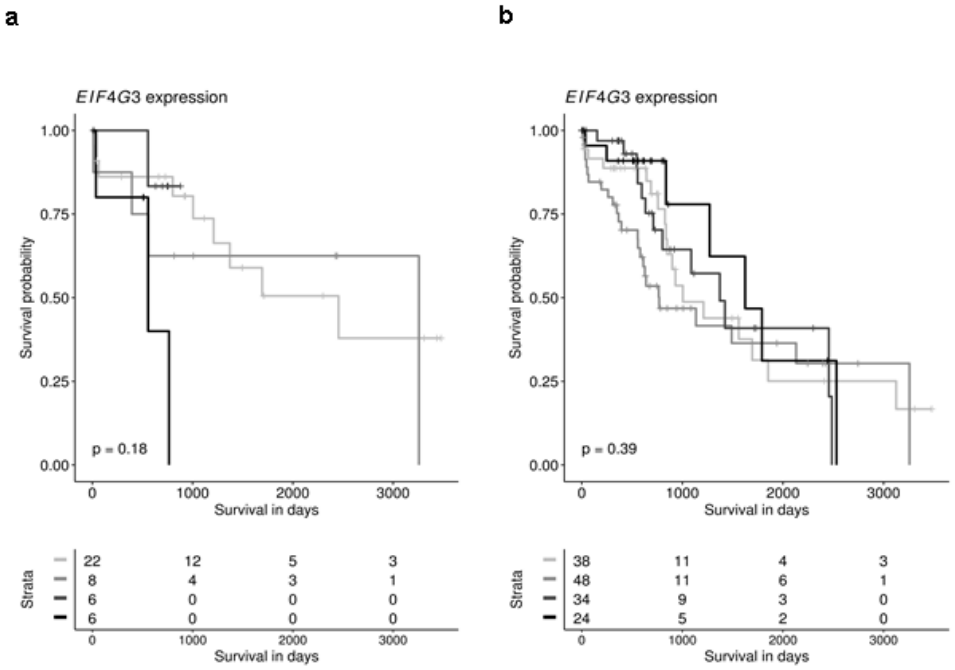

Figure 27: eIF4G3 is a clinically relevant candidate in HCC patients, patients with HBV- and HCV-associated HCC, non-alcoholic and alcoholic livers. Kaplan-Meier curves of eIF4G3 expression on overall survival for HCC, HBV- and HCV-associated HCC, and ASH. Cases are divided in low or high expressers according to whether expression is below or above median and survival are compared using the log-rank test. (a) Represent the HCC dataset, medium grey line displays low gene expression and black line high gene expression for eIF4G3. (b) Comparison between HCC with chronic hepatitis C and B. The light grey lines represent low gene expression for chronic hepatitis B, medium grey lines display high gene expression for chronic hepatitis B, the dark grey lines represent low gene expression for chronic hepatitis C and the black lines high gene expression for chronic hepatitis C [182].

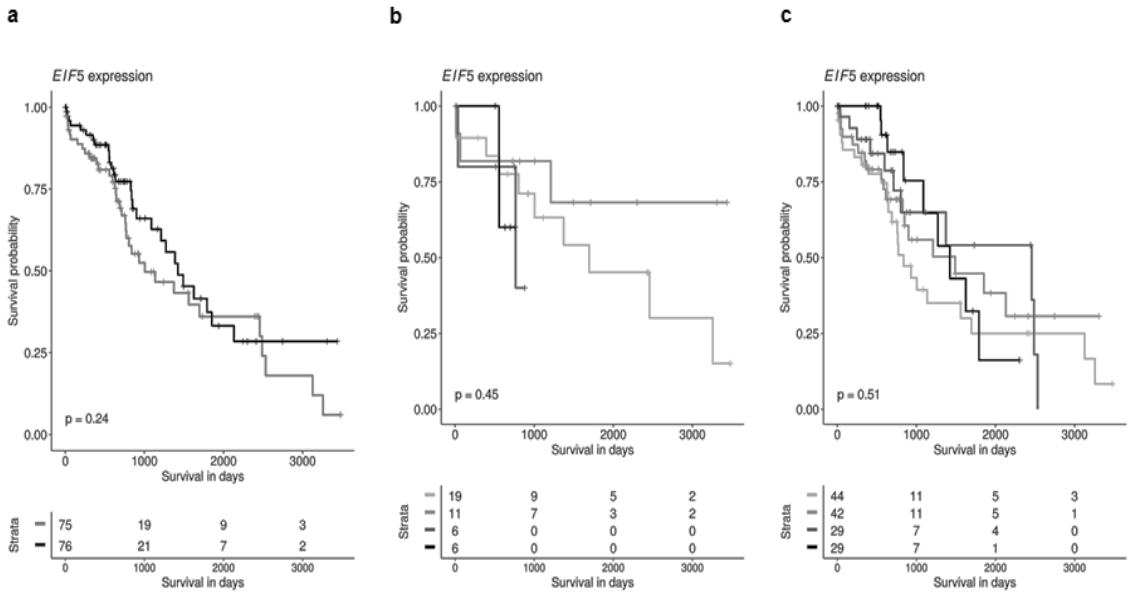

Figure 28: eIF5 is a clinically relevant candidate in HCC patients, patients with HBV- and HCV-associated HCC, non-alcoholic and alcoholic livers. Kaplan-Meier curves of eIF5 expression on overall survival for HCC, HBV- and HCV-associated HCC, and ASH. Cases are divided in low or high expressers according to whether expression is below or above median and survival are compared using the log-rank test. (a) Represent the HCC dataset, medium grey line displays low gene expression and black line high gene expression for eIF5. (b) Comparison between HCC with chronic hepatitis C and B. The light grey lines represent low gene expression for chronic hepatitis B, medium grey lines display high gene expression for chronic hepatitis B, the dark grey lines represent low gene expression for chronic hepatitis C and the black lines high gene expression for chronic hepatitis C. (c) Comparison between ASH and NASH induced HCC. The light grey lines represent low gene expression for NASH, medium grey lines display high gene expression for NASH, the dark grey lines represent low gene expression for ASH and the black lines high gene expression for ASH [182].

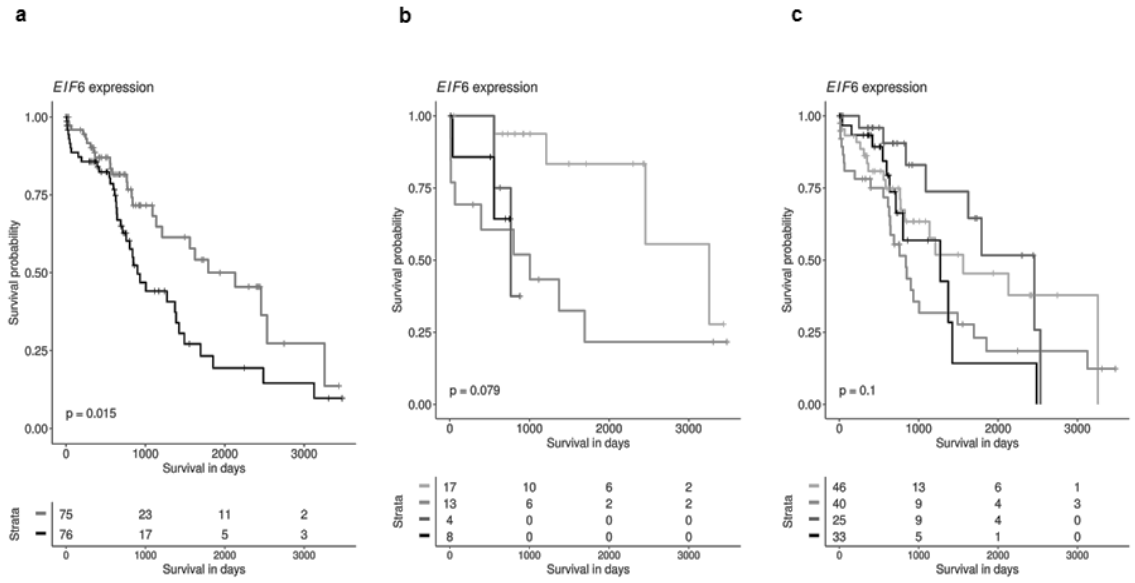

Figure 29: eIF6 is a clinically relevant candidate in HCC patients, patients with HBV- and HCV-associated HCC, non-alcoholic and alcoholic livers. Kaplan-Meier curves of eIF6 expression on overall survival for HCC, HBV- and HCV-associated HCC, and ASH. Cases are divided in low or high expressers according to whether expression is below or above median and survival are compared using the log-rank test. (a) Represent the HCC dataset, medium grey line displays low gene expression and black line high gene expression for eIF6. (b) comparison between HCC with chronic hepatitis C and B. The light grey lines represent low gene expression for chronic hepatitis B, medium grey lines display high gene expression for chronic hepatitis B, the dark grey lines represent low gene expression for chronic hepatitis C and the black lines high gene expression for chronic hepatitis C. (c) Comparison between ASH and NASH induced HCC. The light grey lines represent low gene expression for NASH, medium grey lines display high gene expression for NASH, the dark grey lines represent low gene expression for ASH and the black lines high gene expression for ASH [182].

4.3.1 Cox Regression

eIF5 is significant, both in a single covariate model (p=0.0225) as well as in a model including all available clinical information (p=0.0349). In fact, it is the only covariate which is significant at a level below 0.05 and has a large coefficient. A backward stepwise model selection approach eliminated all covariates except for eIF5, which displayed significance (0.0496) [182].

4.4 Members of the PI3K/AKT/mTOR Signaling Pathway and eIF Expression in Chronic Hepatitis C, HCV-Associated and Non-Virus Induced HCC

We investigated the expression patterns of eIFs and mTOR pathway members in chronic hepatitis C, HCV-associated HCC and non-virus related HCC patient samples using immunoblot analysis.

The protein expression levels of pmTOR and mTOR were significantly increased in HCV-associated HCC and HCC without viral background compared to control tissue (Figure 30, 31 and 32). The protein expression levels of the PI3K/AKT/mTOR pathway members' pmTOR, PTEN, pAKT and AKT were decreased in chronic hepatitis C compared to NNLT (Figure 31, 32 and 33). In comparison, pPTEN, PTEN, pAKT and AKT (Figure 30, 31 and 32) were significantly decreased in HCV-associated HCC and in HCC without viral background.

peIF2α, eIF2α and peIF4B (Figure 30, 32 and Figure 33) showed stronger protein expression in HCV cases, HCV-associated HCC and non-virus related HCC. Interestingly, the eIF3 subunits B, C, D and J as well as eIF4G, eIF6 (Figure 30, 32 and Figure 33) displayed higher protein expression levels in HCV-associated HCC compared to NNT. In HCC without viral background, eIF3C, eIF3I, eIF4E and eIF4G (Figure 30, 32 and Figure 33) showed increased protein levels compared to NNT. Interestingly, eIF5 (Figure 30, 32 and Figure 33) displayed decreased protein expression levels in HCC without viral background in comparison to NNT.

eIF3 subunits B and D as well as eIF4E, displayed decreased protein expression levels in HCV cases (Figure 30, 32 and Figure 33). eIF3H (Figure 30, 32 and Figure 33) showed a significantly downregulated protein level in HCV-associated HCC and HCC without viral background compared to NNT [182].

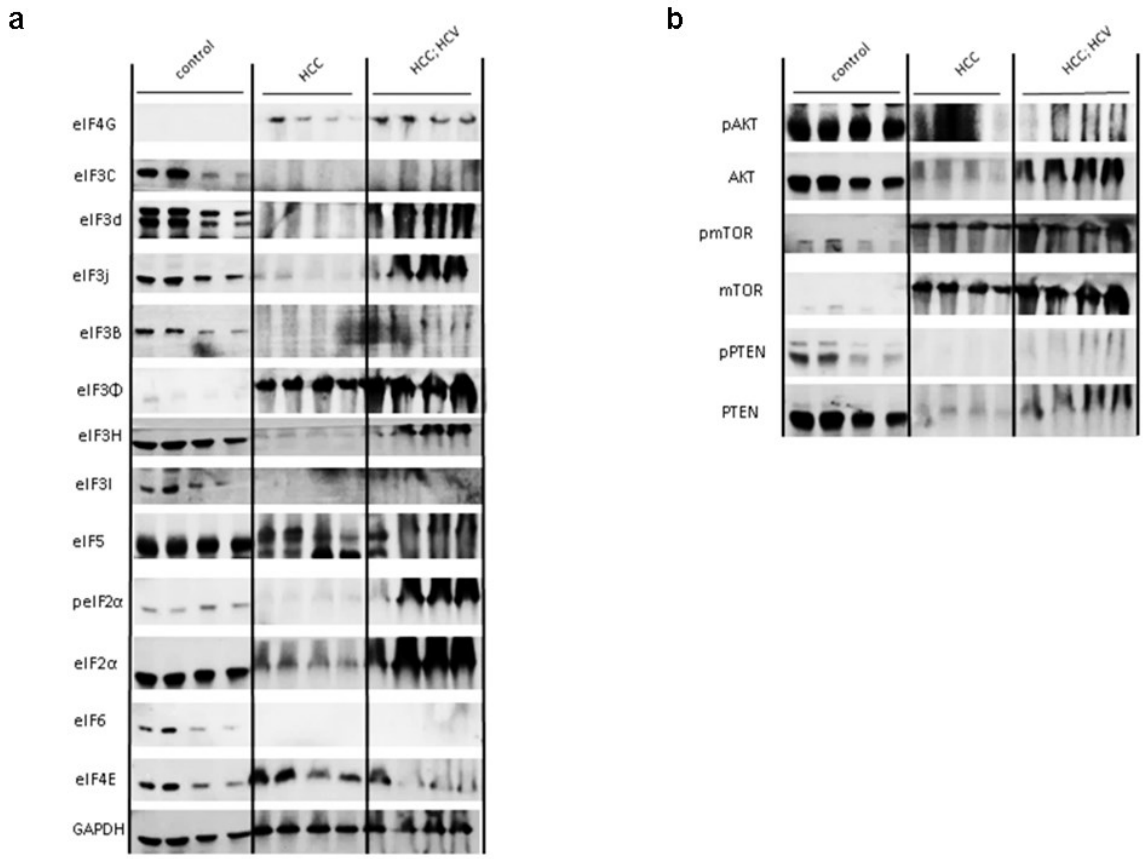

Figure 30: eIF and mTOR expression in HCC and HCV-associated HCC. (a) Immunoblot analyses from HCC and HCV-associated HCC compared to non-neoplastic tissues (NNT). Equal amounts of protein were resolved on SDS PAGE and immunoblotted with eIF subunits 4G, 3C, 3d, 3j, 3B, 3a, 3H, 3I, 5, p2α, 2α, 6, 4E and β-actin (loading control) antibodies. (b) Immunoblot analyses from HCC and HCV-associated HCC compared to NNT. Equal amounts of protein were resolved on SDS PAGE and immunoblotted with pmTOR, mTOR, pAKT, AKT, pPTEN, PTEN and β-actin (loading control) antibodies [182]. Three independent experiments were carried out.

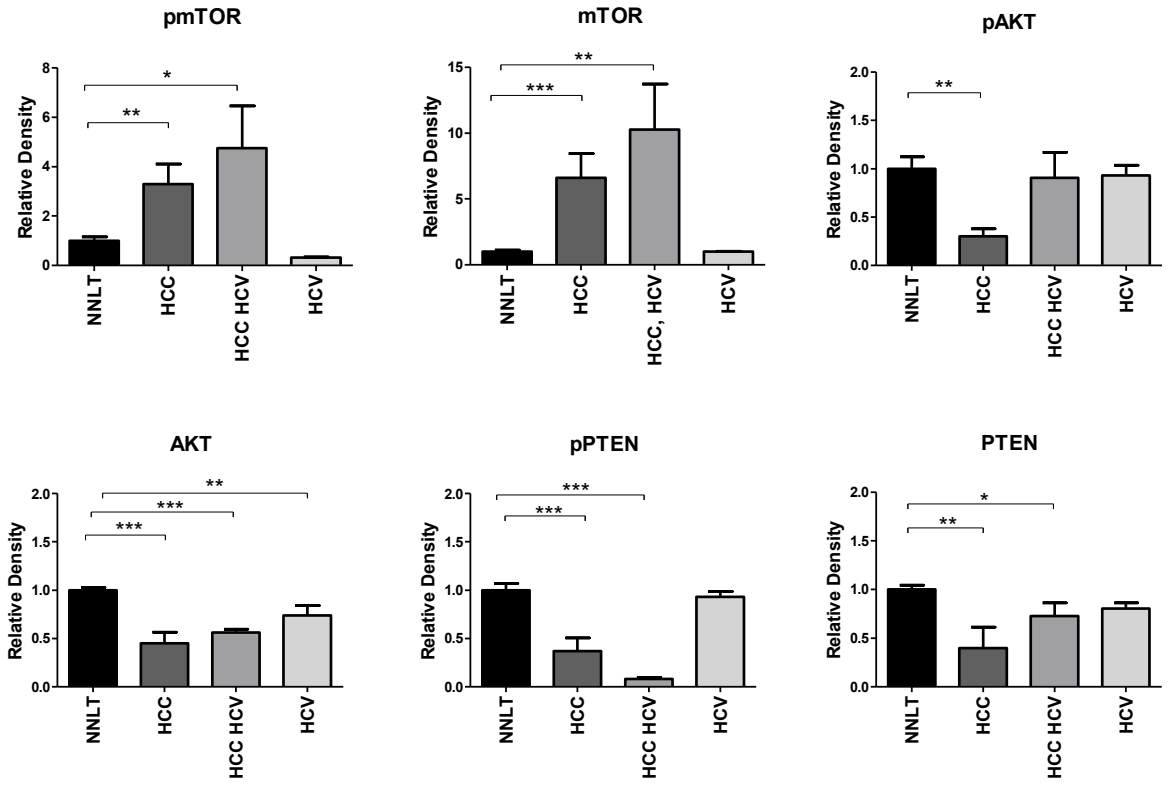

Figure 31: mTOR pathway members in chronic hepatitis C and HCV associated HCC and HCC without viral infection. Members of the mTOR signaling cascade were analyzed on protein level in HCV induced chronic hepatitis, HCV-associated HCC, HCC without viral infection compared to non-neoplastic liver tissue (NNLT) using immunoblot analyses. Densitometric analyses of immunoblots were performed using ImageJ software (NIH, MD, United States). Relative densities were normalized to the loading control (GAPDH). Statistical analyses: 1-way ANOVA with Bonferroni post-test *p< 0.05, **p< 0.01 and ***p< 0.001 [182].

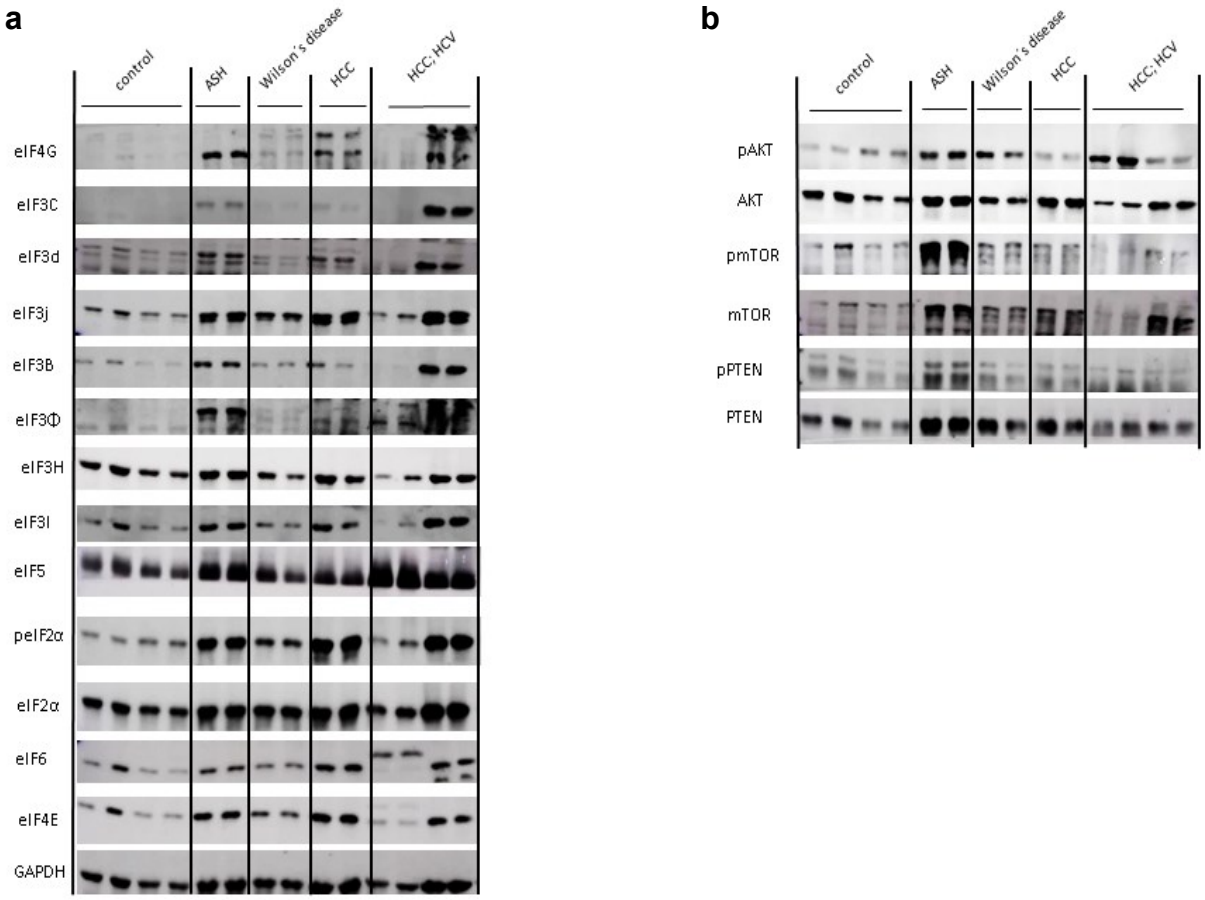

Figure 32: eIF and mTOR expression in ASH, Morbus Wilson, HCC and HCV-associated HCC. (a) Immunoblot analyses from ASH, Morbus Wilson, HCC and HCV-associated HCC. Equal amounts of protein were resolved on SDS PAGE and immunoblotted with eIF subunits 4G, 3C, 3d, 3j, 3B, 3a, 3H, 3I, 5, p2α, 2α, 6, 4E and β-actin (loading control) antibodies. (b) Immunoblot analyses from ASH, Wilson´s disease, HCC and HCV-associated HCC compared to NNLT. Equal amounts of protein were resolved on SDS PAGE and immunoblotted with pmTOR, mTOR, pAKT, AKT, pPTEN, PTEN and β-actin (loading control) antibodies [182]. Three independent experiments were carried out.

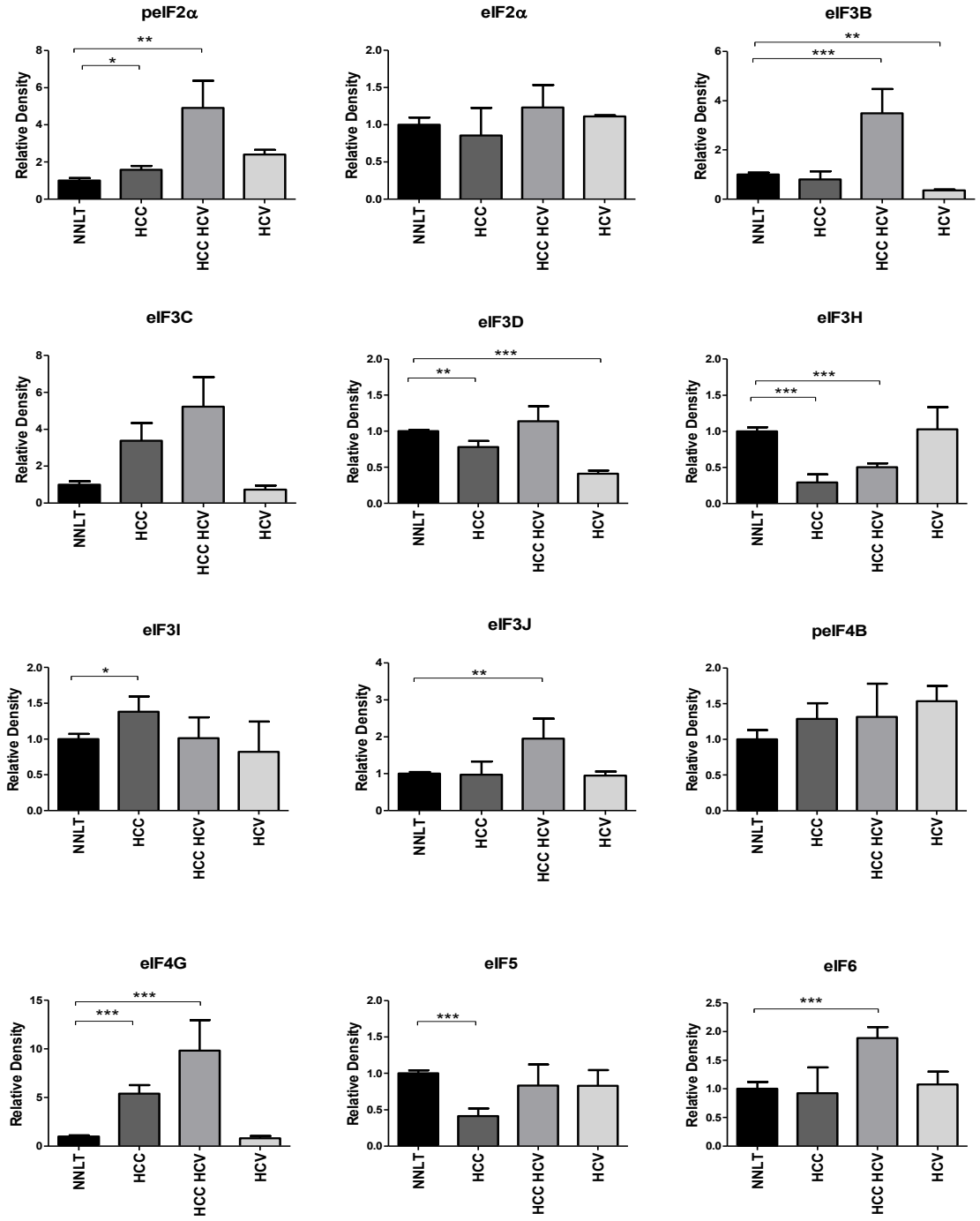

Figure 33: eIF protein expression in HCV - induced chronic hepatitis, HCV-associated HCC and HCC without viral infection.eIF protein expression in HCV, HCV-associated HCC and HCC compared to non-neoplastic tissue (NNT) was analyzed using immunoblot analyses. Alterations in protein expression pattern of peIF2α, eIF2α, eIF3B, eIF3C, eIF3D, eIF3H, eIF3I, eIF3J, peIF4B, eIF4E, eIF4G, eIF5 and eIF6. Densitometric analyses of immunoblots were performed using ImageJ software (NIH, MD, United States). Relative densities were normalized to the loading control (GAPDH).

Statistical analyses: 1-way ANOVA with Bonferroni post-test; *p< 0.05; **p< 0.01 and ***p< 0.001 [182].

4.5 Expression of Mmembers of the PI3K/AKT/mTOR Signaling Pathway and of eIFs in Chronic Hepatitis B, HBV-associated HCC and Non-Virus Induced HCC

We observed that PTEN, pAKT and AKT (Figure 34 and 35) showed significantly decreased protein expression levels in HBV-associated HCC and non-virus induced HCC compared to NNLT. The protein expression of the PI3K/AKT/mTOR pathway members (Figure 34 and 35) pmTOR and mTOR displayed a significant increase in non-virus induced HCC in comparison to NNLT. pPTEN (Figure 34 and 35) was significantly downregulated in non-virus induced HCC in comparison to NNLT. For PTEN (Figure 34 and 35), we observed a significantly increased protein expression level in chronic hepatitis B samples. We also observed downregulated protein levels of AKT (Figure 34 and 35) upon HBV infection when compared to NNLT [182].

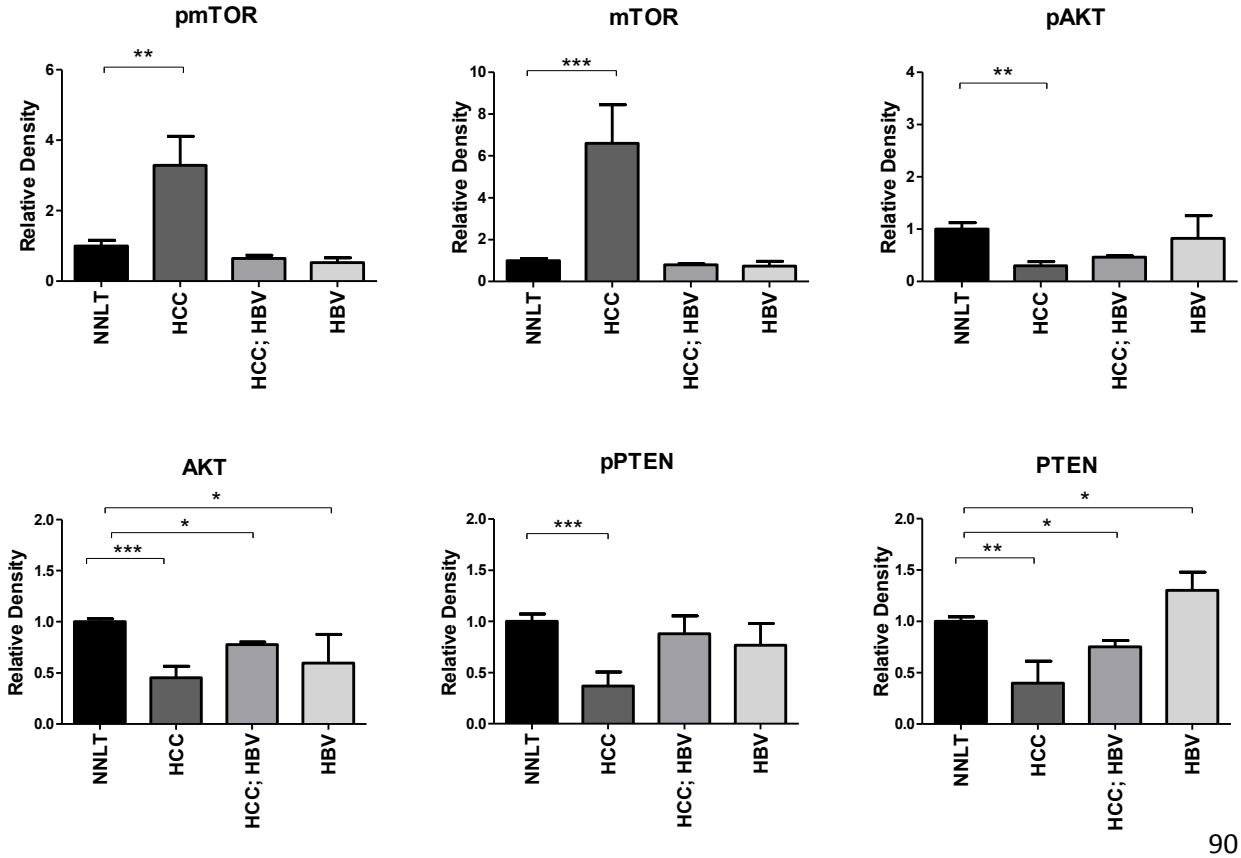

Figure 34: mTOR pathway members in chronic hepatitis B and HBV associated HCC and HCC without viral infection. Members of the mTOR signaling cascade were analyzed on protein level in HBV- induced chronic hepatitis, HBV-associated HCC and HCC without viral infection compared to NNLT using immunoblot analyses. Protein expression of pmTOR (g), mTOR (h), pPTEN (i), PTEN (j), pAKT (k), AKT (l). Densitometric analyses of immunoblots were performed using ImageJ software (NIH, MD, United States). Relative densities were normalized to the loading control (GAPDH). Statistical analyses: 1-way ANOVA with Bonferroni post-test *p< 0.05, **p< 0.01 and ***p< 0.001 [182].

peIF2α, eIF3C, eIF3I, eIF4E and eIF4G (Figure 35 and 36) showed a significantly stronger protein expression in non-virus induced HCC compared to NNLT. For the eIF subunits p2α, p4B, 4G and 5 (Figure 35 and 36), we detected a significant increase on protein level in HBV-associated HCC and HBV in comparison to NNLT. Interestingly, eIF2α, eIF3H, eIF3I, eIF4E and eIF6 (Figure 35 and 36) showed decreased protein expression in HBV-associated HCC and chronic hepatitis B compared to NNLT. Furthermore, eIF3H and eIF5 displayed a significantly lower expression in non-virus induced HCC in comparison to NNLT (Figure 35 and 36). The eIF3 subunits B, D, and J showed decreased protein levels in HBV-associated HCC (Figure 35 and 36) [182].

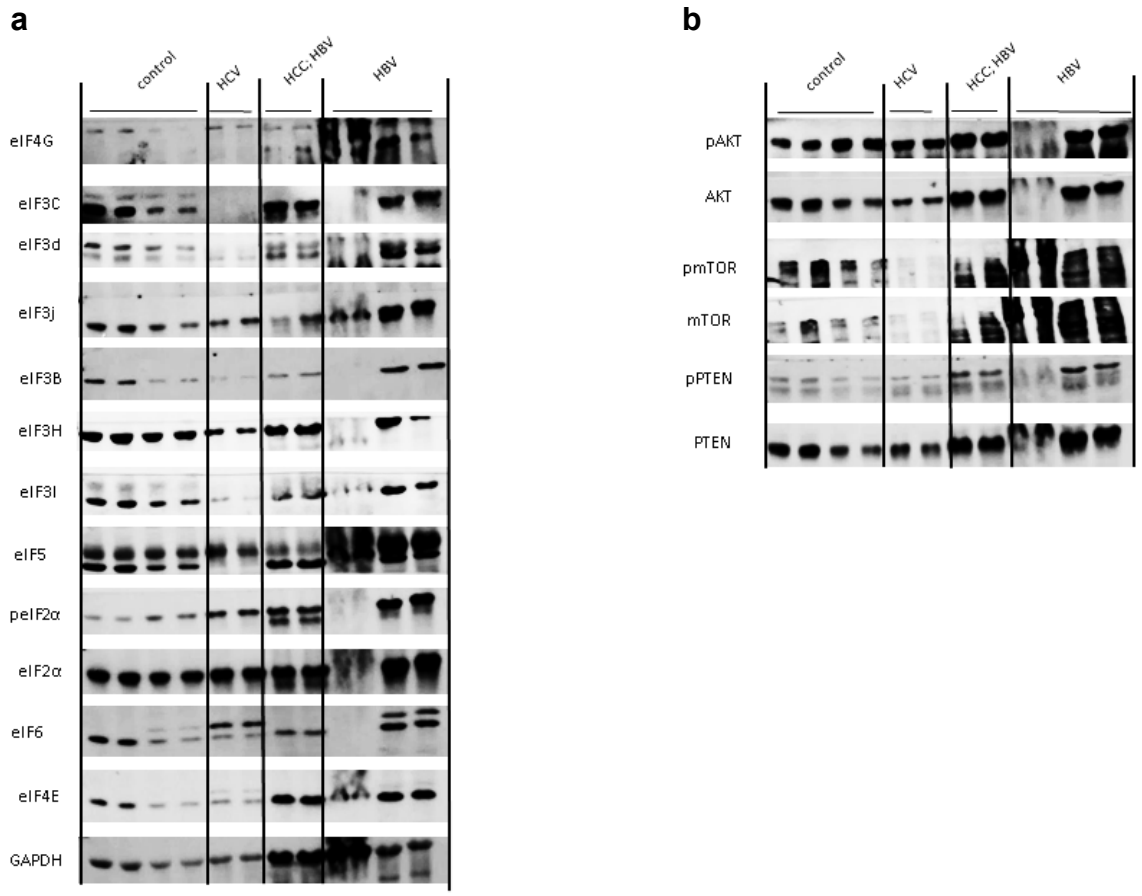

Figure 35: eIF and mTOR expression in chronic hepatitis C, HBV-associated HCC and chronic hepatitis B. Immunoblot analyses from chronic hepatitis C, HBV-associated HCC and chronic hepatitis B. Equal amounts of protein were resolved on SDS PAGE and immunoblotted with eIF subunits 4G, 3C, 3d, 3j, 3B, 3a, 3H, 3I, 5, p2α, 2α, 6, 4E and β-actin (loading control) antibodies. Immunoblot analyses from chronic hepatitis C, HBV-associated HCC and chronic hepatitis B compared to non-neoplastic tissues (NNLT).Equal amounts of protein were resolved on SDS PAGE and immunoblotted with pmTOR, mTOR, pAKT, AKT, pPTEN, PTEN and β-actin (loading control) antibodies [182]. Three independent experiments were carried out.

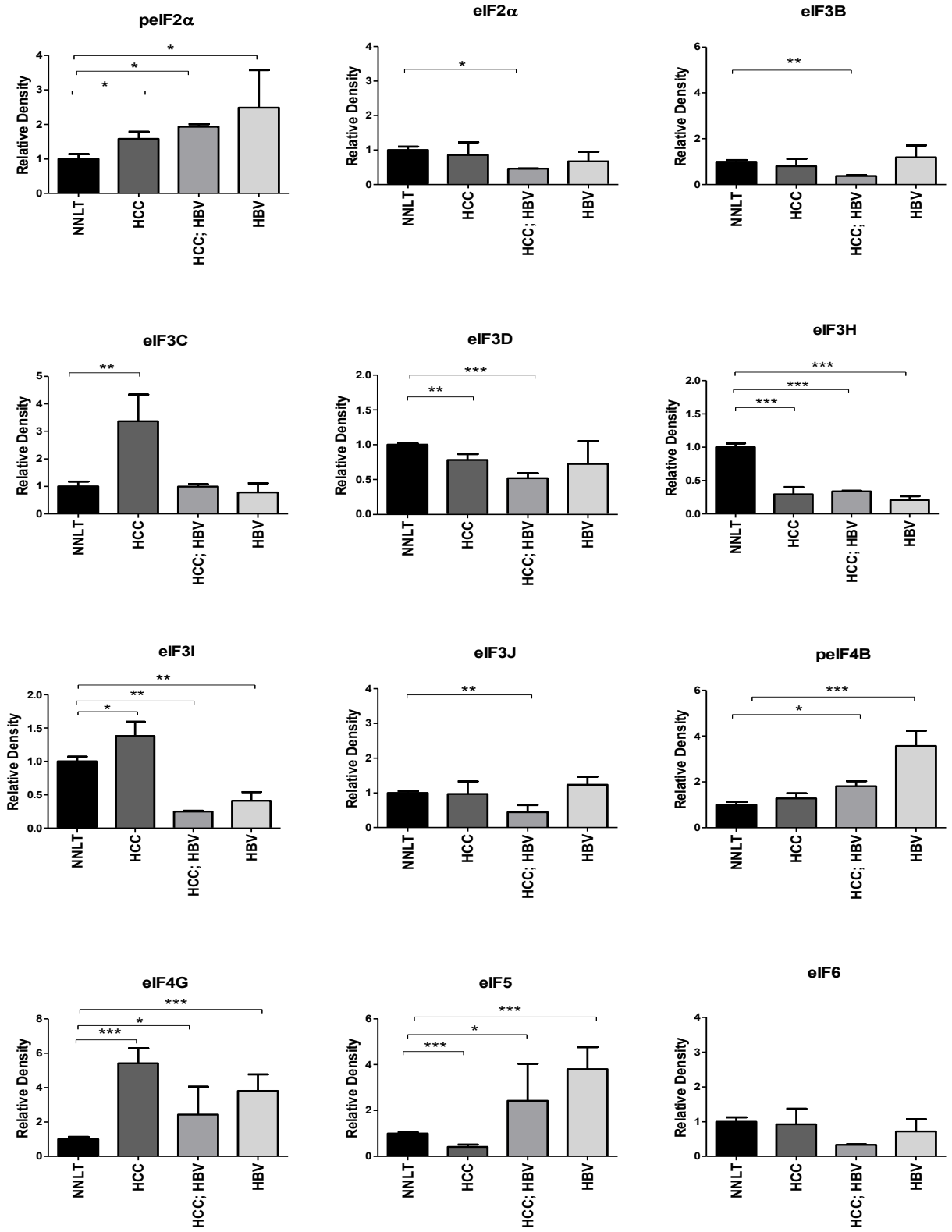

Figure 36: eIF protein expression in chronic hepatitis B, HBV-associated HCC and HCC without viral infection. eIF protein expression in HBV induced chronic hepatitis, HBV-associated HCC and

HCC without viral infection compared to non-neoplastic tissue (NNLT) was analyzed using immunoblot analyses. Alterations in protein expression pattern of peIF2α, eIF2α, eIF3B, eIF3C, eIF3D, eIF3H, eIF3I, eIF3J, peIF4B, eIF4E, eIF4G, eIF5 and eIF6 .Densitometric analyses of immunoblots were performed using ImageJ software (NIH, MD, United States). Relative densities were normalized to the loading control (GAPDH). Statistical analyses: 1-way ANOVA with Bonferroni post-test *p< 0.05; **p< 0.01 and ***p< 0.001 [182].

4.6 Members of the PI3K/AKT/mTOR Signaling Pathway and eIF Expression in Alcoholic Steatohepatitis and Morbus Wilson

The protein expression of the mTOR pathway member's pmTOR, mTOR, PTEN and pAKT was clearly increased in ASH and Morbus Wilson compared to NNLT (Figure 37 and 38). AKT displayed a significant decrease in ASH compared to NNLT (Figure 37 and 38) [182].

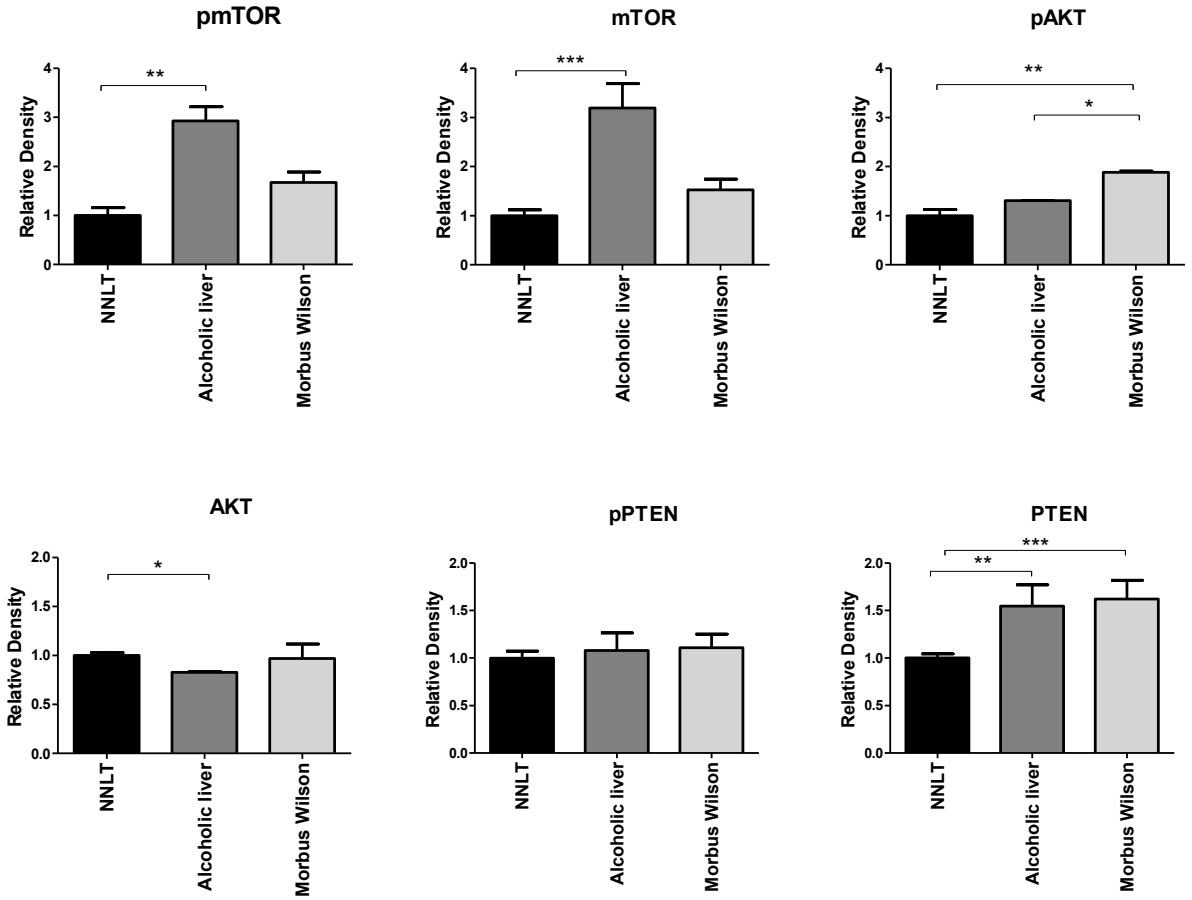

Figure 37: mTOR signaling in alcoholic livers and Morbus Wilson. Members of the mTOR signaling cascade were analyzed on protein level in ASH livers and Morbus Wilson compared to non-neoplastic tissues (NNLT) using immunoblot analyses. Protein expression of pmTOR, mTOR, pPTEN, PTEN, pAKT, AKT .Densitometric analyses of immunoblots using ImageJ software (NIH, MD, United States). Relative densities were normalized to the loading control (GAPDH). Statistical analyses: 1-way ANOVA with Bonferroni post-test; *p< 0.05; **p< 0.01 and ***p< 0.001 [182].

peIF2α, eIF2α, eIF3B, eIF3C, eIF3J, eIF4E, eIF4G and eIF6 were significantly upregulated in ASH and Morbus Wilson compared to NNLT (Figure 39 and 40). Furthermore, eIF3D, eIF3I and peIF4B displayed increased protein expression levels in ASH in comparison to NNLT (Figure 38 and 39). Interestingly, eIF3D, eIF3I and peIF4B (Figure 38 and 39) showed decreased protein expression levels in Morbus Wilson compared to NNLT. We observed decreased eIF3H (Figure 38 and 39) protein expression levels in ASH and Morbus Wilson compared to NNLT [182].

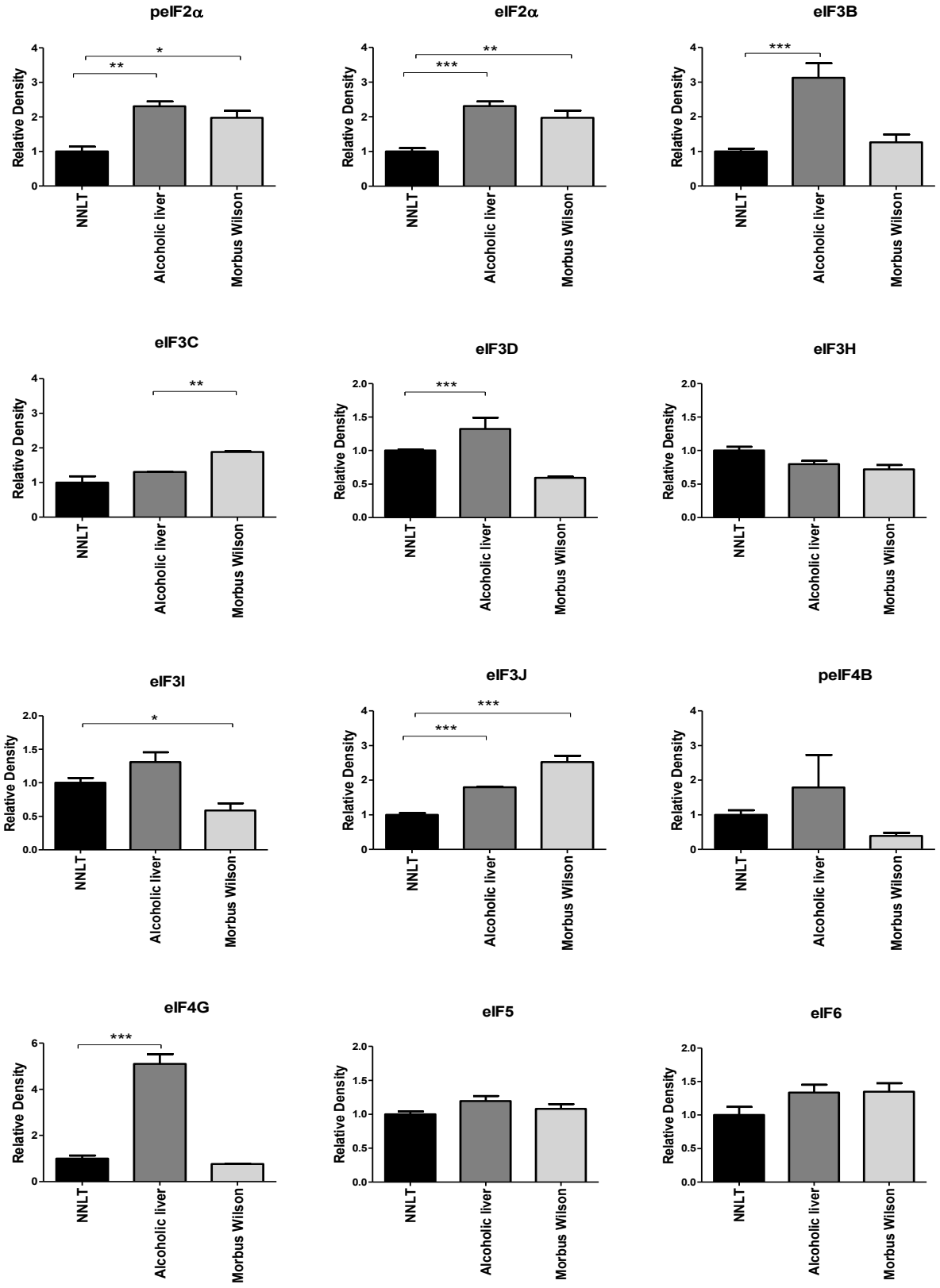

Figure 38: eIF protein expression in ASH and Morbus Wilson. eIF protein expression in alcoholic livers and Wilson´s disease compared to NNLT were analyzed using immunoblot analyses. Alterations

in protein expression patterns of peIF2α, eIF2α, eIF3B, eIF3C, eIF3D, eIF3H , eIF3I , eIF3J , peIF4B , eIF4E , eIF4G , eIF5 and eIF6 . Densitometric analyses of immunoblots were analyzed using ImageJ software (NIH, MD, United States). Relative densities were normalized to the loading control (GAPDH). Statistical analyses: 1-way ANOVA with Bonferroni post-test *p< 0.05; **p< 0.01 and ***p< 0.001 [182].

5 Results Colorectal Carcinoma

5.1 Immunohistochemistry of Primary CRC Patients and Liver Metastases from Primary CRC

The expression of eIF1, eIF2α, eIF3A, eIF3B, eIF3C, eIF4E, eIF4G and eIF6 in CRC patients and liver metastasis from primary CRC patient material was assessed by one experienced and board certified pathologist (J.H.). The distribution of eIF staining was mainly cytoplasmic. Staining intensity, describing the percentage of tumor cells with positive staining, ranged from 0 – 100%. The intensity score (IS) ranged from 0 to 3 resembling the weak to intense, light to dark brown signals, respectively.

The subunits eIF1, 2α, 3H and 4G exhibited stronger staining in the metastatic tissues compared to NNLT (Figure 39 and 40). The staining intensities for eIF3A, eIF3B, eIF4E and eIF6 were increased compared to NNLT, but were weaker for the eIF subunits 1, 2α, 3H, 4G (Figure 39 and 40). eIF3C staining was only weak to moderate in the metastases (Figure 39 and 40). IHC staining intensity of the subunits eIF1, 2α, 3A, 3B, 3H, 4E, 4G and 6 was stronger in the RC metastases, and no staining was found in the NNLT (Figure 42). Only for eIF3C weak to moderate staining was found in RC metastases (Figure 42). The IHC data displayed stronger eIF expression in RC metastases compared to CC metastases (Figure 41 and 42).

In primary CC and RC patients the IHC staining for eIF2α and eIF3H was strong in approximately 100% of CRC tissue samples and non-neoplastic mucosa (NNM) (Figure 41 and 42). Staining for eIF3A, eIF3B, eIF1, eIF4E, eIF4G and eIF6 was strong to weak, with irregular expression patterns (Figure 41 and 42) [181].

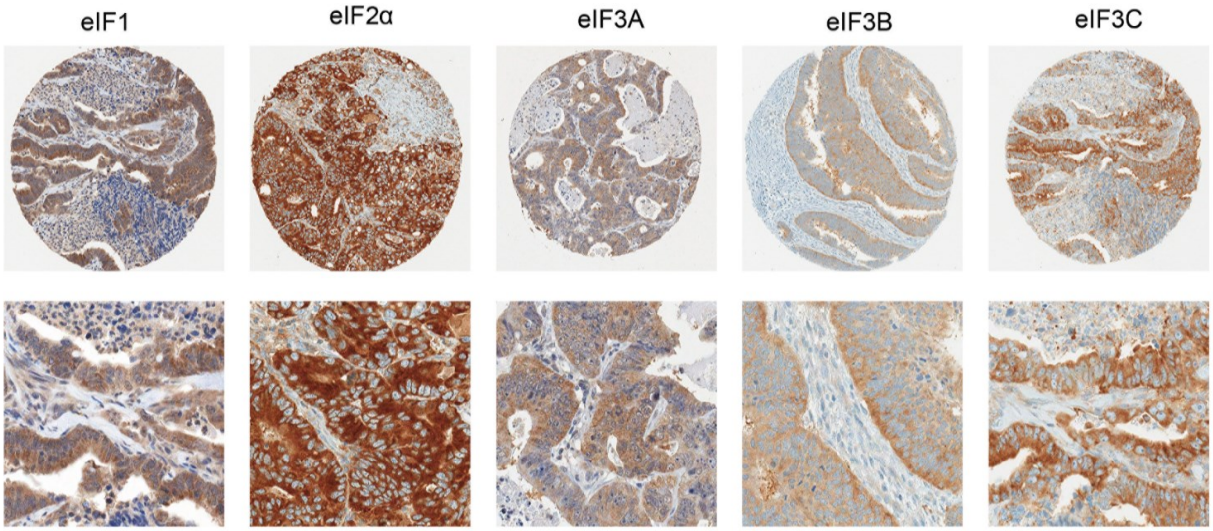

Figure 39: Immunohistochemical distribution for eIF1, eIF2α, eIF3A, eIF3B, eIF3C in low and high grade CC and liver metastases of primary CC. Scale bars: 200 nm and 50nm [181].

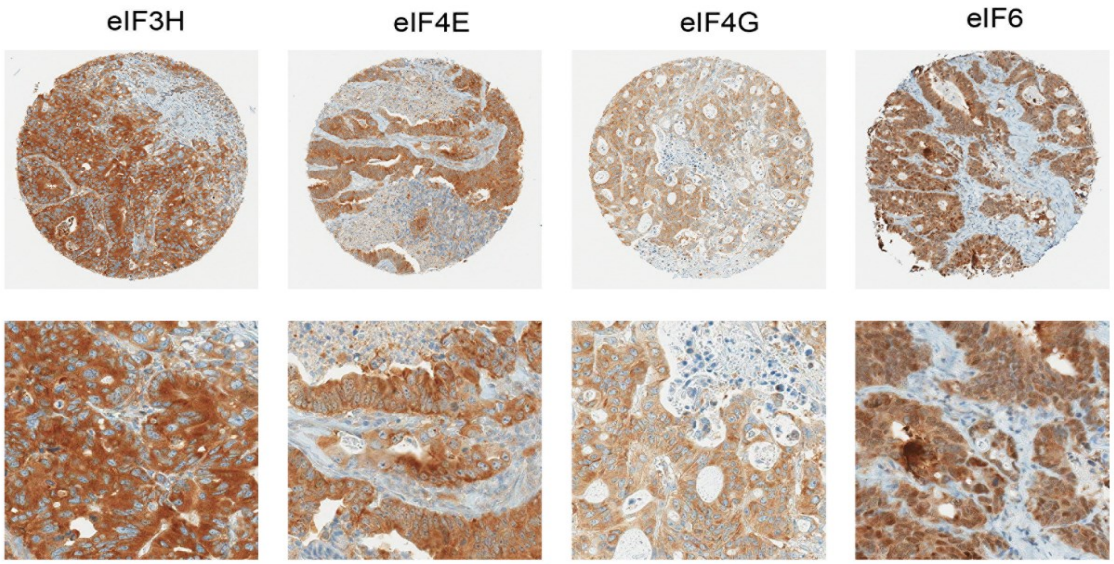

Figure 40: **Immunohistochemical distribution for eIF3H, eIF4E, eIF4G and eIF6 in low and high grade CC and liver metastases of primary CC.** Scale bars: 200 nm and 50nm [181].

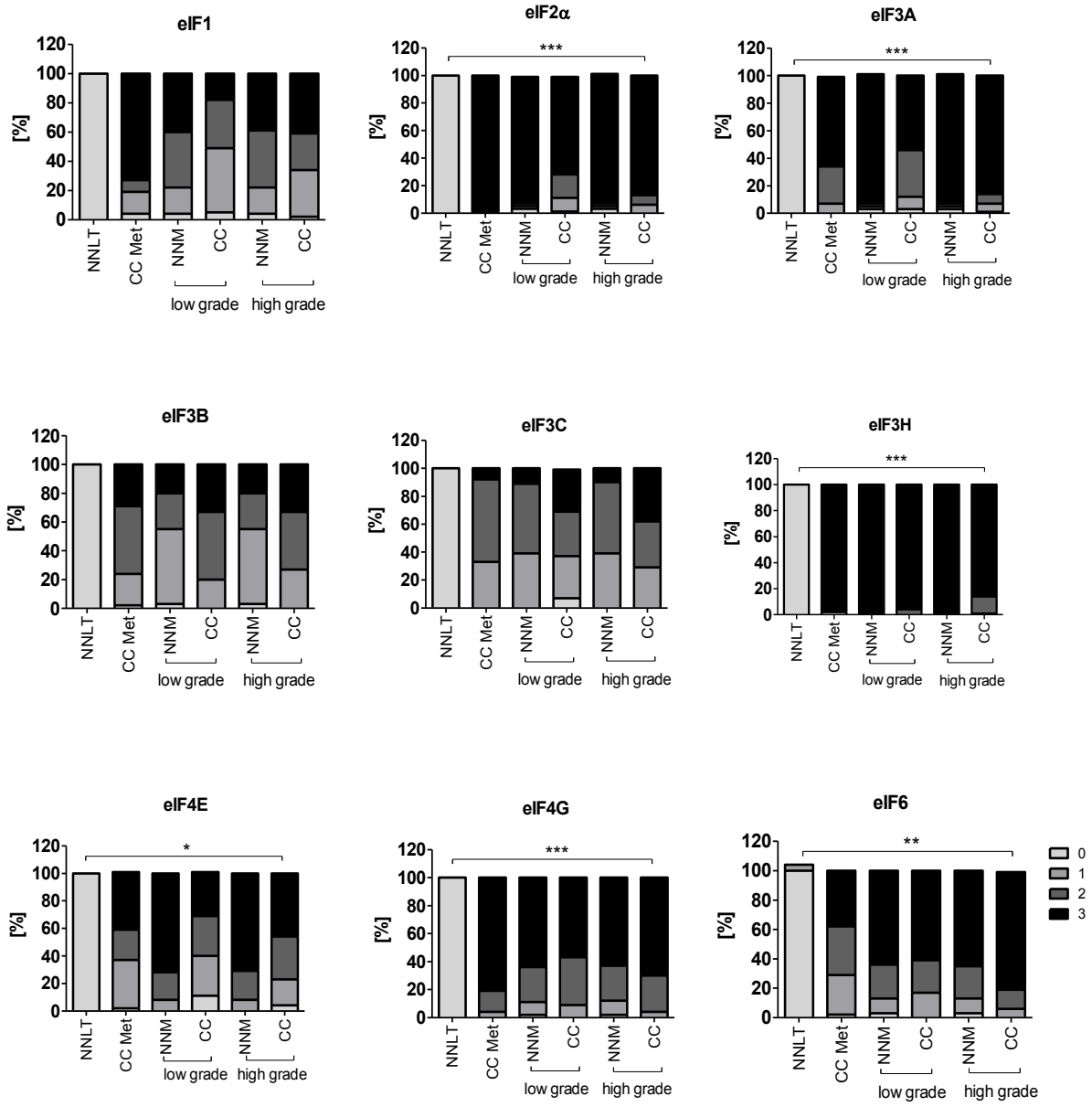

Figure 41: Densitometric analysis of immunohistochemical staining from various eIF subunits in liver metastases of primary colon carcinomas (CC- Met) compared to NNLT and primary colon carcinomas compared to (NNM) [181]. Three independent experiments were carried out. Bars represent mean ± SEM. *p < 0.05, **p < 0.01, ***p < 0.001.

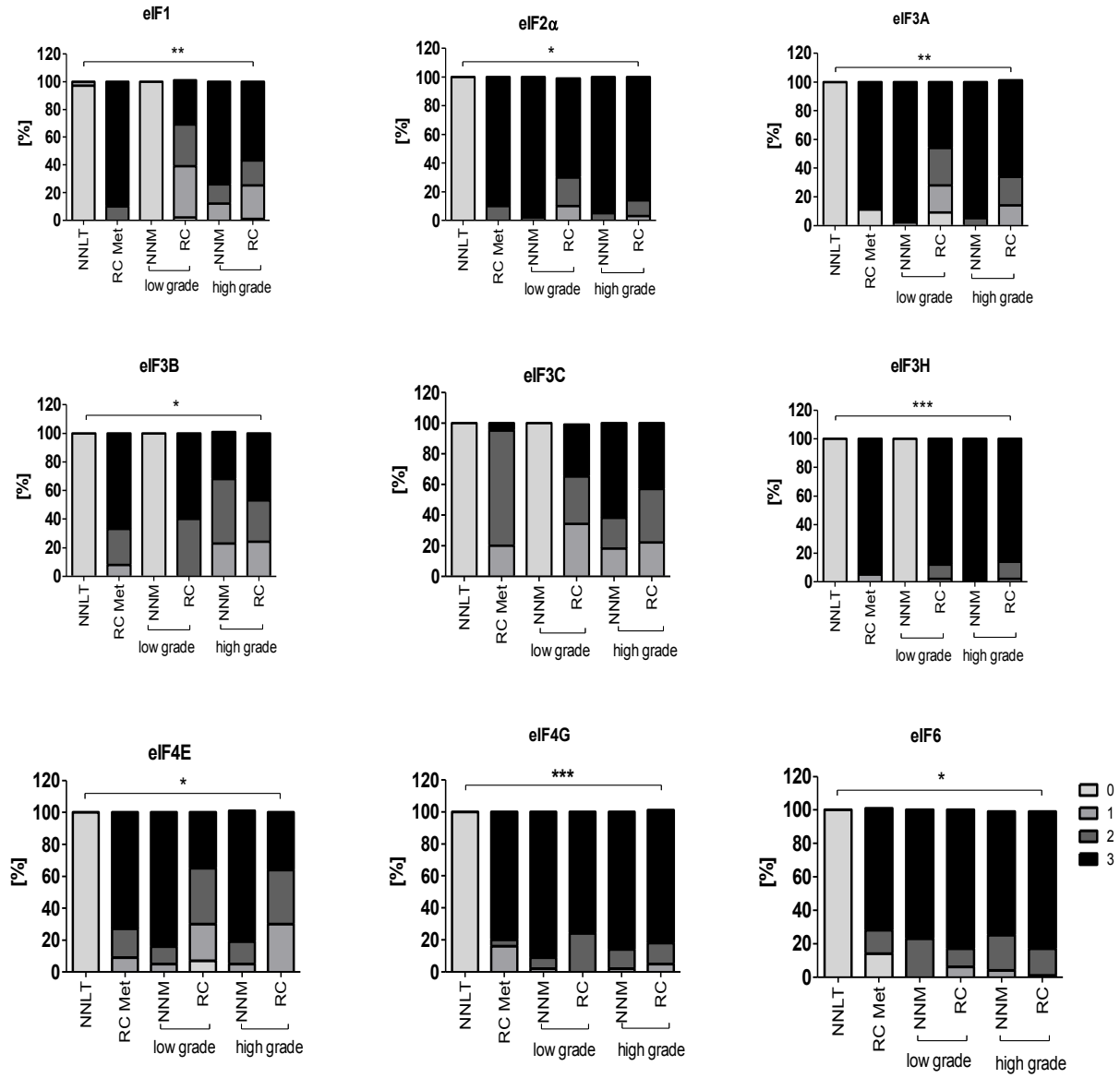

Figure 42: Densitometric analysis of immunohistochemical staining from various eIF subunits in liver metastases of primary rectum carcinomas (RC- Met) compared to NNLT and primary RC compared to NNM [181]. Three independent experiments were carried out. Bars represent mean ± SEM. *p < 0.05, **p < 0.01, ***p < 0.001.

5.2 Kaplan-Meier Curves from Potential mTOR Members and eIFs

Datasets from the TCGA database were investigated to identify mTOR members and eIF genes that were significantly altered in CRC. Kaplan-Meier curves were drawn to assess a potential association of mTOR members and eIF expression with overall survival in CC and RC patients. The median mTOR and eIF mRNA expression in all CC and RC tissues was used as the cutoff point to divide all cases into low and high grade CC (n = 201) and RC (n = 70) groups. As shown in Figure 53 there was a significant difference in the survival between patients with low and high grade CC (eIF1 p = 0.013; eIF5 p = 0.019; eIF6 p = 0.015) group. However, there were no significant differences in overall survival between low and high grade RC groups (Figure 53).

As shown in Figure 43, there was a significant difference in survival between patients with low and high grade CC for mTOR (p = < 0.001), PTEN (p = 0.016), p70S6K (p = 0.016), AKT1 (p = 0.020), AKT2 (p = 0.024) and AKT3 (p = 0.021), but there were no significant differences in overall survival between low and high grade RC groups (Figure 44) for mTOR (p = 0.325), PTEN (p = 0.462), p70S6K (p = 0.157), AKT1 (p = 0.285), AKT2 (p = 0.281) and AKT3 (p = 0.112). As shown in Figure 45, there was a significant difference in survival between patients with low and high grade CC for AMPK1 (p = < 0.010), AMPK2 (p = 0.011), Rictor (p = 0.017), Raptor (p = 0.016) and RPS6 (p = 0.019). There were no significant differences in overall survival between low and high grade RC groups for AMPK1 (p = 0.304), AMPK2 (p = 0.220), Rictor (p = 0.349), Raptor (p = 0.566) and RPS6 (p = 0.197) (Figure 46). As shown in Figure 47, there was a significant difference in survival between patients with low and high grade CC for eIF2S1 (p = 0.024), eIF3A (p = 0.011), eIF3B (p = 0.013), eIF3C (p = 0.013), eIF3D (p = 0.022) and eIF3H (p = 0.024). There were no significant differences in overall survival between low and high grade RC groups for eIF2S1 (p = 0.220), eIF3A (p = 0.258), eIF3B (p = 0.208), eIF3C (p = 0.083), eIF3D (p = 0.242) and eIF3H (p = 0.024) (Figure 48). Figure 49 showed a significant difference in survival between patients with low and high grade CC for eIF3I (p = 0.008), eIF3J (p = 0.026), eIF3K (p = 0.006), eIF3M (p = 0.018), eIF4B (p = 0.004) and eIF4E (p = 0.003). There were no significant differences in overall survival between low and high grade RC groups for eIF3I (p = 0.456), eIF3J (p = 0.311), eIF3K (p = 0.636), eIF4B (p = 0.093) and eIF4E (p = 0.596) (Figure 50). For eIF3M (p = 0.018) there was a significant difference in survival between low and high grade RC groups. There was a significant difference in the survival between patients with low grade and high grade CC for eIF4G1 (p = 0.005), eIF4G2 (p = 0.011), and eIF4G3 (p = 0.011) shown in Figure 51. There were no

significant differences for eIF4G1 (p = 0.247) and eIF4G3 (p = 0.663). For eIF4G2 (p = 0.011) there was a significant difference in the survival between low and high grade RC groups (Figure 52) [181].

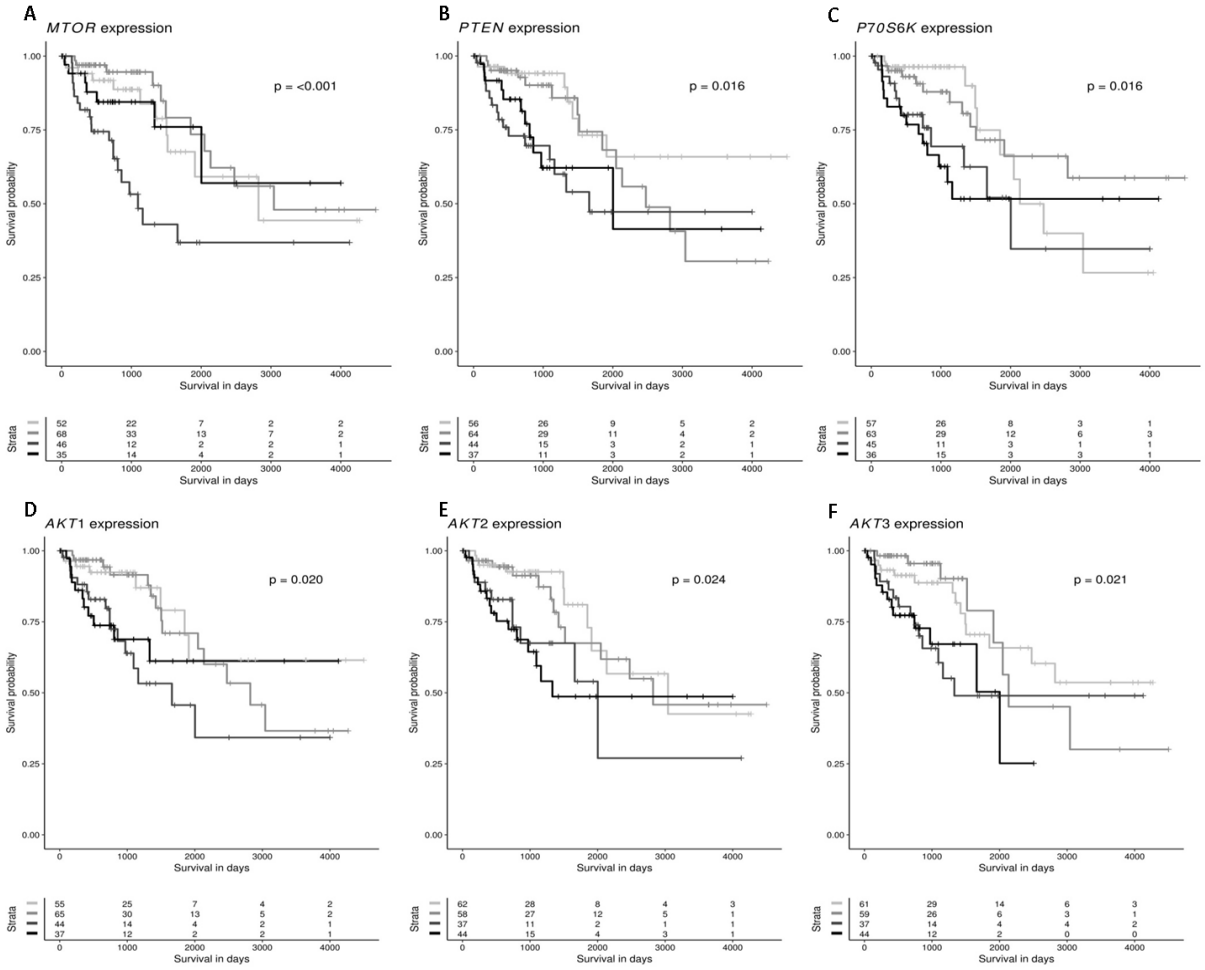

Figure 43: Kaplan-Meier curves of mTOR, PTEN, p70S6K and AKT expression on overall survival for CC. Cases are subdivided in mTOR, PTEN, p70S6K and AKT low or high expressers according to whether expression is below or above median and survival is compared using the log-rank test. The light grey lines represent low tumor grade with low gene expression, medium grey lines display low tumor grade with high gene expression, the dark grey lines represent high tumor grade with low gene expression and the black lines high tumor grade with high gene expression. [A] mTOR dataset; [B] PTEN dataset; [C] p70S6K dataset; [D] AKT1 dataset; [E] AKT2 dataset and [F] AKT3 dataset [181].

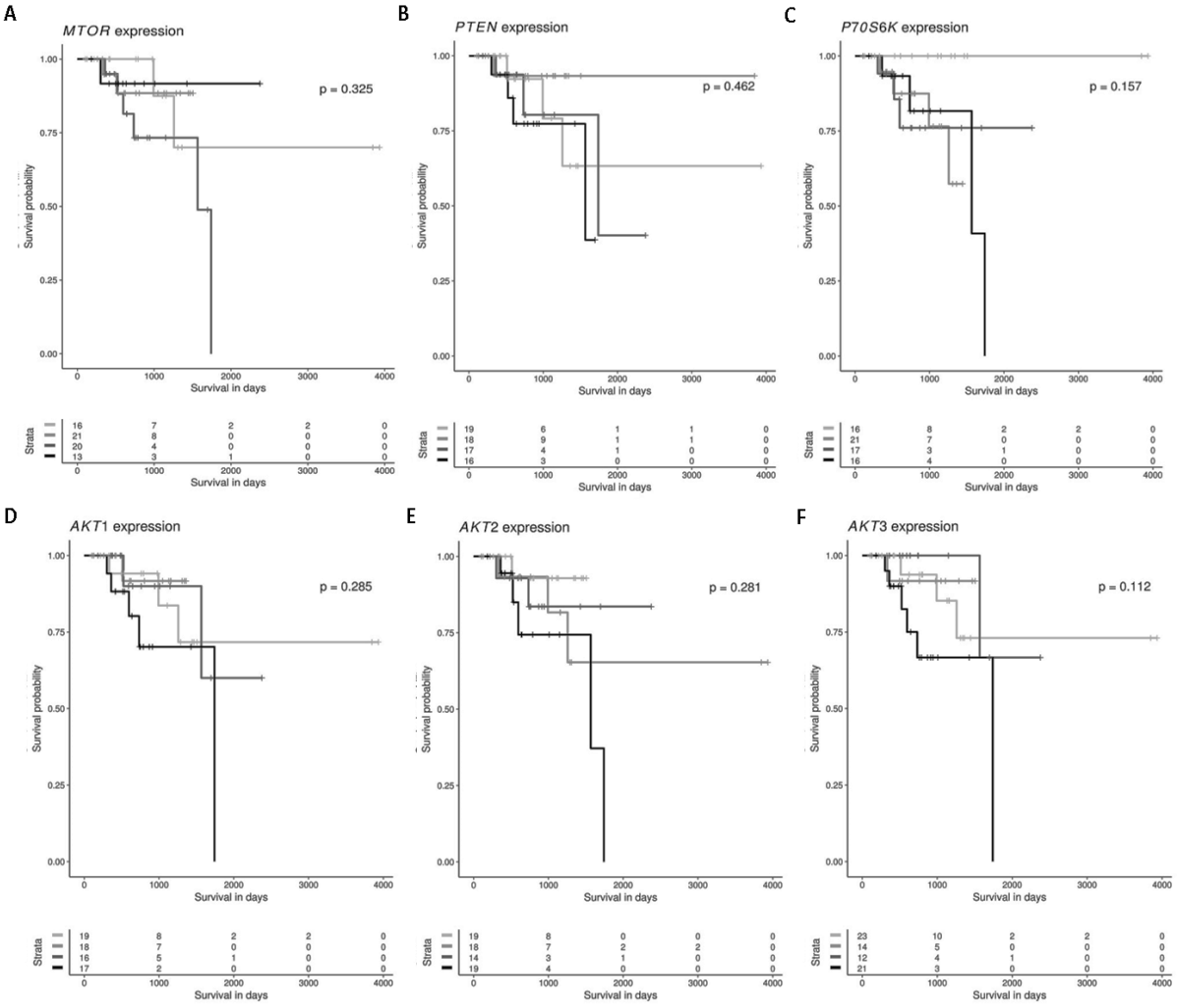

Figure 44: Kaplan-Meier curves of mTOR, PTEN, p70S6K and AKT expression on overall survival for RC. Cases are subdivided in mTOR, PTEN, p70S6K and AKT low or high expressers according to whether expression is below or above median and survival are compared using the log-rank test. The light grey lines represent low tumor grade with low gene expression, medium grey lines display low tumor grade with high gene expression, the dark grey lines represent high tumor grade with low gene expression and the black lines high tumor grade with high gene expression. [A] mTOR dataset; [B] PTEN dataset; [C] p70S6K dataset; [D] AKT1 dataset; [E] AKT2 dataset and [F] AKT3 dataset [181].

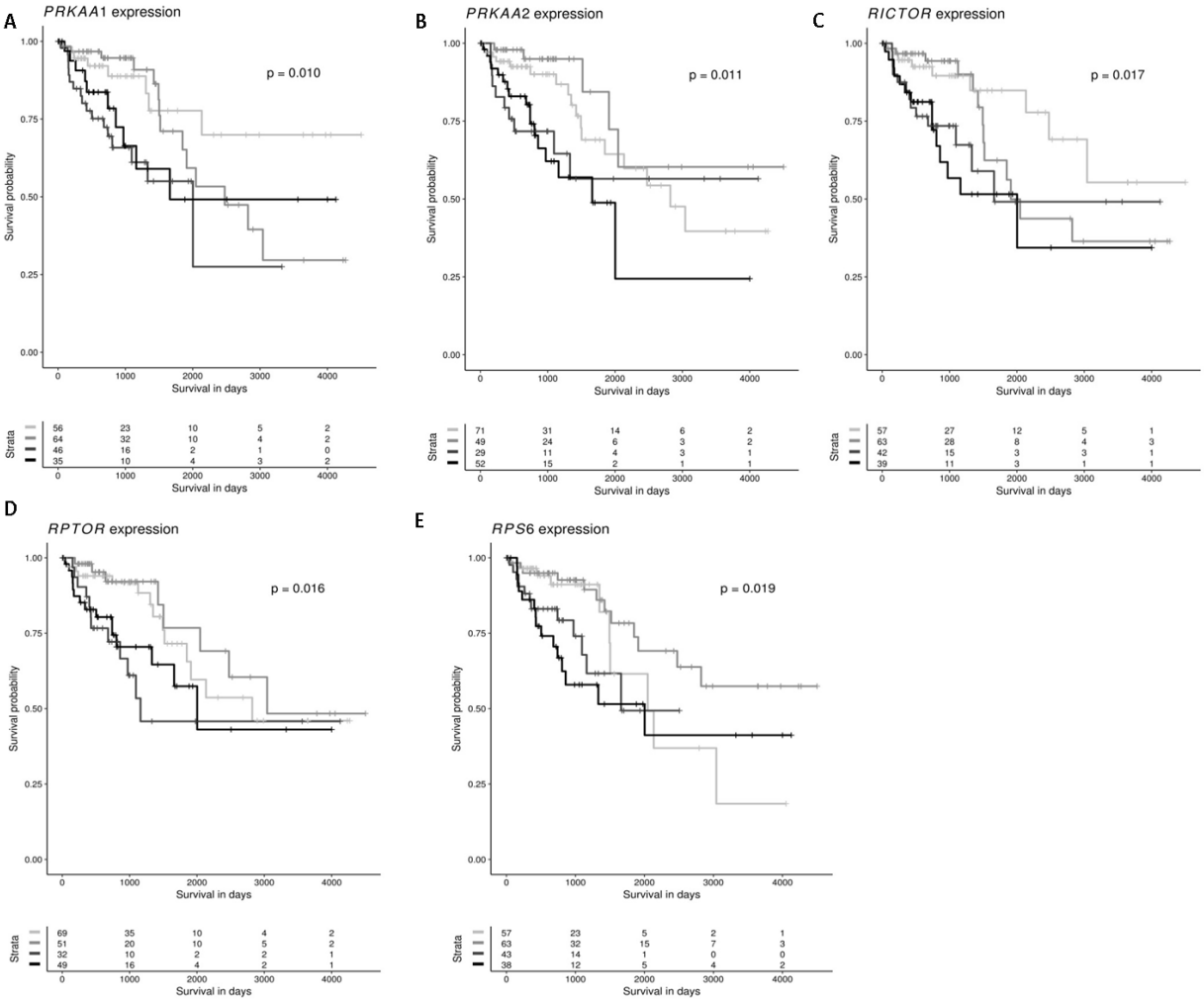

Figure 45: Kaplan-Meier curves of PRKAA1, PRKAA2, Rictor, Raptor and RPS6 expression on overall survival for CC. Cases are subdivided PRKAA1, PRKAA2, Rictor, Raptor and RPS6 low or high expressers according to whether expression is below or above median and survival is compared using the log-rank test. The light grey lines represent low tumor grade with low gene expression, medium grey lines display low tumor grade with high gene expression, the dark grey lines represent high tumor grade with low gene expression and the black lines high tumor grade with high gene expression. [A] PRKAA1 dataset; [B] PRKAA2 dataset; [C] Rictor dataset; [D] Raptor dataset; and [E] RPS6 dataset [181].

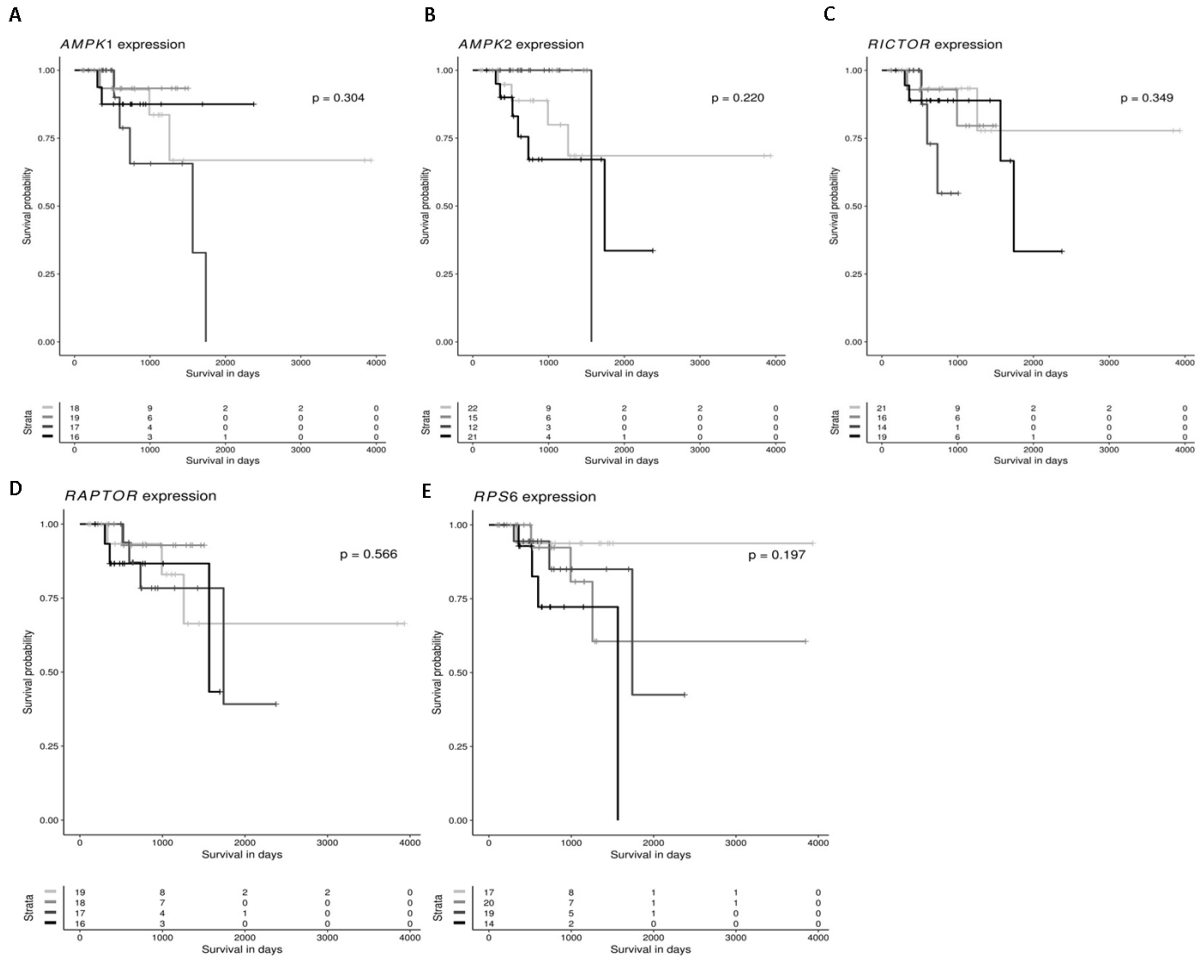

Figure 46: Kaplan-Meier curves of AMPK1, AMPK2, Rictor, Raptor and RPS6 expression on overall survival for RC. Cases are subdivided AMPK1, AMPK2, Rictor, Raptor and RPS6 low or high expressers according to whether expression is below or above median and survival is compared using the log-rank test. The light grey lines represent low tumor grade with low gene expression, medium grey lines display low tumor grade with high gene expression, the dark grey lines represent high tumor grade with low gene expression and the black lines high tumor grade with high gene expression. [A] AMPK1 dataset; [B] AMPK2 dataset; [C] Rictor dataset; [D] Raptor dataset; and [E] RPS6 dataset [181].

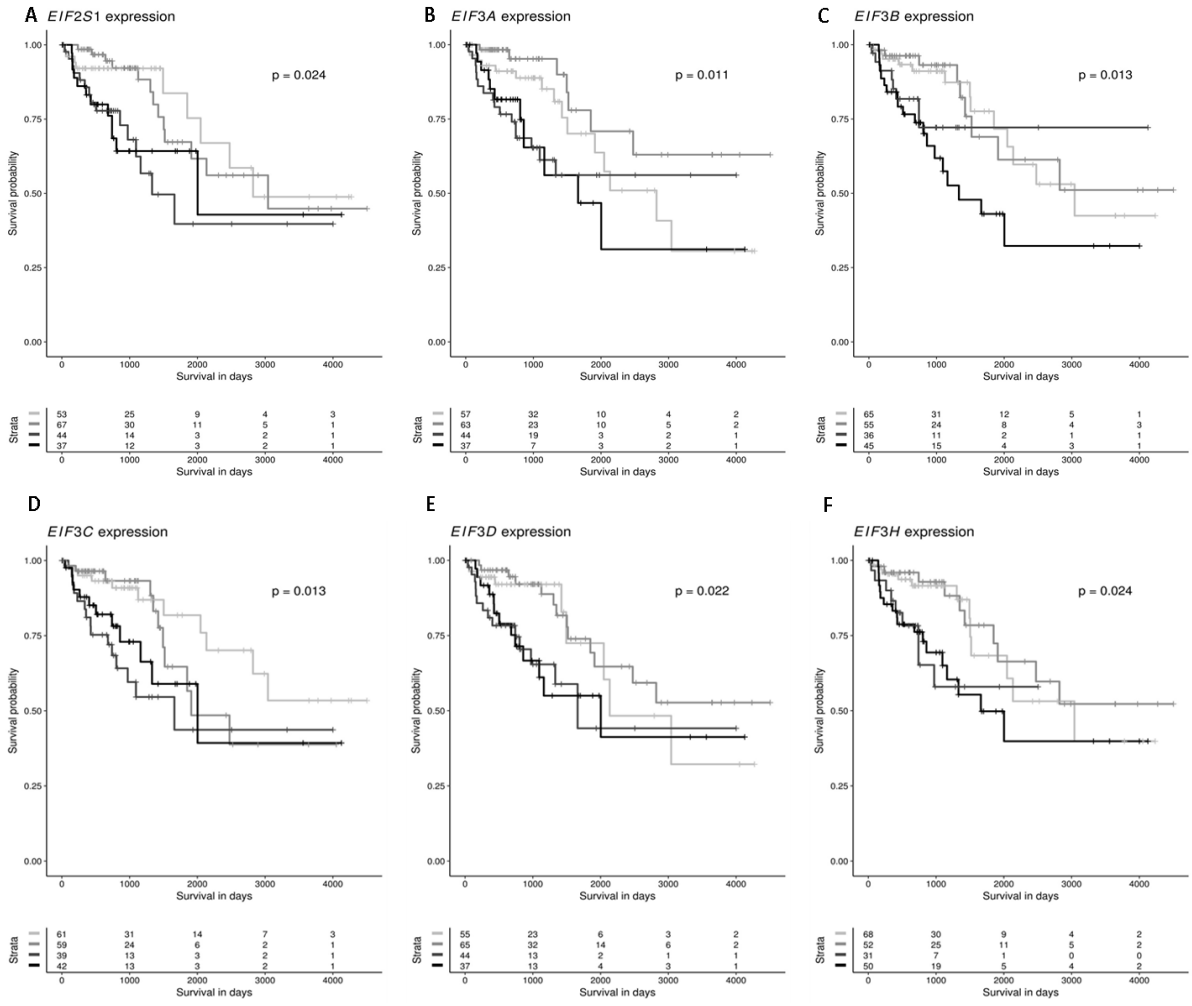

Figure 47: Kaplan-Meier curves of eIF2S1, eIF3A, eIF3B, eIF3C, eIF3D and eIF3H expression on overall survival for CC. Cases are subdivided in eIF2S1, eIF3A, eIF3B, eIF3C, eIF3D and eIF3H low or high expressers according to whether expression is below or above median and survival is compared using the log-rank test. The light grey lines represent low tumor grade with low gene expression, medium grey lines display low tumor grade with high gene expression, the dark grey lines represent high tumor grade with low gene expression and the black lines high tumor grade with high gene expression. [A] eIF2S1 dataset; [B] eIF3A dataset; [C] eIF3B dataset; [D] eIF3C dataset; [E] eIF3D dataset and [F] eIF3H dataset [181].

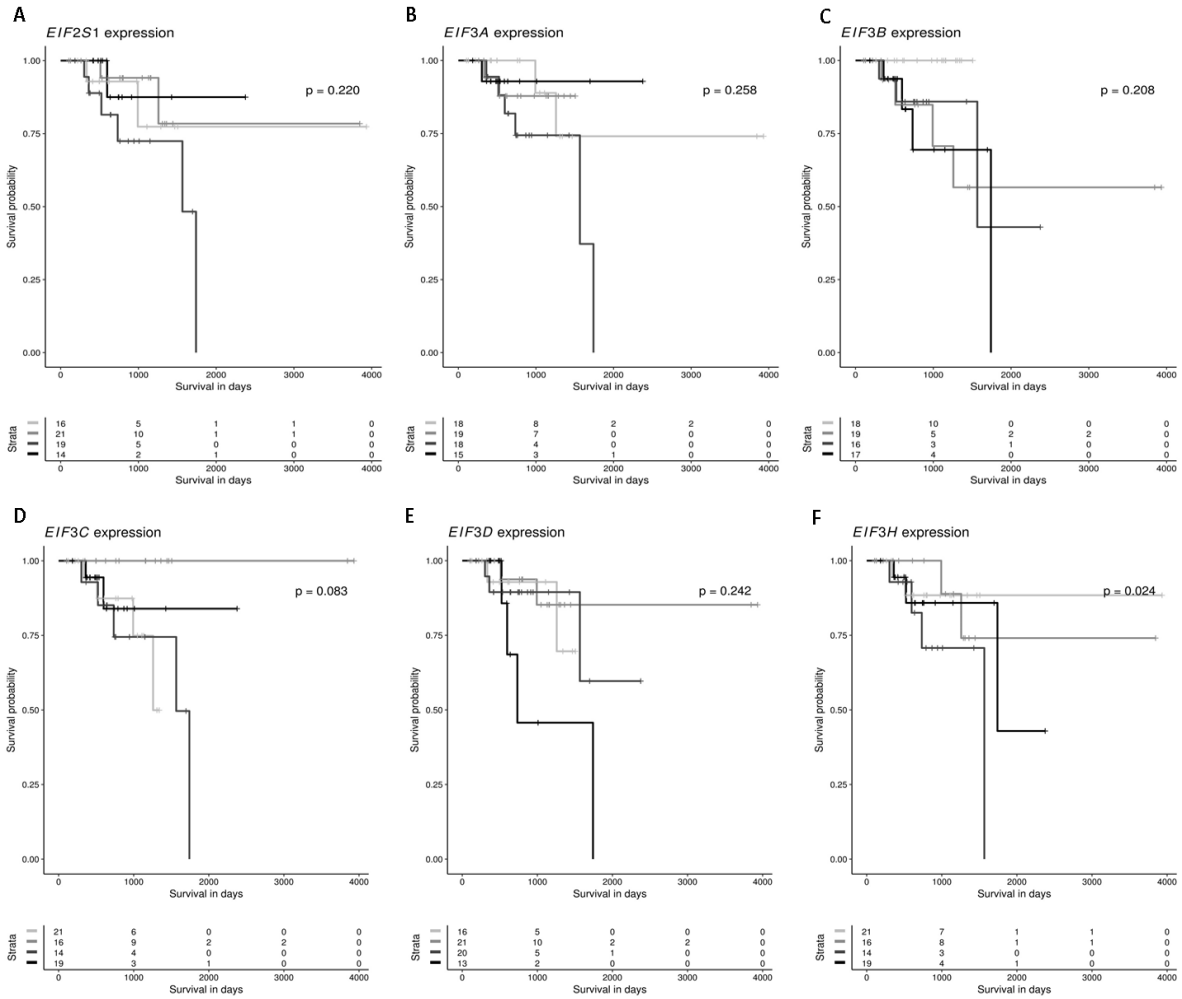

Figure 48: Kaplan-Meier curves of eIF2S1, eIF3A, eIF3B, eIF3C, eIF3D and eIF3H expression on overall survival for RC. Cases are subdivided in eIF2S1, eIF3A, eIF3B, eIF3C, eIF3D and eIF3H low or high expressers according to whether expression is below or above median and survival is compared using the log-rank test. The light grey lines represent low tumor grade with low gene expression, medium grey lines display low tumor grade with high gene expression, the dark grey lines represent high tumor grade with low gene expression and the black lines high tumor grade with high gene expression. [A] eIF2S1 dataset; [B] eIF3A dataset; [C] eIF3B dataset; [D] eIF3C dataset; [E] eIF3D dataset and [F] eIF3H dataset [181].

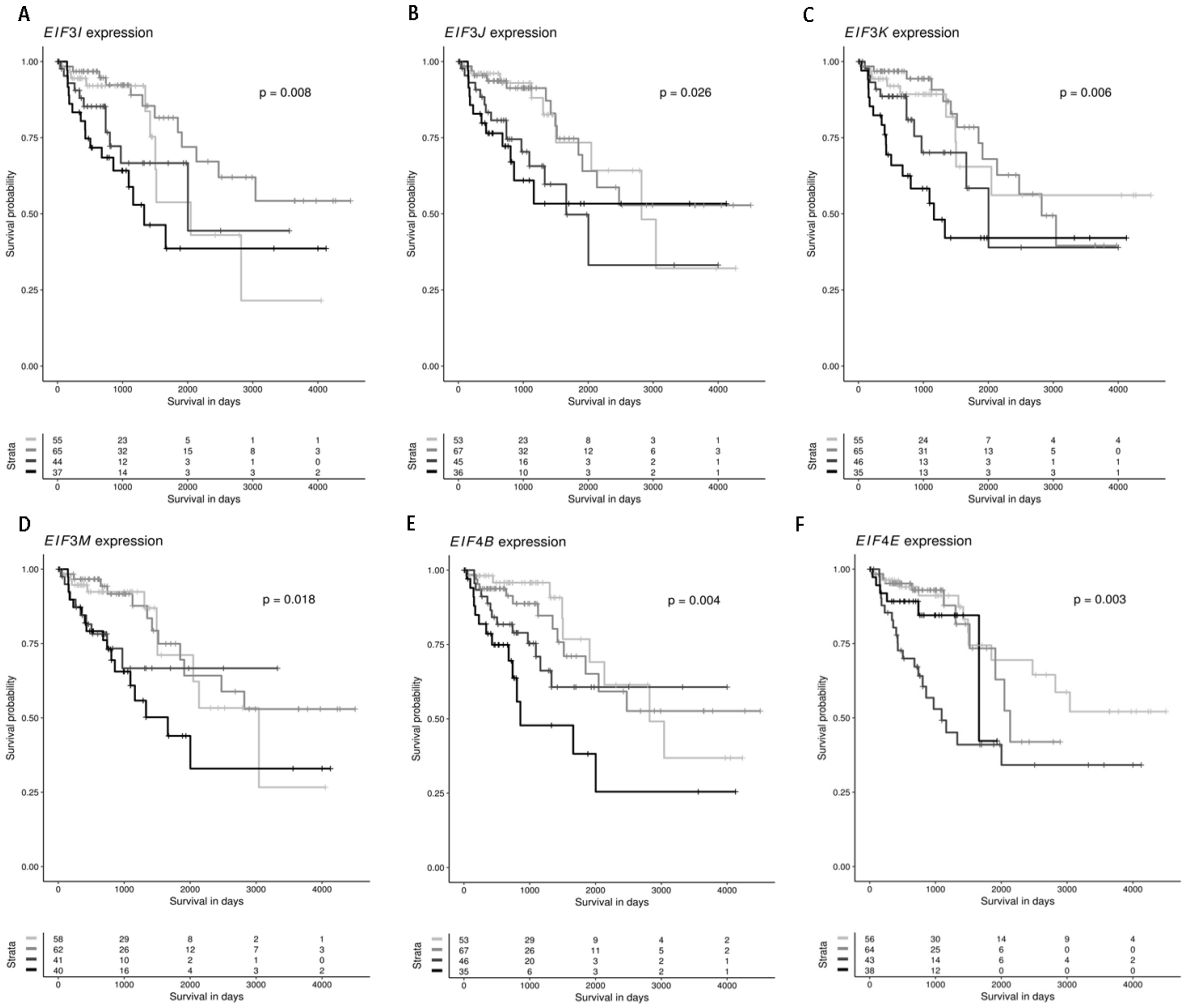

Figure 49: Kaplan-Meier curves of eIF3I, eIF3J, eIF3K, eIF3M, eIF4B and eIF4E expression on overall survival for CC. Cases are subdivided in eIF3I, eIF3J, eIF3K, eIF3M, eIF4B and eIF4E low or high expressers according to whether expression is below or above median and survival is compared using the log-rank test. The light grey lines represent low tumor grade with low gene expression, medium grey lines display low tumor grade with high gene expression, the dark grey lines represent high tumor grade with low gene expression and the black lines high tumor grade with high gene expression. [A] eIF3I dataset; [B] eIF3J dataset; [C] eIF3K dataset; [D] eIF3M dataset; [E] eIF4B dataset and [F] eIF4E dataset [181].

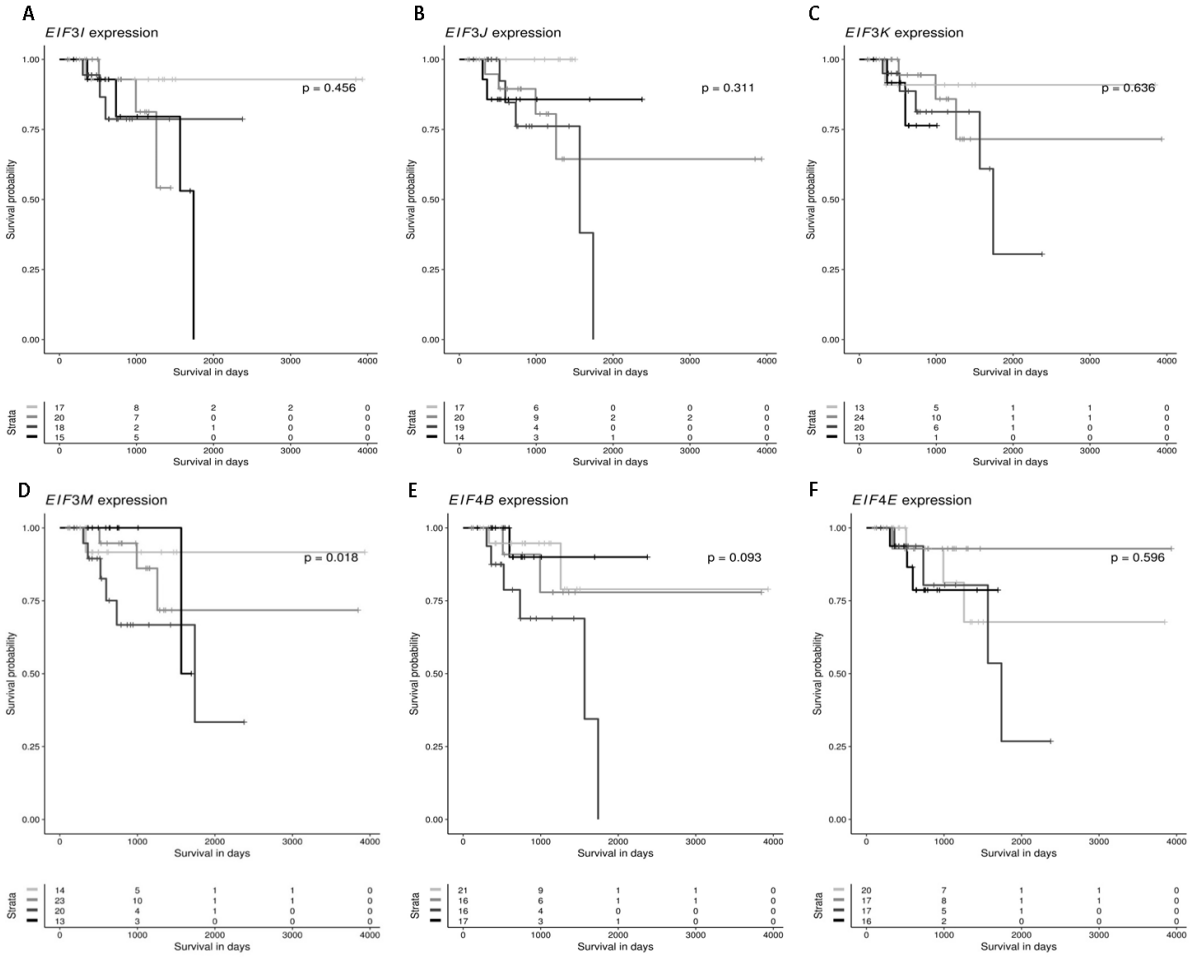

Figure 50: Kaplan-Meier curves of eIF3I, eIF3J, eIF3K, eIF3M, eIF4B and eIF4E expression on overall survival for RC. Cases are subdivided in eIF3I, eIF3J, eIF3K, eIF3M, eIF4B and eIF4E low or high expressers according to whether expression is below or above median and survival is compared using the log-rank test. The light grey lines represent low tumor grade with low gene expression, medium grey lines display low tumor grade with high gene expression, the dark grey lines represent high tumor grade with low gene expression and the black lines high tumor grade with high gene expression. [A] eIF3I dataset; [B] eIF3J dataset; [C] eIF3K dataset; [D] eIF3M dataset; [E] eIF4B dataset and [F] eIF4E dataset [181].

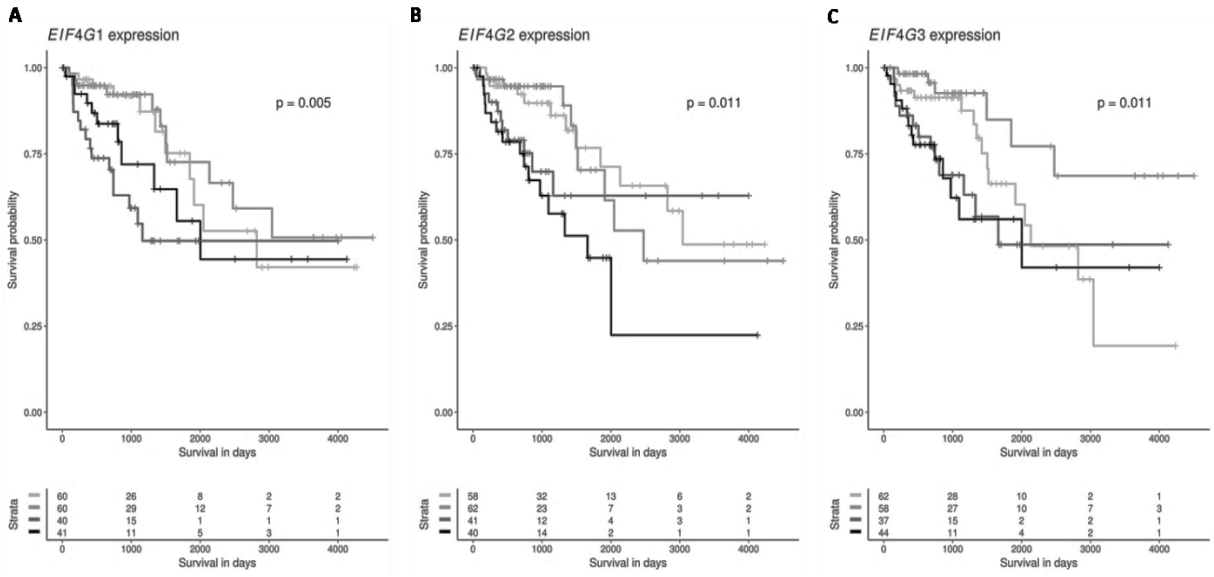

Figure 51: Kaplan-Meier curves of eIF4G1, eIF4G2 and eIF4G3 expression on overall survival for CC. Cases are subdivided in eIF4G1, eIF4G2 and eIF4G3 low or high expressers according to whether expression is below or above median and survival is compared using the log-rank test. The light grey lines represent low tumor grade with low gene expression, medium grey lines display low tumor grade with high gene expression, the dark grey lines represent high tumor grade with low gene expression and the black lines high tumor grade with high gene expression. [A] eIF4G1 dataset; [B] eIF4G2 dataset; [C] eIF4G3 dataset [181].

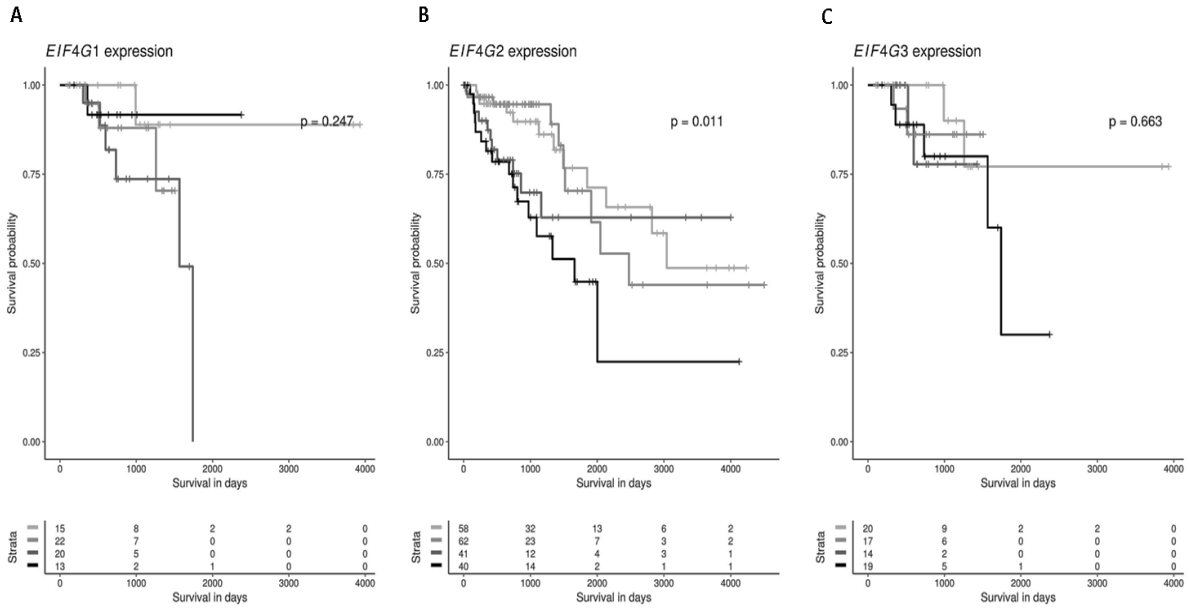

Figure 52: Kaplan-Meier curves of eIF4G1, eIF4G2 and eIF4G3 expression on overall survival for RC. Cases are subdivided in eIF4G1, eIF4G2 and eIF4G3 low or high expressers according to whether expression is below or above median and survival is compared using the log-rank test. The light grey lines represent low tumor grade with low gene expression, medium grey lines display low tumor grade with high gene expression, the dark grey lines represent high tumor grade with low gene expression and the black lines high tumor grade with high gene expression. [A] eIF4G1 dataset; [B] eIF4G2 dataset; [C] eIF4G3 dataset [181].

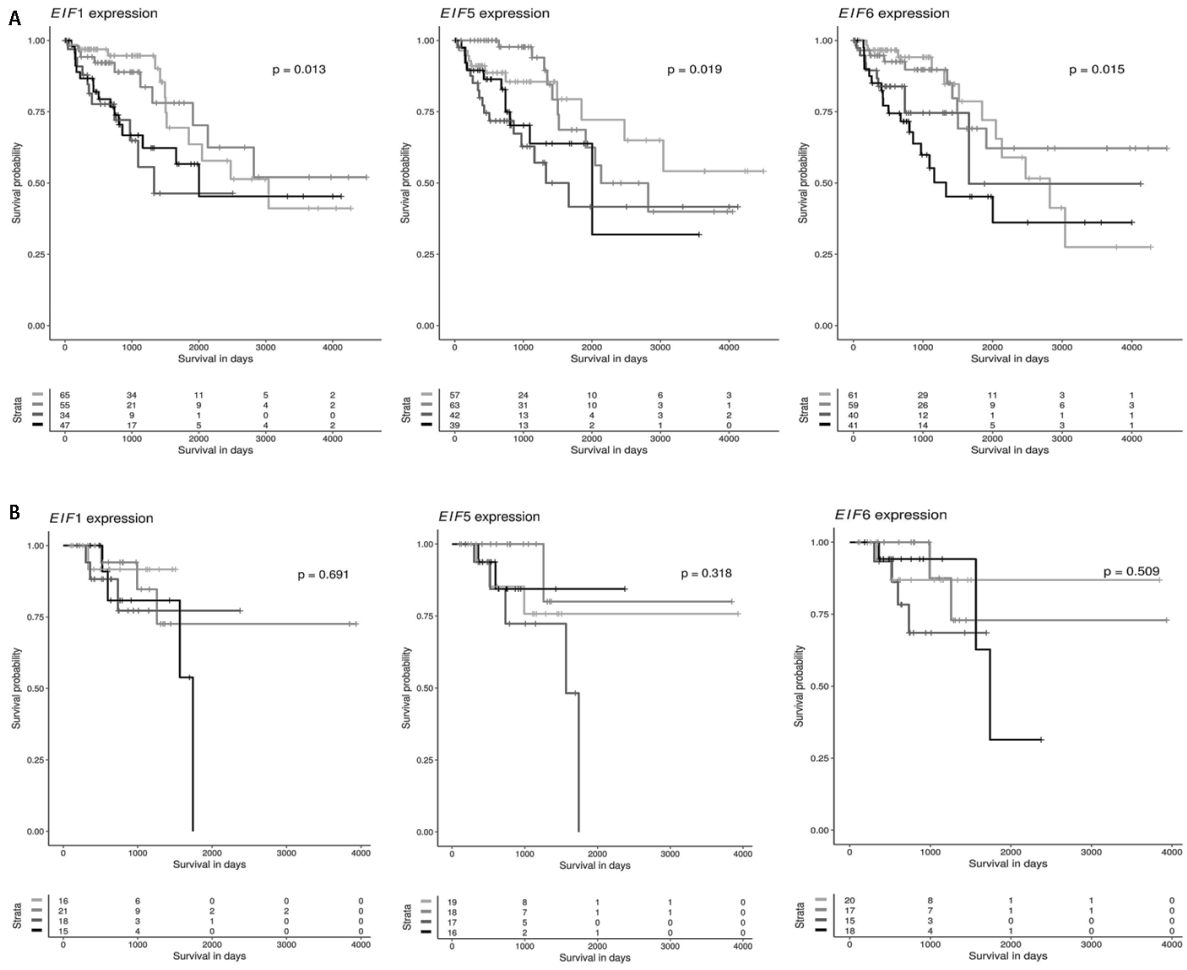

Figure 53: eIF1, eIF5 and eIF6 are clinically relevant candidates in CRC. [A] Kaplan-Meier curves reflect the effect of eIF1, eIF5 and eIF6 expression on overall survival for colon carcinoma. Cases are subdivided in eIF1, eIF5 and eIF6 low or high expressers according to whether expression is below or above median and survival is compared using the log-rank test. [B] Kaplan-Meier curves reflect the effect of eIF1, eIF5 and eIF6 expression on overall survival for rectum carcinoma. Cases are divided in eIF1, eIF5 and eIF6 low or high expressers according to whether expression is below or above median and survival is compared using the log-rank test. The light grey lines represent low tumor grade with low gene expression, medium grey lines display low tumor grade with high gene expression, the dark grey lines represent high tumor grade with low gene expression and the black lines high tumor grade with high gene expression [181].

5.3 Biochemical Analyses of CRC

5.3.1 Immunoblot Analyses of PI3K/AKT/mTOR Pathway Members in Low and High Grade CC and RC

I investigated the expression patterns of mTOR members in CRC patient samples, which we separated into CC and RC, and also into low and high grade tumor samples.

Immunoblot analyses of pmTOR, mTOR, pAKT, AKT and 4E-BP1 revealed a significantly higher expression of these proteins in CRC compared to the corresponding non-neoplastic tissue (NNT) (Figure 54). When we separated the samples into groups of CC and RC, we observed that the overexpression of pmTOR, mTOR, pAKT, AKT and 4E-BP1 was restricted to the RC patients. The CC patient showed no significant change in the expression of mTOR pathway members at the protein level (Figure 54).

Finally, I investigated the influence of tumor grade and compared the protein expression levels after separation into low and high grade CC and RC. Protein expression levels of mTOR, pAKT, AKT and 4E-BP1 were significantly increased in low grade RC compared to low and high grade CC (Figure 54). In comparison, pmTOR, mTOR, pAKT, AKT, pp70S6K, p70S6k and 4E-BP1 were increased in high grade RC at the protein level (Figure 54) [181].

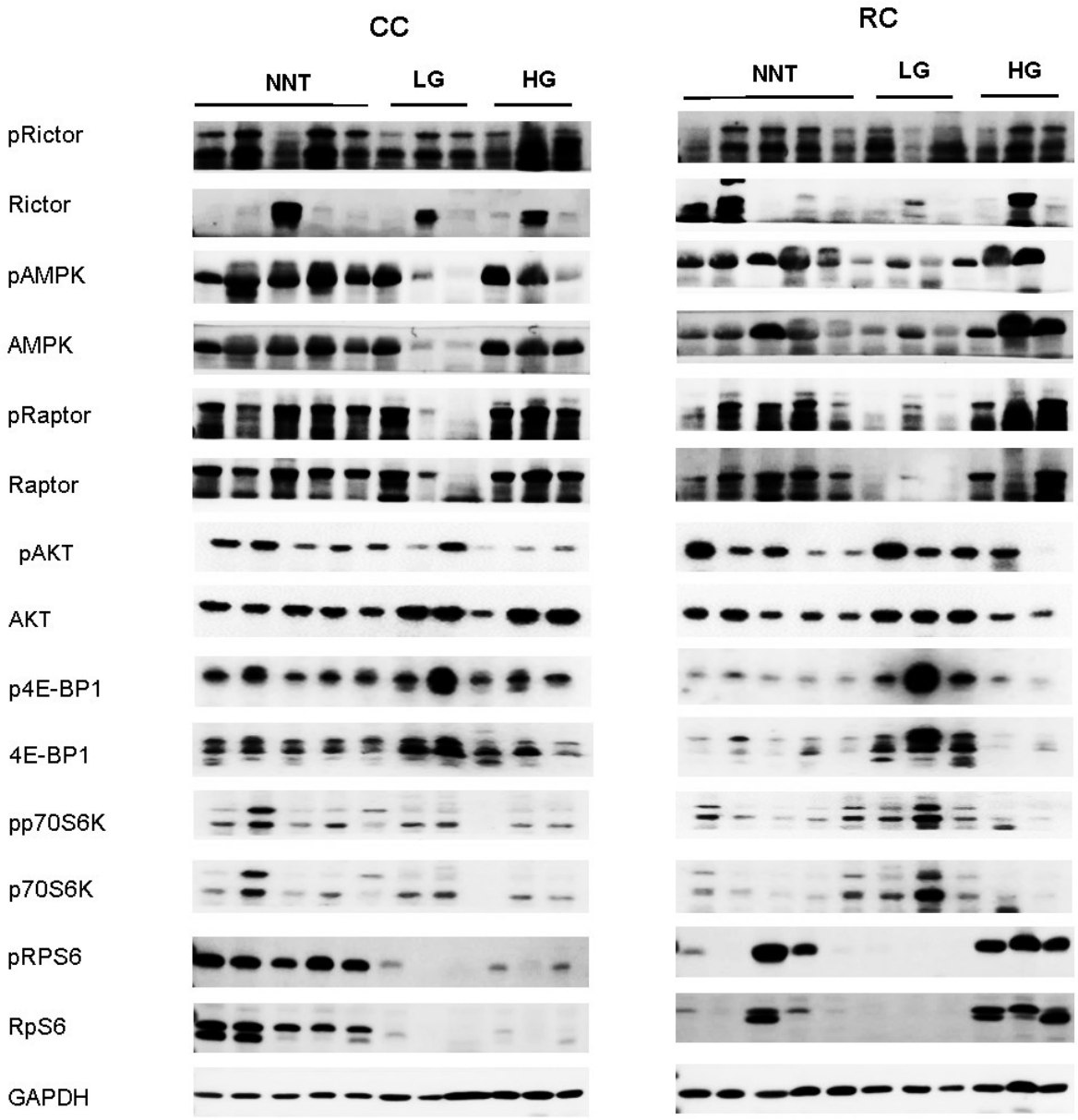

Figure 54: PI3K/AKT/mTOR pathway expression in low and high grade CC and RC. Immunoblot analyses from low grade (LG) and high grade (HG) CC and RC compared to NNT. Equal amounts of protein were loaded on SDS-PAGEs and immunoblotted with pRictor, Rictor, pAMPK, AMPK, pRaptor, Raptor, p4E-BP1, pmTOR, mTOR, pAKT, AKT, pp70S6K, p70S6K, pRPS6, RPS6,p4E-BP1, 4E-BP1 and GAPDH (loading control) antibodies [181]. Three independent experiments were carried out.

5.3.2 mRNA Expression Analysis of PI3K/AKT/mTOR Pathway Members in Low and High grade CC and RC

I investigated the mRNA expression patterns of mTOR members in CRC patient samples, which I separated into CC and RC, and also into low and high grade tumor samples.

Increased mRNA expression levels of *mTOR* and *PTEN* were observed in CRC (Figure 55). Despite the differences in protein expression, increased mRNA expression levels of *mTOR* and *PTEN* (Figure 56) were observed in both, CC and RC.

Increased mRNA expression levels of *mTOR* and *PTEN* (Figure 55) were observed in low grade CC and RC, while there was no difference in the mRNA levels of *mTOR* and *PTEN* in high grade CC and RC compared to NNT (Figure 55) [181].

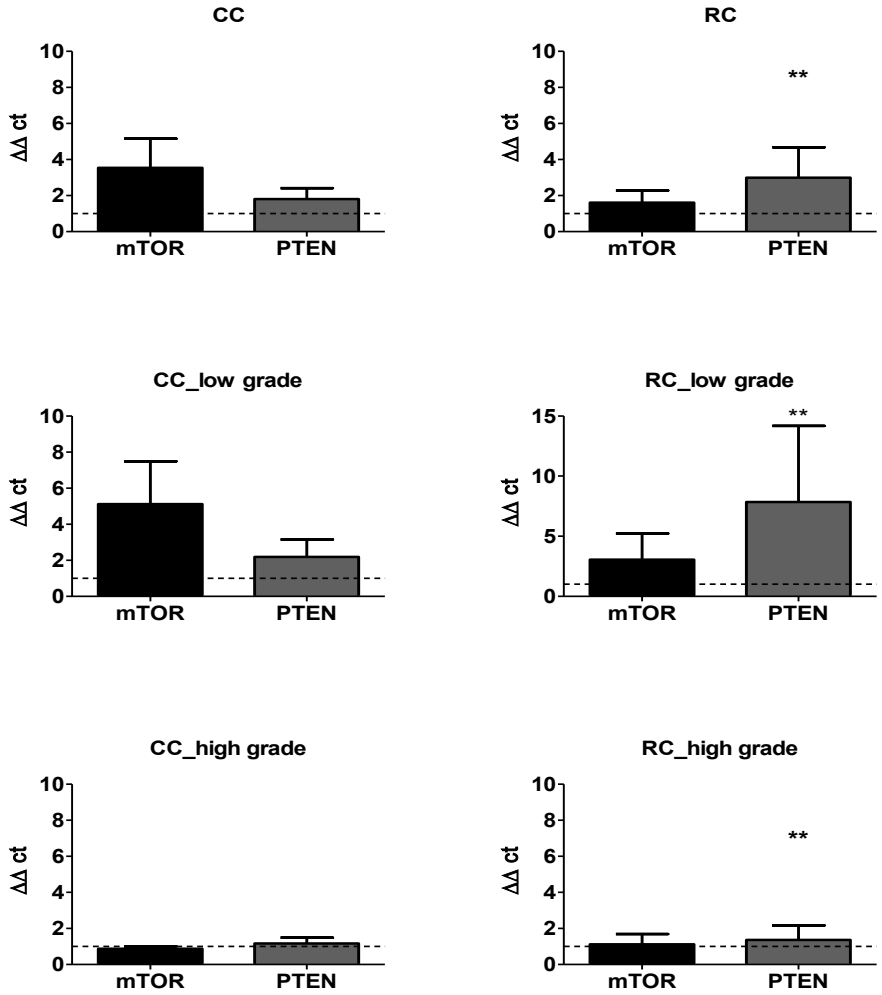

Figure 55: mTOR and PTEN expression in low and high grade CC and RC. qRT-PCR analyses of *mTOR* and PTEN from low grade (LG) and high grade (HG) CCand RC compared to NNT [181]. Three independent experiments were carried out. Bars represent mean ± SEM. *p < 0.05, **p < 0.01, ***p < 0.001.

5.3.3 Immunoblot Analyses of eIFs in Low and High Grade CC and RC

eIF1, peIF2α, eIF2α, eIF3A, eIF3C, eIF3H, eIF3I, peIF4B, eIF4B, eIF4G, eIF5 and eIF6 showed higher protein expression in CRC tumors in compared to NNT (Figure 56).

The expression of several eIF subunits differed between CC and RC. Interestingly, peIF2α, eIF2α and the eIF3 subunits A, B, C, H and I, as well as peIF4B, eIF4G, and eIF6, displayed a higher protein expression relative RC compared to CC and NNT. eIF1, eIF4B and eIF5 showed increased protein levels in CC and RC compared to NNT (Figure 56).

As I noticed dramatic differences in the protein expression between CC and RC patients, I decided to separate the results into low and high grade tumors. In low grade CC, I observed an overexpression of eIF1 and eIF4B at the protein level and in high grade CC only an overexpression of eIF1.

However, in low grade RC, the protein expression levels of the eIF subunits 1, p2α, 2α, 3A, 3C, p4B, 4G, 5 and 6 were significantly increased relative to NNT compared to low grade CC (Figure 56). Increased protein expression levels of eIF1, eIF2α, eIF3A, eIF3B, eIF3C, eIF3I, eIF3H, peIF4B, eIF4B, eIF4E, eIF5 and eIF6 were observed in high grade RC (Figure 56). In line with previous studies, the data presented here indicate increased tumor initiation and progression in CRC [181].

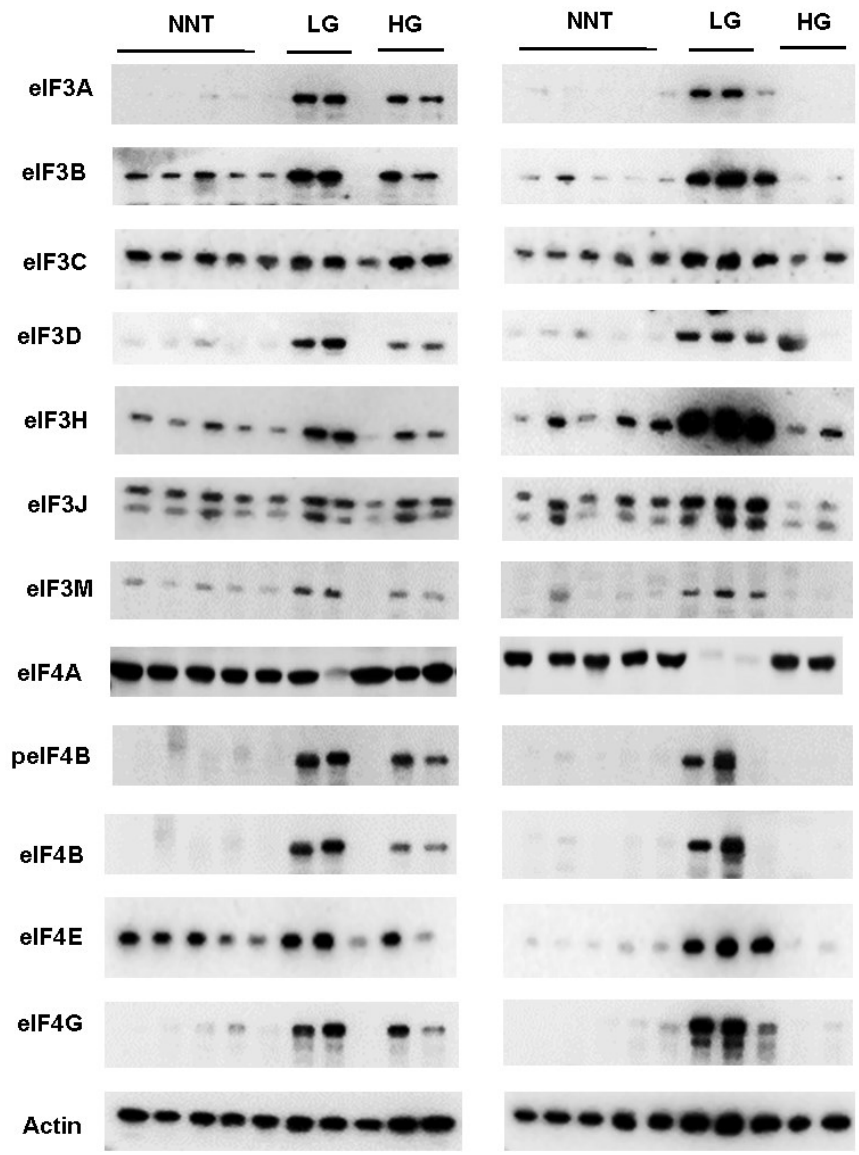

Figure 56: eIF expression in level low and high grade CC and RC. Graph shows Immunoblot analyses of low grade (LG) and high grade (HG) CC and RC compared to NNT. Equal amounts of protein were resolved on SDS-PAGEs and immunoblotted with various eIF subunits and β-actin (loading control) antibodies [181]. Three independent experiments were carried out.

5.3.4 mRNA Expression Analysis of eIFs in Low and High Grade CC and RC

To evaluate the gene expression at the mRNA level, I performed qRT–PCR and measured the transcripts of 13 eIF subunits $2^{-\Delta\Delta CT}$ method. Our results show that transcripts for the eIF

subunits *1, 2α, 3A, 3B, 3C, 3H, 3J, 3M, 4B, 4G, 5* were significantly overexpressed in CRC compared to NNT (Figure 57).

Furthermore, *eIF1, eIF2α, eIF3A, eIF3B, eIF3C, eIF3H, eIF3J, eIF3M, eIF4B, eIF4G* and *eIF6* showed a significantly higher mRNA expression level in CC compared to NNT (Figure 57). For RC patients, we observed mRNA overexpression for the eIF subunits *1, 2α, 3A, 3B, 3C, 3H, 3J, 3M, 4B, 4G, 5* and *6* compared to NNT (Figure 57).

The eIF subunits *1, 2α, 3A, 3C, 3H, 3J, 3M, 4B, 4G* and *6* (Figure 57) showed a significant overexpression at the mRNA level in low grade CCs. In contrast, the eIF subunits *1, 3B, 3C, 3H, 3M, 4B* and *6* revealed a significantly higher expression in high grade CCs (Figure 57).

In high grade RC the eIFs subunits *1, 2α, 3A, 3B, 3C, 3H, 3J, 3M, 4B, 4G, 5* and *6* (Figure 57) showed a significantly higher mRNA expression relative to NNT in contrast to high grade CC.

Increased mRNA expression levels of *eIF* subunits *1, 2α, 3A, 3B, 3C, 3H, 3J, 4B, 4G, 5* and *6* were observed in low grade RC (Figure 57) [181].

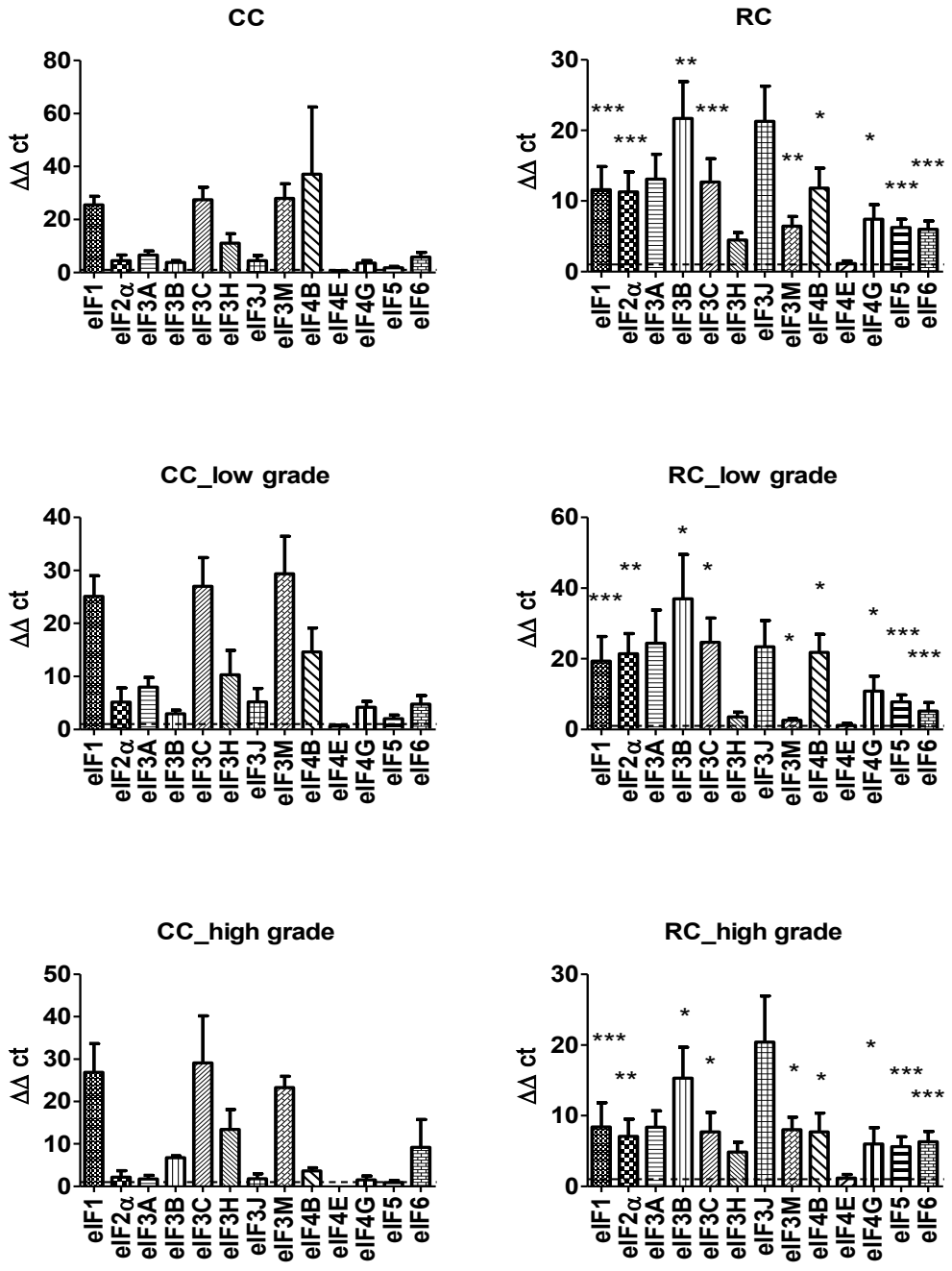

Figure 57: mRNA expression level of various eIF subunits in low and high grade CC and RC. qRT-PCR of various eIF subunits from low grade (LG) and high grade (HG) CC and RC compared to NNT [181]. Three independent experiments were carried out. Bars represent mean ± SEM. *p < 0.05, **p < 0.01, ***p < 0.001.

5.3.5 Immunoblot Analyses of PI3K/AKT/mTOR Members and eIFs in Liver Metastases of Primary CC and RC

Expression profiles of mTOR members and eIFs in CC and RC liver metastases were analyzed by immunoblot analyses and compared to match NNLT.

Regarding the PI3K/AKT/mTOR pathway in the metastases, I found no changes in the expression of pmTOR, mTOR, pAKT, AKT, pPTEN, PTEN, pp70S6K and 4E-BP1 at the protein level in CC Mets and RC Mets (Figure 58).

Immunoblot analyses revealed peIF2α, eIF3B and eIF4E protein expression to be higher in metastatic CC and RC compared to NNLT (Figure 58). For eIF3K, we only observed higher expression in RC Met but no changes in CC Met (Figure 58) [181].

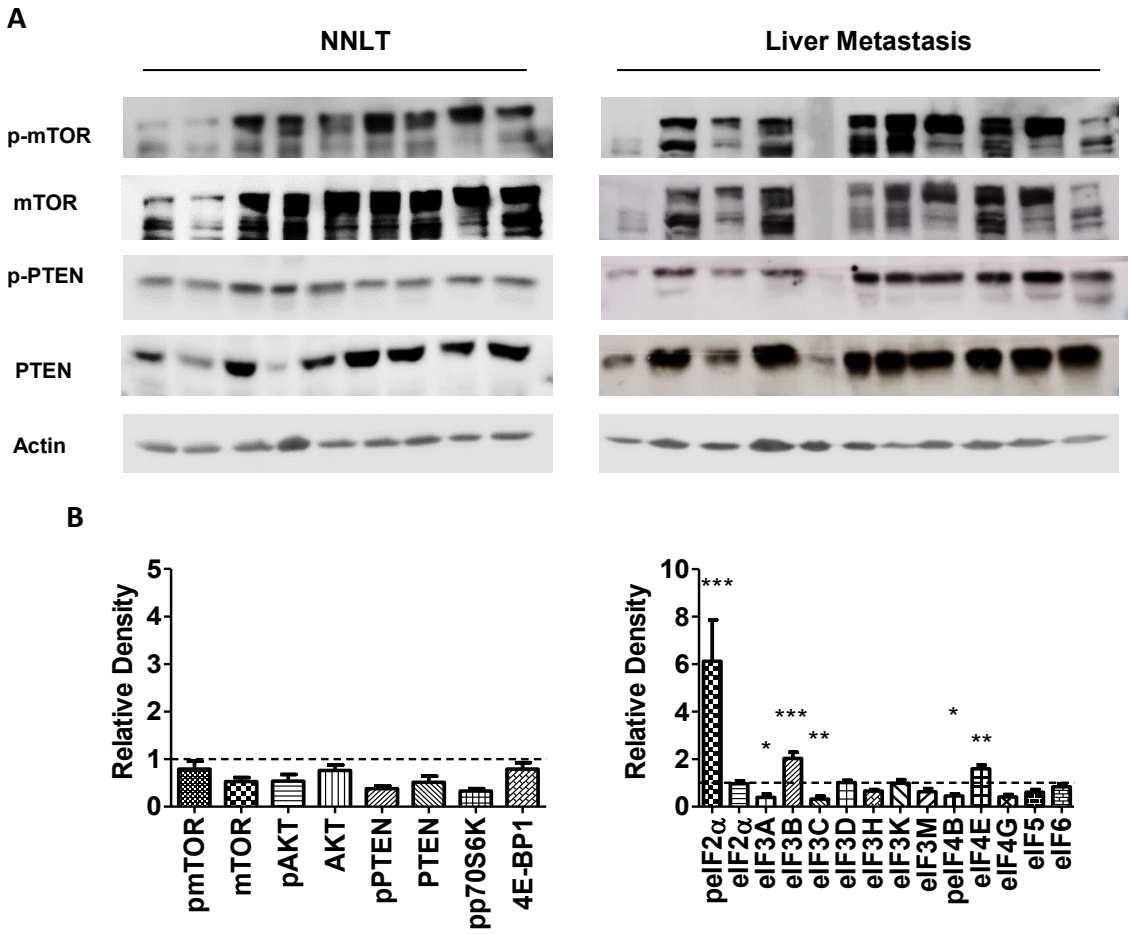

Figure 58: PI3K/AKT/mTOR signaling pathway members and eIF subunits in liver metastases of CRC patients. [A] Protein expression of mTOR members in CRC Met tissues. [B] Densitometric analyses of mTOR members, eIF subunits and β-actin in liver metastases of CRC patient samples compared to NNLT [181]. Three independent experiments were carried out. Bars represent mean ± SEM. *p < 0.05, **p < 0.01, ***p < 0.001.

5.3.6 mRNA Expression of PI3K/AKT/mTOR Members and eIFs in Liver Metastases of Primary CC and RC

Expression profiles of mTOR members and eIFs in CC and RC metastases were analyzed by qRT-PCR compared to match NNLT.

At mRNA level, *mTOR* and *PTEN* were significantly upregulated in CC and RC Met compared to NNLT (Figure 59).

To evaluate the gene expression at the mRNA level, we performed qRT–PCR and measured the transcripts of 13 eIF subunits by relative quantification normalized to ß-actin. AtmRNA level, the eIF subunits *1, 2α, 3A, 3B, 3C, 3H, 3M, 4B, 4E, 4G, 5* and *6* showed a significant overexpression in CC and RC Met compared to NNLT (Figure 59) [181].

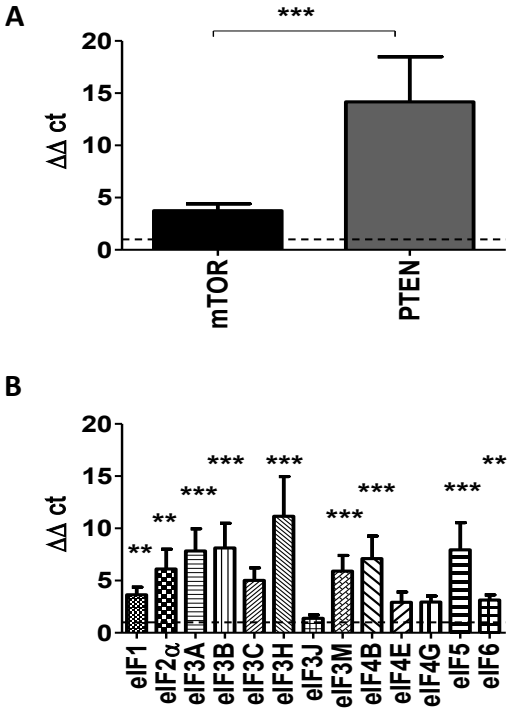

Figure 59: PI3K/AKT/mTOR signaling pathway members and eIF subunits in liver metastases of CRC patients. (A) mRNA expression of mTOR and PTEN in liver metastases of primary CRC patient samples. (B) mRNA expression of eIF subunits in liver metastases of primary CRC patient samples [181]. Three independent experiments were carried out. Bars represent mean ± SEM. *p < 0.05, **p < 0.01, ***p < 0.001.

5.3.7 *In Situ* Detection of Different eIFs by Padlock Probe Approach

In order to localize and analyze the distribution of *eIF1*, *eIF5* and *eIF6* transcripts in CC and RC vs. NNT, we performed an mRNA-based in-situ detection approach (Figure 61). *In situ* detection allows visualization of single mRNA transcripts (Figure 61). In situ detection confirmed an overexpression at the mRNA level of *eIF1* and *eIF5* in CC vs. NNT ($p<0.001$ and $p<0.05$) (Figure 60). In RC tissue, eIF5 was overexpressed compared to NNT ($p<0.05$) (Figure 60) [181].

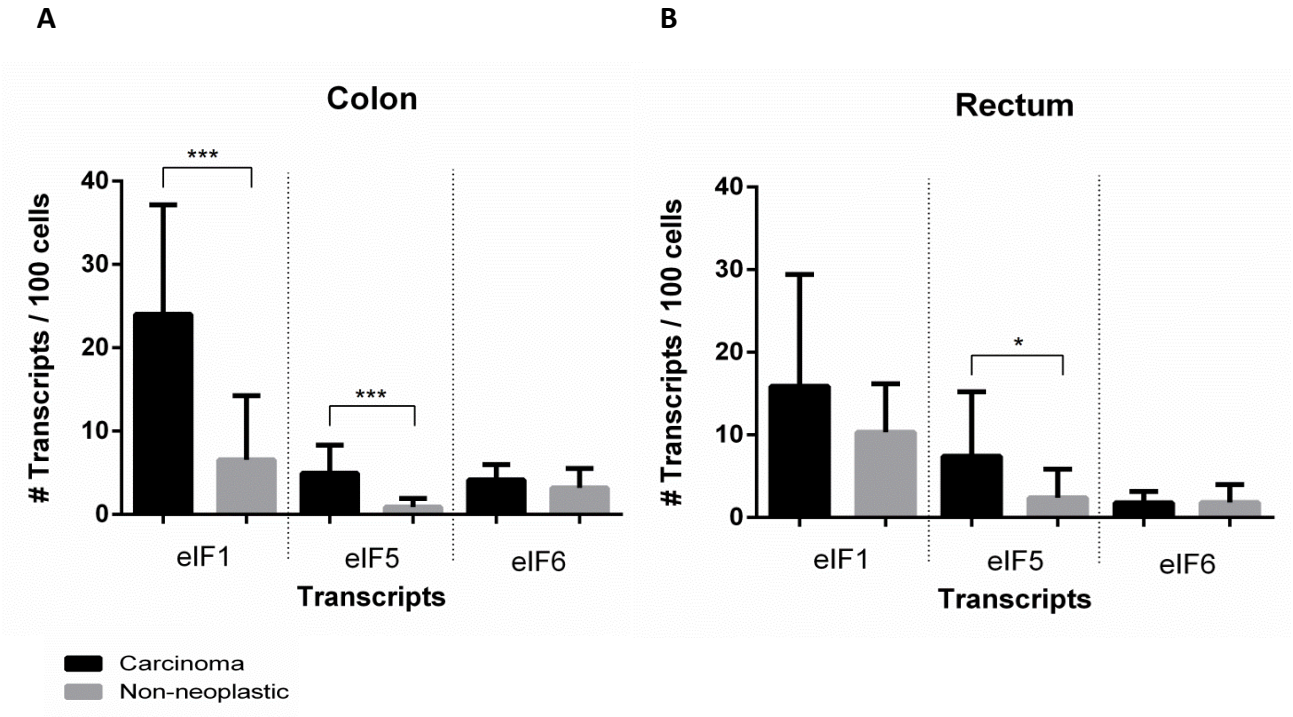

Figure 60: Quantification of *in situ* detected signals of eIF1, eIF5 and eIF6 transcripts in CC and RC vs. NNT. [A] mRNA expression level of eIF1, eIF5 and eIF6 in CC compared to NNT. [B] mRNA expression level of eIF1, eIF5 and eIF6 in RC compared to NNT. Error bars show SEM [181].

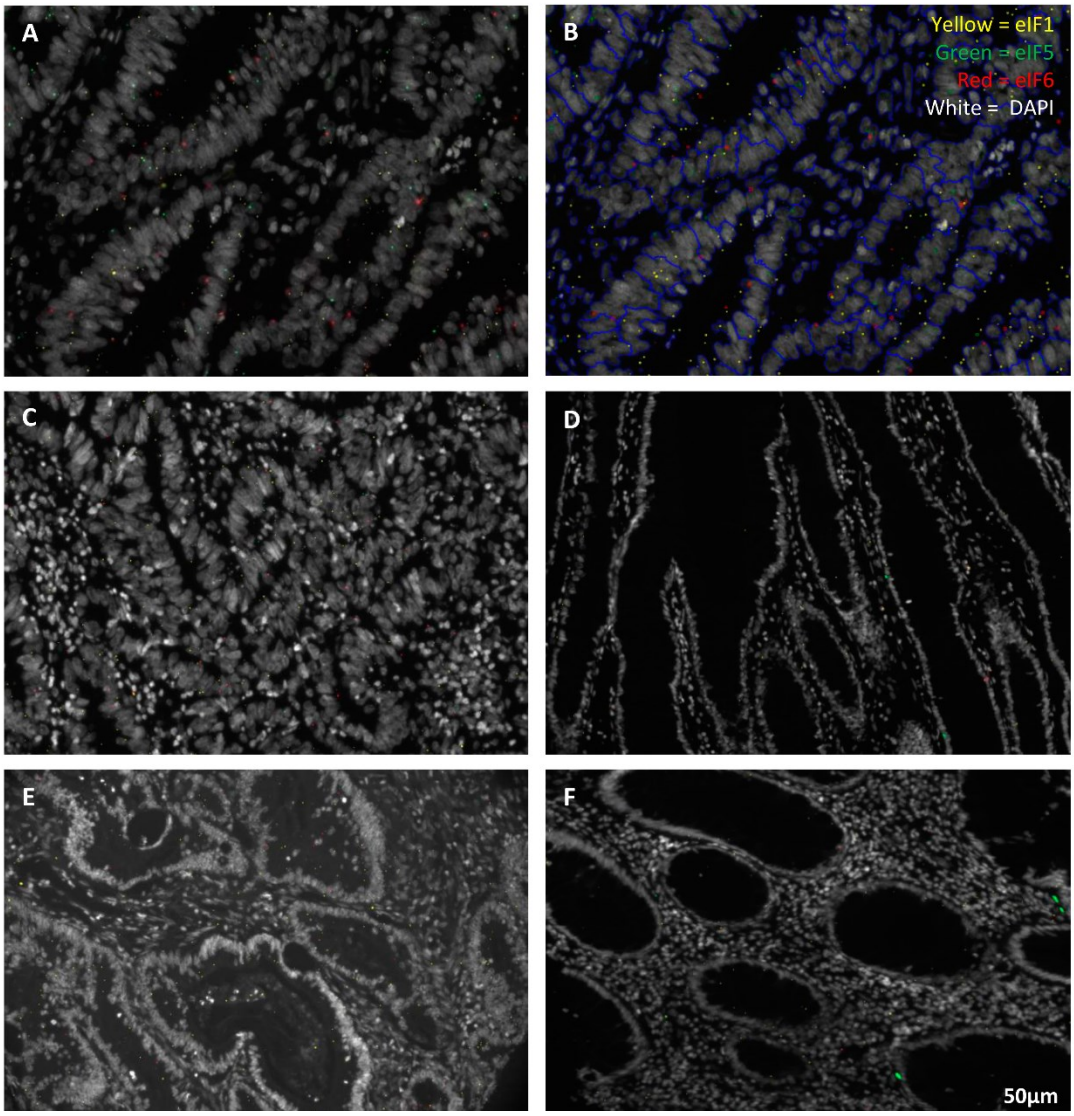

Figure 61: *In situ* detection of eIF transcripts in CRC. [A] The tissue displays eIF1 (yellow), eIF5 (green) and eIF6 (red) transcripts, represented as small fluorescent signals. [B] Output image of the quantification of each signal by the CellProfiler software. [C] The tissue displays small fluorescent signals in RC samples. [D] The tissue displays small fluorescent signals in NNT. [E] The tissue displays small fluorescent signals in CC samples. [F] The tissue displays small fluorescent signals in NNT [181].

5.4 *In vitro* Experiments

5.4.1 siRNA Knockdown of eIF1, eIF5 and eIF6 in HCT116 and HT29 Cells

Based on the results of the eIF characterization in CRC patients (Figure 62), eIF1, eIF5 and eIF6 were identified as the factors with the most significantly overexpression, and therefore as the most promising candidates as targets for future therapeutic intervention [181].

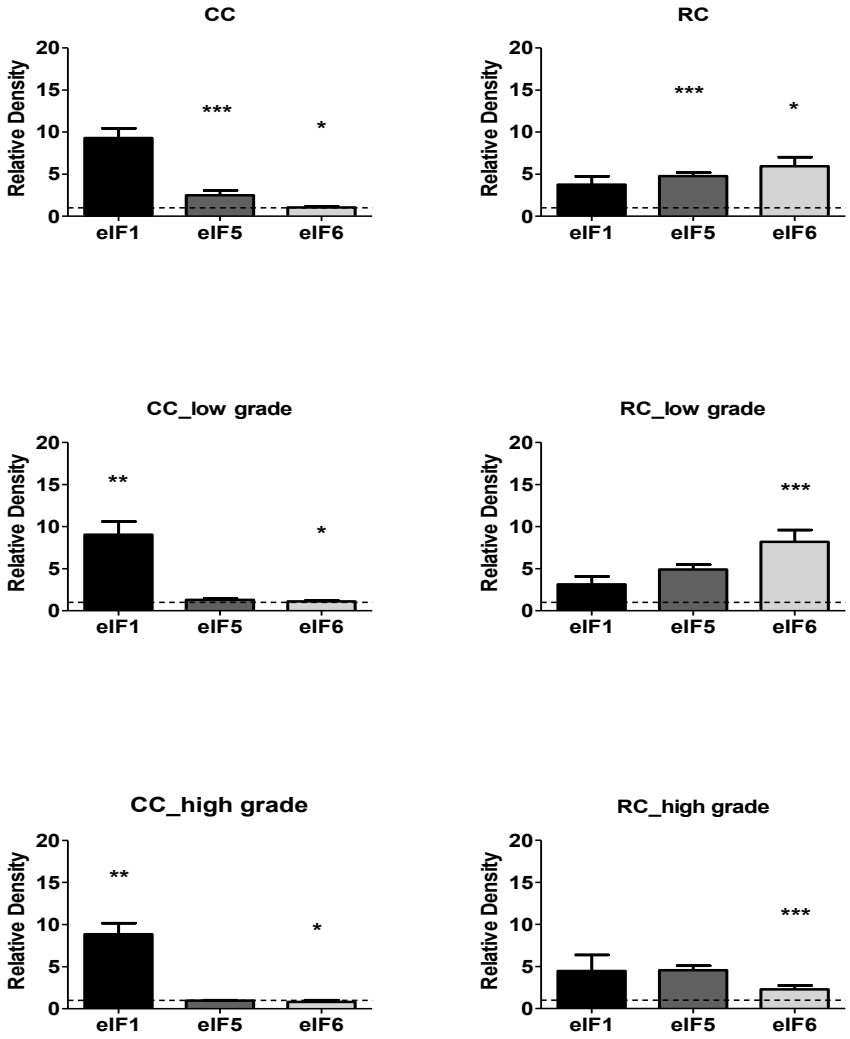

Figure 62: eIF1, eIF5 and eIF6 expression levels in low and high grade CC and RC. Densitometric analyses of immunoblots from eIF1, eIF5 and eIF6 and β-actin in low grade (LG) and high grade (HG) CC and RC compared to NNT [181]. Three independent experiments were carried out. Bars represent mean ± SEM. *p < 0.05, **p < 0.01, ***p < 0.001.

Thus, in order to investigate the effect of silencing eIF1, eIF5 and eIF6, HCT116 cells were transfected with respective siRNAs, and the knockdown effect was subsequently assessed for three time points. An inhibition of protein levels close to 90% was achieved for eIF1 (Figure 63A), eIF5 (Figure 63B) and eIF6 (Figure 63C) at all three time points. The transfection strongly reduced the proliferation of HCT116 cells which expressed eIF1, eIF5 and eIF6 specific siRNAs, but had no effect on MOCK control [181].

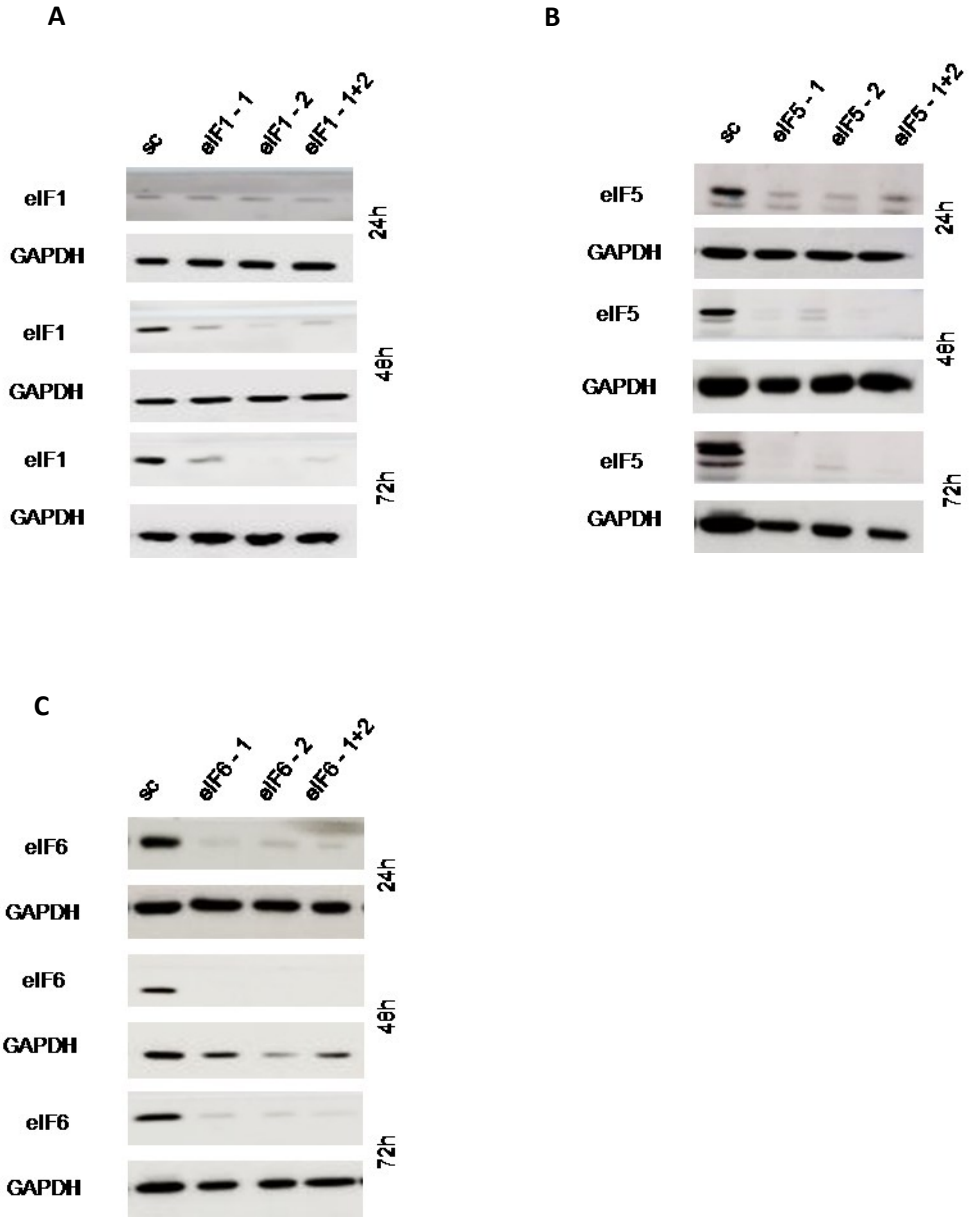

Figure 63: *In vitro* characterization of the effect of eIF1, eIF5 and eIF6 knockdown in HCT116 cells. (A) Protein expression of siRNA knockdown with eIF1 after 24h, 48h and 72h compared to SC

control. (B) Protein expression of siRNA knockdown with eIF5 after 24h, 48h and 72h compared to SC control. (C) Protein expression of siRNA knockdown with eIF6 after 24h, 48h and 72h compared to SC control [181]. Three independent experiments were carried out. Bars represent mean ± SEM. *$p < 0.05$, **$p < 0.01$, ***$p < 0.001$.

Additionally, we evaluated the consequences of siRNA-mediated *eIF1*, *eIF5* and *eIF6* depletion in HT29 cells. The knockdown effect was assessed for three time points (24h, 48h and 72h). A knockdown effect at the protein level close to 60% was achieved for eIF1 (Figure 64A), eIF5 (Figure 64B) and eIF6 (Figure 64C) at all three time points [181].

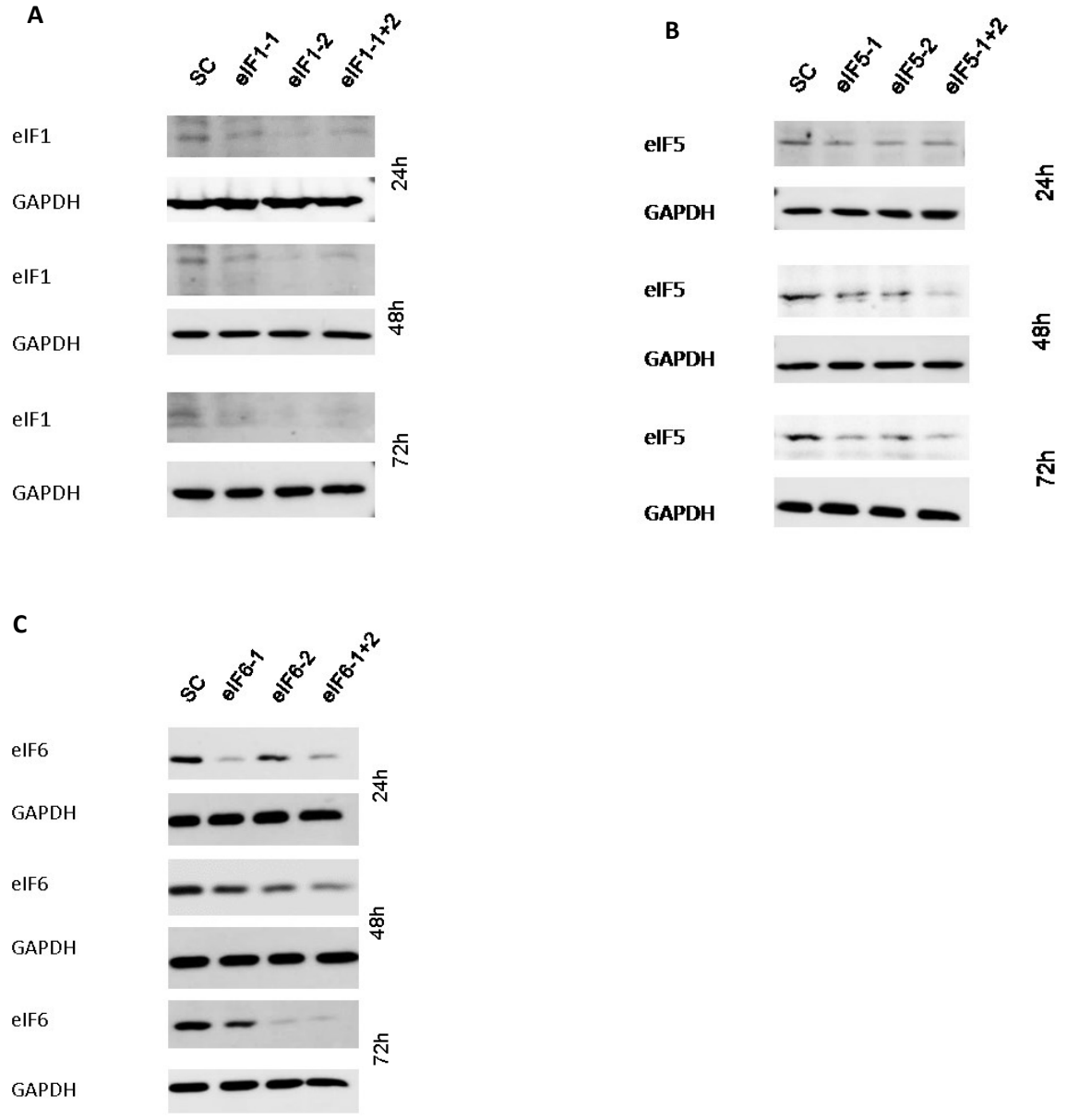

Figure 64: *In vitro* characterization of the effect of eIF1, eIF5 and eIF6 knockdown in HT29 cells. (A) Protein expression of eIF1 siRNA constructs after 24h, 48h and 72h compared to SC control. (B) Protein expression of eIF5 siRNA constructs after 24h, 48h and 72h compared to SC control. (C) Protein expression of eIF6 siRNA constructs after 24h, 48h and 72h compared to SC control [181]. Three independent experiments were carried out. Bars represent mean ± SEM. *$p < 0.05$, **$p < 0.01$, ***$p < 0.001$.

Upon transfecting HCT116 cells for 24h, 48h and 72h with the respective siRNAs, mRNA expression of *eIF1*, *eIF5* and *eIF6* was reduced in all three subunits compared to cells transfected with scrambled RNA (SC) (Figure 65) [181].

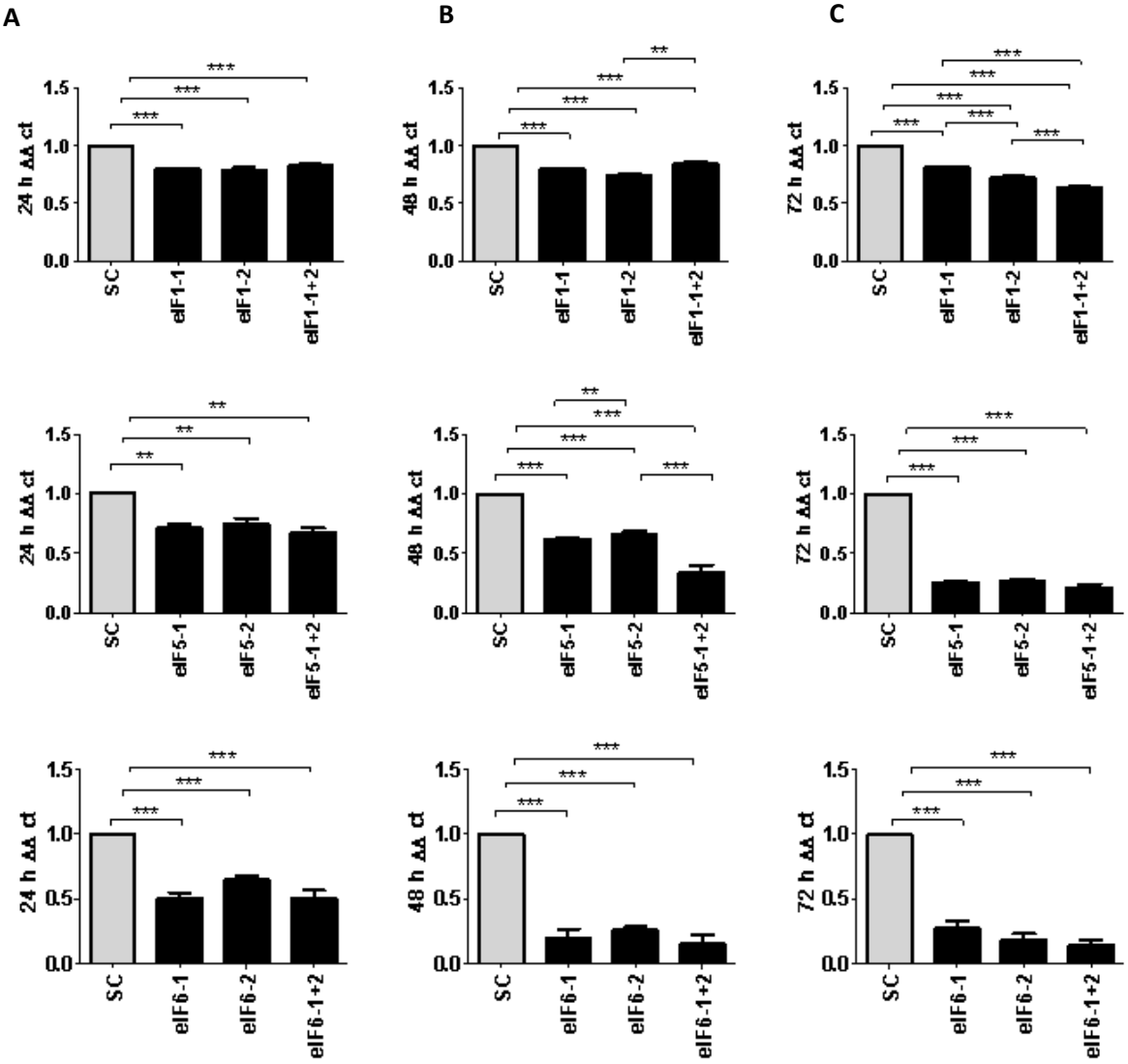

Figure 65: *In vitro* characterization of the effect of eIF1, eIF5 and eIF6 knockdown in HCT116 cells. mRNA expression level of *eIF1* (A), *eIF5* (B) *and eIF6* (C) in HCT116 cells compared to the SC [181]. Three independent experiments were carried out. Bars represent mean ± SEM. *p < 0.05, **p < 0.01, ***p < 0.001.

The mRNA expression of *eIF1, eIF5* and *eIF6* was reduced in all three subunits compared to SC (Figure 66) [181].

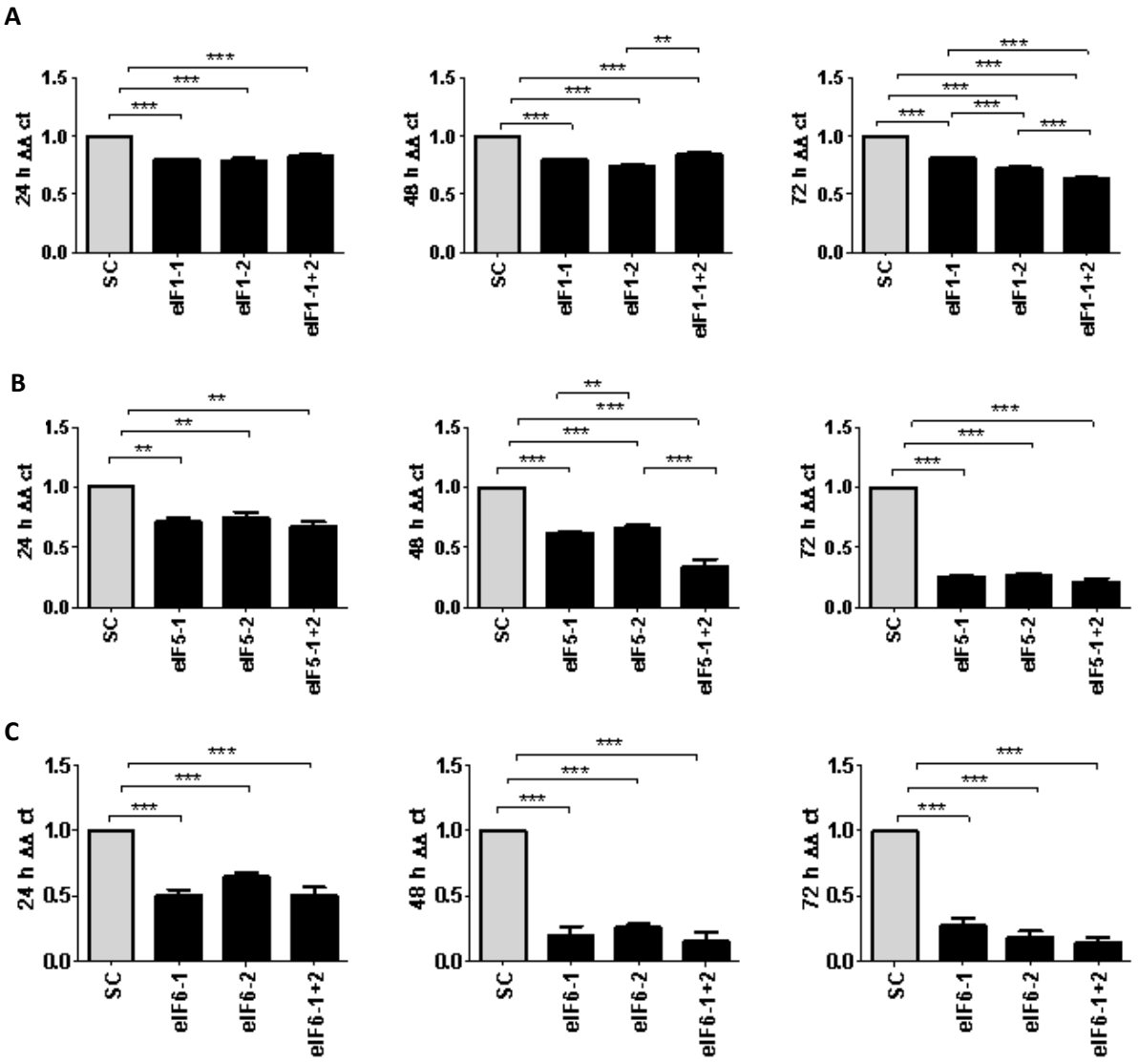

Figure 66: *In vitro* characterization of the effect of eIF1, eIF5 and eIF6 knockdown in HT29 cells. mRNA expression level of *eIF1 (A), eIF5 (B) and eIF6 (C)* in HT29 cells compared to SC [181]. Three independent experiments were carried out. Bars represent mean ± SEM. *p < 0.05, **p < 0.01, ***p < 0.001.

The effect of *eIF1, eIF5* and *eIF6* gene knockdown on apoptosis was analyzed by YO-PRO®-1 staining. The apoptosis rate of cells transfected with *eIF1*, *eIF5* and *eIF6* siRNA knockdown

constructs was significantly decreased compared to SC cells 72h after transfection (Figure 67 and Figure 68) [181].

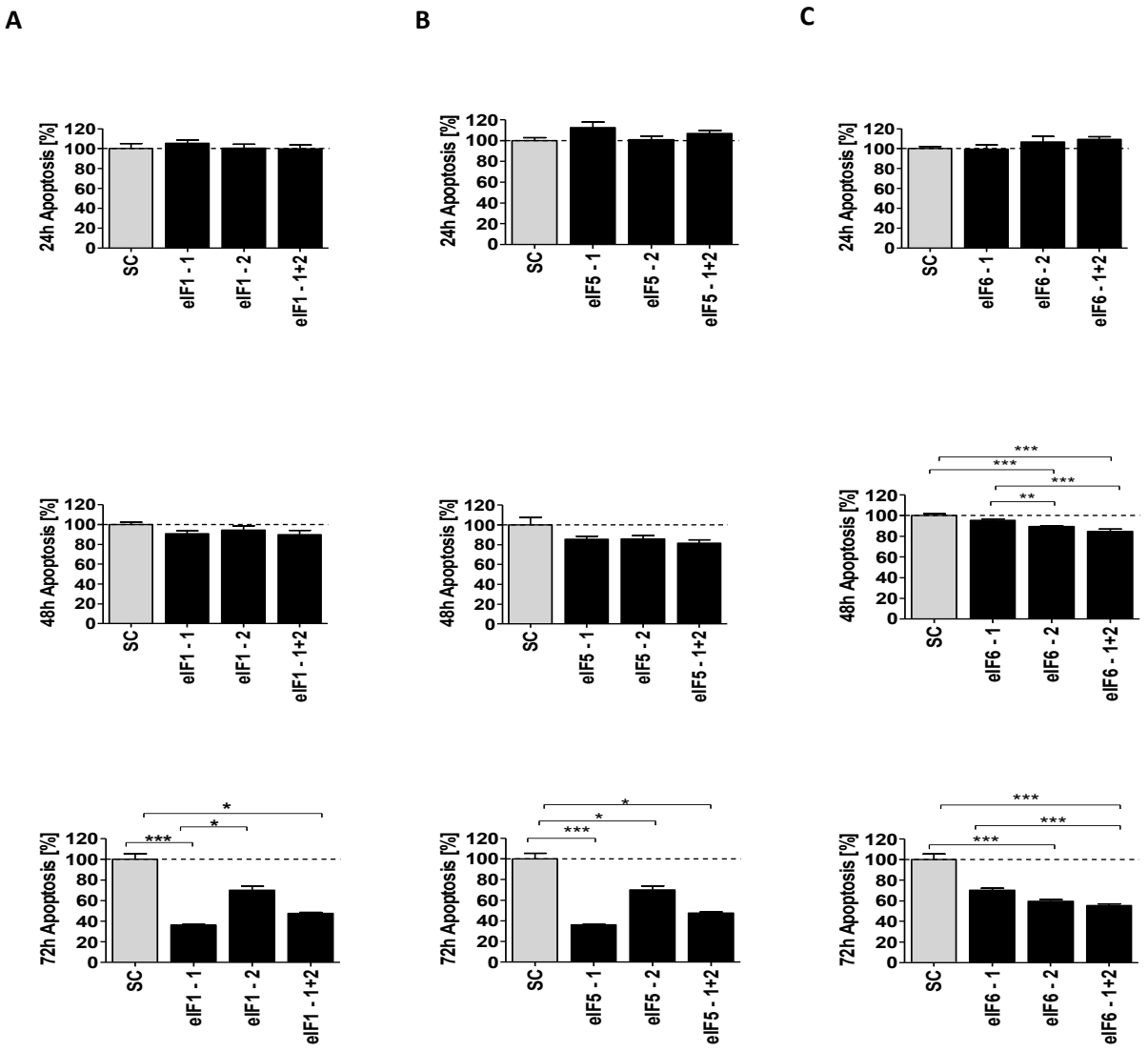

Figure 67: *In vitro* characterization of the effect of eIF1, eIF5 and eIF6 knockdown in HCT116 cells. Graph shows apoptosis rate after eIF1 (A), eIF5 (B) and eIF6 (C) knockdown compared to SC [181]. Three independent experiments were carried out. Bars represent mean ± SEM. *p < 0.05, **p < 0.01, ***p < 0.001.

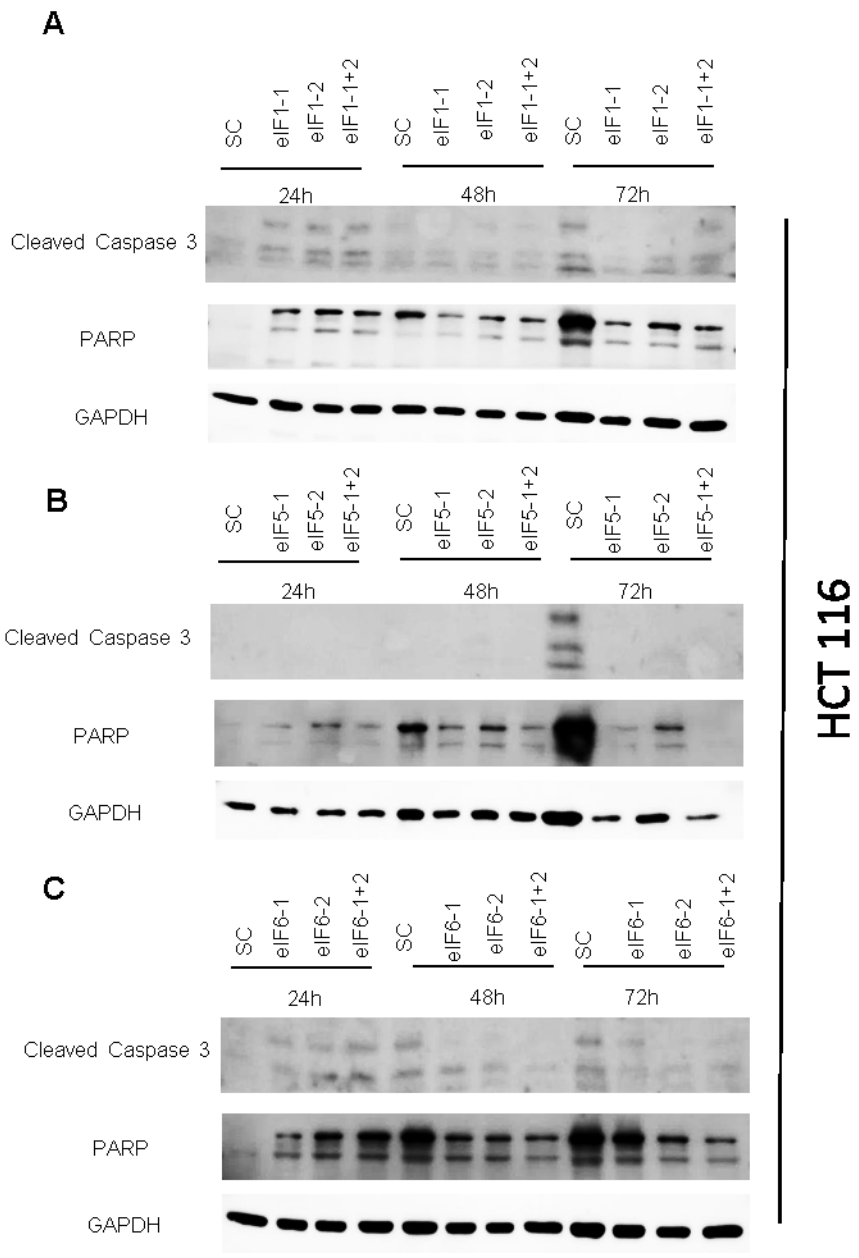

Figure 68: *In vitro* characterization of the effect eIF1, eIF5 and eIF6 knockdown in HCT116 cells on apoptosis rate. [A] Protein expression of cleaved caspase 3 and PARP in sieIF1-transfected HCT116 cells. [B] Protein expression of cleaved caspase 3 and PARP in sieIF5-transfected HCT116 cells. [C] Protein expression of cleaved caspase 3 and PARP in sieIF6-transfected HCT116 cells [181]. Three independent experiments were carried out.

The apoptosis rate of cells transfected with *eIF1*, *eIF5* and *eIF6* siRNA knockdown constructs (Figure 69 and 70) displayed less decrease only at the 72h time point [181].

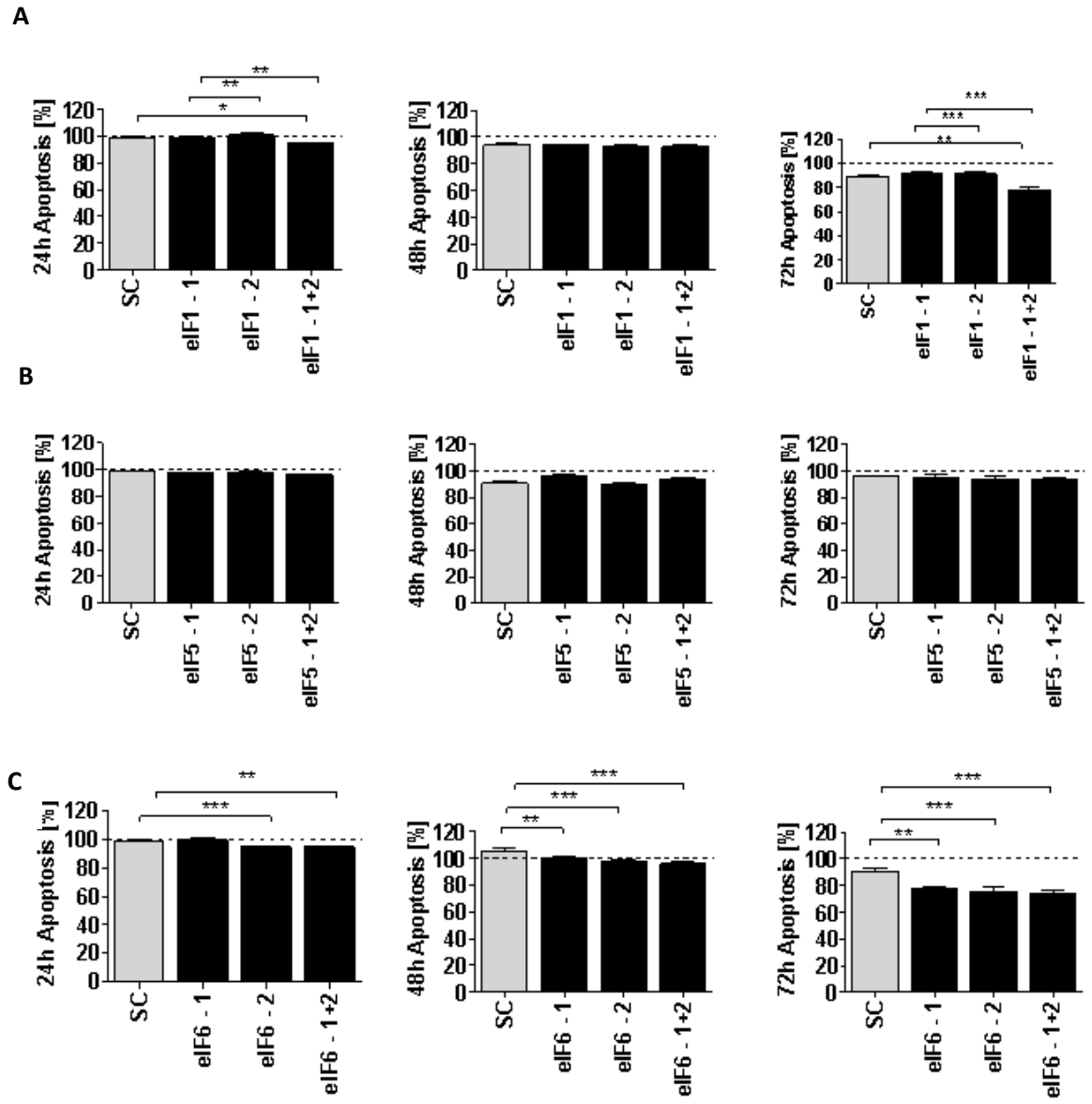

Figure 69: *In vitro* characterization of the effect of eIF1, eIF5 and eIF6 siRNA knockdown in HT29 cells. Graph shows apoptosis rate after eIF1 (A), eIF5 (B) and eIF6 (C) siRNA knockdown compared to SC [181]. Three independent experiments were carried out. Bars represent mean ± SEM. *p < 0.05, **p < 0.01, ***p < 0.001.

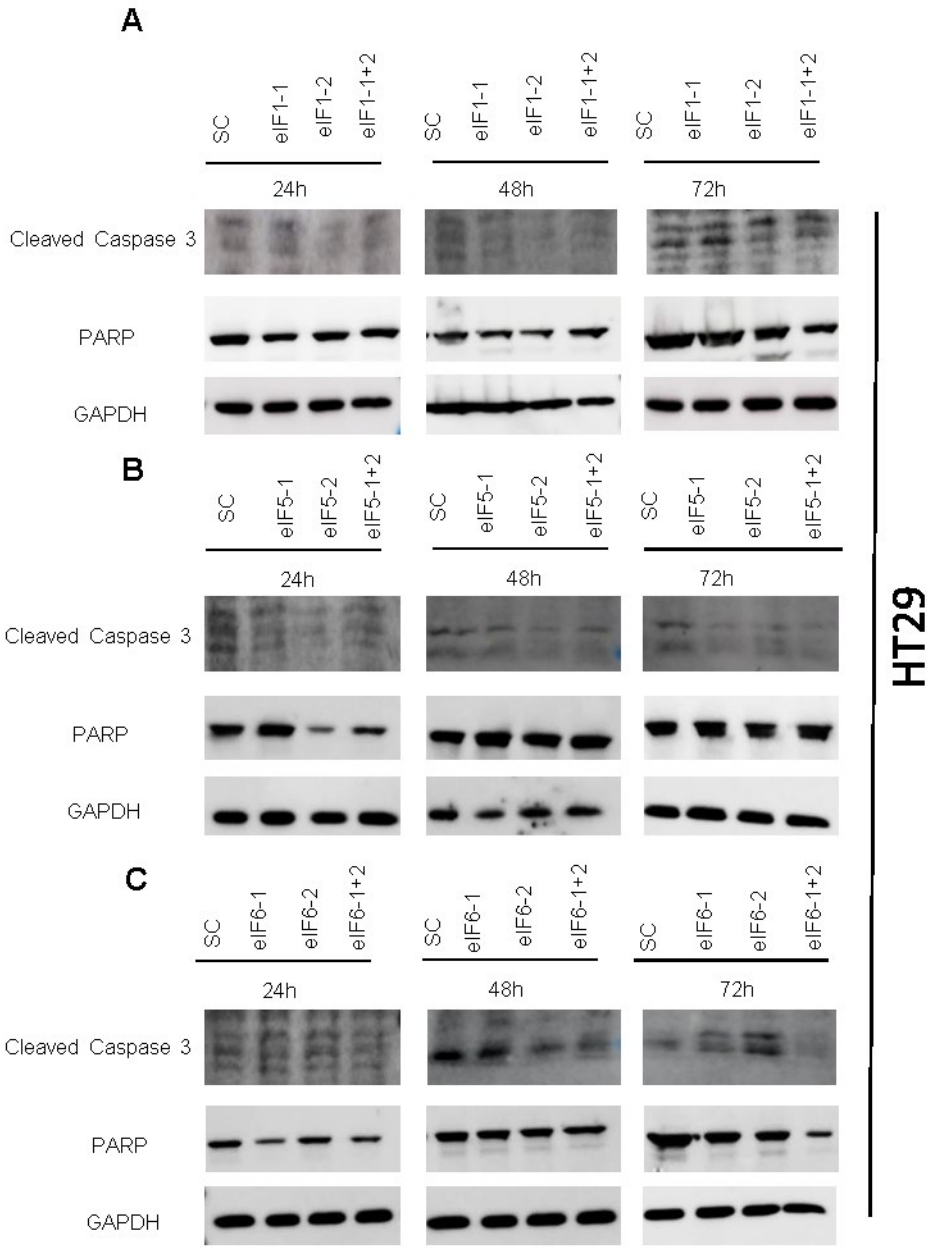

Figure 70: *In vitro* characterization of the effect eIF1, eIF5 and eIF6 siRNA knockdown in HT29 cells on apoptosis rate. [A] Protein expression of cleaved caspase 3 and PARP in sieIF1-transfected HT29 cells. [B] Protein expression of cleaved caspase 3 and PARP in sieIF5-transfected HT29 cells. [C] Protein expression of cleaved caspase 3 and PARP in sieIF6-transfected HT29 cells [181].

Silencing of *eIF1, eIF5* and *eIF6* led to a significant reduction in cell viability at all 3 time points (24h, 48h, 72h) (Figure 71) [181].

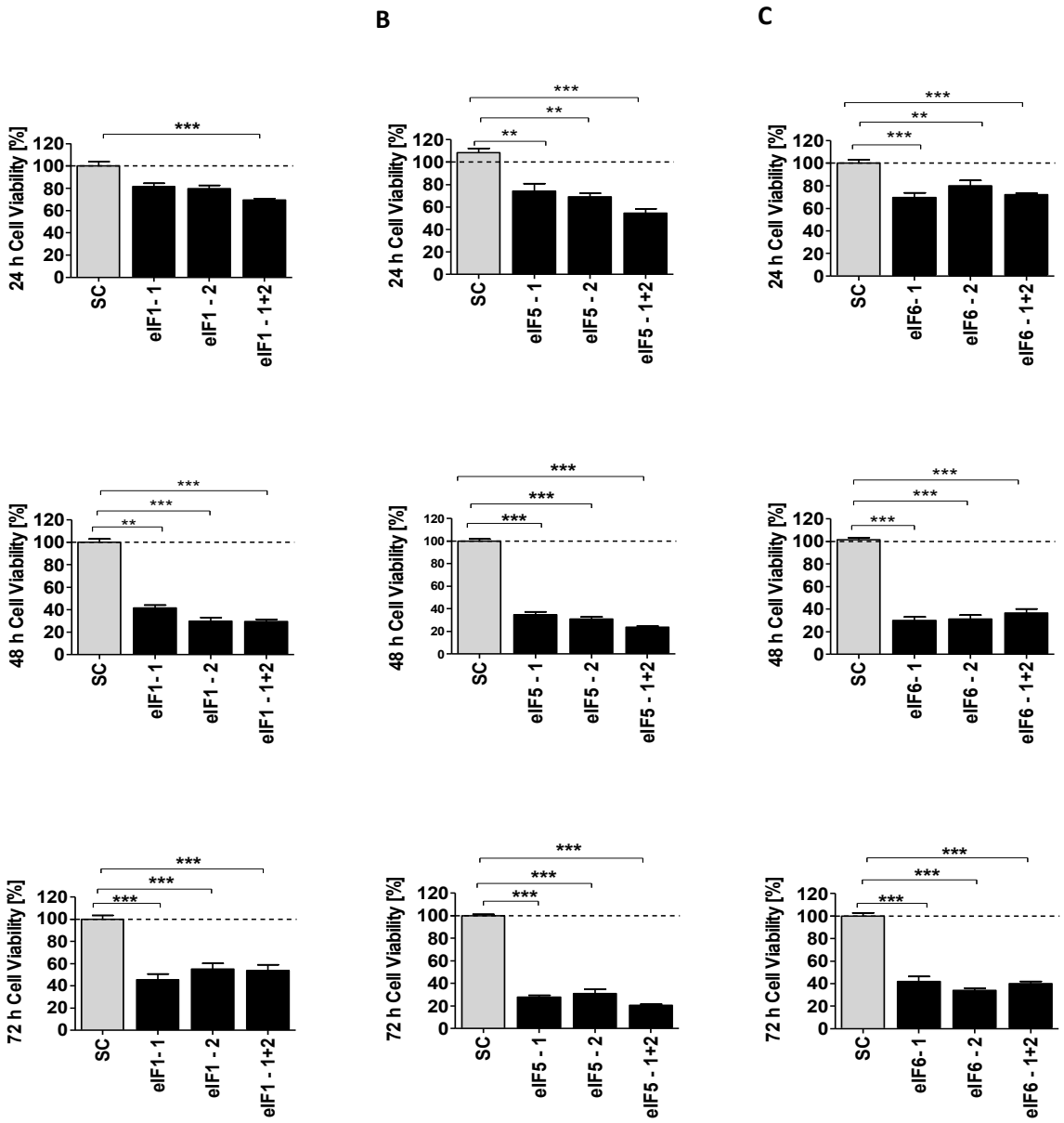

Figure 71: ***In vitro*** **characterization of the effect of eIF1, eIF5 and eIF6 siRNA knockdown in HCT116 cells.** Graph shows cell viability after eIF1 (A), eIF5 (B) and eIF6 (C) siRNA knockdown compared to SC [181]. Three independent experiments were carried out. Bars represent mean ± SEM. *p < 0.05, **p < 0.01, ***p < 0.001.

Silencing of *eIF1, eIF5* and *eIF6* led to less reduction in cell viability at all 3 time points (24h, 48h, 72h) in HT29 cells in comparison to HCT116 knockdown (Figure 71 – Figure 75) [181].

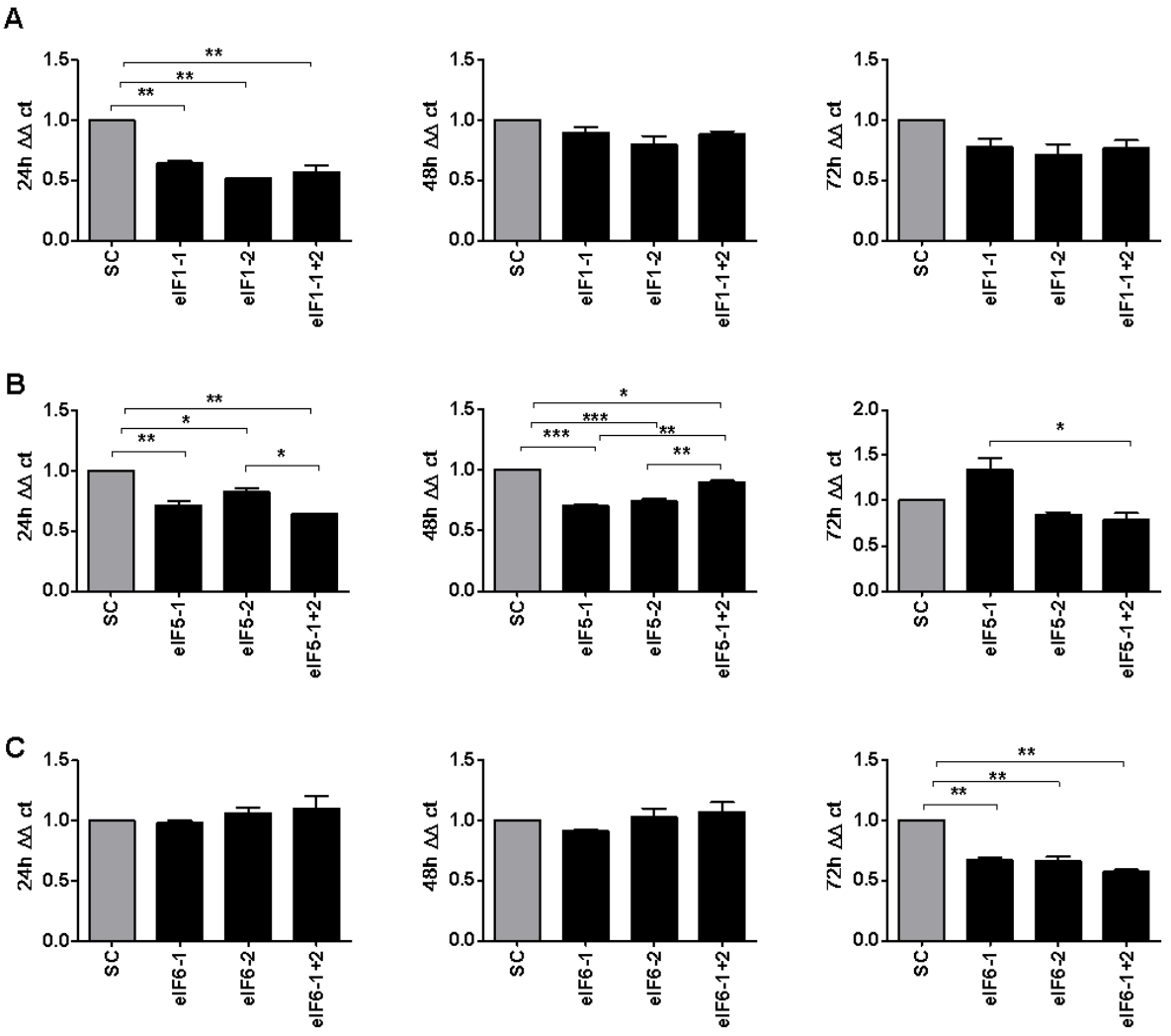

Figure 72: *In vitro* characterization of the effect of eIF1, eIF5 and eIF6 siRNA knockdown in HCT116 cells on Ki67 expression. [A] mRNA expression of Ki67 in sieIF1-transfected HCT116 cells. [B] mRNA expression of Ki67 in sieIF5-transfected HCT116 cells [C] mRNA expression of Ki67 in sieIF6-transfected HCT116 cells [181]. Three independent experiments were carried out. Bars represent mean ± SEM. *p < 0.05, **p < 0.01, ***p < 0.001.

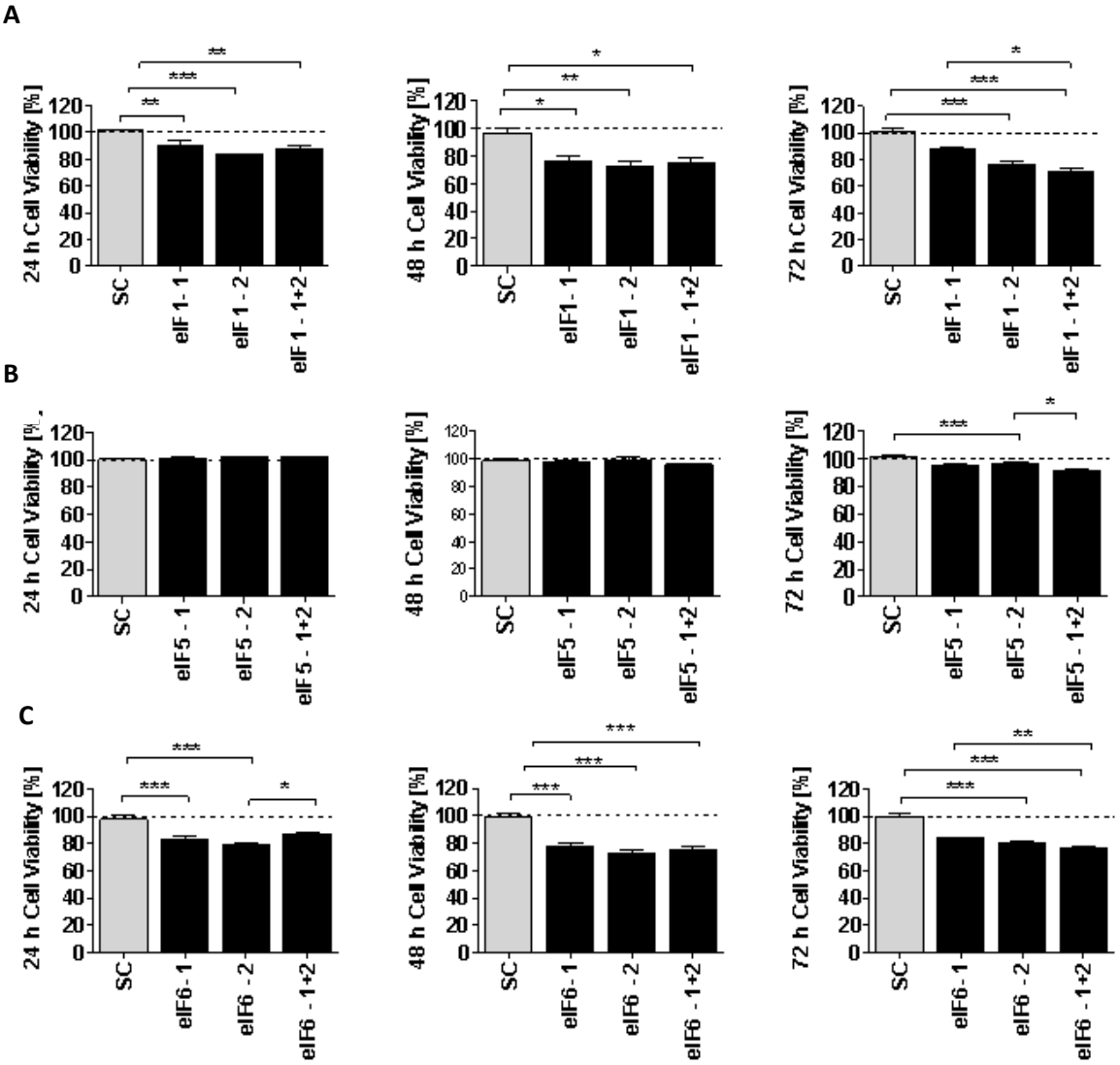

Figure 73: ***In vitro*** **characterization of the effect of eIF1, eIF5 and eIF6 siRNA knockdown in HT29 cells.** Graph shows cell viability after eIF1 (A), eIF5 (B) and eIF6 (C) siRNA knockdown compared to SC [181]. Three independent experiments were carried out. Bars represent mean ± SEM. *p < 0.05, **p < 0.01, ***p < 0.001.

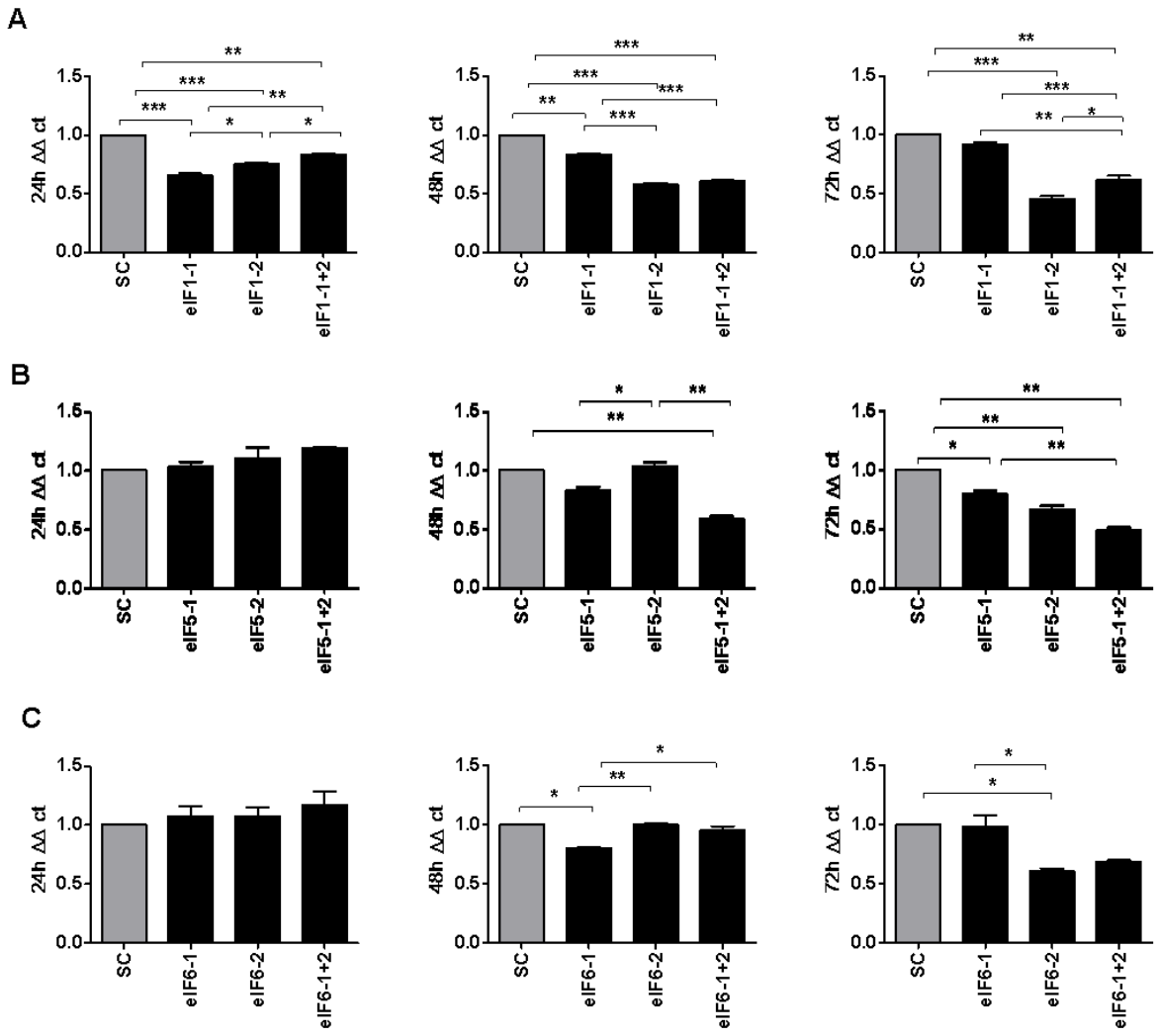

Figure 74: *In vitro* characterization of the effect of eIF1, eIF5 and eIF6 siRNA knockdown in HT29 cells on Ki67 expression rates. [A] mRNA expression of Ki67 in sieIF1-transfected HT29 cells. [B] mRNA expression of Ki67 in sieIF5-transfected HT29 cells [C] mRNA expression of Ki67 in sieIF6-transfected HT29 cells [181]. Three independent experiments were carried out. Bars represent mean ± SEM. *p < 0.05, **p < 0.01, ***p < 0.001.

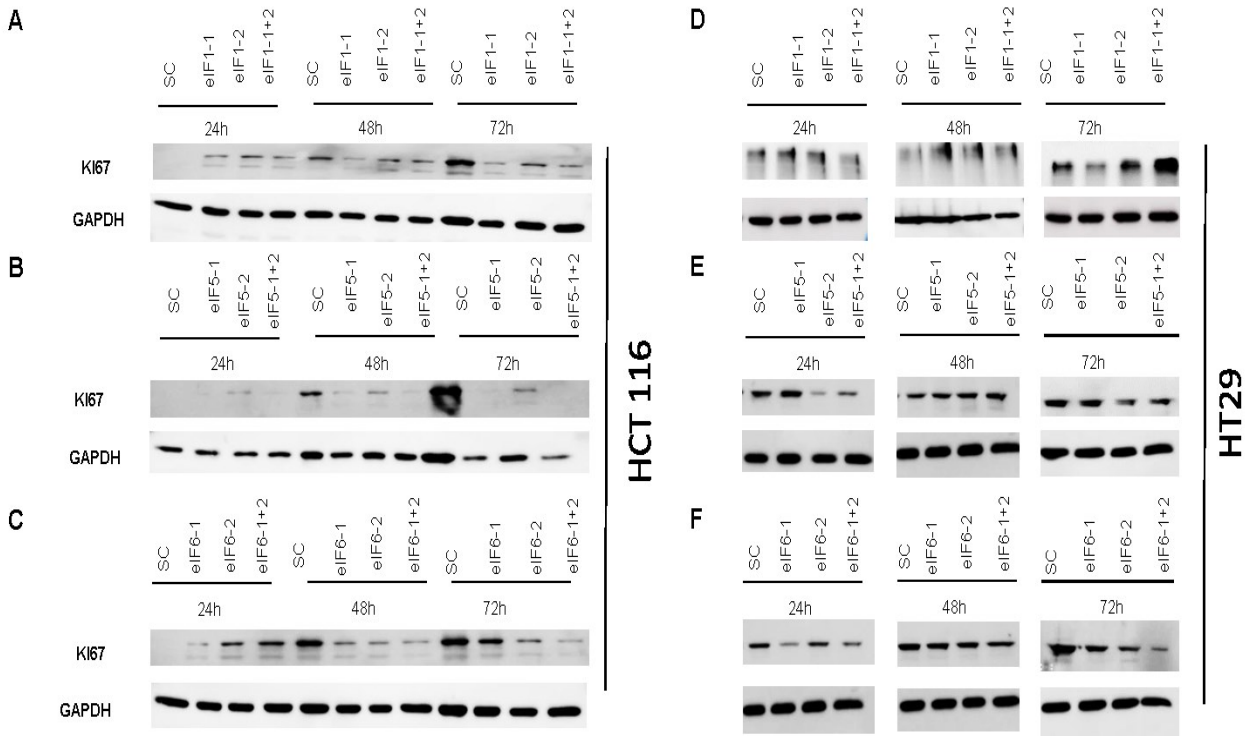

Figure 75: *In vitro* characterization of the effect of eIF1, eIF5 and eIF6 siRNA knockdown in HCT116 and HT29 cells on cell proliferation. [A] Protein expression of Ki67 in sieIF1-transfected HCT116 cells. [B] Protein expression of Ki67 in sieIF5-transfected HCT116 cells. [C] Protein expression of Ki67 in sieIF6-transfected HCT116 cells. [D] Protein expression of Ki67 in sieIF1-transfected HT29 cells. [E] Protein expression of Ki67 in sieIF5-transfected HT29 cells. [F] Protein expression of Ki67 in sieIF6-transfected HT29 cells [181].

Clonogenicity in HCT116 cells was evaluated by Giemsa staining. Colony formation was reduced 21 days after seeding in all siRNA transfected cells (Figure 76) [181].

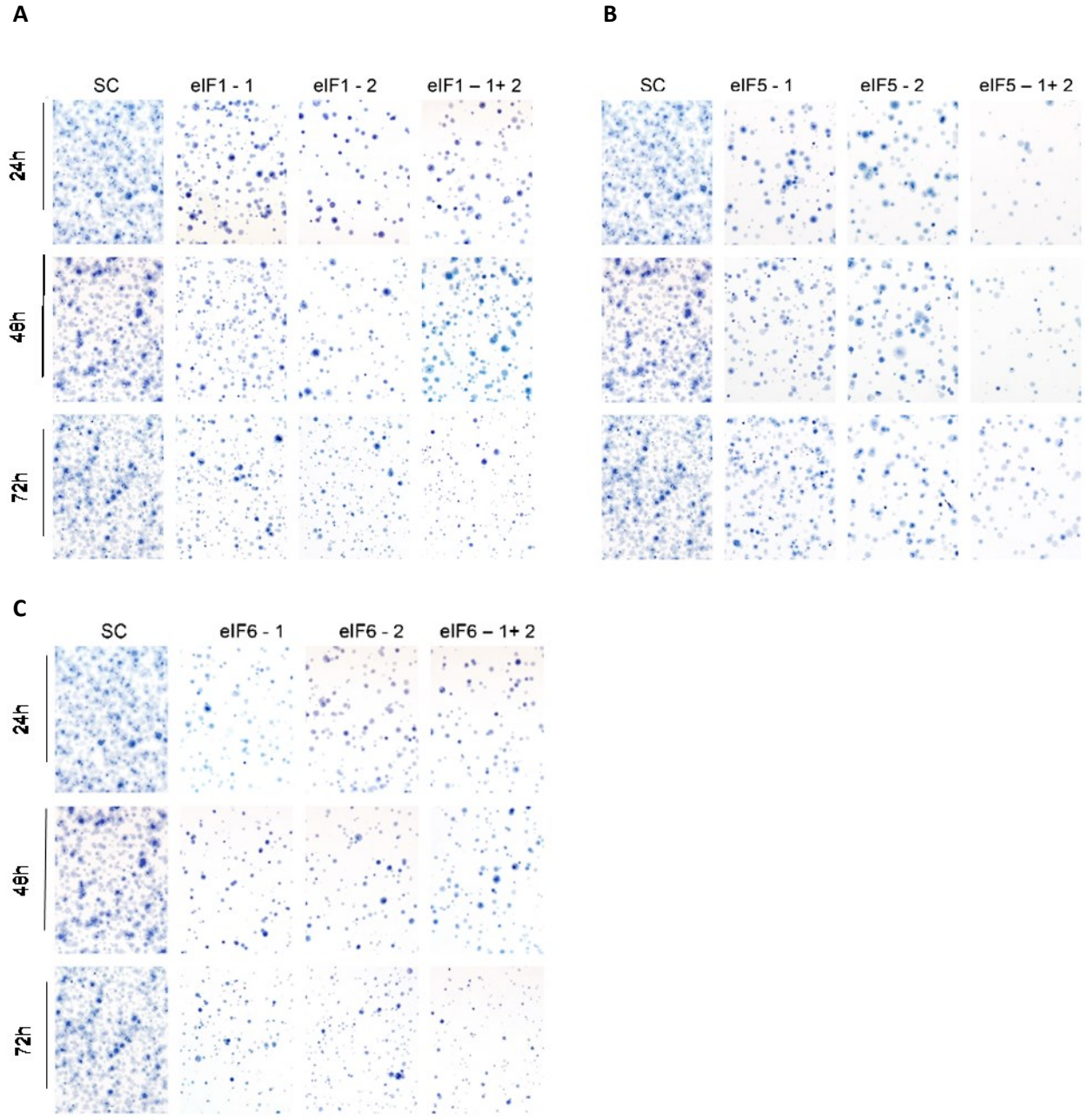

Figure 76: *In vitro* characterization of the effect of eIF1, eIF5 and eIF6 siRNA knockdown in HCT116 cells on clonogenicity. [A] Colony formation after si-eIF1 transfection in HCT116 cells after 21 days. [B] Colony formation after sieIF5 transfection in HCT116 cells after 21 days. [C] Colony formation after sieIF5 transfection in HCT116 cells after 21 days [181].

The effect of *eIF1*, *eIF5A* and *eIF6* siRNA knockdown on CRC cell motility was investigated by assessing the transmigration competence of cells through filters coated with an extracellular matrix. The cells exhibited reduced capability of transmigrating upon *eIF1*, *eIF5* and *eIF6* (Figure 77) siRNA knockdown compared to MOCK [181].

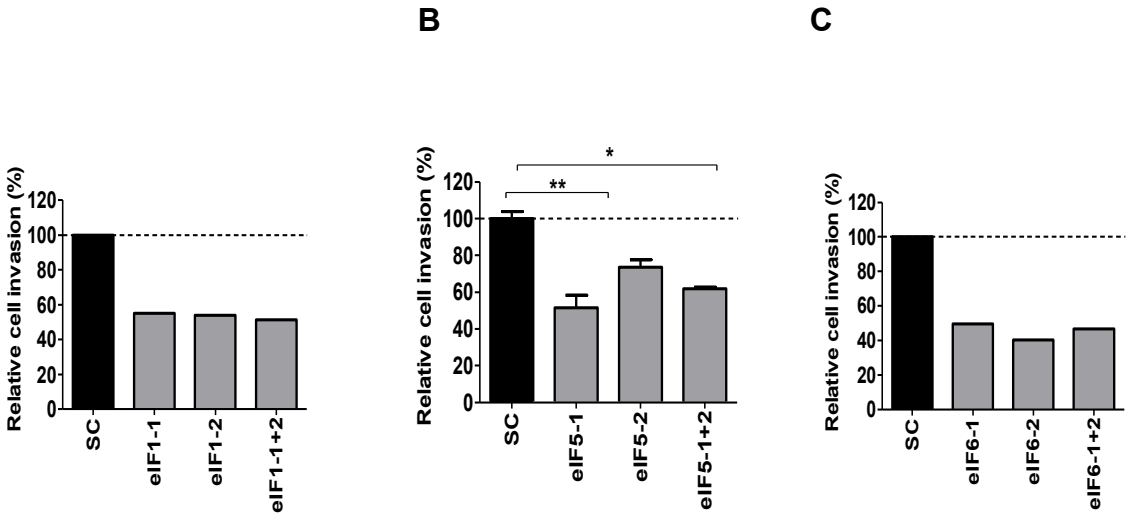

Figure 77*: In vitro* characterization of the effect of eIF1, eIF5 and eIF6 siRNA knockdown in HCT116 cells on invasiveness. [A] Invasive properties of HCT116 cells after eIF1 siRNA knockdown. [B] Invasive properties of HCT 116 cells after eIF5 siRNA knockdown. [C] Invasive properties of HCT116 cells after eIF6 siRNA knockdown [181]. Three independent experiments were carried out. Bars represent mean ± SEM. *p < 0.05, **p < 0.01, ***p < 0.001.

5.4.2 siRNA Knockdown of eIF1, eIF5 and eIF6 Leads to Reduced Translation

The effects of *eIF1*, *eIF5* and *eIF6* siRNA knockdown on translation initiation were investigated by polysome profiling. After sucrose density gradient centrifugation of cell lysates, polysomes, 80S ribosomes and free 40S and 60S subunits were detected by monitoring their A_{254nm} as described in the methods section.

Non-transfected HCT116 cells showed some free 40S and 60S subunits, a large 80S peak and low numbers of polysomes. After *eIF1* siRNA knockdown, increased levels of free 60S subunits and a marked decrease of the 80S peak were observed, suggesting a defect in

translation initiation. Furthermore, fewer polysomes were recorded in the *eIF1* siRNA knockdown profile, indicating reduced translation rates (Figure 78). *eIF5* knockdown also led to decreased levels of polysomes. In addition, the levels of free 40S and 60S ribosomal subunits relative to 80S ribosomes were increased, suggesting less efficient translation initiation (Figure 79). Similarly, *eIF6* siRNA knockdown resulted in a decrease in polysomes and an increase of the levels of free ribosomal subunits relative to 80S ribosomes (Figure 80).

In conclusion, siRNA knockdown of all three initiation factors resulted in a reduction of polysomes consistent with reduced initiation of translation [181].

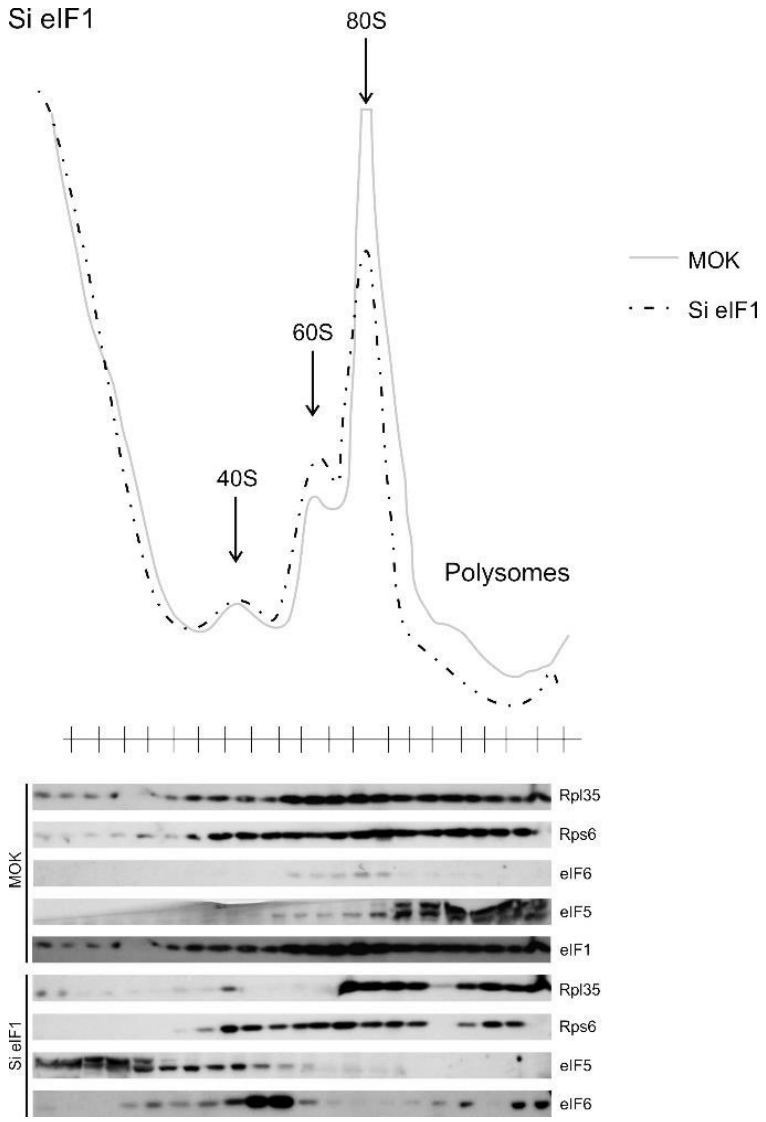

Figure 78: ***In vitro*** **characterization of the effect of eIF1 siRNA knockdown in HCT116 cells.** Sucrose density gradient profiles of HCT116 cells 72h after transfection with sieIF1 and MOCK [181].

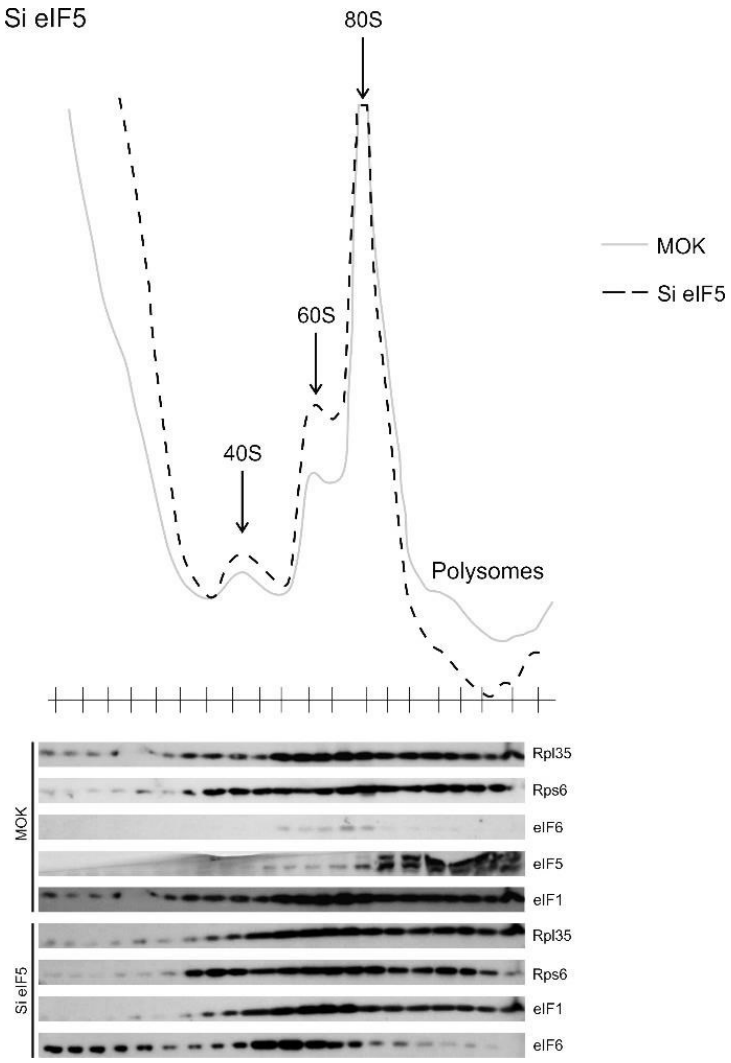

Figure 79: ***In vitro*** **characterization of the effect of eIF5 siRNA knockdown in HCT116 cells.** Sucrose density gradient profiles of HCT116 cells 72h after transfection with sieIF5 and MOCK [181].

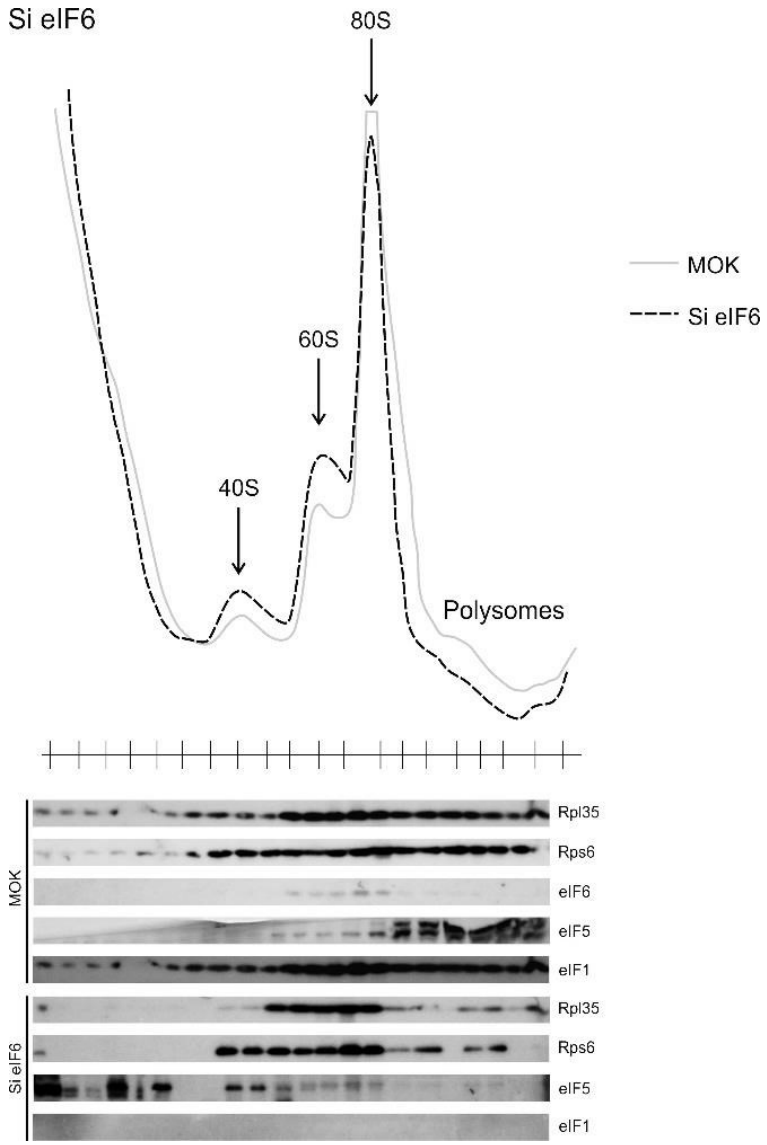

Figure 80: ***In vitro*** **characterization of the effect of eIF6 siRNA knockdown in HCT116 cells.** Sucrose density gradient profiles of HCT116 cells 72h after transfection with sieIF6 and MOCK [181].

5.5 *In vivo* Experiments

5.5.1 Chemosensitivity Testings of Colon Carcinoma Patient Derived Xenografts

The patient derived xenografts (PDX) represent 4 primary colon carcinoma (CC 1 – CC 4) models and one colon metastasis (CC-Met 1) model. The test for sensitivity to specific

chemotherapeutic drugs revealed Irinotecan (T/C=21), 5-FU (T/C=35) and Cetuximab (T/C=42) as the most efficient drugs to enhance growth of primary colon carcinoma. Treatment with IGF 1/2 mAB (T/C=191), AZ1 (T/C=142) and Volitinib (T/C=118) revealed higher tumor growth compared to PBS-treated samples. Treatment of the colon metastasis PDX led to a biologically meaningful reduction in tumor growth under treatment with Cetuximab (T/C=9), Oxaliplatin (T/C=48) and Irinotecan (T/C=34). Tumor growth upon treatment with IGF 1/2 mAB (T/C=251), 5-FU (T/C=110), Afatinib (T/C=111), Nintedanib (T/C=123) and Volitinib (T/C=161) revealed higher tumor growth than with PBS treatment.

Table 19: Chemosensitivity testing of PDX models for primary CC and CC-Met. Table shows treated tumor volumes in comparison to the PBS treated controls (T/C).

Drug	CC 1	CC 2	CC 3	CC 4	CC-Met 1
Oxaliplatin	70	98	62	89	48
Irinotecan	28	16	10	30	34
5-FU	56	50	18	15	110
Cetuximab	60	26	-	40	9
AZD8931	58	35	71	67	63
AZD6244	25	35	45	70	58
Afatinib	84	25	64	89	111
Avastin	37	86	83	103	70
Regorafenib	44	92	82	52	74
Nintedanib	50	77	58	53	123
mTOR FR	80	96	72	24	93
IGF 1/2 mAB	153	363	149	97	251
AZ1	101	260	125	81	-
Volitinib	-	198	84	71	161

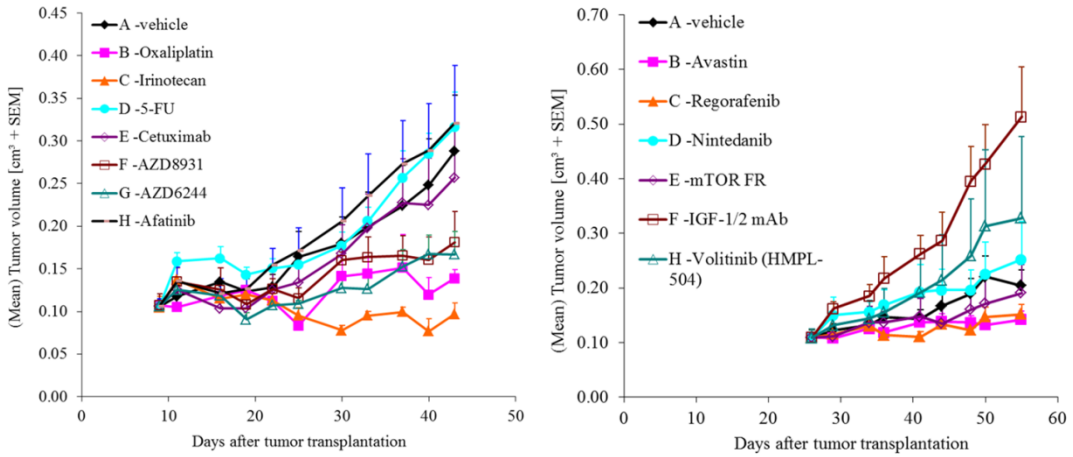

Figure 81: Growth curves of the colon metastasis PDX model (CC-Met 1) upon chemotherapeutic treatment. Growth curves display a biologically meaningful reduction of tumor growth upon treatment with Cetuximab, Oxaliplatin and Irinotecan. N=5/6

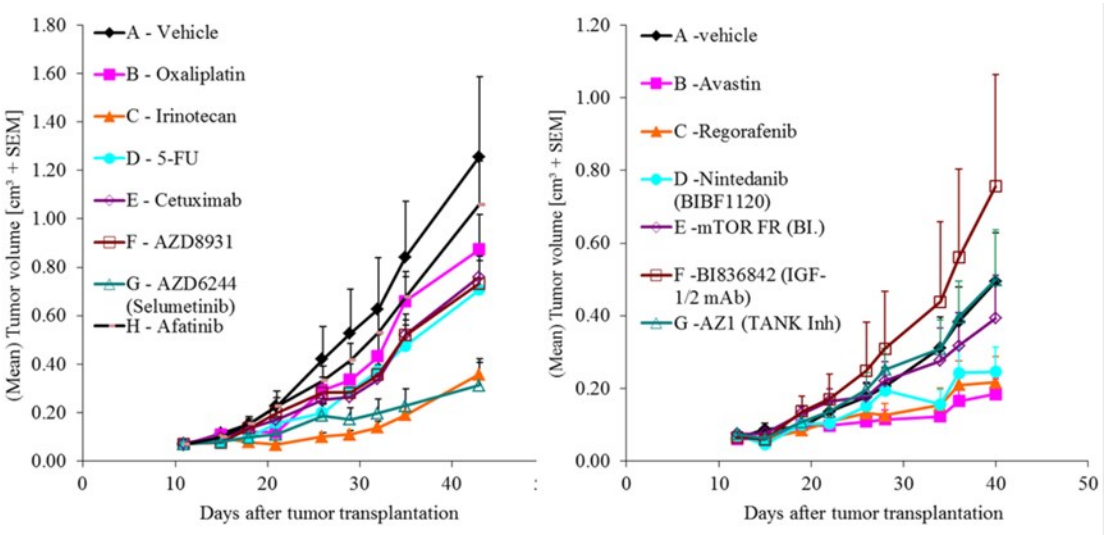

Figure 82: Growth curves of the colon primary carcinoma PDX model CC 1 upon chemotherapeutic treatment. Growth curves of CC 1 display a biologically meaningful reduction of tumor growth upon treatment with Irinotecan, AZD6244, Avastin and Regorafenib. N=5/6

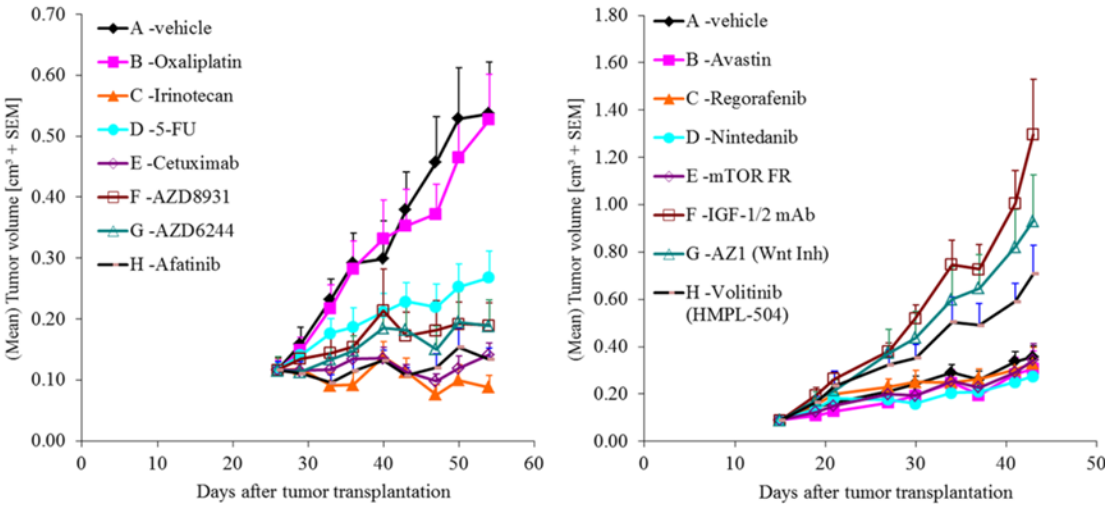

Figure 83: Growth curves of the colon primary carcinoma PDX model CC 2 upon chemotherapeutic treatment. Growth curves of CC 2 display a biologically meaningful reduction of tumor growth upon treatment with Irinotecan, Cetuximab, AZD8931, AZD6244 and Afatinib. N=5/6

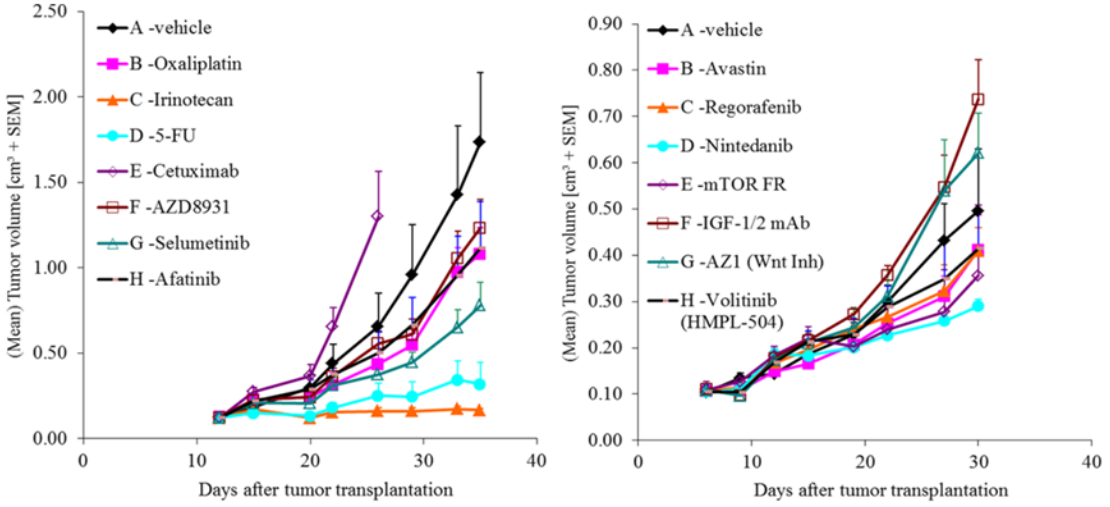

Figure 84: Growth curves of the colon primary carcinoma PDX model CC 3 upon chemotherapeutic treatment. Growth curves of CC 3 display a biologically meaningful reduction of tumor growth upon treatment with Irinotecan, 5-FU and AZD6244 (Selumetinib). N=5/6

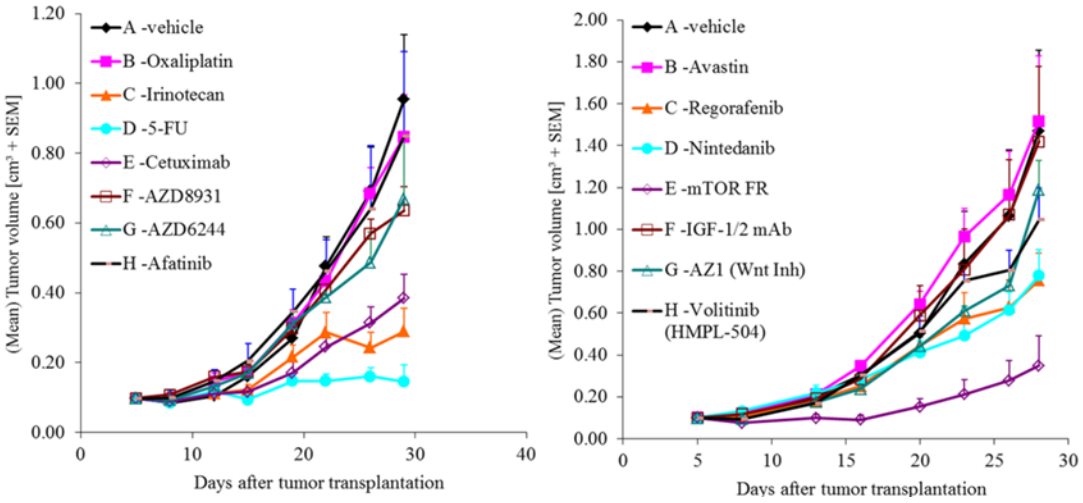

Figure 85: Growth curves of the colon primary carcinoma PDX model CC 4 upon chemotherapeutic treatment. Growth curves of CC 4 displays a biologically meaningful reduction of tumor growth upon treatment with Irinotecan, 5-FU, Cetuximab, Regorafenib, Nintedanib and mTOR FR. N=5/6

5.5.2 Chemosensitivity testings of Rectum Cancer Patient Xenograft Models

The PDX consists of 4 primary RC (RC 1 – RC 4) models and one rectum metastasis (RC-Met 1 and RC-Met 2) model.

The sensitivity testings of specific chemotherapeutic drugs displayed Irinotecan (T/C=16), Avastin (T/C=34), Regorafenib (T/C=34) and mTOR FR (T/C=36) as most efficient drugs to reduce growth of primary rectum carcinomas. Nintedanib (T/C=36), Oxaliplatin (T/C=45), 5-FU (T/C=46) and AZD6244 (T/C=40) also showed a biological meaningful growth reduction. In primary PDX models, tumor growth upon treatment with IGF 1/2 mAB (T/C=126) and AZ1 (T/C=123) was even higher than with PBS/vehicle treatment. For the PDX of the rectum metastases, we revealed the highest reduction in tumor growth upon treatment with Irinotecan (T/C=9), 5-FU (T/C=21), Cetuximab (T/C=26) and mTOR FR (T/C=31). In addition, a biologically meaningful reduction of tumor growth was also observed for Oxaliplatin (T/C=36), Afatinib (T/C=41), Nintedanib (T/C=45) and Avastin (T/C=37).

Table 20: Chemosensitivity testing of PDX models for primary RC and RC-Met. Table shows treated tumor volumes in comparison to PBS/vehicle controls (T/C).

Drug	RC 1	RC 2	RC 3	RC 4	RC-Met 1	RC-Met 2
Oxaliplatin	30	34	50	64	46	26
Irinotecan	4	32	22	8	5	13
5-FU	45	72	30	38	24	19
Cetuximab	76	89	122	19	10	42
AZD8931	82	62	49	78	39	75
AZD6244	32	36	36	55	38	62
Afatinib	49	78	58	75	38	44
Avastin	33	26	41	37	36	38
Regorafenib	39	21	52	26	41	75
Nintedanib	43	20	47	32	33	58
mTOR FR	13	13	62	33	38	24
IGF 1/2 mAB	190	73	130	111	87	83
AZ1	80	70	221	119	75	-
Volitinib	-	-	-	93	-	73

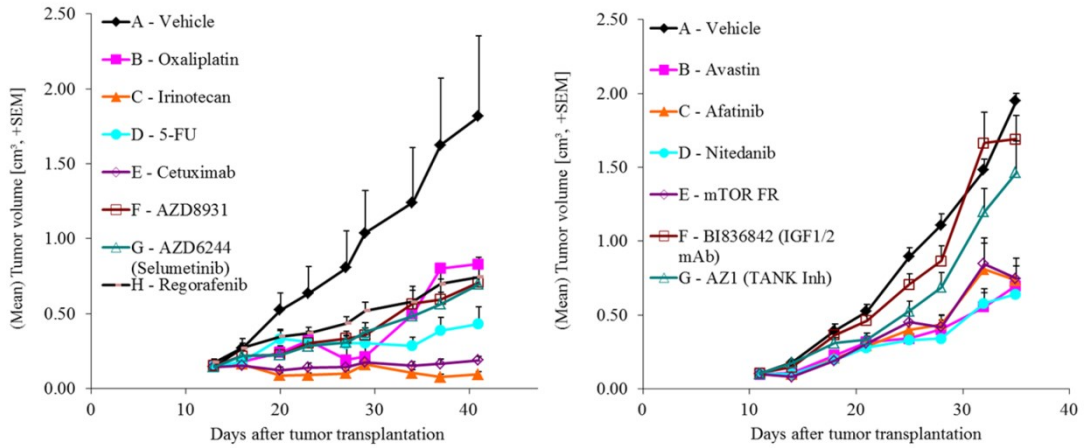

Figure 86: Growth curves of the rectum metastasis PDX model RC-Met 1 upon chemotherapeutic treatment. Growth curves of RC-Met 1 display a biologically meaningful reduction of tumor growth upon treatment with all mentioned drugs except IGF 1/2 mAB and AZ1. N=5/6

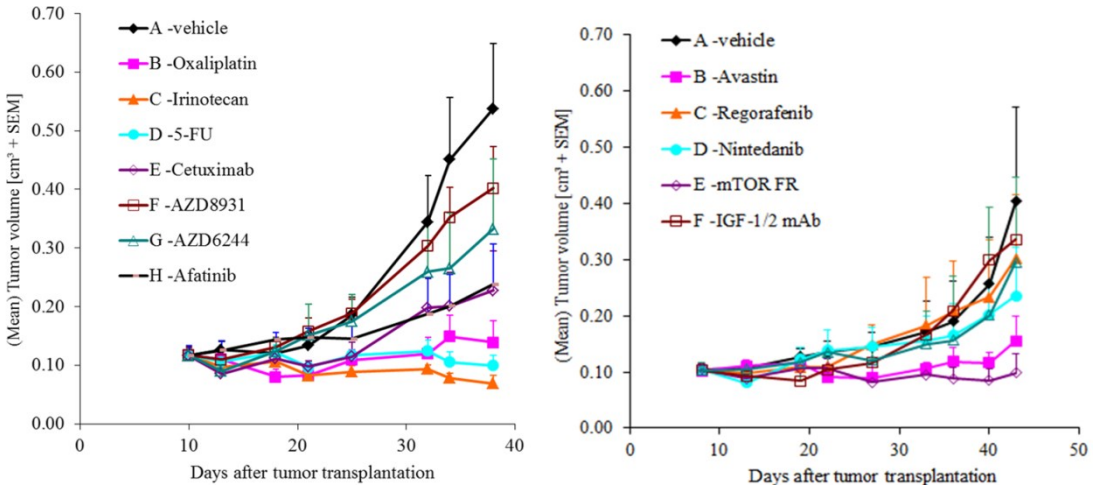

Figure 87: Growth curves of the rectum metastasis PDX model RC-Met 2 upon chemotherapeutic treatment. Growth curves of RC-Met 2 displays a biologically meaningful reduction of tumor growth upon treatment with Oxaliplatin, Irinotecan, 5-FU, Cetuximab, Afatinib, Avastin and mTOR FR. N=5/6

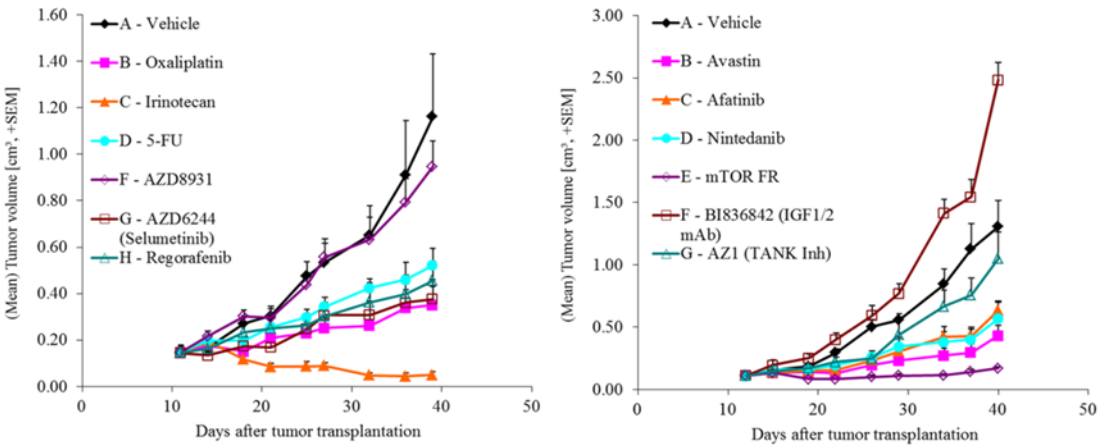

Figure 88: Growth curves of the rectum primary carcinoma PDX model RC 1 upon chemotherapeutic treatment. Growth curves of RC 1 display a biologically meaningful reduction of tumor growth upon treatment with Oxaliplatin, Irinotecan, 5-FU, AZD6244, Avastin, Regorafenib and mTOR FR. N=5/6

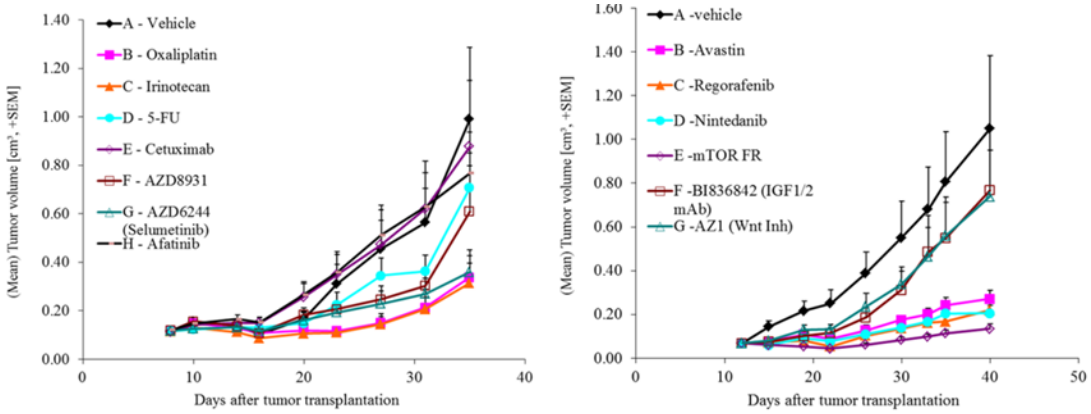

Figure 89: Growth curves of the rectum primary carcinoma PDX model RC 2 upon chemotherapeutic treatment. Growths curves of RC 2 displays a biologically meaningful reduction of tumor growth upon treatment with Oxaliplatin, Irinotecan, AZD6244, Avastin, Regorafenib, Nintedanib and mTOR FR. N=5/6

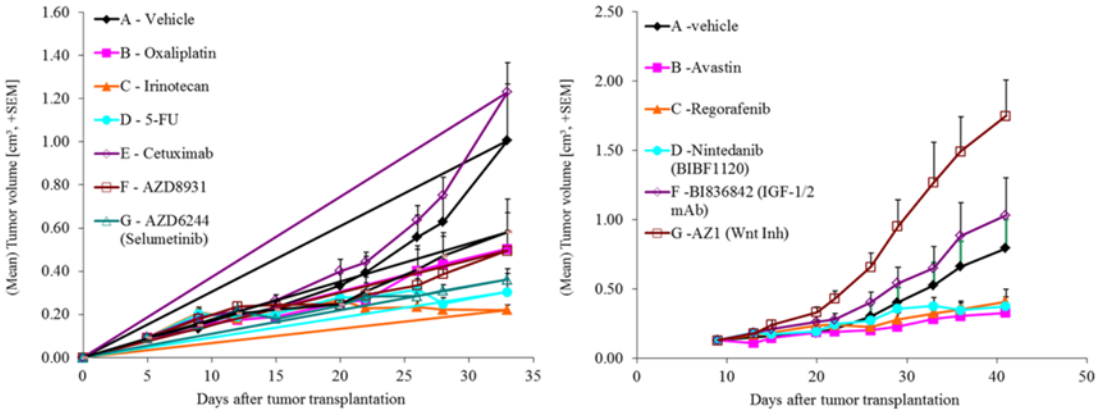

Figure 90: Growth curves of the rectum primary carcinoma PDX model RC 3 upon chemotherapeutic treatment. Growth curves of RC 3 displays a biologically meaningful reduction of tumor growth upon treatment with Irinotecan, 5-FU, AZD6244 and Avastin. N=5/6

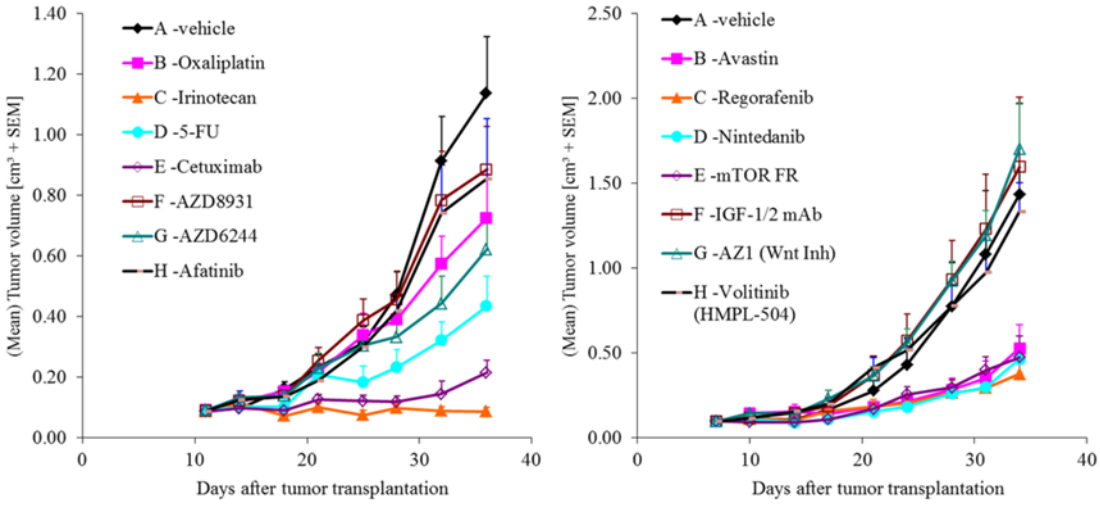

Figure 91: Growth curves of the rectum primary carcinoma PDX model RC 4 upon chemotherapeutic treatment. Growth curves of RC 4 display a biologically meaningful reduction of tumor growth upon treatment with Irinotecan, Cetuximab, Avastin, Regorafenib, Nintedanib and mTOR FR. N=5/6

5.5.3 Protein Expression of eIFs and mTOR Members in Primary CC PDX Models

Using immunoblots, we analyzed protein expression of various eIF subunits and mTOR members in treated PDX models of four primary colorectal carcinoma tissues and one liver metastasis from primary colorectal cancer. During relative quantification, protein levels were normalized to non-neoplastic tissue and untreated controls. Actin was used as a housekeeping gene (Figure 92).

Compared to untreated control, mTOR was upregulated under treatment with Oxaliplatin and Cetuximab in primary colon carcinoma PDX models. A partly downregulation was visible in the AZ1-treated colon carcinoma PDX model. Protein expression of mTOR in the liver metastasis revealed an upregulation under Afatinib treatment. According to untreated controls, mTOR, eIF2α, eIF3J, eIF4B and eIF5 were increased in the Afatinib-treated metastasis. In addition, PTEN seemed to be decreased in Avastin-treated metastasis. Protein expression of PTEN, eIF2α, eIF3A, eIF3J, eIF3B, eIF4B, eIF4G and eIF5 was heterogeneous and displayed no visible changes when comparing untreated and treated colon cancer tissue (Figure 93).

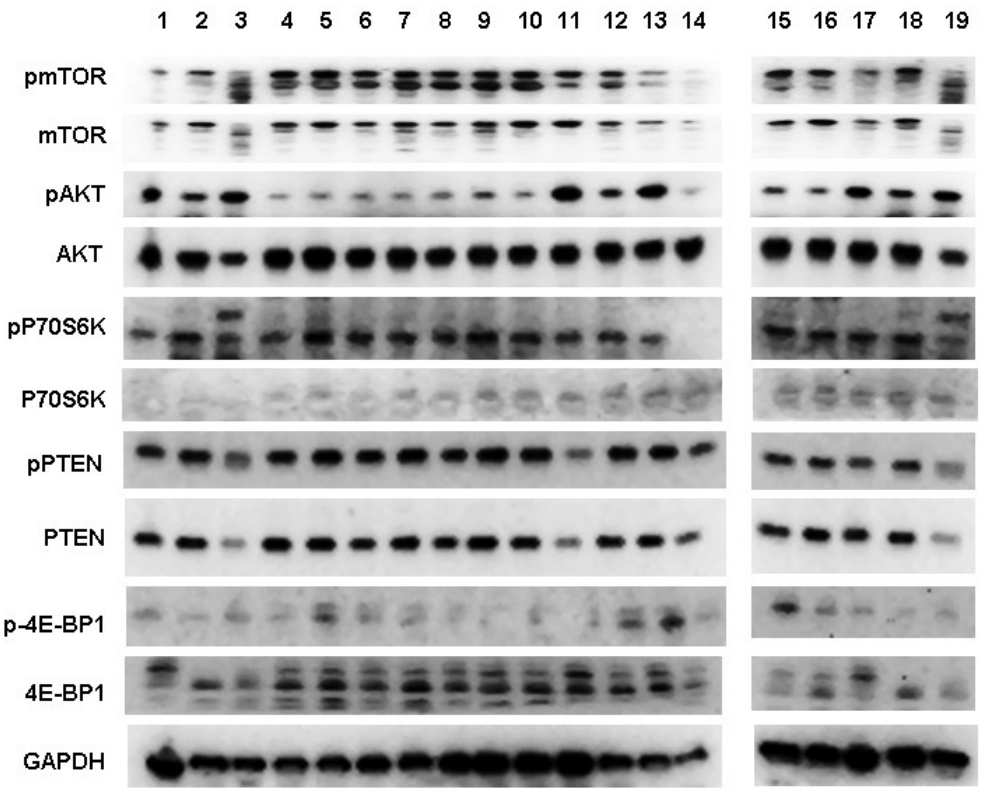

Figure 92: Protein expression of mTOR pathway members in untreated and treated CC PDX models. (1) Vehicle/PBS treated Xenograft; (2) Primary Tumor; (3) non-neoplastic tissue; (4) Oxaliplatin; (5) Irinotecan; (6) Cetuximab; (7) 5-FU; (8) AZD 8961; (9) AZD 6244; (10) Afatinib; (11) Avastin; (12) Regorafenib; (13) Nintedanib; (14) mTOR FR; (15) IGF1/2 mAB; (16) AZ 1; (17) Vehicle/PBS treated Xenograft; (18) Primary Tumor; (19) NNT. GAPDH was used as loading control. Three independent experiments were carried out. Bars represent mean ± SEM. *$p < 0.05$, **$p < 0.01$, ***$p < 0.001$.

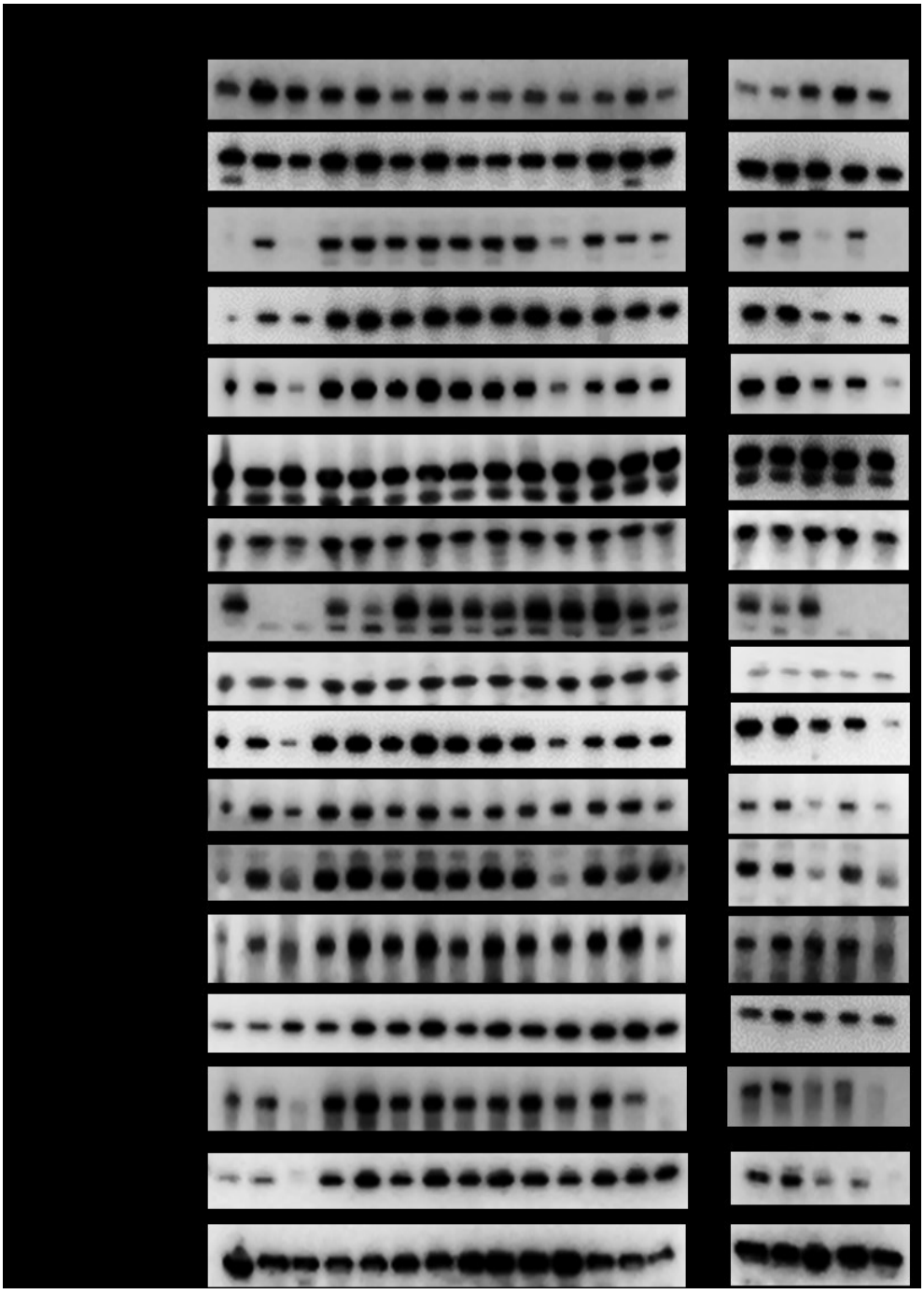

Figure 93: Protein expression of various eIF subunits in untreated and treated CC PDX models. (1) Vehicle/PBS treated Xenograft; (2) Primary Tumor; (3) non-neoplastic tissue; (4) Oxaliplatin; (5) Irinotecan; (6) Cetuximab; (7) 5-FU; (8) AZD 8961; (9) AZD 6244; (10) Afatinib; (11) Avastin; (12) Regorafenib; (13) Nintedanib; (14) mTOR FR; (15) IGF1/2 mAB; (16) AZ 1; (17) Vehicle/PBS treated; (18) Primary Tumor; (19) NNT. GAPDH was used as loading control. Three independent experiments were carried out. Bars represent mean ± SEM. *p < 0.05, **p < 0.01, ***p < 0.001.

5.5.4 Protein Expression of eIFs and mTOR Members in Primary RC PDX Models

Four primary RCs and two liver metastases from primary RC PDX models were analyzed. Protein expression of eIF3J showed downregulation in liver metastases upon treatment with Nintedanib, mTOR FR and IGF 1/2 mAB. In addition, these models displayed downregulation of eIF3A upon treatment with Irinotecan, 5-FU, Avastin, Regorafenib, Nintedanib and mTOR FR. Protein expression of eIF4G was increased in Oxaliplatin and Cetuximab-treated primary RC PDX (Figure 94 and Figure 95).

Protein expression of PTEN, eIF2α, eIF3J, eIF3B, eIF4B and eIF5 was heterogeneous and displayed no visible changes when comparing untreated and treated RC tissue (Figure 96 and Figure 97).

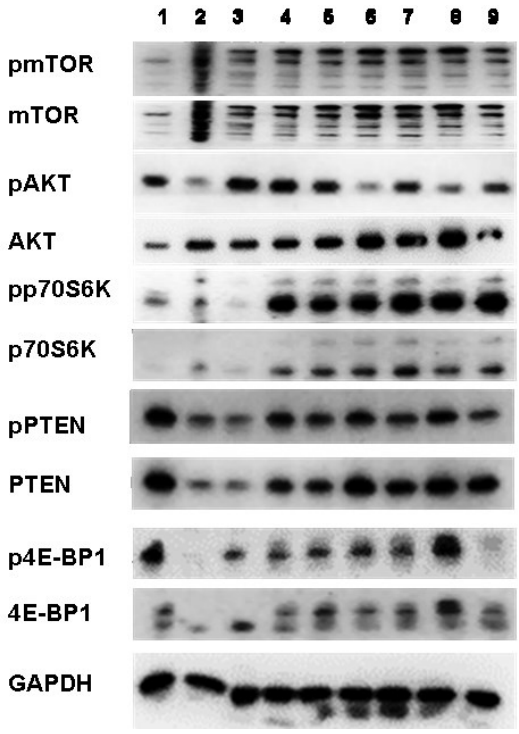

Figure 94: Protein expression of mTOR pathway members in untreated and treated RC PDX models. (1) Vehicle/PBS treated Xenograft; (2) Primary Tumor; (3) NNT; (4) Irinotecan; (5) Cetuximab; (6) AZD 8961; (7) Regorafenib; (8) Afatinib; (9) mTOR FR. GAPDH was used as loading control. Three independent experiments were carried out. Bars represent mean ± SEM. *p < 0.05, **p < 0.01, ***p < 0.001.

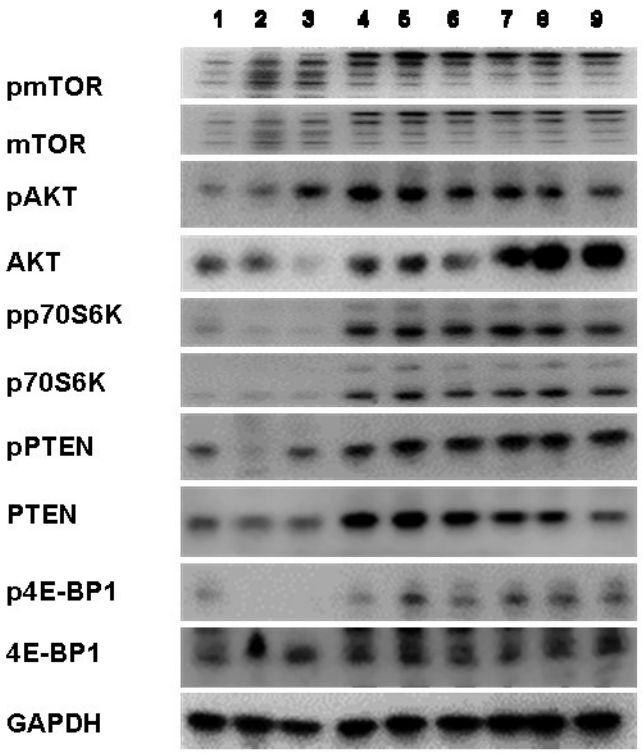

Figure 95: Protein expression of mTOR pathway members in untreated and treated RC PDX models. (1) Vehicle/PBS treated Xenograft; (2) Primary Tumor; (3) NNT; (4) 5-FU; (5) AZD6244; (6) Avastin; (7) Nintedanib; (8) IGF 1/2 mAB; (9) AZ 1. GAPDH was used as loading control. Three independent experiments were carried out. Bars represent mean ± SEM. *p < 0.05, **p < 0.01, ***p < 0.001.

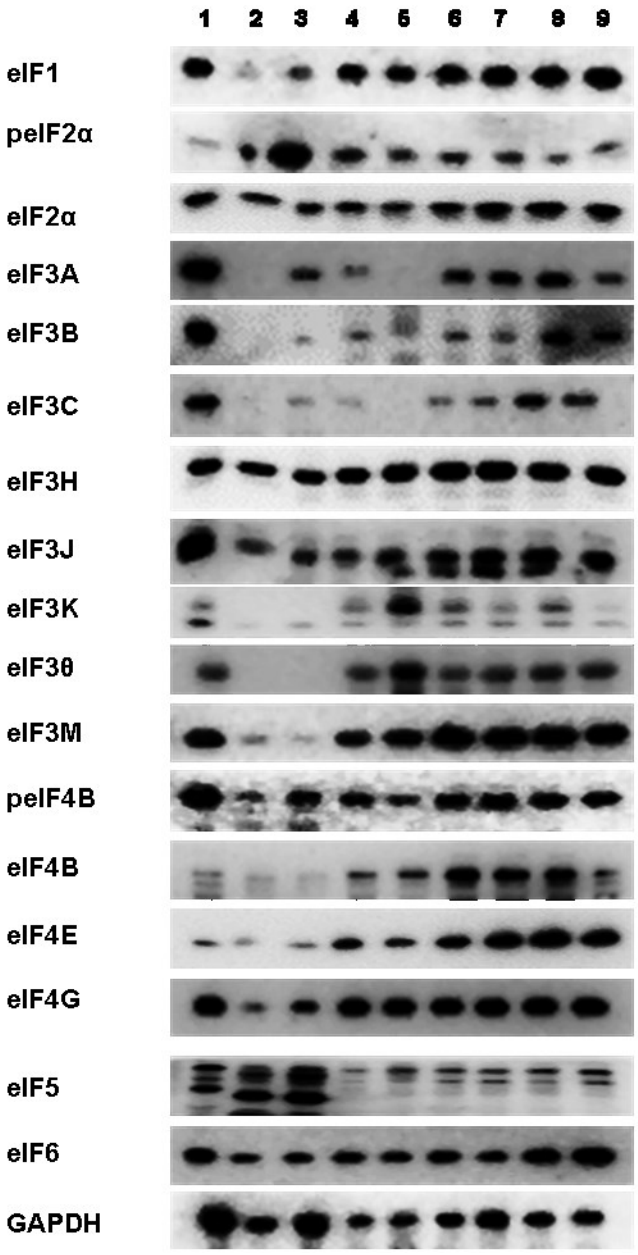

Figure 96: Protein expression of various eIF subunits in untreated and treated RC PDX models. (1) Vehicle/PBS treated Xenograft; (2) Primary Tumor; (3) NNT; (4) Irinotecan; (5) Cetuximab; (6) AZD 8961; (7) Regorafenib; (8) Afatinib; (9) mTOR FR. GAPDH was used as loading control. Three independent experiments were carried out. Bars represent mean ± SEM. *p < 0.05, **p < 0.01, ***p < 0.001.

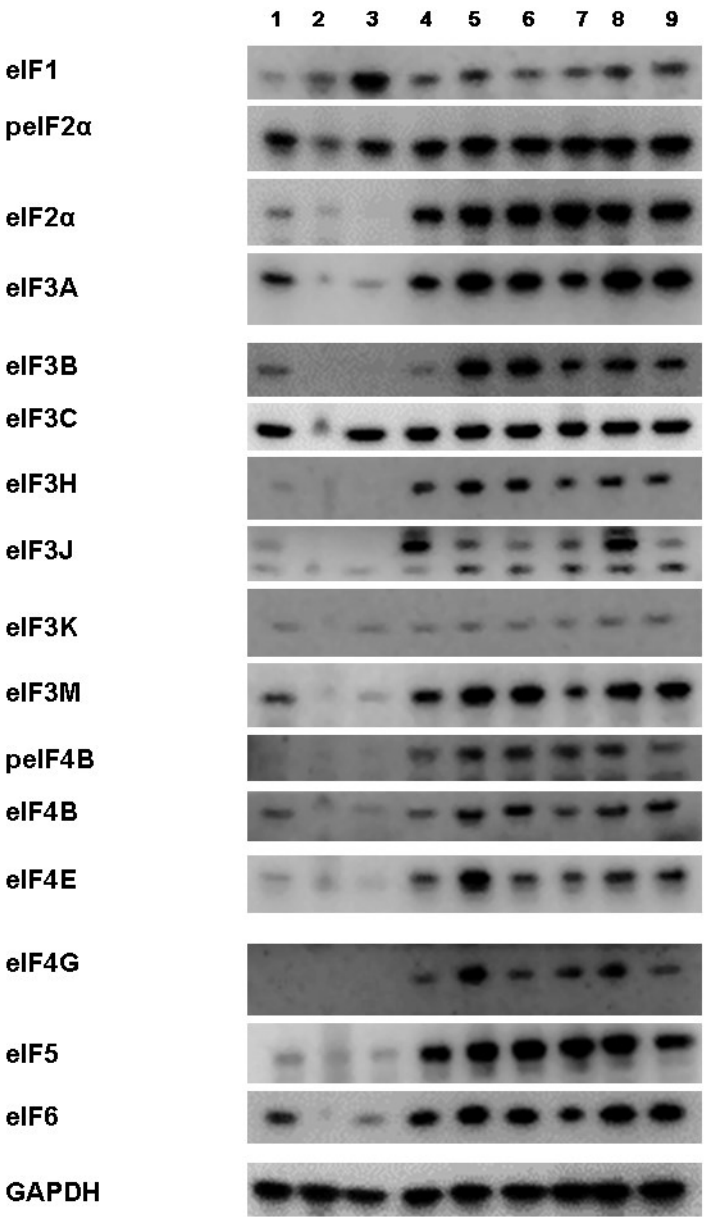

Figure 97: Protein expression of various eIF subunits in untreated and treated RC PDX models. (1) Vehicle/PBS treated Xenograft; (2) Primary Tumor; (3) NNT; (4) 5-FU; (5) AZD6244; (6) Avastin; (7) Nintedanib; (8) IGF 1/2 mAB; (9) AZ 1. GAPDH was used as loading control. Three independent experiments were carried out. Bars represent mean ± SEM. *p < 0.05, **p < 0.01, ***p < 0.001.

6 Discussion

The results obtained within this PhD project indicate that eIF5 are prognostic biomarkers in HBV, HCV, HBV- and HCV-associated HCC, non-virus related HCC, ASH and Morbus Wilson. Biomarkers are indispensable for prognostic reasons and future tailored therapy. We investigated HBV, HCV, HBV- and HCV-associated HCC, non-virus related HCC, ASH and Morbus Wilson tissue samples and analyzed them biochemically for the expression of mTOR signaling pathway members and eIFs.

There are differences in the expression pattern of mTOR pathway members and eIFs between NNLT and HBV, HCV, HBV- and HCV-associated HCC and non-virus related HCC. Thus, differentiation of the before mentioned tumor types is recommended not only because of their different prognosis, but also because of their distinct molecular profiles.

The findings indicate a prognostic clinical impact when separating etiology based chronic HBV, HCV, HBV- and HCV-associated HCC and non-virus related HCC and emphasizes the potential of eIF5 as a biomarker for non-virus related and virus related HCC [182].

In the second part of this thesis human CRC tissue samples were analyzed biochemically for the expression of mTOR signaling pathway members and eIFs, continued by the subclassification into CC and RC as well as low and high grade tumors. It was revealed that eIFs are also prognostic biomarkers in CRC patients, in particular eIF1, eIF5 and eIF6 and support the hypothesis that eIF1, eIF5 and eIF6 are involved in the carcinogenesis in this tumor entity. eIF1, eIF5 and eIF6 are differentially expressed in CC and RC as well as in low and high grade CC and RC.

The third part of this thesis investigated CRC cell lines in which a siRNA-knockdown was established and cellular changes upon reduction of eIF1, eIF5 and eIF6 were analyzed. These autonomous approaches argue in conclusion, that eIF1, eIF5 and eIF6 are important parts in the translation initiation and show characteristics of prognostic as well as predictive biomarkers in CRC. Changes with eIF1, eIF5 and eIF6 siRNA-knockdown were observed, including reduced protein and mRNA expression as well as reduced proliferation, cell motility and increase apoptosis rate. I also analyzed the knockdown effects of eIF1, eIF5 and eIF6 on translation initiation by sucrose density gradient profiling. The control showed some free 40S and 60S subunits, a large 80S peak and low numbers of polysomes. eIF1 reduction revealed increased levels of free 60S subunits and a marked decrease of the 80S peak were observed suggesting a defect in translation initiation. eIF5 profiles led to increased levels of free 40S

and 60S ribosomal subunits relative to 80S ribosomes, suggesting less efficient translation initiation. Additionally, decreased amounts of polysomes were detected. Similarly, eIF6 siRNA-knockdown was indicative of increased levels of free ribosomal subunits relative to 80S ribosomes and a decrease in polysomes. In conclusion, knockdown of all three initiation factors resulted in a relative increase of free ribosomal subunits relative to 80S ribosomes and polysomes, consistent with reduced initiation of translation.

Even though in literature CC and RC are frequently summarized under the term CRC, these results emphasize a probable prognostic impact when separating low and high grade CC and RC and eIF1, eIF5 and eIF6 play a major role in the translation initiation in CC and RC [181].

6.1 Characterization of mTOR Members and eIFs in HCC

eIFs are involved in the translation of growth factors, proteins influencing cell cycle, apoptosis and malignant transformation. mTOR pathway members and eIFs are overexpressed in malignancies, such as head and neck squamous cell carcinoma, lung, thyroid, breast cancer and other cancer types [150], but data on eIFs in HCC are still poor.

Significant differences in the expression levels of mTOR signaling pathway members and various eIF subunits in HBV, HCV, HBV- and HCV-associated HCC, non-virus related HCC, ASH and Morbus Wilson were found.

One of the major pathways involved in regulation of protein synthesis, cell growth and proliferation is the PI3K/AKT/mTOR pathway [151 -153]. In our study, we found an overexpression of mTOR, pAKT, AKT, pPTEN and PTEN in non-virus related HCC, HCV-associated HCC, ASH and Morbus Wilson. Moreover, we observed a downregulation for pmTOR and mTOR in HBV, HCV and HBV-associated HCC. We and others, observed a downregulation of PTEN in HCV associated HCC; HBV associated HCC and also HCV as well as in non-virus related HCC. Patients with HBV infection showed an increased protein level of PTEN but a downregulation of AKT. It seems that the involvement of PTEN triggers uncontrolled or increased protein expression in HBV.
Previous studies investigated a large patient cohort and observed an increase for mTOR in non-virus related HCC [154]. However, the downregulation of pmTOR and mTOR did not seem to be a driver of tumor growth in HBV, HCV and HBV-associated HCC. Animal studies

suggest mTOR as a crucial driver of carcinogenesis at early stages of the disease, but not in advanced liver cancer [155, 156].

Former studies have shown an overexpression of eIF4E and eIF3I in different cancers, including non-virus related HCC [150, 157]. This supports the results presented here, that eIF4E and eIF3I are involved in non-virus related HCC formation and also in the pathogenesis of ASH and Morbus Wilson. Downregulation of eIF4E and eIF3I was observed for HBV- and HCV- associated HCC, as well as for HBV and HCV.

The results of the PhD thesis revealed that, on the one hand, eIF5 showed a downregulation in non-virus related HCC, HCV-associated HCC and HCV. On the other hand, HBV-associated HCC and HBV displayed an overexpression for eIF5. eIF5 overexpression has been reported as a predictive tumor marker in different cancers [158], but not in HCV-associated HCC and HCV. The results presented within this thesis regarding eIF5 expression were similar to those of lymphoma studies [159]. To evaluate the potential predictive power of eIF5 we conducted a number of proportional hazard models, also referred to as Cox regressions. The backward stepwise model selection approach eliminated all covariates, except for eIF5, which again emphasizes the potential of eIF5 as a biomarker for non-virus related and virus related HCC.

Strong correlation of altered levels of specific eIF3 subunits and cancer suggests that eIF3 subunits may play a causative role in malignant transformation. However, it still needs to be clarified how increased levels of particular eIF3 subunits promote translation and support tumorigenesis [160, 151]. Previous studies have shown an overexpression of eIF6 in some cancer types, such as head and neck cancer, lung metastasis and malignant mesothelioma. The question of which mechanistic factor leads to eIF6 upregulation in cancer still needs to be answered [161, 162].

These studies also support the results presented here, which show that the eIF subunits p2α, 2α, 3B, 3C, 3D, 3J, p4B, 4G, as well as 6 were significantly upregulated in HCV-associated HCC, and that the subunits 2α and p4B were increased upon HCV infection. In contrast, we observed for the eIF3 subunits B, C, I and for eIF4E, eIF4G and eIF5 a reduction in protein expression in HCV. Our protein data from HBV-associated HCC and HBV revealed a significant overexpression of peIF2α, peIF4B and eIF4G. Another study has reported overexpression of eIF4G in different liver cell lines, and these were also linked to carcinogenesis [162]. In contrast to these data, we observed a downregulation for eIF2α, eIF3D, eIF3H, eIF3I, eIF3J, eIF4E and eIF6 in HBV-associated HCC and HBV.

In this study, the eIF subunits p2α, 2α, 3B, 3J and 6 were overexpressed in ASH and Morbus Wilson and eIF3D, peIF4B and eIF4G showed a significantly upregulated protein expression level in livers with alcohol induced injury. In contrast, we observed a downregulation in Wilson´s disease for eIF subunits 3D, 3H and p4B.

Significant differences were noticed in the expression pattern between chronic hepatitis B and C, HBV- and HCV-associated HCC and non-virus related HCC [182].

6.2 Characterization of mTOR Members and eIFs in CRC

Recent studies on mRNA transcription and protein synthesis in cancer have demonstrated a key role for translational control in tumorigenesis [163]. Activation of mTOR signaling has been shown to be a hallmark of cancer [164] and has been linked to cell growth and cell cycle progression [181].

In the PhD thesis, the expression patterns of mTOR pathway components in CRC patients were investigated. We also separated CRC patients into CC and RC and noticed dramatic differences in the expression patterns between these two groups. The final step was to sub-classify CC and RC patient samples into low and high grade tumors. mTOR and its upstream target AKT as well as the downstream targets p70S6K and 4E-BP1 displayed an overexpression only in RC, but not in CC. The tendency was the same in low and high grade RC tumors. Upstream and downstream targets of mTOR seem to be involved in cancer progression in low and high grade RC while in low grade and high grade CC the mTOR pathway members play a less important role [181].

Previously, a significant increase of eIF3 subunits in CRC was found [165]. Concurring with previous results, we found that eIF3 subunits were differentially expressed on protein and mRNA level in CC and RC. It is known from literature, that eIF3A, eIF3B and eIF3M overexpression has been detected in the CC cell line SW1116 [166]. eIF3C was found to be an oncogene and was shown to be increased in cancer cells [167], which is confirmed by our findings in CRC. eIF3H has been associated with higher CRC risk and was therefore suggested to act as CRC susceptibility gene [165]. We confirmed the CRC data from the literature and reported differences in the expression pattern of eIF3 subunits in low and high grade CC and RC [181].

Previous studies have reported an overexpression of eIF4G and eIF4E in different cell lines, including CRC cell lines, and they have also been linked to carcinogenesis [168]. This supports the results presented here showing that eIF4B displayed an overexpression in CRC and eIF4G was overexpressed in RC. eIF1, eIF2, eIF3 and eIF5 have been reported to be essential for translation initiation [169 - 171]. Previously, eIF2a was described to be transiently expressed only in normal cells, whereas constitutive overexpression supported tumor initiation and progression. Knockdown of eIF3D in HCT116 cells attenuated proliferation and increased stress-driven apoptosis [172, 181].

eIF4E is one of the most thoroughly investigated translation factors involved in cancer biology, especially in CRC. Together with eIF4A and eIF4G it forms the trimetric eIF4F complex. eIF4E plays a major role in the regulation of tumor growth, invasion and metastasis formation [171, 173]. Compared to previous studies, we also showed that eIF2α, eIF4B, eIF4E and eIF4G were significantly overexpressed on protein and mRNA level in CRC. This implies the influence of the eIF4F complex in protein translation in CRC [181].

Translational control and eIFs have been displayed to play major roles in growth, cell cycle regulation, proliferation, differentiation and tumorigenesis. However, the mechanism of eIF contribution in tumorigenesis is not yet finally understood [181].

6.3 Characterization of mTOR Members and Eukaryotic Translation Initiation Factors in Liver Metastases of Primary Colorectal Carcinoma

Approximately 20% of CRC patients have liver metastases at the time of diagnosis and 60% of patients develop liver metastases during the course of disease [174 - 176]. Current clinical management strategies include surgery, chemotherapy, radiation and palliative care, but they are not as effective as previously expected [172]. Various drugs have been reported to be effective against primary or metastatic CRC, but still the efficacy of current medications needs to be further improved [181].

In this study, regarding the PI3K/AKT/mTOR pathway in the metastases, we found no changes in the expression of pmTOR, mTOR, pAKT, AKT, pPTEN, PTEN, pp70S6K and 4E-BP1 on protein level for CC Mets and RC Mets. The IHC staining pattern of eIF subunits 1,

2α, 3A, 3B, 3C, 3H, 4E, 4G and 6 displayed a strong staining intensity in the CC and RC liver metastases but no staining was found in the NNLT [181].

As these eIF subunits turned out to be significantly overexpressed in liver metastases of primary CRC one might state that eIFs are major parts in the translation initiation of liver metastases of primary CRC carcinogenesis.

Nevertheless, little is known about eIFs and their antitumor activity in liver metastases of primary CRC. This PhD thesis here characterized for the first time the differences in the expression pattern of mTOR members and eIFs between NNCRM and primary CC and RC as well as NNLT and liver metastasis derived from primary CC and RC [181].

6.4 siRNA-Knockdown of eIF1, eIF5 and eIF6 *in vitro*

eIF6 expression limits cell growth and transformation [177]. eIF6 is known as part of a multi-protein complex connected with the RISC complex, which is the major complex regulating miRNA activity. Previous studies have reported eIF6 overexpression in ovarian serous carcinoma, leukemia, head and neck carcinoma, as well as CRC [177 - 180]. We also saw a significant increase of eIF6 in low and high grade RC at protein and mRNA level. This finding suggests that eIF6 may play a central role in the translation initiation of RC [181].

eIF5 overexpression has been reported in different cancer types and is considered to be a predictive tumor marker [169]. eIF1 has been demonstrated to bind eIF5 and thereby potentially interferes with its GAP function [169, 181].

As the eIF subunits 1, 5 and 6 turned out to be the most promising candidates in targeting CRC we investigated them in more detail in siRNA-knockdown experiments. After successful knockdown of eIF1, eIF5 and eIF6, both the proliferation rate and the clonogenicity of HCT116 and HT29 cells were significantly reduced. Apoptosis significantly increased after longer treatment periods (72h). The knockdown of *eIF1*, *eIF5* and *eIF6* resulted in a reduction of polysomes, indicating reduced overall translation [181].

To gain deeper mechanistic insights into the multifaceted role of eIF1, eIF5 and eIF6 in carcinogenesis future studies are needed. However, it can be concluded that, in low and high grade CRC eIF1, 5 and 6 might serve as prognostic tumor markers [181].

6.5 Analyses of Colorectal Cancer Patient Derived Xenograft Models

In addition to primary CRC analyses, chemosensitivity of various treated colon and rectum cancer PDX models was tested. Chemosensitivity testing for specific chemotherapeutic drugs revealed the standard CRC chemotherapeutic drugs Irinotecan, 5-FU, Oxaliplatin and Cetuximab as most efficient drugs to reduce the growth of colon and rectum carcinomas. Treatment with novel drugs like IGF 1/2 mAB, AZ1 and Volitinib did not display a biological meaningful reduction in tumor growth. They even seem to promote higher tumor growth compared to untreated controls in various CRC PDX models.

In addition to chemosensitivity testing, CRC PDX models were analyzed on protein level. No significant changes in eIF expression patterns could be observed comparing CRC and respectively PBS treated control tissue.

Less is known about the detailed mechanisms of eIFs in the deregulation of cell proliferation and malignant transformation, and this makes eIFs attractive targets for cancer therapy. Many eIFs are regulated through post-translation modifications such as phosphorylation. One possibility to inhibit eIFs and mRNA translation for cancer treatment is targeting the upstream kinases or phosphatases. If eIFs could serve as predictive biomarkers, not for only cisplatin and related therapies, will be subject of intense research in the following years.

7 Literature

1. International Agency for Research on Cancer (2013) GLOBOCAN 2012: estimated cancer incidence, mortality and prevalence worldwide in 2012. Lyon (France): Inerational Agency for Research on Cancer, 2013.

2. Kim JH, Sohn BH, Lee HS, Kim SB, Yoo JE, et al. Genomic predictors for recurrence patterns of hepatocellular carcinoma: Model derivation and validation. PLOS Medicine, 2014, 11(12): e1001770.

3. El Serga HB.Hepatocellular carcinoma: recent trends in the United States. Gastroenterology 2004; 127: 27-34.

4. Davila JA, Morgan RO, Shaib Y, McGlynn KA, El Serage HB.Heapitis C Infection and the increasing incidence of hepatocellular carcinoma: a population-based study. Gastroenterology 2004; 127(5): 1372-1380.

5 Kwon SK, Yun SS, Kim HJ, Lee DS. The risk factors of early recurrence after hepatectomy in hepatocellular carcinoma. Ann Surg Treat Res. 2014; 86(6): 283–288.

5. Llovet JM, Fuster J, Bruix J. Intention-to-treat analysis of surgical treatment for early hepatocellular carcinoma: resection versus transplantation. Hepatology 1999; 30(6): 1434-1440.

6. Poon RT, Fan ST, Ng IO, Lo CM, Lui CL, et al. Different risk factors and prognosis for early and late intrahepatic recurrence after resection of hepatocellular carcinoma. Cancer 2000; 89(3): 500-507.

7. Mantovani A, Allavena P, Sica A, Balkwill F. Cancer-related inflammation. Nature 2008; 454(7203): 436-444.

8. Bosch FX, Ribes J, Cleries R, Diaz M. Epidemiology of hepatocellular carcinoma. Clin Liver Dis 2005; 9(2): 191-211.

9. Sun B, Karin M. Inflammation and liver tumorgenesis. Front Med 2013; 7(2): 242-254.

11 Dvorak HF. Tumors: wounds that do not heal. Similarities between tumor stroma generation and wound healing. N Engl J Med 1986; 315(26): 1650-1659.

12 Haybaeck J. Mechanisms of Molecular carcinogenesis Volume 2. ISBN 978-319-53660-6. Springer International Publishing AG 2017.

13 Schlageter M, Terracciano LM, D'Angelo S, Sorrentino P. Histopathology of hepatocellular carcinoma. World J Gastroenterol. 2014; 20(43): 15955–15964.

14 The International Agency for Research on Cancer. WHO Classification of Tumours of the Digestive System (IARC WHO Classification of Tumours). 4th ed. In: Bosman FT, Carneiro F, Hruban RH, Theise ND, editors. Publisher: World Health Organization; 2010, 9789283224327.

15 Shafizadeh N, Kakar S. Diagnosis of well-differentiated hepatocellular lesions: role of immunohistochemistry and other ancillary techniques. Adv Anat Pathol. 2011; 18(6):438–45.

16 Nakashima O, Sugihara S, Kage M, Kojiro M. Pathomorphologic characteristics of small hepatocellular carcinoma: a special reference to small hepatocellular carcinoma with indistinct margins. Hepatology. 1995; 22(1):101-5.

17 Nakashima Y, Nakashima O, Hsia CC, Kojiro M, Tabor E. Vascularization of small hepatocellular carcinomas: correlation with differentiation. Liver. 1999; 19(1):12–18.

18 Craig JR, Peters RL, Edmondson HA, Omata M. Fibrolamellar carcinoma of the liver: a tumor of adolescents and young adults with distinctive clinico-pathologic features. Cancer. 1980; 46(2):372–379.

19 El-Serag HB, Davila JA. Is fibrolamellar carcinoma different from hepatocellular carcinoma? A US population-based study. Hepatology. 2004; 39(3):798–803.

20 Soreide O, Czerniak A, Bradpiece H, Bloom S, Blumgart L. Characteristics of fibrolamellar hepatocellular carcinoma. A study of nine cases and a review of the literature. Am J Surg. 1986; 151(5):518–523.

21 Van Eyken P, Sciot R, Brock P, Casteels-Van Daele M, Ramaekers FC, Desmet VJ. Abundant expression of cytokeratin 7 in fibrolamellar carcinoma of the liver. Histopathology. 1990; 17(2):101-7.

22 Schlageter M, Terracciano LM, D'Angelo S, Sorrentino P.Histopathology of hepatocellular carcinoma. World J Gastroenterol. 2014; 20(43): 15955–15964.

23 Yamaguchi R, Yano H, Iemura A, Ogasawara S, Haramaki M, Kojiro M. Expression of vascular endothelial growth factor in human hepatocellular carcinoma. *Hepatology 1998*, 28(1):68-77.

24 Matsuura S, Aishima S, Taguchi K, Asayama Y, Terashi T, Honda H, Tsuneyoshi M. 'Scirrhous' type hepatocellular carcinomas: a special reference to expression of cytokeratin 7 and hepatocyte paraffin 1. Histopathology. 2005; 47(4):382–390.

25 Yang SH, Watanabe J, Nakashima O, Kojiro M. Clinicopathologic study on clear cell hepatocellular carcinoma. Pathol Int. 1996; 46(7):503–509.

26 Buchanan TF, Huvos AG. Clear-cell carcinoma of the liver. A clinicopathologic study of 13 patients. Am J Clin Pathol. 1974 ;61:529–539.

27 Salomao M, Yu WM, Brown RS, Emond JC, Lefkowitch JH. Steatohepatitic hepatocellular carcinoma (SH-HCC): a distinctive histological variant of HCC in hepatitis C virus-related cirrhosis with associated NAFLD/NASH. Am J Surg Pathol. 2010; 34(11):1630–1636.

28 Park HS, Jang KY, Kim YK, Cho BH, Moon WS. Hepatocellular carcinoma with massive lymphoid infiltration: a regressing phenomenon? Pathol Res Pract. 2009; 205(9):648-52.

29 Emile JF, Adam R, Sebagh M, Marchadier E, Falissard B, Dussaix E, Bismuth H, Reynès M. Hepatocellular carcinoma with lymphoid stroma: a tumour with good prognosis after liver transplantation. Histopathology. 2000; 37:523–529.

30 Compton CC and Greene FL. "The staging of colorectal cancer: 2004 and beyond.," *CA. Cancer J. Clin.*, 2004; 54(6): 295–308.

31 Ramos-Lopez O, Martinez-Lopez E, Roman S, Fierro NA, Panduro A. Genetic, metabolic and environmental factors involved in the development of liver cirrhosis in Mexico. World J Gastroenterol. Nov 7, 2015; 21(41): 11552-11566.

32 Jemal A, Bray F, Center MM, Ferlay J, Ward E, Forman D. Global Cancer statistics. *CA Cancer J Clin* 2011; 61(2):69-90.

33 Parsyan A, Hernàndez G, Meterissian S. Translation initiation in colorectal cancer. Cancer Metastasis Rev 2012; 31: 387. doi:10.1007/s10555-012-9349-9.

34 Diab-Assaf M, Abou-khouzam R, Saadallah-Zeidan N, Habib K, Bitar N, Karam W, Liagre B, Harakeh St, Azar R. Expression of eukaryotic initation factor 4E and 4E binding protein 1 in colorectal carcinogenesis. Int J ClinExpPathol 2005; 8 (1):404-413.

35 Wang XW, Zhang YJ. (2014). Targeting mTOR network in colorectal cancer therapy. World J Gastroenterol 2014; 20(15): 4178-4188.

36 Hisamuddin IM and Yang VW. Molecular Genetics of Colorectal Cancer: An Overview. *Curr Colorectal Cancer Rep*. 2006; 2(2): 53–59.

37 Bogaert J and Prenen H. Molecular genetics of colorectal cancer. *Ann Gastroenterol 2014; 27 (1): 9-14.*

38 Moore PA, Fidler WJ. Adenocarcinoma of the colon and rectum in patients less than 40 years of age. Am Surg. 1984 Jan; 50(1):10-4.

39 Amersi F, Agustin M, Ko CY. Colorectal Cancer: Epidemiology, Risk Factors, and Health Services. Clinics in Colon and Rectal Surgery, 2005; 18:(3) 133-40.

40 Li FY, Lai MD. Colorectal cancer, one entity or three. J Zhejiang Univ Sci B. 2009; 10(3):219-29.

41 Hartmann M, Pabst MA, Schmied R, Caluba HC, Dohr G. Zytologie, Histologie und Mikroskopische Anatomie. Licht- und elektronenmikroskopischer Bildatlas. Facultas; 3-85076-679-9.

42 Young B . *Wheater's Functional Histology*, 2006; 5th ed. Churchill Livingstone.

43 http://middlesexsurgical.com/colorectal-surgery/

44 Prasad S. Practical Histology for Medical Students, 2007; 1st ed. Jaybee Brothers.

45 Flemming M, Ravula S, Tatishchev F, Wang H.L. Colorectal carcinoma: Pathological aspects. J Gastrointest Oncol 2012; 3(3):153–173.

46 Leopoldo S, Lorena B, Cinzia A, et al. Two subtypes of mucinous adenocarcinoma of the colorectum: clinicopathological and genetic features. Ann Surg Oncol 2008; 15(5):1429-39.

47 https://anatomytopics.wordpress.com/2008/12/21/21-anatomy-histology-embryology-of-the-large-intestine/

48 Kang H, O'Connell JB, Maggard MA, Sack J, Ko CY. A 10-year outcomes evaluation of mucinous and signet-ring cell carcinoma of the colon and rectum. Dis Colon Rectum. 2005; 48(6):1161-8.

49 Chen JS, Hsieh PS, Chiang JM, et al. Clinical outcome of signet ring cell carcinoma and mucinous adenocarcinoma of the colon. Chang Gung Med J 2010; 33(1):51-7.

50 Makino T, Tsujinaka T, Mishima H, Ikenaga M, Sawamura T, Nakamori S, Fujitani K, Hirao M, Kashiwazaki M, Masuda N, Takeda M, Mano M. Primary signet-ring cell carcinoma of the colon and rectum: report of eight cases and review of 154 Japanese cases. Hepatogastroenterology. 2006; 53(72):845-9.

51 Thirunavukarasu P, Sathaiah M, Singla S, et al. Medullary carcinoma of the large intestine: a population based analysis. Int J Oncol 2010; 37(4):901-7.

52 Hinoi T, Tani M, Lucas PC, et al. Loss of CDX2expression and microsatellite instability are prominent features of large cell minimally differentiated carcinomas of the colon. Am J Pathol 2001;159(6):2239-48.

53 Alexander J, Watanabe T, Wu TT, et al. Histopathological identification of colon cancer with microsatellite instability. Am J Pathol 2001; 158(2):527-35.

54 Abdalla E, Adam R, Bilchik A, and Jaeck D, “Improving resectability of hepatic colorectal metastases: expert consensus statement,” *Ann Surg Oncol.*, 2006; 13(10): 1271–1280.

55 Donadon M, Ribero D, Morris-Stiff G, Abdalla E, and Vauthey J. “New paradigm in the management of liver-only metastases from colorectal cancer,” *Gastrointest Cancer Res.*, 2007; 1(1): 20–27, 2007.

56 Schwenk W, Böhm B, and Müller JM. “Postoperative pain and fatigue after laparoscopic or conventional colorectal resections. A prospective randomized trial.,” *Surg. Endosc.*, 1998; 12:(9)1131–1136.

57 A. C. Society, “Colorectal Cancer Facts & Figures 2014-2016,” A. C. Society, 2014; 1–32.

58 http://picbear.linkpc.net/art/rectal-cancer-pictures-stages-of-lung.html

59 Hartmann M, Pabst M, Schmied R, Caluba H and Dohr G. *Zytologie, Histologie and Mikroskopische Anatomie*. 2005.

60 Young B. *Wheater's Functional Histology*, 5th ed. Churchill Livingstone, 2006.

61 Gayowski TJ, Iwatsuki S, Madariaga JR, Selby R, Todo S, Irish W, Starzl TE. "Experience in hepatic resection for metastatic colorectal cancer: Analysis of clinical and pathologic risk factors," *Surgery. Author Manuscr.*, 1994; 116(4): 703–711.

62 Martenson J, Willett C, Sargent D, Mailliard J, and Donohue J. "Phase III study of adjuvant chemotherapy and radiation therapy compared with chemotherapy alone in the surgical adjuvant treatment of colon cancer: results of intergroup protocol 0130," *J. Clin. Oncol.*, 2004; 22(16): 3277–3283.

63 Balch E, De Meo A, and Guillem J. "Modern management of rectal cancer," *World J Gastroenterol*, vol. 2006; 12(20): 3185–3195.

64 "Treatment Strategies for Rectal Cancer." Available: http://www.cancer.gov/cancertopics/pdq/treatment/rectal/HealthProfessional/page4/page4.

65 Prasad S. *Practical Histology for Medical Students*, 1st ed. Jaybee Brothers, 2007.

66 Marzouk O, Schofield J. Review of Histopathological and Molecular Prognostic Features in Colorectal Cancer. Cancers, 2011; 3(2) 2767-2810.

67 De la Chapelle, A. Microsatellite Instability. *N. Engl. J. Med*. 2003, 17;349(3):209-10.

68 Boland, C.R.; Thibodeau, S.N.; Hamilton, S.R.; Sidransky, D.; Eshleman, J.R.; Burt, R.W.; Meltzer, S.J.; Rodriguez-Bigas, M.A.; Fodde, R.; Ranzani, G.N.; *et al.* National Cancer Institute Workshop on microsatellite instability for cancer detection and familial predisposition: Development of international criteria for the determination of microsatellite instability in colorectal cancer. *Cancer Res.* 1998, *58*(52): 5248-5257.

69 Aaltonen, L.A.; Peltomäki, P.; Leach, F.S.; Sistonen, P.; Pylkkänen, L.; Mecklin, J.P.; Järvinen, H.; Powell, S.M.; Jen, J.; Hamilton, S.R.; *et al.* Clues to the pathogenesis of familial colorectal cancer. *Science* 1993, 260(5109):812-6.

70 Kinzler, K.W.; Vogelstein, B. Lessons from hereditary colorectal cancer. *Cell* 1996, 87(2):159-70.

71 Lawes, D.A.; SenGupta, S.; Boulos, P.B.; The clinical importance and prognostic implications of microsatellite instability in sporadic cancer. *Eur. J. Surg. Oncol*. 2003, 29(3):201-12.

72 Peyssonnaux, C.; Eychène, A. The Raf/MEK/ERK pathway: New concepts of activation. *Biol. Cell* 2001, 93(1-2):53-62.

73 Davies, H.; Bignell, GR.; Cox, C.; Stephens, P.; Edkins, S.; Clegg, S.; Teague, J.; Woffendin, H.; Garnett, MJ.; Bottomley, W.; *et al.* Mutations of the BRAF gene in human cancer. *Nature* 2002, 417(6892):949-54.

74 Wellbrock, C.; Karasarides, M.; Marais, R. The RAF proteins take centre stage. *Nat. Rev. Mol. Cell Biol*. 2004, **5**(11):875-85.

75 Garnett, M.J.; Rana, S.; Paterson, H.; Barford, D.; Marais, R. Wild-type and mutant B-RAF activate C-RAF through distinct mechanisms involving heterodimerization. *Mol. Cell* 2005, 20(6):963-9.

76 Richman, S.D.; Seymour, M.T.; Chambers, P.; Elliott, F.; Daly, C.L.; Meade, A.M.; Taylor, G.; Barrett, J.H.; Quirke, P. KRAS and BRAF mutations in advanced colorectal cancer are associated with poor prognosis but do not preclude benefit from oxaliplatin or irinotecan, results from the MRC FOCUS trial. *J. Clin. Oncol*. 2009, 27(35):5931-7.

77 Vogelstein, B.; Kinzler, K.W. Cancer genes and the pathways they control. *Nat. Med*. 2004, *10*, 789-799.

78 Rajagopalan, H.; Bardelli, A.; Lengauer, C.; Kinzler, KW.; Vogelstein, B.; Velculescu,VE. Tumorigenesis, RAF/RAS oncogenes and mismatch-repair status. *Nature* 2002, 418(6901):934.

79 Worthley, D.L.; Whitehall, V.L.; Spring, K.J.; Leggett, B.A. Colorectal carcinogenesis: Road maps to cancer. *World J. Gastroenterol*. 2007, 13(28): 3784–3791.

80 Tabernero, J.; Van Cutsem, E.; Diaz-Rubio, E.; Cervantes, A.; Humblet, Y.; Andre´ T.; Van Laethem, J-L.; Soulie, Ṕ.; Casado, E.; Verslype, C.; *et al.* Phase II trial of cetuximab in combination with fluorouracil.; leucovorin.; and oxaliplatin in the first-line treatment of metastatic colorectal cancer. *J. Clin. Oncol*. 2007, 25(33):5225-32.

81 Amado, R.G.; Wolf, M.; Peeters, M.; Van Cutsem, E.; Siena, S.; Freeman, D.J.; Juan, T.; Sikorski, R.; Suggs, S.; Radinsky, R.; *et al.* Wild-type KRAS is required for panitumumab efficacy in patients with metastatic colorectal cancer. *J. Clin. Oncol*. 2008, 26(10):1626-34.

82 Roth, A.D.; Tejpar, S.; Delorenzi, M.; Yan, P.; Fiocca, R.; Klingbiel, D.; Dietrich, D.; Biesmans, B.; Bodoky, G.; Barone, C.; *et al.* Prognostic role of KRAS and BRAF in stage II and III resected colon cancer, results of the translational study on the PETACC-3.; EORTC 40993.; SAKK 60-00 trial. *J. Clin. Oncol*. 2010, 28(3):466-74.

83 Ogino, S.; Meyerhardt, J.A.; Irahara, N.; Niedzwiecki, D.; Hollis, D.; Saltz, L.B.; Mayer, R.J.; Schaefer, P.; Whittom, R.; Hantel, A.; *et al.* KRAS mutation in stage III colon cancer and clinical outcome following intergroup trial CALGB 89803. *Clin. Cancer Res*. 2009, 15(23):7322-9.

84 Samowitz, W.S.; Sweeney, C.; Herrick, J.; Albertsen, H.; Levin, T.R.; Murtaugh, M.A.; Wolff, R.K.; Slattery, M.L. Poor survival associated with the BRAF V600E mutation in microsatellite-stable colon cancers. *Cancer Res*. 2005, 65(14):6063-9.

85 Roth, A.D.; Tejpar, S.; Delorenzi, M.; Yan, P.; Fiocca, R.; Klingbiel, D.; Dietrich, D.; Biesmans, B.; Bodoky, G.; Barone, C.; *et al.* Prognostic role of KRAS and BRAF in stage II and III resected colon cancer, results of the translational study on the PETACC-3.; EORTC 40993.; SAKK 60-00 trial. *J. Clin. Oncol*. 2010, *28*(3): 466-474.

86 Di Nicolantonio, F.; Martini, M.; Molinari, F.; Sartore-Bianchi, A.; Arena, S.; Saletti, P.; De Dosso, S.; Mazzucchelli, L.; Frattini, M.; Siena, S.; *et al.* Wild-type BRAF is required for response to panitumumab or cetuximab in metastatic colorectal cancer. *J. Clin. Oncol*. 2008, 26(35):5705-12.

87 Bardelli, A.; Siena, S. Molecular mechanisms of resistance to cetuximab and panitumumab in colorectal cancer. *J. Clin. Oncol*. 2010, 28(7):1254-61.

88 Sartore-Bianchi, A.; Di Nicolantonio, F.; Nichelatti, M.; Molinari, F.; De Dosso, S.; Saletti, P.; Martini, M.; Cipani, T.; Marrapese, G.; Mazzucchelli, L.; *et al.* Multi-determinants analysis of molecular alterations for predicting clinical benefit to EGFR-targeted monoclonal antibodies in colorectal cancer. *PLoS One* 2009, 4(10):e7287.

89 Sonnberg N, Hinnebush AG. Regulation of translation initiations in eukaryotes: mechanisms and biological targets. Cell 2009; 136(4):731-45.

90 Hinnebush AG, Lorsch JR. The mechanism of eukaryotic initiation: new insights and challenges. Cold Spring Harb Perspect Biol. 2012; 4(10): a011544.

91 Jackson Rj, Hellen CU, Pestova TV. Termination and post-termination events in eukaryotic translation. Adv Protein Chem Struct Biol 2012; 86:45-93.

92 Spilka R, Ernst C, Kuldeep Mehta A, Haybaeck J. Eukaryotic translation initiation factors in cancer development and progression. Cancer Lett. 2013; 28; 340(1):9-21.

93 Matsuo H, Li H, McGuire Am, Flechter CM, Gingras AC, Sonenberg N, Wagner G. Structure of translation factor eIF4E bound to m7GDP and interaction with 4E-binding protein. Nat Struct Biol 1997; 4(9):717-24.

94 Spilka R, Laimer K, Bachmann F, Spizzo G, Vogetseder A, Wieser M, Müller H, Haybaeck J, and Obrist P. "Overexpression of eIF3a in squamous cell carcinoma of the oral cavity and its putative relation to chemotherapy response," *J. Oncol.*, vol. 2012, 901956, doi:10.1155/2012/901956.

95 Jackson R, Hellen C, and Pestova T. "The mechanism of eukaryotic translation initiation and principles of its regulation," *Nat. Rev. Cell Biol.*, 2010; 11(2):113-27.

96 Passmore LA, Schmeing TM, Maag D, Applefield DJ, Acker MG, Algire MA, Lorsch JR, Ramakrishnan V.The Eukaryotic Translation Initiation Factors eIF1 and eIF1A induce an Open Conformation of the 40S Ribosome. Molecular CellArticle. 2007, 13; 26(1):41-50.1:41–50.

97 Jackson R, Hellen C, and Pestova T. "The mechanism of eukaryotic translation initiation and principles of its regulation," *Nat. Rev. Cell Biol.*, 2010; 11(2):113-27.

98 Fletcher CM, Pestova T, Hellen C, Wagner G. Structure and interactions of the translation initiation factor eIF1, EMBO J. 1999; 18(9): 2631**–**2637.

99 Miyasaka H, Endo S, Shimizu H. Eukaryotic translation initiation factor 1 (eIF1), the inspector of good AUG context for translation initiation, has an extremely bad AUG context, J. Biosci. Bioeng. 2010; 109(6):635-7. .

100 Yoon HJ, Donahue TF. The suil suppressor locus in Saccharomyces cerevisiae encodes a translation factor that functions during tRNA(iMet) recognition of the start codon, Mol. Cell. Biol. 1992; 12(1):248–260.

101 J. Rush, A. Moritz, K.A. Lee, A. Guo, V.L. Goss, E.J. Spek, H. Zhang, X.M. Zha, R.D. Polakiewicz, M.J. Comb, Immunoaffinity profiling of tyrosine phosphorylation in cancer cells, Nat. Biotechnol. 2005; 23(1):94-101.

102 Fenner BJ, Scannell M, Prehn JH. Expanding the substantial interactome of NEMO using protein microarrays, PLoS One 2010; 5(1):e8799.

103 Nanda JS, Saini AK, Munoz AM, Hinnebush AG, Lorsch. Coordinated movments of eukaryotic translation inititation factors eIF1, eIF1A, and eIF5 trigger phosphate

release from eIF2 in response to start codon recognition by the ribosomal preinitiation complex. J Biol Chem 2013; 288(8):5316-29.

104 Suragani R, Ghosh S, Ehtesham NZ, Ramaiah KV. Expression and purification of the subunits of human translation inititation factor 2 (eIF2): phosphorylation of eIF2 alpha and beta. Protein Expr Purif 2006; 47:225-233.

105 Roll-Mecak A, Alone P, Cao C, Dever TE, Burley SK. X-ray structure of translation initiation factor eIF2gamma: implications for tRNA and eIF2alpha binding. J Biol Chem 2004; 279:10634-10642.

106 Thompson GM, Pacheco E, Melo EO, Castilho BA. Conserved sequences in the beta subunit of archaeal and eukaryal translationinitiation factor 2 (eIF2), absent from eIF5, mediate interaction with eIF2gamma. Biochem J 2002; 347(3):703-709.

107 Cho S, Hoffmann DW. Structure of the beta subunits of translation initiation factor 2 from the archaeon Methanococcus jannaschii: a representative of the eIF2beta/eIF5 family of proteins. BioChemistry 2002; 41: 5730-5742.

108 Ito T, Marintchev A, Wagner G. Solution structure of human initiation factor 2alpha reveals homology to the elongation factor eEF1B. Structure (Camb) 2004; 12(9):1693-704.

109 Yang W. Hinnebush AG. Identifation of a regulatory subcomplex in the guanine nucleotide exchange factor eIF2B that mediates inhibition by phosphorylated eIF2. Mol Cell Biol 1996; 16(11):6603-16.

110 Zhou M, Sandercock AM, Fraser CS, Ridlova G, Stephens E, Schenauer MR, Yokoi-Fong T, Barsky D, Leary JA, Hershey JW, Doudna JA, Robinson CV. Mass spectrometry reveals modularity and a complete subunit interaction map of the eukaryotic translation factor eIF3, PNAS 2008; 105(47):18139-44.

111 Sun C, Todorovic A, Querol-Audí J, Bai Y, Villa N, Snyder M, Ashchyan J, Lewis CS, Hartland A, Gradia S, Fraser CS, Doudna JA, Nogales E, Cate JH. Functional reconstitiution of human eukaryotic translation initiation factor 3 (eIF3). PNAS 2011; 108(51):20473-8.

112 Bachmann F, Banziger R, Burger MM. Cloning of a novel protein overexpressed in human mammary carcinoma, Cancer Res. 1997; 57:988-994.

113 Pincheira R, Chen Q, Zhang JT. Identification of a 170-kDa protein overexpressed in lung cancers, Br. J. Cancer 2001; 84(11): 1520–1527.

114 Chen G, Burger MM. p150 overexpression in gastric carcinoma: the association with p53, apoptosis and cell proliferation. Int J Cancer. 2004; 112(3):393-8.

115 Xu TR, Lu RF, Romano D, Pitt A, Houslay MD, Milligan G, Kolch W. Eukaryotic translation initiation factor 3, subunit a, regulates the extracellular signal-regulated kinase pathway, Mol. Cell. Biol. 2012; 32(1):88-95.

116 Scoles DR, Yong WH, Qin Y, Wawrowsky K, Pulst SM. Schwannomin inhibits tumorigenesis through direct interaction with the eukaryotic initiation factor subunit c (eIF3c), Hum. Mol. Genet. 2006; 15 (7): 1059-1070.

117 Kim HK, Choi IJ, Kim CG, Kim HS, Oshima A, Michalowski A, Green JE. A gene expression signature of acquired chemoresistance to cisplatin and fluorouracil combination chemotherapy in gastric cancer patients, PLoS ONE 2011; 18;6(2):e16694.

118 Sudo H, Tsuji AB, Sugyo A, Kohda M, Sogawa C, Yoshida C, Harada YN, Hino O, Saga T. Knockdown of COPA, Identified by Loss-of-Function Screen, Induces Apoptosis and Suppresses Tumor Growth in Mesothelioma Mouse Model. Genomics. 2010; 95(4):210-6.

119 Marchetti A, Buttitta F, Miyazaki S, Gallahan D, Smith GH, Callahan R. Int- 6, a highly conserved, widely expressed gene, is mutated by mouse mammary tumor virus in mammary preneoplasia, J. Virol. 1995; 69(3):1932–1938.

120 Rasmussen SB, Kordon E, Callahan R, Smith GH. Evidence for the transforming activity of a truncated Int6 gene, in vitro. Oncogene 2001, 20: 5291–5301.

121 Doldan A, Chandramouli A, Shanas R, Bhattacharyya A, Cunningham JT, Nelson MA, Shi J. Loss of the eukaryotic initiation factor 3f in pancreatic cancer, Mol. Carcinog. 2008; 47(3): 235–244.

122 Doldan A, Chandramouli A, Shanas R, Bhattacharyya A, Leong SP, Nelson MA, Shi J. Loss of the eukaryotic initiation factor 3f in melanoma, Mol. Carcinog. 2008; 47(10): 806–813.

123 Rauch J, Ahlemann M, Schaffrik M, Mack B, Ertongur S, Andratschke M, Zeidler R, Lang S, Gires O. Allogenic antibody-mediated identification of head and neck cancer antigens, Biochem. Biophys. Res. Commun. 2004; **323**(1):156-62.

124 Joseph P, Lei YX, Ong TM. Up-regulation of expression of translation factors – a novel molecular mechanism for cadmium carcinogenesis, Mol. Cell.Biochem. 2004; 255: 93. doi:10.1023/B:MCBI.0000007265.38475.f7

125 Goh SH, Hong SH, Lee BC, Ju MH, Jeong JS, Cho YR, Kim IH, Lee YS. eIF3m expression influences the regulation of tumorigenesis-related genes in human colon cancer, Oncogene 2011; 30(4):398-409.

126 Gingras AC, Raught B, Sonenberg N. EIF4 initiation factors: effectors of mRNA recruitment to ribosomes and regulators of translation, Annu. Rev. Biochem.1999; 68:913–963.

127 Lazaris-Karatzas A., Sonenberg N. The mRNA 5' cap-binding protein, eIF-4E, cooperates with v-myc or E1A in the transformation of primary rodent fibroblasts. Mol. Cell. Biol. 1992; 12:1234–1238.

128 Kroczynska B, Kaur S, Katsoulidis E, Majchrzak-Kita B, Sassano A, Kozma SC, Fish EN, Platanias LC. Interferon-dependent engagement of eukaryotic initiation factor 4B via S6 kinase (S6K)- and ribosomal protein S6K-mediated signals, Mol. Cell. Biol. 2009; 29(10):2865-75.

129 Peffley DM, Sharma C, Hentosh P, Buechler RD. Perillyl alcohol and genistein differentially regulate PKB/Akt and 4E-BP1 phosphorylation as well as eIF4E/eIF4G interactions in human tumor cells, Arch. Biochem. Biophys. 2007; 465(1):266-73.

130 Jia Y, Chiu TL, Amin EA, Polunovsky V, Bitterman PB, Wagner CR. Design, synthesis and evaluation of analogs of initiation factor 4E (eIF4E) cap-binding antagonist Bn7-GMP, Eur. J. Med. Chem. 2010; 45(4): 1304–1313.

131 Assouline S, Culjkovic B, Cocolakis E, Rousseau C, Beslu N, Amri A, Caplan S, Leber B, Roy DC, Miller WH, Borden KL. Molecular targeting of the oncogene eIF4E in acute myeloid leukemia (AML): a proof-of-principle clinical trial with ribavirin, Blood 2009; 114(2):257-60.

132 Chen L, Aktas BH, Wang Y, He X, Sahoo R, Zhang N, Denoyelle S, Kabha E, Yang H, Freedman RY, Supko JG, Chorev M, Wagner G, Halperin JA. Tumor suppression by small molecule inhibitors of translation initiation. Oncotarget 2012; 3(8):869-81.

133 Jennings MD, Pavitt GD. eIF5 has GDI activity necessary for translational control by eIF2 phosphorylation, Nature 2010; 465(7296):378-81.

134 Singh CR, Lee B, Udagawa T, Mohammad-Qureshi SS, Yamamoto Y, Pavitt GD, Asano K. An eIF5/eIF2 complex antagonizes guanine nucleotide exchange by eIF2B during translation initiation, EMBO J. 2006; 25(19):4537-46.

135 Maier B, Ogihara T, Trace AP, Tersey SA, Robbins RD, Chakrabarti SK, Nunemaker CS, Stull ND, Taylor CA, Thompson JE, Dondero RS, Lewis EC, Dinarello CA, Nadler JL, Mirmira RG. The unique hypusine modification of eIF5A promotes islet beta cell inflammation and dysfunction in mice, J. Clin. Invest. 2010; 120(6):2156-70.

136 Balabanov S, Gontarewicz A, Ziegler P, Hartmann U, Kammer W, Copland M, Brassat U, Priemer M, Hauber I, Wilhelm T, Schwarz G, Kanz L, Bokemeyer C, Hauber J, Holyoake TL, Nordheim A, Brummendorf TH. Hypusination of eukaryotic initiation factor 5A (eIF5A): a novel therapeutic target in BCR-ABL-positive leukemias identified by a proteomics approach, Blood 2007; 109(4):1701-11.

137 Miluzio A, Beugnet A, Volta V, Biffo S. Eukaryotic initiation factor 6 mediates a continuum between 60S ribosome biogenesis and translation, EMBO Rep. 2009; 10(5):459-65.

138 Benelli D, Marzi S, Mancone C, Alonzi T, la Teana A, Londei P. Function and ribosomal localization of aIF6, a translational regulator shared by archaea and eukarya. Nucleic Acids Res. 2009; 37(1):256-67.

139 Gandin V, Miluzio A, Barbieri AM, Beugnet A, Kiyokawa H, Marchisio PC, Biffo S. Eukaryotic initiation factor 6 is rate-limiting in translation, growth and transformation, Nature 2008; 455(7213):684-8.

140 Chendrimada TP, Finn KJ, Ji X, Baillat D, Gregory RI, Liebhaber SA,. Pasquinelli AE, Shiekhattar R. MicroRNA silencing through RISC recruitment of eIF6, Nature 2007; 447(7146):823-8.

141 Guertin DA, Sabatini DM. An exlanding role form TOR in cancer. Trends Mol Med 2005; 11:353-361.

142 Parsyan A.. Translation and its regulation in cancer biology and medicin. Springer 2014; ISBN 978-94-017-9077-2.

143 Laplante M, Sabatini DM. mTOR signaling in growth control and disease. Cell 2012; 149(2):274-93.

144 Zoncu R, Bar-Peled L, Efeyan A, Wang S, Sancak Y, Sabatini DM. mTORC1 senses lysomal amino acids through an inside-out mechanism that requires the vacuolar h(+)-ATPase. Science 2011; 334(6056):678-83.

145 Carriere A, Romeo Y, Acosta-Jaquez HA, Moreau J, Bonneij E, Thibault P, Fingar DC, Roux PP. ERK1/2 Phosphorylate Raptor to Promote Ras-dependent Activation of mTOR Complex 1 (mTORC1).J. Biol. Chem. 2011; 286(1):567-77.

146 Singh AS and. Sau AKS, “Tissue Microarray: A powerful and rapidly evolving tool for high-throughput analysis of clinical specimens,” *Int. J. Case Reports Images*, 2010; 01:1-6.

147 http://www.cell.com/cms/attachment/580971/4371271/gr4.jpg

148 Radhakrishnan R, Solomon M, Satyamoorthy K, Martin LE, Lingen MW. Tissue microarray – a high-throughput molecular analysis in head and neck cancer. J Oral Pathol Med 2008; 37(3):166-76.

149 http://www.bio-protocol.org/e251

150 Wang XL, Cai HP, Ge JH, Su XF. Detection of eukaryotic translation initiation factor 4E and its clinical significance in hepatocellular carcinoma. World J Gastroenterol 2012; 18(20): 2540–2544.

151 Parsyan A. Translation and ist regulation in caner biology and medicine. Springer 2014; ISBN 978-94-017-9077-2.

152 George A, Panda S, Kudmulwar D, Chhatbar SP, Nayak SC, Krishnan HH. Hepatitis C virus NS5A binds to the mRNA cap-depending eukaryotic translation initiation 4F (eIF4F) complex and up-regulates host translation initiation machinery through eIF4F-binding protein 1 inactivation. J Biol Chem 2012; 287(7):5042-58.

153 Guertin DA, Sabatini DM. The pharmacology of mTOR inhibition. SciSignal 2009; 2(67):pe24.

154 Villanueva A, Chiang DY, Newell P, Peix J, Thung S, Alsinet C, Tovar V, Roayaie S, Minguez B, Sole M. et al.. Pivotal role of mTOR signaling in hepatocellular carcinoma. Gastroenterology 2008; 135(6):1972-83.

155 Stelzer MK, Pilot HC, Liem A, Lee D, Kennedy GD, Lambert PF. Rapamycin inhibits anal carcinogenesis in two preclinical animal models. Cancer Prev Res (Phila) 2010; 3(12): 1542–1551.

156 Bello DM, Ariyan CE, Carvajal RD. Melanoma mutagenesis and aberrant cell signaling. Cancer Control. 2013; 20(4):261-81.

157 Wang J, Guo Y, Chu H, Guan Y, Bi J, Wang B. Multiple functions of the RNA-binding HuR in cancer progression, treatment response and prognosis. Int J Mol Sci 2013; *14*, 10015-10041.

158 Yang GF., Xie D, Liu JH, Luo JH,. Li LJ,. Hua WF, Wu HM, Kung HF, Zeng YX, Guan XY. Expression and amplification of EIF-5A2 in human epithelial ovarian tumors and overexpression of EIF-5A2 is a new independent predictor of outcome in patients with ovarian carcinoma, Gynecol. Oncol. 2009; 112(2):314-8.

159 Scuoppo C, Miething C, Lindqvist L, Reyes J, Ruse C, Appelmann I, Yoon S, Krasnitz A, Teruya-Feldstein J, Pappin D. et al. . A tumor suppressor network relying on the polyamine hypusine axis. Nature 2012; 487(7406):244-8.

160 Silvera D, Formenti S, Schneider R. Translation control in cancer, Nat Rev Cancer *2010;* 10(4):254-66.

161 Martin B, Sanz R, Aragues R, Olivia B, Sierra A. Functional clustering of metastasis proteins describes plastic adaption resources of breast-cancer cells to new microenvironments. J Proteome Res 2008; 7(8):3242-3253.

162 Rosso P, Cortesina G, Sanvito F, Donadini A, Di Benedetto B, Biffo S, Marchisio PC Overexpression of p27BBP in head and neck carcinomas and their lymph node metastases. Head Neck 2004; 26(5):408-17.

163 Pestova TV, Kolupaev VG. The role of individual eukaryotic translation initiation factors in ribosomal scanning and initiation codon selection. Genes Dev. 2002; **16**(22):2906-22.

164 Shahbazian D, Parsyan A, Petroulakis E, Hershey J, Sonenberg N.. eIF4B controls survival and proliferation and is regulated by proto-oncogenic signaling pathways. Cell Cycle 2010; 9(20): 4106–4109.

165 Wang Z, Chen J, Sun J, Cui Z, Wu H.. RNA interference-mediated silencing of eukaryotic translation initiation factor 3, subunit B (EIF3B) gene expression inhibits proliferation of colon cancer cells. World J Surg Oncol. 2012; 10:119.

166 Liu Z, Dong Z, Yang Z, Chen Q, Pan Y, Yang Y, Cui P, Zhang X, Zhang JT.. Role of eIF3a (eIF3 p170) in intestinal cell differentiation and its association with early development. Differentiation 2007; 75(7):652-61.167 Song N, Wang Y, Gu X, Chen Z, Shi L. . Effect of siRNA-mediated knockdown of EIF3C gene on the survival of colon cancer cells. BJZUS 2013; 14(6): 451–459.

168 Fukuchi-Shimogori T, Ishii I, Kashiwagi K, Mashiba H, Ekimoto H, Igarashi K. (1997). Malignant transformation by overproduction of translation initation factor eIF4G. Cancer Res. 1997; 57(22):5041-4.

169 Yang GF, Xie D, Liu JH, Luo JH, Li LJ, Hua WF, Wu HM, Kung HF, Zeng YX, Guan XY. . Expression and amplification of EIF-5A2 in human epithelial ovarian tumors and overexpression of EIF-5A2 is a new independent predictor of outcome in patients with ovarian carcinoma, Gynecol. Oncol. 2009; 112(2):314-8.

170 Nielsen KH, Behrens MA, He Y, Oliveira CL, Sottrup Jensen L, Hoffmann SV, Pedersen JS, Andersen GR. Synergistic activation of eIF4A by eIF4B and eIF4G, Nucleic Acids Res. 2011; 39(7):2678-89.

171 Xu T, Zong Y, Peng L, Kong S, Zhou M, Zou J, Liu J, Miao P, Sun X, Li L. (2016). Overexpression of eIF4E in colorectal cancer patients is associated with liver metastasis. Onco Targets Ther. 2016; 9: 815–822.

172 Yu X, Zheng B, Chai R. Lentivirus-mediated knockdown of eukaryotic translation initiation factor 3 subunit D inhibits proliferation of HTC116 colon cancer cells. Biosci. Rep.2014; 34(6): e00161.

173 Showkat M, Beigh MA, Andrabi KI. mTOR Signaling in Protein Translation Regulation : Implications in Cancer Genesis and Therapeutic Interventions. Nat. Rev. 2015; 2014:686984.

174 Clark ME, Smith RR. Liver-directed therapies in metastatic colorectal cancer. J GastrointestOncol 2014; 5(5): 374–387.

175 Hohla F, Winder T, Greil R, Rick FG, Block NL, Schally AV. (2014). Targeted therapy in advances metastatic colorectal cancer: Current concepts and prespectives. World j Gastroenterol 2014; 20(20):6102-6112.

176 Zhang W, Song T. (2014). The progress in adjuvant therapy after curative resection of liver metastasis from colorectal cancer. Drug Discoveries & Therapeutics 2014; 8(5):194-200.

177 Gandin V, Miluzio M, Barbieri AM, Beugnet A, Kiyokawa H, Marchisio PC, Biffo S. Eukaryotic initiation factor 6 is rate-limiting in translation, growth and transformation. Nature 2008; 455(7213):684-8

178 Rosso P, Cortesina G, Sanvito F, Donadini A, Di Benedetto B, Biffo S, Marchisio PC. Overexpression of p27BBP in head and neck carcinomas and their lymph node metastases. Head Neck 2004; 26(5):408-17.

179 Miluzio A, Beugnet A, Volta V, Biffo S. Eukaryotic initiation factor 6 mediates a continuum between 60S ribosome biogenesis and translation. EMBO Rep. 2009; 10(5):459-465.

180 Chendrimada TP, Finn KJ, Ji X, Baillat D, Gregory RI, Liebhaber SA, Pasquinelli AE, Shiekhatter R. MicroRNA silencing through RISC recruitment of eIF6. Nature 2007; 447(7146):823-8.

181 Golob-Schwarzl N, Schweiger C, Koller C, Krassnig S, Gogg-Kamerer M, Gantenbein N, Toeglhofer AM, Wodlej C, Bergler H, Pertschy B, Uranitsch S, Holter M, El-Heliebi A, Fuchs J, Punschart A, Stiegler P, Keil M, Hoffmann J, Henderson D, Lehrach H, Reinhard C, Regenbrecht C, Schicho R, Fickert P, Lax S, Haybaeck J. Separation of low and high grade colon and rectum carcinoma by eukaryotic translation initiation factors 1, 5 and 6. Oncotarget, 2017; in Revision.

182 Golob-Schwarzl N, Krassnig S, Toeglhofer AM, Park YN, Gogg-Kamerer M, Vierlinger K, Schröder F, Rhee H, Schicho R, Fickert P, Haybaeck J. New liver cancer biomarkers: PI3K/AKT/mTOR pathway members and eukaryotic translation initiation factors. European Journal of Cancer 2017, 83:56-70.